Development of Glucose Biosensors Using Nanostructured Composites

Hadi Wali Saheb Al-Sagur

A thesis submitted in partial fulfilment of the requirements of

Sheffield Hallam University

for the degree of Doctor of Philosophy

August 2018

DECLARATION

I hereby declare that this thesis submitted for the degree of PhD is the result of my own research and that this thesis has not been submitted for higher degree to any other university or institution.

Hadi Wali Saheb Al-Sagur

DEDICATION

To my late father who is resting in peace, my mother and siblings

To my nephew (Sarmad) and niece (Hajar)

This effort is a small gift for all of you

Hadi Wali Saheb Al-Sagur

ACKNOWLEDGEMENT

First and foremost, I would like to express my appreciation and acknowledgement to my director of study and supervisor Dr Aseel Hassan, without the support and guidance of you, this work would not have been possible. Your patience, motivation, interest, and massive knowledge have helped me in all the time of research and writing of this thesis.

I gratefully acknowledge the guidance and support provided by Prof Alexei Nabok, Dr Akram Khan, and Dr Shanmugasundaram Komathi through their second supervisory roles in this thesis.

The support and supply of chemicals by Prof Tamara Basova, Prof Mahmut Durmuş, and Prof Ayşe Gürek is gratefully acknowledged.

Special thanks to my mother and my siblings for their support, patience and understanding throughout the course of my studies.

I would also like to acknowledge the financial sponsorship provided by the Ministry of Higher Education and Scientific Research (MOHESR) in Iraq. Special thanks, to the Iraqi Cultural Attaché in London for their support during my PhD research.

Thi-Qar University, College of Medicine, Physiology and Medical Physics department are gratefully acknowledged for the continuing support during my study.

The support of staff in the Materials and Engineering Research Institute (MERI) was so vital to make life easy during my study; to mention but a few, Prof Alan Smith, Prof Papken Hovsepian, Dr Nicholas Farmilo, Prof Chris Sammon, Dr Francis Clegg, Miss Deeba Zahoor for her great training sessions and support, Mr Paul Allender for the training and technical support, Dr Tony Bell, Mr Gary Robinson, Mr Stuart Creasey,

Jane Wright, Rachael Toogood, Gail Hallewell, Corrie Houton, Clare Mills Roberts, Leo Olowookere, Ekaterina Nikolova, Yuvini Hettiarachchi, and Amy McNally.

I am so thankful for my PhD colleagues and friends for making life interesting during the three years together; Abdusalam Essa, Ronak Janani, Abubakar Mohammed, Matthew Kitchen, Jorge Otero, Hassan Judah, Vitalijus Slizys, Vishal Bajaj, Samantha Harvey, Mirjam Skof, Magdi Mussa, Eman El-Buaishi, Oliver Duncan, Yaqub Rahaq, Ojo Ayotunde, Zaid Al-Jlaihawi, Ranjika Gunathilaka, Nimra Shahab, Oluwaseum Tope Oluwafemi, Deborah Fisher, Shruti Mandhani, Rebecca Chadwick, Magda Kaminska, and Murtadha Kareem.

Finally, special thanks to the International Experience Team in Sheffield Hallam University for all support and help they offered to me during my course of study in SHU.

ABSTRACT

Developing a biosensor capable of measuring glucose and other whole blood analytes for monitoring diabetes has been a major challenge for over four decades. In this thesis, an attempt has been made to develop three different novel metallophthalocyanine-based (MPcs) biosensors for this purpose. Three novel enzymatic biosensors have been fabricated to monitor glucose concentration and other whole blood analytes in vitro. The first fabricated biosensor is based on conducting multifunctional hydrogel (PAA-rGO/VS-PANI/$LuPc_2$/GOx-MFH) utilising reduced graphene oxide (rGO) and lutetium phthalocyanine ($LuPc_2$) dissolved in chloroform to produce three-dimensional (3D) matrix as platform to enhance the sensing performance. Utilising the aqueous properties of a novel water-soluble iron phthalocyanine (FePc) derivative on the other hand, added more simplicity for the fabrication process of another biosensor (PAA-CP/GPL-FePc/GOx-CH) for enzymatic detection of glucose. Graphene nanoplatelets (GPL) have been attached non-covalently to the FePc resulting in a conducting hydrogel-based platform (CH). A third novel bioprobe (SiO_2($LuPc_2$)-PANI(PVIA)/GOx-CNB) based on silica nanoparticles (SiO_2) grafted polyaniline (PANI) has formed a conducting nanobeads (CNB)-based biosensor. The latter is employed as an enzymatic biosensor platform for the detection of glucose with enhanced sensitivity. Full characterisation has been carried out for all the raw studied materials as well as prepared biosensing platforms. UV-Visible and FT-IR spectroscopies as well as SEM, TEM, XRD, and EDX have been employed in order to help gaining full understanding of the nature and properties of the studied materials. The electrochemical properties of the newly developed biosensing platforms have been fully studied using common analytical methods such as cyclic voltammetry (CV), amperometry, and electrochemical impedance spectroscopy (EIS). The freeze dry system alongside the Brunauer-Emmett-

Teller (BET) method were employed to characterise the surface area of the produced platforms.

The sensitivity of MFH biosensor studied in the range 2-12 mM of glucose is found to fall in the region of 15.31 μA mM^{-1} cm^{-2} with low detection limit of 25 μM. The biosensor based on CH platform exhibited a broad linear behaviour when glucose in the range 1-20 mM is studied, with high sensitivity of 18.11 μA mM^{-1} cm^{-2} and low detection limit of 1.1503 ng/mL. The conducting nanobeads-based biosensor (CNB) has led to a further improvement the sensitivity of glucose detection (38.53 μA mM^{-1} cm^{-2}) with wide linear range of 1-16 mM and detection limit of 0.1 mM. All three biosensing platforms have exhibited excellent selectivity when examined against whole blood components.

LIST OF ABBREVIATIONS

2D	Two-dimension
3D	Three-dimensional networks
A	Absorbance
A	Electrode area
AA	Ascorbic acid
A_{acs}	Adsorbate cross sectional area
AC	Alternating current
ACV	Alternating current voltammetry
AD	Amperometric detection
ADA	Americans with Disabilities
Au	Gold
β	beta
BET	Brunauer-Emmett-Teller
c	Concentration
CA	Chronoamperometry
C_b	Bulk concentration
C_{dl}	Double layer capacitance
CE	Counter electrode
CGM	Continuous glucose monitoring
CH	Conducting hydrogel
CNB	Conducting nanobeads
CNT	Carbon nanotube
CNT-CUM	Carbon nanotube-Cumarin
CNT-Pyrene	Carbon nanotube-Pyrene
COUL	Coulometric Detection
C_{ox}	Bulk concentration of oxidized species
CP	Conducting polymer
C_{Red}	Bulk concentration of reduced species
CV	Cyclic voltammetry
CV	Cyclic voltammetry
CVs	Cyclic voltammograms
d	inter-atomic distance

DA	Dopamine
DC	Direct current
DET	Direct electron transfer
D_i	Diffusion
DM	Diabetes mellitus
DBU	1,8-diazabicyclo [5.4.0] undec-7-ene
DPV	Differential pulse voltammetry
$DyPc_2$	Dysprosium phthalocyanine
ε	Absorption coefficient
E	Nernst potential
E_p^a	Anode potentials
E_p^c	Cathode potentials
$E^{o'}$	Formal potential
EC	Equivalent circuit
Ecoli	Escherichia coli
EDX	Energy dispersive X-ray
EIS	Electrochemical impedance spectroscopy
EMS	Electronic Micro Systems
EPO	Erythropoietin
$EuPc_2$	Europium phthalocyanine
F	Faraday's constant
FA	Fast amperometry
FAD	Flavin adenine dinucleotide
FePc	Iron phthalocyanine
FESEM	Field Emission Scanning Electron Microscope
FT-IR	Fourier-transform Infrared
GDH	Glucose dehydrogenase
GDM	Gestational diabetes mellitus
$GdPc_2$	Gadolinium phthalocyanine
GOx	Glucose oxidase
GPL	Graphene nanoplatelets
H_2O_2	Hydrogen peroxide
HOMO	Highest occupied molecular orbital

I	Current
ICP	Intrinsic conducting polymer
IDDM	Insulin dependent diabetes mellitus
IDEAU	Interdigitated gold electrodes
IDEs	Interdigitated electrodes
IDF	International Diabetes Federation
I_{ion}	Current carried by the ions
ISFET	ion-sensitive field-effect transistor
iZ'	Imaginary impedance
JACS	Journal of American chemical society
l	Length of cell
LA	Lactic acid
LLBs	Lanthanide luminescent bioprobes
LMCT	Ligand-to-metal charge transfer
LOD	Limit of detection
LPR	Linear polarization resistance
LSP	Linear sweep potentiometry
LSV	Linear sweep voltammetry
LUMO	Lowest unoccupied molecular orbital
$LuPc_2$	Lutetium phthalocyanine
M	Molecular weight
MFH	Multifunctional conducting hydrogel
MPcs	Metallophthalocyanines
mRNA	Messenger ribonucleic acid
MWCNTs	Multi-walled carbon nanotubes
n	Number of electrons
N	The Avagadro's number
NCIVN	National Cardiovascular Intelligence Network
NDP	Normal pulse voltammetry
$NdPc_2$	Neodymium phthalocyanine
NIDDM	Non-insulin dependent diabetes mellitus
NPs	Nanoparticles
NPV	Normal pulse voltammetry

Ω	Ohm
p	Equilibrium gas pressure
p_o	Saturation pressure
PAA	Polyacrylic acid
PAD	Pulsed amperometric detection
PANI	Polyaniline
PB	Prussian Blue
PC	Professional computer
Pcs	Phthalocyanines
PDT	Photodynamic therapy
PEDOT	Poly(3,4-ethylenedioxythiophene
PEG	Poly(ethylene glycol) diamine
PEI	Polyethyleneimine
PHE	Public Health England
POT	Potentiometric detection
PPy	Polypyrrole
PSAF	Potentiometric stripping analysis (faradaic)
PSAG	Potentiometric stripping analysis (galvanostatic)
PT	Polythiophene
PtPb	Platinum modified lead
PVIA	Poly(vinyl alcohol-vinyl acetate) itaconic acid
Q	The reaction quotient
R	Universal gas constant
R_{ct}	Charge transfer resistance
RE	Reference electrode
R_{et}	Electron transfer resistance
rGO	Reduced graphene oxide
R_s	Electrolyte resistance
RSD	Relative standard deviation
R_W	Warburg diffusion element
SEM	Scanning electron microscopy
SiO_2	Silica nanoparticles
$SmPc_2$	Samarium phthalocyanine

SPCEs	Screen-Printed carbon electrodes
SPR	Surface plasmon resonance
SWCNTs	Single-walled carbon nanotubes
T	Temperature
t	Time
T1DM	Type-1 diabetes mellitus
T2DM	Type-2 diabetes mellitus
TEM	Transmission electron microscopy
TLC	Thin layer chromatography
TPA	Terephthalaldehyde
UA	Uric acid
UV	Ultra-violent
v	Adsorbed volume
v	Wavenumber
v_m	Adsorbed monolayer volume
VS	Vinyl substituted
VS-PANI	Vinyl substituted polyaniline
WADA	World Anti-Doping Agency
WE	Working electrode
WHO	World Health Organisation
XRD	X-ray diffraction
XRF	X-ray fluorescence
YSI	Yellow Spring Instrument
Z	Real impedance
ZCP	Zero current potentiommetry
ZRA	Zero resistance amperometry
θ	The angle
λ	Wavelength
π	Constant =3.14159

LIST OF PUBLICATIONS

- **Al-Sagur, H.**, Komathi, S., Khan, M. A., Gurek, A.G & Hassan, A. A novel glucose sensor using lutetium phthalocyanine as redox mediator in reduced graphene oxide conducting polymer multifunctional hydrogel. Biosensors & Bioelectronics, 92 (2017) 638-645.
- Ahmet Şenocak, Cem Göl, Tamara V. Basova, Erhan Demirbaş, Mahmut Durmuş, **Hadi Al-Sagur**, Burak Kadem, Aseel Hassan. Preparation of single walled carbon nanotube-pyrene 3D hybrid nanomaterial and its sensor response to ammonia. Sensors and Actuators B: Chemical, 256 (2018) 853-860.
- **Al-Sagur, H**., Komathi, S., Karakaş, H., Atilla, D., Gürek, A.G., Basova,T., Farmilo, N., Hassan, A.K. A glucose biosensor based on novel Lutetium bis-phthalocyanine incorporated silica-polyaniline conducting nanobeads. Biosensors & Bioelectronics, 102 (2018) 637-645.

CONFERENCES

- **Al-Sagur, H.**, Komathi, S., Nabok, A., & Hassan, A. Development of chemical/bio-sensors using Graphene-based materials. Winter poster event of MERI_BMRC conference, (17th December 2015), Sheffield Hallam University, UK. (Poster)
- **Al-Sagur, H.**, Komathi, S. & Hassan, A. Preparation of polyaniline/Europium phthalocyanine janus nanocomposite electrochemical probe for reagentless detection of glucose. The Nanoparticles with Morphological and Functional Anisotropy: Faraday Discussion, (4th-6th July 2015) in the University of Strathclyde, Glasgow, UK. (Poster)
- **Al-Sagur, H.**, Komathi, S., Nabok, A., & Hassan, A. Development of chemical/bio-sensors using Graphene-based composites. MERI research Symposium, (17th-18th May 2016), Sheffield Hallam University, UK. (Poster)
- **Al-Sagur, H.**, Komathi, S., Khan, M. A., Gurek, A.G & Hassan, A. A novel glucose sensor using lutetium phthalocyanine as redox mediator in reduced graphene oxide conducting polymer multifunctional hydrogel. The 26th Anniversary World Congress on Biosensors, (25th-27th May 2016) Gothenburg, Sweden. (Poster)
- **Al-Sagur, H.**, Komathi, S., & Hassan, A. Lutetium phthalocyanine doped silica-polyaniline "bead-on-bead" nanostructures: A novel electrochemical probe for glucose biosensor application. Winter poster event of BMRC/MERI conference, (15th December 2016), Sheffield Hallam University, UK. (Poster)
- **Al-Sagur, H.**, Komathi, & Hassan, A. A glucose biosensor based on novel Lutetium bis-phthalocyanine incorporated silica-polyaniline conducting nanobeads . The 5th International Conference on Bio-Technology, (7th-10th May 2017) Riva Del Garda, Italy. (Poster)
- **Al-Sagur, H.**, Komathi, Nabok, A. & Hassan, Development of biosensors using graphene-based composites. MERI research Symposium (7th-10th May 2017) Sheffield Hallam University, UK. (Poster)
- **Al-Sagur, H.**, Komathi, S., & Hassan, A. The 60th anniversary of the Nikolaev Institute of Inorganic Chemistry, Novosibirsk, Russia. (15th-22nd October 2017) (Collaboration and training course)

- **Al-Sagur, H.**, Komathi, S., Khan, M. A., Gurek, A.G & Hassan, A. A novel glucose sensor using lutetium phthalocyanine as redox mediator in reduced graphene oxide conducting polymer multifunctional hydrogel. The 10th Man Met Postgraduate Research Conference 'PROVOKING DISCOURSE' (7^{th} March 2018), Manchester, UK. (Poster)

- **Al-Sagur, H.**, Komathi, S., & Hassan, A. A novel water soluble iron phthalocyanine as a redox mediator integrated to multifunctional hydrogel based graphene nanoplatelets for glucose monitoring. Deutsche Physikalische Gesellschaft e.V., (11^{th}-16^{th} March 2018), Berlin, Germany. (Poster)
- **Al-Sagur, H.**, Komathi, S., & Hassan, A. Construction and glucose biosensing performance of a water processable iron phthalocyanine functionalised graphene nanoplatelets distributed conducting hydrogel. The 28th Anniversary World Congress on Biosensors (12^{th}-15^{th} June 2018) Miami, Florida, USA. (Poster)

PRIZES AND AWARDS

- Best third poster in BMRC/MERI winter poster event, (15^{th} December 2016), Sheffield Hallam University, UK.
- Sponsor award from the representative of the research sponsor, the Iraqi Cultural Attaché in London (17^{th} January 2017).
- Best third PhD student talk at the MERI symposium, (17^{th} May 2017), Sheffield Hallam University, UK.

LIST OF FIGURES

LIST OF TABLES

TABLE OF CONTENTS

Chapter: 1 Introduction

1.1 Rationale

Diabetes mellitus (DM) is a global public health crisis affecting more than 425 million people and is estimated to increase to up to 642 million people by 2040 (International Diabetes Federation, 2017). The United Kingdom (UK) is facing a massive increase in the number of people with diabetes, which has been frequently reported, with the number of people diagnosed with the disease having doubled since 1996 to reach 2.9 million. This number is projected to almost double again over the next ten years (Diabetes UK, 2012). More than a million people died due to diabetes-related diseases and they expected to be the leading cause of death by the end of 2030, according to World Health Organization (WHO). Figure 1-1 shows the aproximate statistics of people living with diabetes in 2013 around the world, according to the International Diabetes Federation (IDF) which appeared in their diabetes atlas, sixth edition 2013 (International Diabetes Federation, 2013).

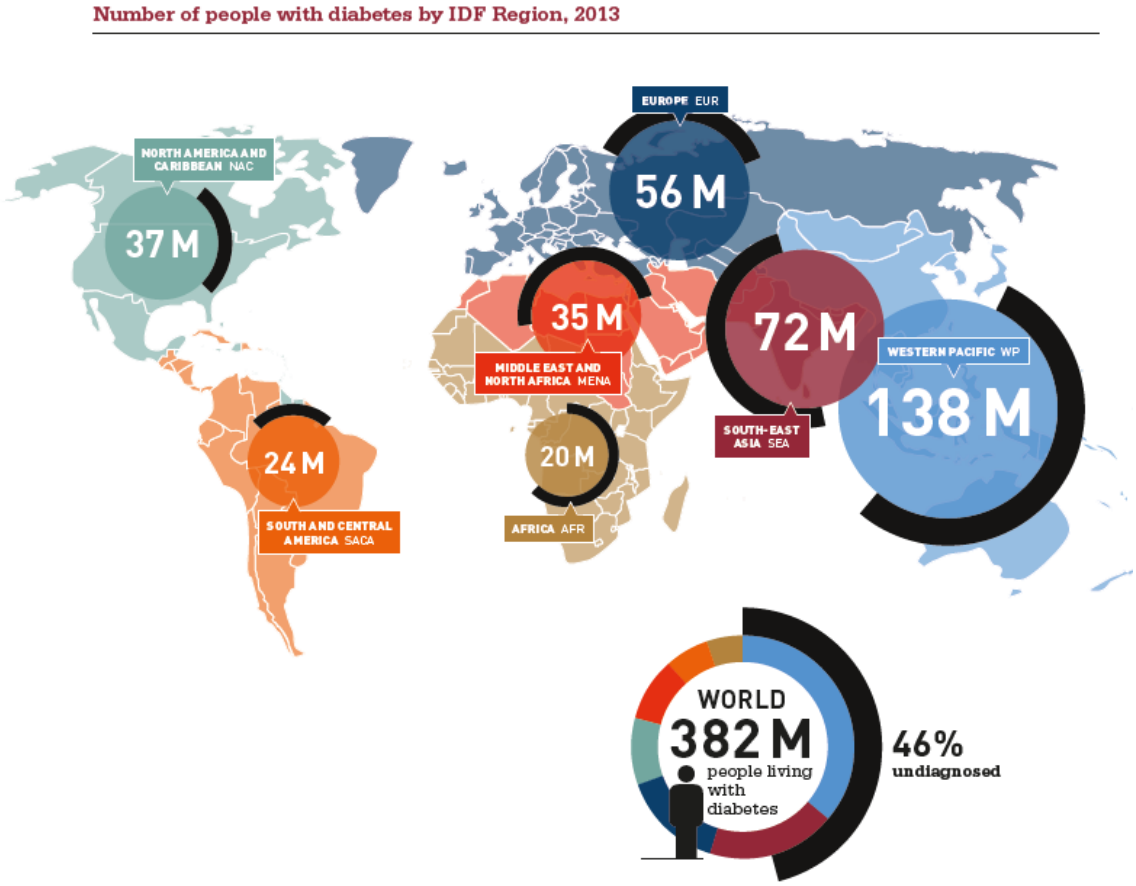

Figure 1-1 Number of people with diabetes by IDF region, 2013

Today's biosensor market is dominated by glucose biosensors. In 2004, glucose biosensors accounted for approximately 85% of the world market which amounts to ~5 billion US dollars (Newman and Turner, 2005). According to a recent report by Global Industry Analysts, Inc., the global market for glucose biosensors and strips will reach several billions of US dollars by 2020. Recently, a market research platform called DATA BRIDGE stated that the global glucometer market was estimated to be 5.2 billion US dollars in 2016 and the top major player companies in the market are Johnson & Johnson Services, Inc., Abbott, Bayer AG, and F. Hoffmann-La Roche Ltd. (DATA BRIDGE, 2018). Geographically, Asia Pacific, North America, Europe, the

Middle East, and Africa are the segments of the glucose biosensor market but it was estimated to be mainly led by North America (Transparency Market Research, 2018). However sensor and biotechnology companies work together to develop reliable devices, where many comparative studies between glucose meter and laboratory-based glucose oxidase have suggested that the available commercial devices are not satisfactory to monitor hypoglycemia for new-borns and infants (Ekhlaspour et al., 2017; Garingarao et al., 2014; Sreenivasa et al., 2015). Hence, the development of biosensors for self-monitoring of blood glucose to control elevated levels of blood sugar is inevitable to tackle this global issue (Wang, 2008, 2001). Therefore, there is a significant need by large number of patients for such simple, reliable, and portable device, which can provide fast and accurate reading (Wang, 2008).

Since the initial concept of glucose enzyme electrodes proposed in 1962 by Clark and Lyons (Clark and Lyons, 1962), a tremendous research activity in the field of glucose biosensors carried out forward development of devices for diabetes control (Davis and Higson, 2009; Klonoff et al., 2017; Turner, 2013). This is a reflection of the significant market demand incurred by users for simple to use, reliable, and low cost devices (Eggins, 2002; Wang, 2008). Regardless of the available conventional methods for the detection of glucose, electrochemical detection of glucose has shown promising results due to its reliable characteristics and low power consumption (Liu and Yu, 1997). In addition to its simplicity and low cost, electrochemical method does not require skilled labour or large instrumentation for its operation (Rahman et al., 2010). Due to the

natural combination of the biosensor-based electrochemical reactions, many technologies have been carried out to develop the performance of the biosensors. Figure 1-2 is the world's first portable glucometer that was launched in 1969 by Bayer's Miles Laboratories (PRESSEPORTAL, 2015).

Figure 1-2 The world's first portable glucometer that was launched in 1969 by Bayer's Miles Laboratories

Several technologies have been employed to develop the electrochemical reactions-based electrode surfaces which are largely applied in electrochemical sensors. Non enzymatic electrochemical sensors have been developed in order to produce efficient sensor for glucose detection purposes (Chaiyo et al., 2018; Kim et al., 2017; Mei et al., 2016; Shamsipur et al., 2017). Despite the considerable attention devoted by large number of researchers and the significant number of papers published in the field, non-enzymatic sensors exhibit poor performance in selectivity and suffer from interference

from other electrochemically active molecules (Tian et al., 2014; Toghill and Compton, 2010). Enzymatic electrochemical detection on the other hand has attracted great attention due to its accurate and stable performance. Glucose oxidase (GOx) is the widely studied enzyme for amperometric glucose sensing since its inception from Clark and Lyons in 1962 (Claussen et al., 2012; Wang, 2001). The key factor for an efficient GOx-based electrochemical biosensor is to obtain electron transfer from the active centre, flavin adenine dinucleotide (FAD) enwrapped within thick protein shell which makes it inaccessible for direct communication (Heller and Feldman, 2008; Wilson and Turner, 1992). Disposable enzyme sensors are basically based on the following reaction (Hu et al., 2017) (More details are found in section 10.2):

$$GOx\ (FAD) + 2H^+ + 2e^- \leftrightarrow GOx(FADH_2) \qquad (1)$$

To achieve direct electron transfer (DET) between the enzyme and the electrode, nanomaterials have expressed the ability of enhancing the catalytic surface area and enabling better mass transport of species within the enzymatic reactions (Salimi et al., 2004; Xie et al., 2007).

Graphene-based derivatives have been proposed as interface material mainly due to their excellent conductivity and large surface area (Geim and Novoselov, 2007; Kuila et al., 2011; Unnikrishnan et al., 2013; Wang et al., 2011). Moreover, immobilisation of GOx to the electrode surface requires suitable host for secure attachment purposes. An ideal biosensor must be stable for long-term application and accurate measurements

with significant operational lifetimes. Therefore, several organic and inorganic nanostructures have been proposed to enhance the immobilization of GOx and improve the conducting properties of the biosensing electrode (Wu et al., 2015); these include conductive polymers (Chen et al., 2006), polyacrylonitrile (Zheng et al., 2002) and silica nanoparticles (Sun et al., 2016).

Hydrogel-based polyaniline (PANI) three-dimensional networks (3D) have been used as conducting matrices for electrochemical applications due to their physiochemical properties and biocompatibility (Gerard et al., 2002; Guo et al., 2015; Taşdelen, 2017).

Silica nanoparticles have been employed to work as bioprobes for glucose detection purposes (Al-Sagur et al., 2018; Hasanzadeh et al., 2012; Ma et al., 2015). Silica nanoparticles are inorganic materials which possess unique properties, such as size tunability, large surface area, and biocompatibility, making them suitable as host matrix for enzyme immobilisation for glucose biosensing applications (Sun et al., 2016). To overcome the poor conductivity of silica nanoparticles, grafting organic to inorganic has been found valuable to develop electron transfer capability, bioactivity, accessibility of analytes, as well as the associated large surface area (Gopalan et al., 2009).

Metallophthalocyanines (MPcs) have been frequently used to develop the electrochemical biosensor performance due to their excellent electrocatalytic activity and chemical stability (Akinbulu and Nyokong, 2010; Martin et al., 2016; Ozoemena et al., 2005; Teo et al., 2016). When GOx catalyses the oxidation of glucose, an electron-

acceptor will be converted to hydrogen peroxide (H_2O_2) and that will lead to estimating the glucose concentrations on the electrodes. Therefore, modification the platform-based biosensors with MPcs (non-water soluble or water-soluble) will enhance the electrocatalytic activity as well as reduce the potential requirement for H_2O_2 oxidation (Han et al., 2016; Ozoemena et al., 2005; Wang et al., 2005). MPcs have been fabricated and loaded onto conducting hydrogels and silica nanoparticles, and the results have demonstrated fast direct electron transfer on the electrode surfaces which contributed towards highly improved sensitivity (Armengol et al., 1999; Buber et al., 2017; Jędrzak et al., 2018; Trzebinski, 2011).

Extensive studies were carried out to develop the sensitivity of biosensors, for instance, Ozoemena and Nyokong have developed cobalt phthalocyanine-based glucose biosensor with sensitivity approaching 0.024 $\mu A/mM^{-1}cm^{-1}$ but the response time was to slow at ~5 second (Ozoemena and Nyokong, 2006). Komathi and coworkers have produced nanoparticle-based PANI enzymatic glucose sensor which exhibited sensitivity in the region of 3.97 $\mu A/mM^{-1}cm^{-1}$ and response time of ~5 second (Komathi et al., 2009a). More recently, Ren and coworkers have fabricated triethylenetetramine-functionalised graphene-based amperometric glucose biosensor achieving sensitivity of 19.9 $\mu A/mM^{-1}cm^{-1}$ and response time of 6 second (Ren et al., 2016).

In this thesis, three different biosensors have been fabricated for the purpose of enzymatic whole blood detection. The first is a scalable synthesis of multifunctional conducting polyacrylic acid (PAA) hydrogel (MFH) integrated with reduced graphene oxide (rGO), vinyl substituted polyaniline (VS-PANI) and lutetium phthalocyanine ($LuPc_2$) as 3D robust matrix for glucose oxidase (GOx) immobilisation (PAA-rGO/VS-

PANI/$LuPc_2$/GOx-MFH). New glucose biosensor-based water processable iron phthalocyanine (FePc) functionalised graphene nanoplatelets (GPL) dispersed polyacrylic acid (PAA) 3D conducting hydrogel (PAA-CP/GPL-FePc/GOx-CH). Finally, a highly sensitive electrochemical bioprobe based on water-soluble lutetium phthalocyanine incorporated into silica nanoparticles ($SiO_2(LuPc_2)$) grafted with Poly(vinyl alcohol-vinyl acetate) itaconic acid (PANI(PVIA)) doped polyaniline conducting nanobeads employed as host to immobilise GOx to produce ($SiO_2(LuPc_2)$PANI(PVIA)/GOx-CNB) enzymatic biosensor used as sensitive electrochemical bioprobe for glucose detection. Figure 1-3 explains the structures of the three fabricated biosensors.

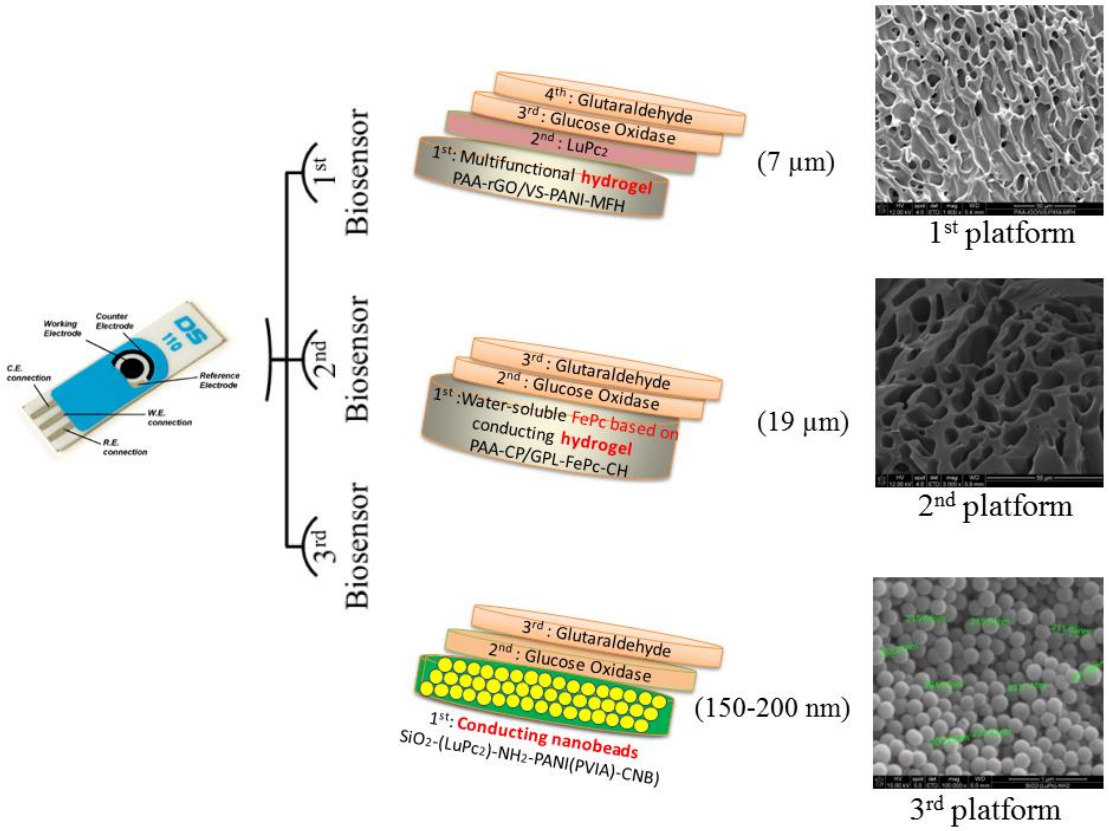

Figure 1-3 The three fabricated biosensors

1.2 Aim and objectives

The principle aim of this research is to develop new biosensor for whole blood monitoring based on metal phthalocyanine incorporated hydrogels and conducting nanobeads. Novel conducting hydrogel-based graphene derivatives or silica nanoparticles modified electrodes have been developed for the ultrasensitive detection of biomolecules including glucose. These electrodes work as electrochemical biosensor devices with high sensitivity and selectivity towards biological analytes. The project involves the preparation of the sensing platforms, characterisation of the used materials to understand their physio-chemical properties, modification of the electrodes with some novel materials and detection of analyte molecules.

The main objectives of the proposed research program can be summarised as follows:

1. Production of multifunctional platform for the ultrasensitive detection of biomolecules such as glucose using electrochemical detection methods and develop a critical comparative analysis to justify the proposed approach.
2. Functionalisation of graphene derivatives or incorporation of silica nanoparticles with metallophthalocyanines.
3. Using different composites such as polyaniline (PANI) and metallophthalocyanines are essential to build a three-dimensional robust matrix to enhance the conductivity and redox properties during the electrochemical detection of the analytes.
4. Control the physical and chemical properties of the hydrogels in order to obtain insoluble hydrophilic polymeric network with the capability to swell in the presence of aqueous solution or biological fluids.
5. The enhancement of the linear range detection of glucose biosensors will also be developed in addition to investigating the interference between the glucose

and other chemical components in whole blood such as ascorbic acid and uric acid. The detection of the analyte molecules will be carried out by electrochemical technique using a three-electrode cell setup.

6. Other key challenges in this research is to achieve low detection limit range of glucose concentrations; this is carried out throughout the program by altering composition of the sensing hydrogel using different MPcs such as $LuPc_2$ and FePc.

Chapter: 2 Literature review

2.1. Biosensors in general

Sensors are devices that record a physical, chemical, or biological change and convert that change into a measurable signal (Eggins, 2002). Biosensors are the analytical tools that monitor changes in the presence of biological analytes such as blood samples, antibody antigen reaction, and so on. A biosensor in general consists of main two components; a bioreceptor (recognition element) and a transducer (Wilson, 2005). The recognition element is originally isolated from living systems, for instance glucose oxidase (GOx) was extracted from three fungi, *Aspergillus niger, Penicillium amagasakiense, and Penicillieeum notatum* (Swoboda and Massey, 1965). The recognition element determines the function and type of the sensor for a particular use of a specific analyte where the selective response of the sensor to an analyte or a group of analytes depends on that element. The most common recognition elements in biosensors are receptors, enzymes, antibodies, nucleic acids, aptamers, molecular imprints and lectins (Chambers et al., 2002). The other main component of the sensor is the transducer. It represents the detector device that produces a signal and this is followed by a signal processor, which collects, amplifies, and output in a display the obtained signal as shown in Figure 2.1. Basically, the recognition element interacts with the targeted sample and the response will be converted by the transducer as an electrical, optical, thermal or mechanical signal. Sensors gained enormous attention in biology due to their powerful ability in gathering biological information. The first reported biosensor was developed by Clark and Lyons in 1962. Later biosensors have shown immense potential for biomolecular detection. Based on the simplicity in operation, higher sensitivity, ability to perform multiplex analysis, and capability to be

integrated with different function at the same platform, biosensors gained outstanding popularity in sensing wide range of analytes in medical diagnosis (Patel et al., 2016).

Biosensors have been used in a variety of applications; in food safety, biosensors have been employed to monitor food contaminations in the industry (Lv et al., 2018). Pathogen detecting biosensors have stood as an urgent need since 1999 with a market size of $563 million (Alocilja and Radke, 2003). Bacteria such as *Salmonella typhimurium*, DH5-α and *Escherichia coli* (*Ecoli*) strains have been detected via impedance based biosensors (Ali et al., 2018); polluting agents, water contamination, and toxins have been studied also (Hernandez-Vargas et al., 2018; Randviir and Banks, 2013). In medicine, a review article stated that biosensors are of great value for use in clinical testing; the diagnosis and treatment monitoring of cancer and cardiac diseases have been commonly investigated by immunosensors and biomarkers (Bahadir and Sezgintürk, 2015). The diagnosis of other diseases have been reported using biosensors, for instance, celiac disease biomarkers have been diagnosed in full blood by using biosensors (Pasinszki and Krebsz, 2018). Surface plasmon resonance (SPR)-based biosensor was employed for the detection of Ebola virus (Yu et al., 2006), while chronic kidney has been monitored at early stage by applying portable biosensor (Desai et al., 2018). Despite the availability of conventional techniques, biosensors in low-resource settings have been used for the detection of malaria infection in the early stages which will help in preventing the spreading of the disease (Ragavan et al., 2018). Recently, biomarkers of Alzheimer's disease have been detected using bio-transduction methods such as electrochemical and surface plasmon resonance methods (Shui et al., 2018). Environmental applications have been already studied using biosensors (Felix and Angnes, 2018); for instance, hand-held biosensor technology has been developed for the monitoring of homeland security in the USA and some other countries (Fuji-Keizai USA, Inc., 2004). In 2001, Mulchandani and coworkers in the university of California

have developed flow injection amperometric enzyme based biosensor for the determination of organophosphate nerve agents (Mulchandani et al., 2001). Vital work has been carried out in developing biosensors for the detection of sugar in diabetics. Several studies related to enzymatic glucose detection cited suitable range of sugar in blood; for instance, Zhang et al. obtained a good wide linear range by their optimized biosensor that starts from 0.5-1000 μM, which is appropriate for glucose detection in the body fluids (Zhang et al., 2015). Another glucose biosensor constructed by Feng et al. shows much wider range (10-1480 μM) and this explains the good conductivity of this device. In addition their constructed device was compared with the results of glucose detection range which was conducted in a hospital using a biomedical analyser (Hitashi 7600) where the measurements demonstrated an excellent sensitivity of their biosensor (Feng et al., 2015). In a similar manner, a new study conducted in 2015 confirmed a suitable measured concentration of glucose, which was in the range 10-1000 μM (ul Hasan et al., 2015).

The high sensitivity of biosensors play vital role in cancer and drugs detection alike (Bohunicky and Mousa, 2011; Higson, 2012; Holford et al., 2012; Lourencao et al., 2015; Ruiyi et al., 2018; Wang, 2006; Xiao et al., 2017). Highly sensitive nano-electrochemical biosensors have been developed to detect the biomarkers of human epidermal growth factor receptor 2 ($HER2^{+}$) which inappropriate activation leads to human breast cancer (Salahandish et al., 2018). Chemical sensors have been employed to monitor the level of prostate-specific antigen (PSA) in the human blood to help detect prostate cancer (Santonico et al., 2014). Furthermore, electrochemical biosensors have been utilised for the determination of drugs such as paracetamol in commercial tablets and human serum samples (Zhang et al., 2016), Luteolin in pharmaceutical scenarios (Li et al., 2018), and the cytotoxicity of anticancer drug such as arsenic trioxide which was used to evaluate the viability of leukemia K562 cells (Yu et al., 2014).

For "clean sport" the World Anti-Doping Agency's president has expanded funding research that lead to detect doping in sport (WADA, 2016), hence there has been an official call by WADA for scientists to take active role in supporting this call (Minunni et al., 2008). Therefore, and because of the point-of-care diagnostics abilities of electrochemical biosensors (Higson, 2012; Wang, 2006), several studies were carried out to monitor doping in sport. Testosterone has been detected by competitive amperometric immunosensor as sensing platform to set the basis for more developments (Laczka et al., 2011). An immunosensor was constructed based on a new type of redox nanoprobe to detect Erythropoietin (EPO) which is one of blood doping agents (Han et al., 2015). However the lack of research to develop the anti-doping domain and the gap between experts and scientists (Deoim and Moller, 2018), there are complicated issues such as the lack of cooperation between governments and WADA in addition to the negative impact of stakeholders (Overbye, 2016).

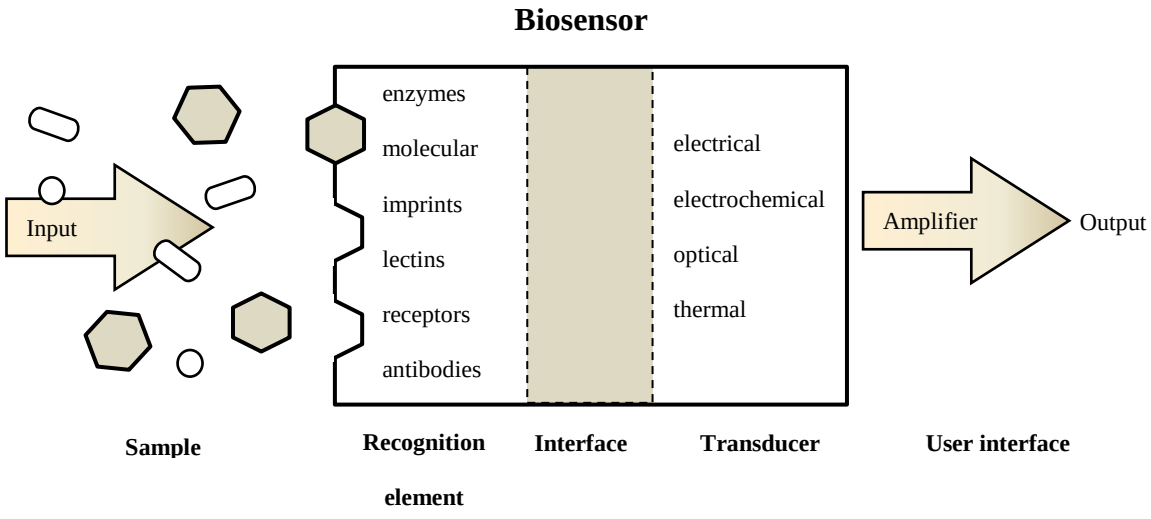

Figure 2-1 Configuration of a biosensor showing biorecognition element, interface, and transduction elements

Biosensors can be classified according to the transduction mechanism; these are (i) resonant biosensors, (ii) optical-detection biosensors, (iii) thermal-detection biosensors,

(iv) ion-sensitive field-effect transistor (ISFET) biosensors, and (v) electrochemical biosensors (Lee et al., 2009). Electrochemical biosensors have proved to be an essential technique to analyse biomolecules species due to the direct conversion of a biological event to electric signal. One of the main advantages of electrochemical biosensors over the other methods is that their electrodes can detect the bio-analytes without interfering with the system (Kuila et al., 2011). In general, a biosensor device utilises biological components such as enzymes to indicate the amount of biomolecules present within an environment. It can simply be defined, in a first approach as a device that intimately associates a biological sensing element and a transducer (Erdem et al., 2000). Blood glucose monitoring is one of the major applications of biosensors due to the high demand in the market. First commercial biosensor was Yellow Springs Instruments glucose biosensor which was launched to the market in 1975 and was based on amperometric detection of hydrogen peroxide (Setford and Newman, 2005). Similar to any other technology, biosensors have developed clearly through the advantage of combining the biomolecules and nanomaterials with appropriate approaches such as the use of nanoparticles in the electrochemical biosensors (Pakchin et al., 2017) and immunosensors arrays (Tang et al., 2012).

Nanoparticles have proven their potential in the development of bio-sensing platforms through enhancing the sensitivity of the sensing platform, due to their excellent high-performance electrical, mechanical or optical properties (Sun et al., 2013). Therefore, combining the rules of biology, chemistry, and the physics of nanostructures have demonstrated an encouraging direction for the fabrication of synthetic platforms from biomaterial structures to be used in biomedical applications (Bitar et al., 2012). Thus, nanoparticles through their bioavailability and bio-distribution of particles (Mohanraj et al., 2006) as well as their biocompatibility have become attractive materials to biosensors and to drug delivery applications as well (Liu et al., 2013).

Table 2-1 History of biosensor development (Setford and Newman, 2005)

Date	Event
1916	First report on the immobilization of proteins: adsorption of invertase on activated charcoal
1922	First glass pH electrode
1956	Invention of the oxygen electrode
1962	First description of a biosensor: an amperometric enzyme electrode for glucose
1969	First potentiometric biosensor: urease immobilized on an ammonia electrode to detect urea
1970	Invention of the ion-selective field-effect transistor (ISFET)
1972-75	First commercial biosensor: Yellow Springs Instruments glucose biosensor
1975	First microbe-based biosensor First immunosensor: ovalbumin on a platinum wire Invention of the pO2/pCO2 optode
1976	First bedside artificial pancreas (Miles)
1980	First fibre optic pH sensor for in vivo blood gases
1982	First fibre optic-based biosensor for glucose
1983	First surface plasmon resonance (SPR) immunosensor
1984	First mediated amperometric biosensor: ferrocene used with glucose oxidase for the detection of glucose
1987	Launch of the MediSense ExacTech blood glucose biosensor
1990	Launch of the Pharmacia BIACore SPR-based biosensor system
1992	i-STAT launches hand-held blood analyser
1996	Glucocard launched
1996	Abbott acquires MediSense for $867 million
1998	Launch of LifeScan FastTake blood glucose biosensor
1998	Merger of Roche and Boehringer Mannheim to form Roche Diagnostics
2001	LifeScan purchases Inverness Medical's glucose testing business for $1.3 billion
2003	i-STAT acquired by Abbott for $392 million
2004	Abbott acquires Therasense for $1.2 billion

2.2. Diabetes

Diabetes mellitus (DM) is a major public health problem affecting more than 425 million adults worldwide (International Diabetes Federation, 2017). DM occurs due to malfunctioning of pancreatic β cells responsible for the production of insulin that controls glucose level in the blood (Schuit et al., 2001). The predictions show that the rate of diabetic people will increase globally by about 58% by 2025 (380 million) and it is the fourth prevalent cause of death (International Diabetes Federation, 2006;

Tirimacco et al., 2010). Other statistics show that about 5% of the world's population (3.9 million people in the UK alone) are living with diabetes (Diabetes UK, 2015). Table 2-2 shows a summary of countries with highest number of estimated cases of DM for 2000 and 2030 (Wild et al., 2004). In addition, government organizations such as Public Health England (PHE) and National Cardiovascular Intelligence Network (NCIVN) have produced prevalence model to target DM and have estimated that 3.8 million people live with the disease. The elevated level of glucose (normal range 4.4–6.6 mM or 80–120 mg/dl) poses serious health problems in diabetic patients and accounts for 4 million deaths worldwide every year (Wild et al., 2004). The human body tightly regulates glucose levels, however, abnormalities in blood sugar levels, hyperglycemia (high) or hypoglycemia (low) result in serious, potentially life-threatening complications (Peters et al., 2015). Damage to the heart, nerves, blood vessels, eyes, and kidneys are results of elevating blood glucose level over time, according to the World Health Organisation (WHO). Therefore, an early diagnosis of blood glucose level could provide management and timely recognition for patients. Frequent self-monitoring of glucose may provide data for optimizing and/or changing insulin uptake in patients (Canadian Diabetes Association, 2008).

Table 2-2 List of countries with highest number of estimated cases of DM for 2000 and 2030 (Wild et al., 2004)

	2000		2030	
Ranking	Country	People with DM (millions)	Country	People with DM (millions)
1	India	31.7	India	79.4
2	China	20.8	China	42.3
3	U.S.	17.7	U.S.	30.3
4	Indonesia	8.4	Indonesia	21.3
5	Japan	6.8	Pakistan	13.9
6	Pakistan	5.2	Brazil	11.3
7	Russian Federation	4.6	Bangladesh	11.1
8	Brazil	4.6	Japan	8.9
9	Italy	4.3	Philippines	7.8
10	Bangladesh	3.2	Egypt	6.7

2.3. Types of diabetes mellitus

The most common DM types are the type-2 diabetes mellitus (T2DM), which is a result of combination of insulin resistance and an insulin secretory defect. T2DM cases represent ~90−95% of all diabetics who are mainly in people with age over 40 years. The second common type is the type-1 diabetes mellitus (T1DM) and it's known as deficiency of the hormone secretion; there are approximately 5−10% patients carry the conditions (Karalliedde and Gnudi, 2016). T1DM targets ages amongst 6 months to young adulthood. This classification with the Arabic numerals, T1DM and T2DM, has been adopted by the WHO and Americans with Disabilities Act (ADA) in 1998 to replace the old classifications, the insulin dependent diabetes mellitus (IDDM) and non-insulin dependent diabetes mellitus (NIDDM) and this became a necessity to avoid any clinical management complications (Raubenheimer, 2010).

Labelling a particular type of diabetes is less important than pathogenesis understanding of the hyperglycemia as well as its efficient treatment. Diagnosing the type of DM could be misleading due to the dependency on present circumstances during the test. For instance, gestational diabetes mellitus (GDM) might develop to hyperglycemia after delivery or may be assigned that the person has T2DM. Alternatively, developing diabetes due to steroids overdose may become normoglycemic if the glucocorticoids, class of steroid hormones works as glucose homeostasis regulator (Dutta and Sharma, 2003). Another study has demonstrated that recurrent episodes of pancreatitis might later improve to diabetes (American Diabetes Association, 2010). Experimental study on sixty mice has shown that combined insulin and steroid hormones restored the hormonal caused by diabetes (Fávaro and Cagnon, 2010). These different findings illustrate the significant complications of diabetes.

2.4. Insulin functions

Insulin is a hormone secreted by the pancreatic β cells and it's the only hormone that has powerful regulation of glucose metabolism in the human body (Rorsman and Braun, 2013). It has been discovered by the two Canadians, the orthopedic surgeon Frederick Banting and the medical student Charles Best on July 30, 1921 (Karamitsos, 2011). Insulin is the key factor of glucose regulation; Figure 2-2 illustrates the general description of the regulation of metabolism by insulin. Various stimuli such as glucose, arginine, sulphonylureas are responsible of secreting insulin from beta cell (Joshi et al., 2007), however, insulin biosynthesis is mostly controlled by glucose metabolism (Poitout et al., 2006). The glucose metabolism stimulates insulin gene transcription and mRNA translation. In vitro studies showed that insulin mRNA stability has been reduced under low glucose and increased under high glucose concentrations (Knopp RH et al., 1985; Welsh et al., 1985).

Other hormones have contributed relatively to control the glucose in the metabolism activity in the human body. Glucagon is a hormone produced by the alpha or islet cells in the pancreas. It has important role and acts as glucose movement but opponent of insulin (Aronoff et al., 2004). To regulate the glucose in the blood, glucagon will signal the liver to break down glycogen and stored starch in order to release them as glucose in the blood stream. The second hormone is amylin, which is released from beta cells along with insulin. It has significant role through decreasing the body's glucagon level, which leads to the reduction of glucose produced in the liver during meals to prevent getting high level of glucose in the blood. In addition, epinephrine, cortisol, and growth hormone separately have certain impacts on the glucose regulation (Diabeteshealth, 2015).

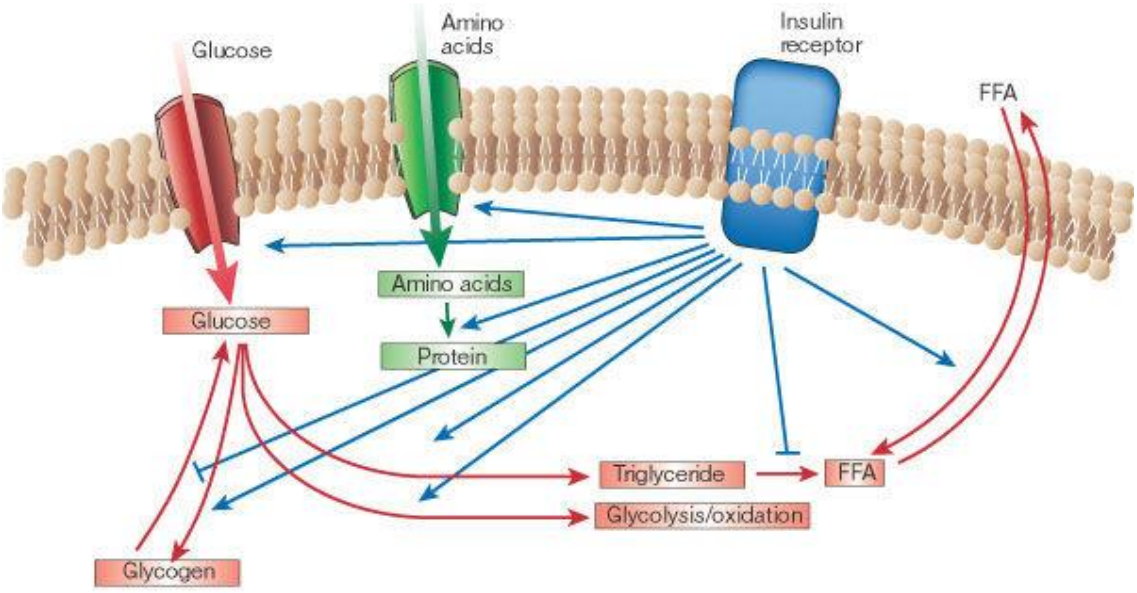

Figure 2-2 The regulation of metabolism by insulin (Rorsman and Braun, 2013)

2.5.Glucometers

A glucometer is a medical device for determining the concentrations of glucose of both hypoglycemic and hyperglycemic disorders. It has significant contribution in reducing the risk of serious secondary clinical complications. In 1941, Anton H. (Tom) Clemens invented the first glucometer at the Ames Division of Miles Laboratories in Elkhart, Indiana USA (Smith, 2013). This electronic blood glucose device was called Ames Reflectance Meter, a diagram of which could be seen in Figure 1-2; it weighs around one kilogram and it could be purchased in the 70's for about $400. Despite the fact that the glucose meter was a successful achievement and an important landmark technology, Ames Reflectance Meter has been used to monitor the glucose level in urine and wasn't treated as a biosensor device until 1965, three years after Clark's glucose biosensor (Clark and Lyons, 1962). Initially, Ames device was made to estimate glucose level in urine, Figure 2-3, and it was based on generating heat. The glucose in the urine was oxidised as a result of heating and the blue cupric sulphate was reduced through changing in colour to determine the glucose level (Clarke and Foster, 2012; Free and Free, 1984). Ames research team have produced the Dextrostix which was the first

blood glucose test strip, however presenting Clark's idea as a commercial biosensor became reality in 1975 by Yellow Springs Instrument Company (YSI) in Ohio, USA (Setford and Newman, 2005). An early version of this YSI commercial biosensor is shown in Figure 2-4.

Figure 2-3 Ames products in 1945, Clinitest and urine glucose test

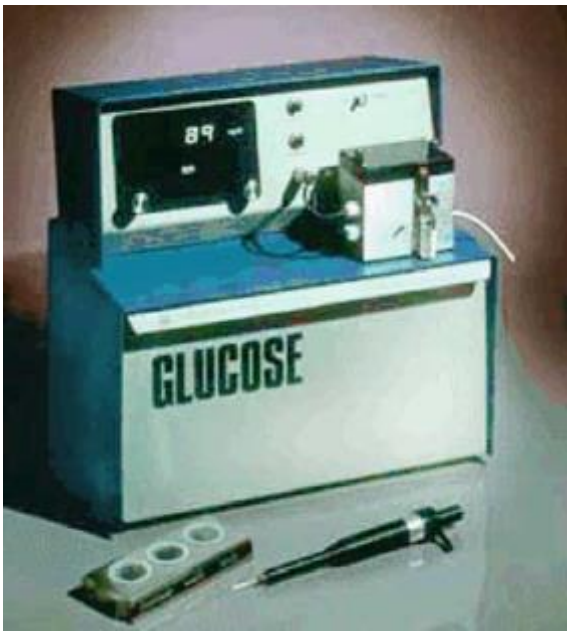

Figure 2-4 An early version of YSI model 23A

As the significant role of the transducer has been described in section 2.1, several potential transduction methods have been developed to measure glucose level in the blood which include optical, piezoelectric, and electrochemical methods (Luong et al., 2008).

2.6. Commercial generations of glucometers

After the invention of Ames Reflectance Meter, various other companies were motivated to develop and produce new types of glucometers. The early 80's were an evolutionary years to the glucose meters to become simple to use, small in size, and more developed, associated with software memory to store and reclaim results. They were barcoded and of good quality, and most importantly, a smaller volume of blood on the strips was required to provide the necessary information. Ames produced two types of glucometers in 1981 and in 1986, Glucometer I that was portable, digital, and light and Glucometer II that was precise and has push-button programming facility, respectively. All these glucometers were not biosensing-based devices until MediSense launched in 1987 the first blood glucose biosensors, the ExacTech, that used an enzyme electrode strip developed at Cranfield and Oxford Universities in the United Kingdom. Between 1991 and 2000, smaller meters have entered the market and patients have become able to monitor their blood sugar level at home.

2.7.Electrochemical biosensor

Since Michael Faraday’s, an English scientist known for his great contribution to the fields of electromagnetism and electrochemistry, and for this invention of electrolysis effects, where the electrolytic magnitude can be expressed through quantitative law. Faraday’s law states that during electrolysis, the liberated element of a mass is directly proportional to the current and time of the process. This law plays crucial role to study the electrochemical reactions between the substrates and analytes, which led to open the

gate for a tremendous growth of research that are applying the electrochemical methods. Chronoamperometry, voltammetry, and electrochemical impedance spectroscopy are the most powerful methods that fundamentally work based on electrochemistry. Electron-transfer rate, background current, and accumulation of analytes are the most significant parameters in these methods. For example, in voltammetry, these parameters are mostly affected by the surface modification of the working electrode, hence, the sensitivity and selectivity could be optimised (Ghadimi et al., 2017).

Electrochemical sensors provide valuable interpretation of the chemical reactions that take place between the electrode and the analyte of interest to produce an electric signal. This electroanalytical technique has been demonstrated to show promising outcome through both qualitative and quantitative analysis to the biological and chemical analytes. Bioelectronics treats the application of the principle of electronics to biology and medicine (Karunakaran et al., 2015). A special type of device of bioelectronics that is used to analyse the biological species is the biosensor. The oxygen electrode invention in 1956 by the father of biosensors, Leland C.Clark Jr., has introduced a new concept to the biosensor filed (Clark, 1956). This successful work has inspired researchers to further develop a variety of biomedical applications (Clark and Lyons, 1962). Clinical, food, agricultural, environmental, biothreat/biowarfare agents have been widely monitored by biosensors (Maduraiveeran et al., 2018; Mercante et al., 2017; Murugaboopathi et al., 2013; Pérez-López and Merkoçi, 2011), however glucose biosensors are still fundamentally dominating the market.

Enzymatic and non-enzymatic detection of glucose research has been carried out due to the urgent need to improve quality of monitoring devices to target diabetes mellitus (Shamsipur et al., 2017; Zhai et al., 2013). As a result, several designs of portable electrochemical devices have been developed and made available for users during the

last two decades (Turner, 2013). Due to the need for reliable devices with high stability, good sensitivity and low cost, bio-interface materials are the key factor for gaining a good performance from the electrochemical reaction that takes place on the material surfaces (Sun et al., 2011). Different materials have been proposed as the interface materials due to their good conductivity (Geim and Novoselov, 2007) and biocompatibility (Kuila et al., 2011) such as graphene, reduced graphene oxide, and carbon nanotubes (Unnikrishnan et al., 2013; Wang et al., 2011). Owing to their remarkable physico/chemical properties, nanomaterials and nanostructures have been widely investigated to play a significant role in terms of developing the sensitivity and selectivity of the electrochemical biosensors through enhancing the surface area and improving enzyme immobilization. High performance glucose detection has been achieved as a result of employing superfine polyaniline nanoflowers grafted onto nanodiamonds for glucose detection (Komathi et al., 2017a). In a review article by Zhu and co-workers it has been reported that thousands of articles written about biosensor studies were published in just two years (Zhu et al., 2015).

2.8. Glucose

Glucose is a sugar that is derived from the digested carbohydrate in the body. Breaking the carbohydrate into glucose is a metabolic process called Glycogenolysis. In addition, glucose or glycogen can be synthesised from non-carbohydrate route through a metabolic pathway process called Gluconeogenesis (Mcmillin, 1990). The glucose then is converted into energy inside the cells after being absorbed into the bloodstream and circulated through the body (Fitzpatrick, 2015). Glucose is the main source of energy in the human body; the brain receives 20% of it (Mergenthaler et al., 2013) however glucose concentration in the body needs to be regulated. The human body tightly regulates glucose levels, however, abnormalities in blood sugar levels hyperglycemia

(high) or hypoglycemia (low) result in serious, potentially life-threatening complications (Peters et al., 2015).

2.9. Glucose oxidase

Glucose oxidase (GOx) is a widely studied enzyme for amperometric glucose detection since its inception from Clark and Lyons in 1962 (Claussen et al., 2012; Wang, 2001), particularly with respect to direct electron transfer (DET). The key factors for an efficient GOx-based sensor is to obtain electron transfer from the active centre, flavin adenine dinucleotide (FAD) enwrapped within thick protein layer, and maintain biological activity, high enzyme loading and avert enzyme leeching. Glucose oxidase (GOx from Aspergillus niger) is a homodimer enzyme, which contains one iron atom and one flavin adenosine dinucleotide cofactor which catalyses the conversion of β-d-glucose to d-glucono-1,5-lactone (Galant et al., 2015). There are three basic enzymes used in sensor applications, which are glucose oxidase, glucose dehydrogenase (GDH), and hexokinase, however GOx is still the most widely used enzyme for glucose detection. Nevertheless there have been several improvements to device structure since the 1960's (Fang et al., 2003). GOx has been widely used in the determination of glucose due to its excellent specificity to the analyte as well as its catalysing activity (Piao et al., 2015; Zebda et al., 2011). Yet, there are still major challenges in the development of GOx-based amperometric biosensors; these are (i) higher loading of enzyme (sensitivity), (ii) stability of immobilized enzyme, and (iii) reduction in high overpotentials (Singh et al., 2009). In general the host matrix and the immobilization strategy employed synergistically influence the performance of the biosensors (Li et al., 2000). Many based-amperometric enzyme biosensors modified materials, such as carbon based nanomaterials, polymers, metal nanoparticles, have been fabricated to enhance the sensor sensitivity (Barsan et al., 2007; Braik et al., 2016; Heller, 1996; Zhu et al., 2014). Thus, GOx has been immobilised successfully onto substrates modified

with different functional materials to fabricate a chemical sensor for the use of monitoring chemical processes and biological systems. Zhu and coworkers have encapsulated the enzyme into alginated hydrogel microspheres for producing implantable glucose biosensors (Zhu et al., 2005)

2.10. Glucose detection

The principle of detecting glucose by glucose meters is based on two essential processes, enzymatic interaction and detection (Tonyushkina and Nichols, 2009). The enzymatic interaction generally occurs between the glucose and one of three typical enzymes: glucose oxidase (GOx), glucose-1-dehydrogenase (GDH), and hexokinase. The latter is the typical enzyme used in the spectrophotometry technique which is applied in the clinical laboratories (Yoo and Lee, 2010). This structure of meters incorporates the enzymes into a biosensor, which basically generates electronic current that is detected by the meter.

Extensive number of research publications in the field of biosensors focusing on device assemblies, immobilisation strategies and applications of new nanomaterials as electrode-surface modifiers have enables this field of research and development to be one of the most attractive fields in science area (Chung et al., 2016; Klonoff et al., 2017; Newman and Turner, 2005; Turner, 2013; Zhu et al., 2015). Glucose biosensors have progressed through three generations of devices until the current developed version of biosensors device has been achieved. They have been classified according to the integration degree of the biorecognition molecule (bioreceptor) to the signal indicator (transducer). The first generation of glucose biosensors relies on oxygen as the main factor in the enzymatic reaction to ensure the catalytic regeneration of the flavin adenine dinucleotide (FAD) centre (Hecht, H.J., Schomburg, D., Kalisz, H. and Schmid, 1993; Wang, 2001). However, there have been two major problems in this type of detection

process, which are the high oxygen dependency and the interference with other species in the blood. An oxygen deficit was noticed in these biosensors to efficiently maintain the glucose oxidation; equation (1) explains the chemical reaction that takes place in this process (Yoo and Lee, 2010):

$$GOx(FADH_2) + O_2 \rightarrow GOx(FAD) + H_2O_2 \qquad (1)$$

The second generation of glucose biosensors has introduced alternative co-substrates to solve the first generation problems (Cass et al., 1984). Electron-accepting mediators are synthesised to improve the electron transfer (Toghill and Compton, 2010). The mediator has however exhibited some drawbacks in its operation, which include the difficulty of maintaining the presence of the mediator near the enzyme on the electrode surface; molecules diffusion and redox interfacing between the mediator and the immobilized enzyme have reduced the stability and performance of this type of glucometers. Ferricyanide and ferrocene have been the most common mediators used in the blood sugar detection (O'Hare, 2014). In order to overcome the complications caused by the mediators, the third generation of glucose biosensors has involved direct electron transfer (DET) between the enzyme and the electrode to solve the problems associated with the previous two generations (Freire et al., 2003; Kempahanumakkagari et al., 2017). The electron transfer activity is associated with or occurs during the catalytic transformation of the substrate to the product (Freire et al., 2003). As long as the third generation biosensors are free from electron mediator or oxygen usage the enzyme is directly immobilised onto the transducer (Higson, 2012). The DET main advantage is eliminating toxic artificial electron mediators and avoiding errors due to variation in the concentration of oxygen in blood samples (Ferri et al., 2011). It is known that the thick protein layer that protects the redox active centre in the enzyme is the biggest challenge of achieving DET (Toghill and Compton, 2010). The use of nano and porous materials

has resulted in a significant increase in the electrode surface area and has thus led to overcoming the challenge produced by the thick protein layer, which surrounds the flavin redox centre. Furthermore, the nanomaterials exhibit electron transfer activity, conductivity, and large surface area, to enhance electrons shuttle from the redox centre of the enzyme to the electrode surface (Davis and Higson, 2009; Wang, 2001). The most significant achievement of the third generation design is the improvement in the device selectivity and sensitivity of these biosensors. Figure 2-5 illustrates the operation of the three generations of glucose biosensors described above (Toghill and Compton, 2010).

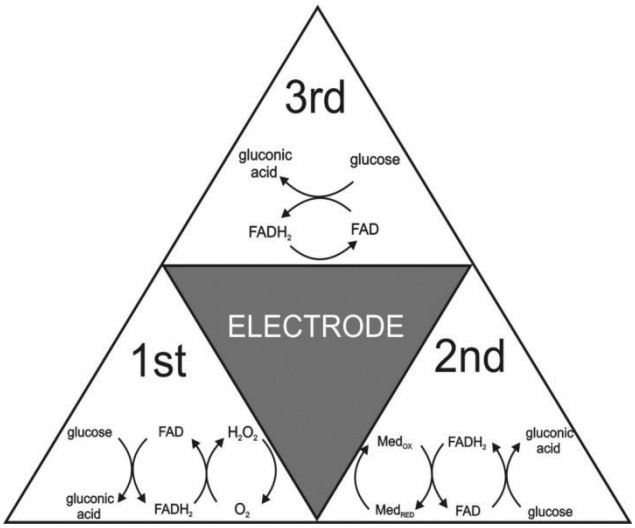

Figure 2-5 The three generation sensors and summary of the enzymatic glucose oxidations

2.10.1. Non-enzymatic glucose detection

Due to the fragility of the enzyme against several environmental factors such as temperature, humidity, pH and chemical reagents, a non-enzymatic glucose biosensor provides a direct oxidation of glucose on the electrode surface (Zhu et al., 2012). The non-enzymatic research and development have been carried out alongside the enzymatic detection for decades. Several composite materials have been employed in the fabrication of efficient platforms for this purpose. Nanostructured materials have received great attention as platforms used for the development of enzymeless glucose

sensors (Jayanth Babu et al. 2017; Hussain et al., 2015; Shan et al., 2010). Noble metal nanoparticles, such as platinum and gold, have been employed as an electrocatalyst in the detection of glucose (Basu and Hazra, 2017; Cherevko and Chung, 2009). For instance, platinum has been used in several sensing forms, such as Pt surfaces modified with Pb in mesoporous platinum (Park et al., 2003). Platinum-Nanotubule arrays have exhibited good performance against glucose concentrations with negligible interference from physiological levels of ascorbic acid and uric acid and good sensitivity of 0.1 μA mM^{-1} cm^{-2} (Yuan et al., 2005). In 2008, Wang and his coworkers have reported 3D nanoporous platinum modified lead (PtPb) bimetallic networks to fabricate non-enzymatic sensors which showed strong and sensitive current response to glucose concentrations (Wang et al., 2008).

Gold nanoparticles (AuNPs) have been employed in non-enzymatic glucose sensors due to the friendly microenvironment for biomolecules and their highly sensitive performance (Fu et al., 2014). Another study has been carried out to fabricate an efficient platform by incorporating organic within inorganic materials; hybrid supramolecular assembly containing polyaniline supported copper (I) ion, which acts as a catalytic centre, has shown good stability for the detection of glucose and sensitivity of 0.47 μA mM^{-1} cm^{-2} (Choudhary et al., 2014).

Zhao and co-workers have demonstrated the electrocatalytic activity of the oxidation of glucose through the fabrication of non-enzymatic sensor based on cubic Cu nanoparticles and multi-walled carbon nanotubes (MWCNTs) (J. Zhao et al., 2013). The sensor has exhibited a response time within 1 second and sensitivity in the range 922 μA mM^{-1} cm^{-2} with a detection range between 0.5–7.5 mM. Figure 2-6 illustrates the reaction that takes place in the non-enzymatic biosensors reaction. Despite the short linear range when compared to the enzymatic sensors, non-enzymatic sensors are simple

in fabrication at low cost, as well as being stable, and reproducible (Mei et al., 2016; Shenoy, 2013).

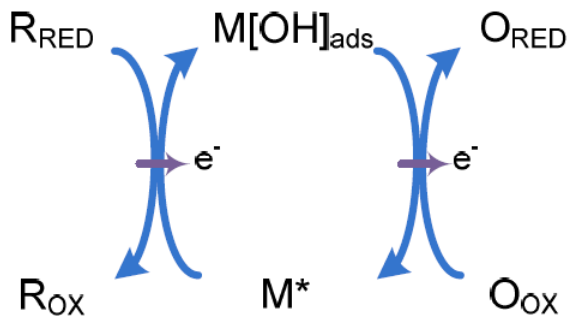

Figure 2-6 Non-enzymatic reaction mechanism, where M* is a reductive metal adsorption, $M[OH]_{ads}$ is an oxidative adsorbed hydroxide radical (Shenoy, 2013)

2.10.2. Enzymatic glucose detections

Glucose oxidase (GOx) is the most widely studied enzyme for amperometric glucose sensing since its inception from Clark and Lyons in 1962 (Claussen et al., 2012; Wang, 2001). The key factors for an efficient GOx-based sensor is to obtain electron transfer from the active centre, flavin adenine dinucleotide (FAD) enwrapped within thick protein layer, maintain biological activity, ensure high enzyme loading and prevent enzyme leeching. Additionally, an ideal biosensor has to be stable for long-term application, and accurate in sensor-to-sensor measurements with significant operational lifetimes. To achieve these factors, large number of substrates as recognition elements have been proposed for GOx immobilization; these include carbon nanotubes (Zhu et al., 2012), graphene (Unnikrishnan et al., 2013), inorganic nanostructures (Wu et al., 2015), conductive polymers (Chen et al., 2006; Garjonyte and Malinauskas, 1999), cellulose acetate (Ren et al., 2009), and polyacrylonitrile (Zheng et al., 2002).

In principle enzyme based biosensors take advantage of catalysing the reactions that are associated with the consumption or generation of detectable compounds such as O_2, CO_2, H_2O_2, NH_3, and H^+ (Nigam and Shukla, 2015). Another aspect that makes enzymes of particular interest in biosensing research is the activation or inhibition of the enzyme activity by the analyte and this can be easily detected by the designated transducers (Patel et al., 2016). There are several techniques applied in the immobilisation of the these biocatalysts on the transducers' interface; these include gel entrapment technology, covalent bonding, and physical adsorption (Mohamad et al., 2015). In addition to the unique properties of enzymes based biosensors, their medical applicability, commercial availability, and ease of enzyme isolation and purification from different sources are factors that make enzymes at the top of priorities of researcher's attention (Laschi et al., 2000). Figure 2-7 illustrates the reaction that takes place between the GOx and the glucose.

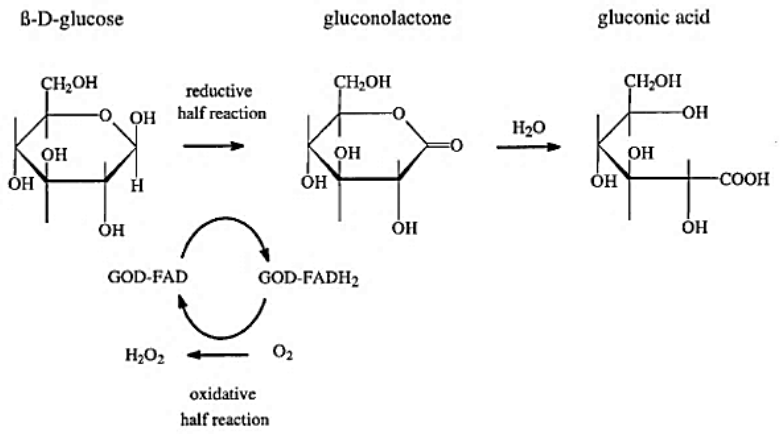

Figure 2-7 Schematic illustration of the reaction catalyzed by glucose oxidase

2.11. Enzymes immobilization

Immobilization of enzymes is an effective technique to produce biosensors, which are robust, reusable, and resistant to environmental changes (Homaei et al., 2013; Kowalewska and Jakubow, 2017). This can be achieved through attachment of the

recognition element such as enzymes, receptors, antibodies, nucleic acids, molecular imprints or lectins into assortment of platforms which are applied in biodetection. Immobilization technologies can be established through linking molecules such as single-wall carbon nanotubes with the enzyme (GOx) (Besteman et al., 2003) or through construction of bioprobes based on silica nanoparticles loaded with GOx (Al-Sagur et al., 2018; Hartmann and Kostrov, 2013). Moreover, GOx immobilisation can be achieved through combining physical entrapment and/or chemical bonding; for instance, the GOx was immobilised on polyethyleneimine (PEI) and carbon nanotubes (CNTs) in order to fabricate a conductive polymer (GOx/PEI/CNT) (Chung et al., 2016). In addition, physical cross-linking by terephthalaldehyde (TPA) which entrap GOx on a substrate based on a polyethyleneimine to produce TPA/[GOx/PEI/CNT] as an enzymatic catalysts to enhance the performance of biofuel cells. Entrapment of GOx and CNT in biologically synthesized silica will introduce simple integration into biodevices in addition to facilitated mediator-free DET coupled to the oxidation of glucose (Ivnitski et al., 2008). Other strategy of immobilisation is through chemical cross-linking; for example, an amperometric GOx biosensor was demonstrated based on single-walled carbon nanotubes (SWCNTs) (Carpani et al., 2008), or through multifunctional conducting hydrogel entrapped with GOx (Al-Sagur et al., 2017) to enhance the performance of glucose biodetection. Furthermore, there have been several other technologies reported in the literature for the immobilization of glucose oxidase on the biosening probe. Among those, adsorption (Spahn and Minteer, 2008), covalent binding (Fu et al., 2011), and affinity immobilization (Sardar et al., 2000).

2.12. Materials used as probing elements in biosensors

2.12.1. Graphene

Graphene is an allotrope of carbon which consist of one atom thick carbon sheet with atoms interconnected together by sp^2 hybridised bonds and arranged in two dimensions (Novoselov et al., 2004). Graphene (sp^2 bonded), carbon nanotubes (CNTs) (sp^2 bonded), diamond (sp^3 bonded), nanodiamonds, and graphite are the well-known other allotropes of carbon. Graphene is a one-atom carbon layer, which is strongly packed in a two-dimensional honeycomb lattice, as depicted in Figure 2-8 (Geim and Novoselov, 2007). Every hundred 2D layers could constitute 3D thin film, making it the thinnest two dimensional carbon materials (Huang et al., 2012). It is a zero-gap semimetal with a small overlap between its valence and conduction bands (Geim and Novoselov, 2007). The theoretical surface area was found to be 2630 m^2/g. (Stoller et al., 2008). Graphene exhibits an excellent thermal stability and conductivity (3000-5000 $Wm^{-1}K^{-1}$) (Balandin et al., 2008; Shinohara et al., 2015). Based on the cell culture experiments, graphene/pegylated graphene oxide are reported to be biocompatible and therefore suitable for biomedical applications (Chen et al., 2008).

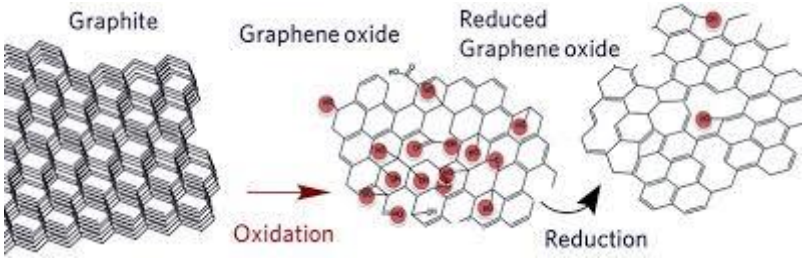

Figure 2-8 The honeycomb lattice form of reduced graphene oxide (Geim and Novoselov, 2007)

The development of graphene-based electrochemical biosensors is found to offer a significantly improved sensitivity to bio-analytes such as glucose. The excellent conductivity of graphene is ascribed to the large surface area; the graphene therefore plays the role as the ‘electron wire’ between the protein or enzyme redox centres and an electrode (Kuila et al., 2011). Due to these properties graphene and its derivatives have an excellent potential in a broad range of industrial and medical applications (Ghibaudi et al., 2017). This interest in graphene has started at 2004 when Novoselvo and Geim were awarded the Nobel Prize in physics in 2010 for their ground-breaking experiments in developing the two-dimensional graphene material (Song et al., 2014). Nowadays, significant volume of research has been dedicated to the study and applications of graphene as well as graphene-based materials. Figure 2-9 shows graphene sheet which is the basic building block for graphitic materials (Geim and Novoselov, 2007); incorporating these nanomaterials into electrochemical biosensors has greatly enhanced the sensitivity (Higson, 2012).

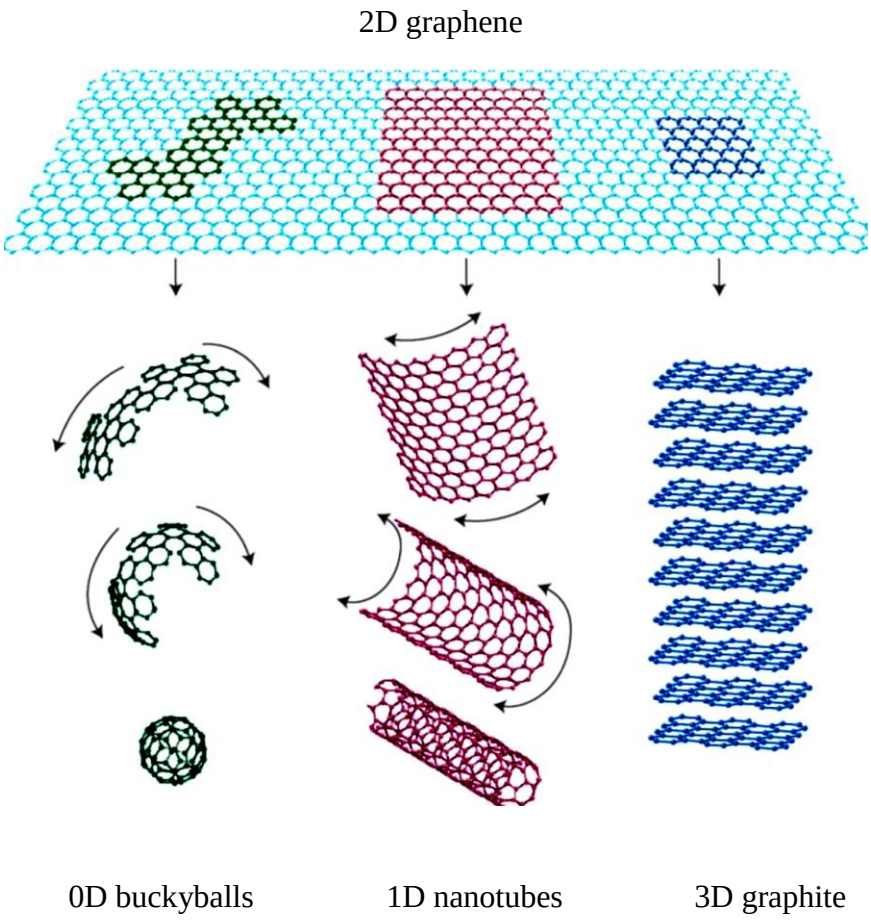

Figure 2-9 Mother of all graphitic forms. Graphene is a 2D building material for carbon materials of all other dimensionalities. It can be wrapped up into 0D buckyballs, rolled into 1D nanotubes or stacked into 3D graphite

2.12.2. Polyaniline

Polyaniline (PANI) is an intrinsic conducting polymer (ICP) which offers potential use in various applications such as corrosion protection, microelectronics (Inzelt et al., 2000), chemical sensing (Maduraiveeran et al., 2018), and biosensing (Xia et al., 2010). Conducting polymers (CPs) were discovered by Shirakawa, Heeger and MacDiarmid in the 1970s (Shirakawa et al., 1977) for which they awarded the Nobel Prize in Chemistry in 2000 (Nguyen and Yoon, 2016). There are however a large variety of other CPs, including, polypyrrole (PPy), polythiophene (PT), poly(3,4-ethylenedioxythiophene) (PEDOT), and other PT derivatives, which have been widely investigated for similar

types of applications (Nguyen and Yoon, 2016). PANI has attracted most interests due the wide range of conductivity, low cost and ease of synthesis (Lee et al., 2010).

In addition to its conductivity, which ranges from the insulating to the metallic regime, PANI has magnificent features, such as its redox tunability and stability (Lee et al., 2010; Y. Wang et al., 2014). There are several factors affecting the conductivity of any polymer such as oxidation state, molecular weight, temperature, humidity, counter ion doping, and proton doping (K. P. Lee et al., 2010; Quy, 2011). In general, PANI consists of oxidized and reduced units; the former contains one benzenoid ring, one quinoid ring, and two imine groups whereas the latter contains two benzenoid rings with two amine groups. This is an important difference in the ratio of these units within the polymer (Stejskal and Gilbert, 2006) which leads to provide a wide range of different oxidation states for PANI. For instance, the partially oxidised (emeraldine E) form is the most conductive oxidation states in comparison with the fully reduced (leucoemeraldine LE) form or the other form which is fully oxidised (pernigraniline); Figure 2-10 illustrates the different forms and units of PANI.

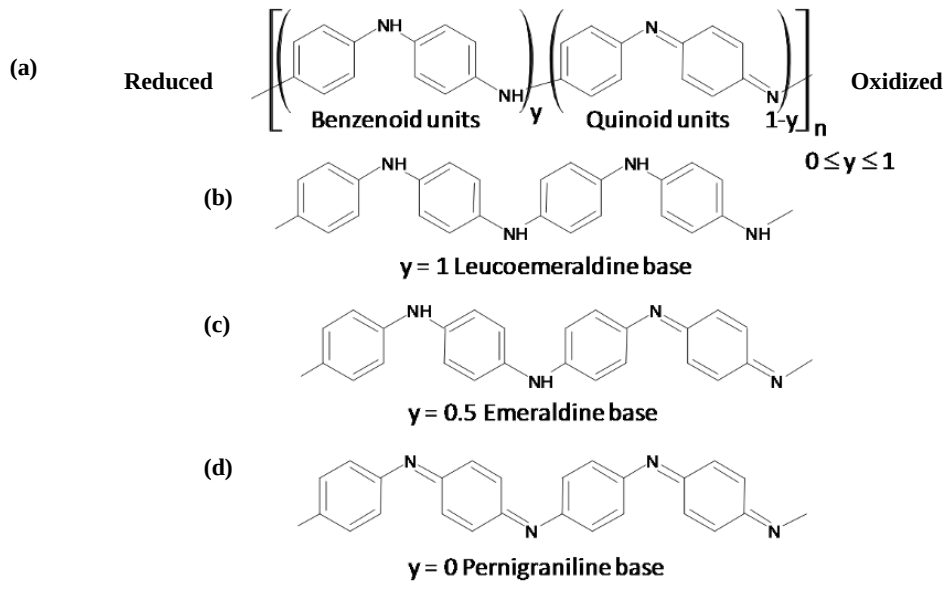

Figure 2-10 Schematic representation of PANI and its common forms

PANI based conducting hydrogels that combine the properties of both conducting polymers and hydrogels mechanical properties have shown potential application in the fields of electrochemical energy storage, metal corrosion resistance and biological and chemical sensors (Guo et al., 2015; Wang et al., 2014; Nath et al., 2014; Ding et al., 2015). The inbuilt properties of hydrogels such as its good biocompatibility and permeability to water-soluble biochemicals in combination with the excellent electronic properties of PANI would provide an ideal matrix for enzyme immobilization and preserving their bioactivity for electrochemical detection. Moreover, the 3D conducting polymer network offers sufficient charge collection capacity to the hydrogel. Overall the synthetic method can be easily manipulated to construct intricately patterned electrodes at low cost (Heller, 2006; Åsberg and Inganäs, 2003). Pan and coworkers have reported the synthesis of hierarchical nanostructured PANI hydrogel, in which phytic acid was used as the gelator and dopant to directly form a conducting polymer network (Pan et al., 2012).

Metal nanoparticles have been combined with PANI to develop the surface area and the catalytic activity of the composite. For example, AU@PANI composite films have been introduced to improve the sensing technology for melamine detection (Rao et al., 2017). Therefore nanostructured polyaniline (PANI) became very popular and important conducting polymer (CP) due to its tunable electrical conductivity and capability of enhancing the conductivity performance when associated with other inorganic species, such as metals (Ag, Au, and Pd), metal oxides (NiO, Cu_2O, ZnO, Fe_2O_3, and MnO_3) and chalcogenides(Bi_2S_3, CdSe, CdS, and CdTe) (Nguyen and Yoon, 2016; Tang et al., 2011).

PANI-based platforms have been widely used and for different purposes due to their potential technological applications; for instance, carbonized PANI has been employed

as a conductive glue and connector of carbon nanotubes (CNTs) to build 3D network in order to enhance the enzymatic biofuel cell performance (Kang et al., 2018).

Hybridisation or incorporation of PANI with silica nanoparticles has improved the mechanical and thermal properties of probes used in biodetection (Azioune et al., 2004). This arises from the flexibility, ductility, and processability of the PANI as well as the rigidity, high thermal stability, and the larger surface area of the silica nanoparticles (Ribeiro et al., 2014). Therefore these hybrids have received much attention due to their applications in adhesion, protective coatings, and biomaterials as drug delivery vehicles (Zou et al., 2008a). Furthermore, silica/PANI nanocomposites exhibit a supercapacitive performance and superior stability during the electrochemical reaction at the facile surface of silica/PANI platform (Wei et al., 2013a). However, loading an electrocatalysts such as phthalocyanines will provide efficient electron mediator for biosensing devices (Fernandes et al., 2011); these electrocatalysts have been used to accelerate the electrochemical process on the electrode surfaces (Appleby, 1971).

2.12.3. Hydrogels

Gels and hydrogels are used alternately by food and biomaterials scientists to define polymeric cross-linked network structures. Scientists define the term gels as a significantly dilute cross-linked system and they are basically categorised as weak or strong depending on their flow behaviour in steady-state. Gels find wide use in industrial applications but mainly in the food industry where it is edible and mostly used for gelling polysaccharides (i.e. hydrocolloids) (González-Pérez and Arellano, 2009; Gulrez et al., 2011). Hydrogels are physically or chemically three-dimensional cross-linked, insoluble hydrophilic polymeric network with the capability to swell in the presence of aqueous solution or biological fluids (Barakat and Sahiner, 2008; Sezgin

and Balkaya, 2015). Naturally, hydrogels can be found in tissue, tendons, stomach, the intestines, the lungs, and blood vessels (Kim, 1999).

In the past 50 years hydrogels have become an important subject to the biomaterials field. Several characteristics enable hydrogels to be used in biomedical applications such as biosensors, drug delivery systems, tourniquets, and so on (Ahmed, 2015; Guiseppi-Elie, 2010; Ulijn et al., 2007). The significant features that make the characteristics unique are the swelling capacity of the low molecular weight biomaterials that have high permeability, and low interfacial tension which decreases the adsorption of protein and therefore biofouling and cell adhesion (Guiseppi-Elie, 2010; Li et al., 2004; Ulijn et al., 2007). Furthermore the hydrophilic functional group, which is linked to the backbone, enables the hydrogels to absorb water, however the cross-links between network chains are responsible for the resistance of dissolution (Ahmed, 2015). Hydrogels are synthesized to cover large variety of applications (Gulrez et al., 2011). What makes the hydrogel unique is their electrochemical properties; redox hydrogels provide 3D electron conducting matrix in addition to the high water content, and that will enable the water soluble biochemicals to diffuse towards a certain enzyme which offers appropriate environment that leads to improve the stability of the sensing platform (Etchenique and Calvo, 1997).

The mechanism through which that gels and hydrogels are formed is called gelation where the macromolecular chains link together and that leads to gradually forming polymers depending on the structure of the starting material; Figure 2-11 elucidates the different types of gelation mechanisms.

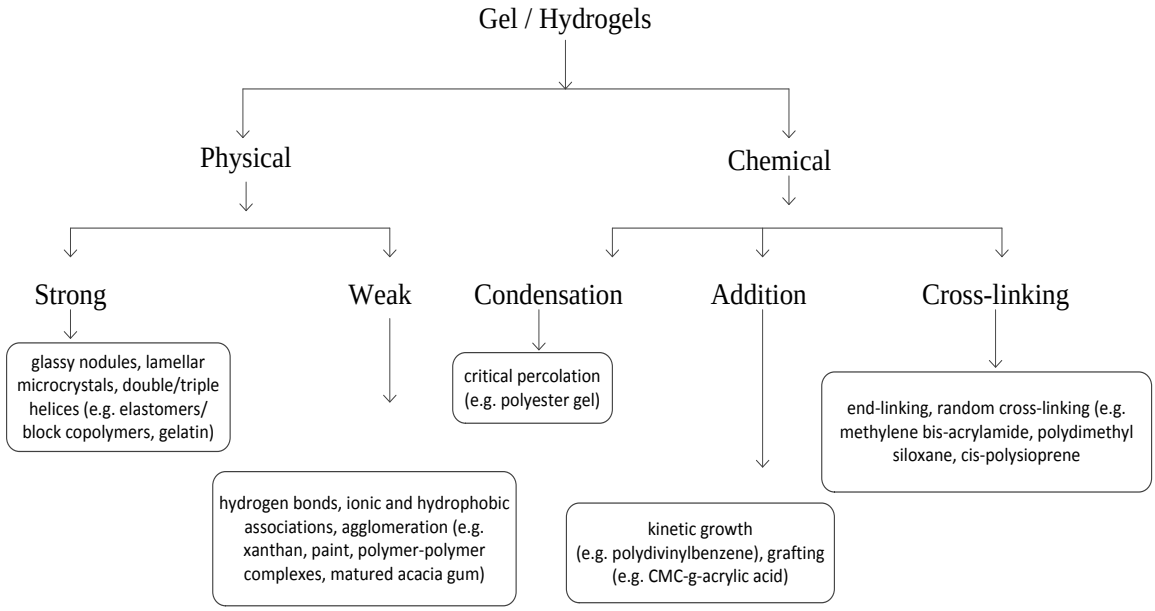

Figure 2-11 Classification of gelation mechanisms (Gulrez et al., 2011)

2.12.4. Silica nanoparticles

Nanoparticles have been employed widely to develop the performance of probing element in biosensors due to their synergetic impact amongst conductivity, catalytic activity, and biocompatibility (Zhu et al., 2015). Different nanostructured materials such as silica NPs, gold NPs and carbon nanotubes have emerged as promising inorganic alternative materials to organic materials to be used in applications as in drug delivery systems as well as in several other biomedical applications (Tang and Cheng, 2013). Due to their unique chemical and physical properties as well as the tunability of the shape and size of the particles (Mamaeva et al., 2013), silica NPs have been widely used in food industry and biomedical engineering/medicine (Jaganathan and Godin, 2012). Several electrodes modifying materials such as carbon based nanomaterials, polymers, metal nanoparticles and silica nanostructures or their hybrids have been widely employed for GOx immobilization (Zhu et al., 2014). Among them silica being inert, non-toxic, with tunable porosity and inexpensive to synthesize will suit for this potential application (He et al., 2010; Y. Zhao et al., 2009). Further, silica imparts

biocompatibility and hydrophilicity for the immobilized enzyme and prevents enzyme leakage (Jaganathan and Godin, 2012). However, mere higher loading of GOx alone is not enough when the immobilized enzyme needs to show higher activity too. The relatively poor conductivity of pristine silica makes it difficult to use in practical electrochemical biosensor applications (Fang et al., 2015). Therefore grafting organic to inorganic materials is the key to develop electron transfer capability, bioactivity, accessibility of analytes, and the large surface area (Gopalan et al., 2009). Harnessing these characteristics, silica-based organic-inorganics structures as new hybrid nanocomposites provide significant enhancement in the performance of electrochemical biosensors. Amperometric glucose sensor, core-shell Fe_3O_4@silica@Au hybrid NPs exhibited a broad linear range, good selectivity and stability (A. J. Wang et al., 2012). Briefly, under solvothermal conditions, Fe_3O_4 was synthesized then silica and gold (Au) were functionalised successively to construct glucose sensor. Recently, a highly sensitive electrochemical bioprobe have been fabricated through combined silica-PANI conducting nanobeads and a high precision sensor for measuring glucose was achieved (Al-Sagur et al., 2018).

Inorganic nanoparticles-based biosensors have been introduced for the first time in 2000 by Bharathi and Lev through encapsulation of GOx in a copolymer comprising Prussian Blue (PB) (Bharathi and Lev, 2000). Significant improvement in this field has been achieved through the early trials of using nanostructured materials to obtain excellent electrocatalytic properties and large surface area which is vital to the electrochemical sensors; this has been proven by Peng and co-workers through synthesising three-dimensional nanoporous Pt networks (Peng et al., 2004).

NPs have enhanced the sensing functionality of biosensors through increasing the electron transfer activity between the platforms and electrodes surface. Thus,

nanostructured-based sensors are promising to have the potential to dramatically develop continuous glucose monitoring (CGM) capabilities and improve patient quality of life (Cash and Clark, 2010).

2.12.5. Phthalocyanines

Phthalocyanines (Pcs) are a fascinating group of synthetic analogues of the naturally occurring porphyrins such as chlorophyll or hemoglobin. An extensive number of phthalocyanine molecules with different substituents and with almost every metal atom as the central atom have been synthesized and extensively studied for a broad range of applications as in photodynamic therapy, catalysis, chemical sensors and so on (Leznoff and Lever, 1993; Simic-Glavaski, 1989).

Pcs were invented in 1907 by accident when Braun and Tschernic isolated a blue compound as part of preparing orthocyanobenzamide but identified later as the metal-free phthalocyanine (Braun and Tcherniac, 1907). In 1928, preparation of phthalimide was carried out at Scottish Dyes Ltd. but the team of scientists observed a greenish compound to be defined later iron phthalocyanine. Thereafter, Scottish Dyes Ltd patented copper phthalocyanine in 1929 (Lomax, 2005). Pcs have been typically used as dyes and catalysts, however, they have recently become important photosensitising agents for photodynamic therapy (PDT) as tumor-targeting material (Carrión, 2018). Water-soluble zinc phthalocyanine has been applied to assess the cytotoxic effect of mesothelioma cells (Saydan et al., 2009), while another study has reported the use of 15 selected phthalocyanine derivatives to be applied as antimicrobial active agent (Kalhotka et al., 2012; Ryskova et al., 2012). Pcs have also been used for industrial purposes as in solar cell development (Nouri et al., 2018) and for polyphenol determination in tea industry (Maximino et al., 2016).

Metallophthalocyanines (MPcs) are described as electron mediators in electrochemical sensors due to their excellent electrocatalytic activity and chemical stability (Martin et al., 2016). For example, the double-decker rare-earth lutetium bisphthalocyanine found interest as material for sensing applications due to its physiochemical properties such as intrinsic semiconductivity and their rich electrochemical properties (De Saja and Rodríguez-Méndez, 2005; Kadish et al., 2001). Fernandes et al. have reported the immobilisation of $LuPc_2$ in biomimetic sensors for phenol detection where they have confirmed the catalytic activity of $LuPc_2$ and proved suitability of the sensor to detect polyphenols in real samples (Fernandes et al., 2011).

MPcs show good electrocatalysis in the oxidation of several industrially and biologically important molecules (Barrera et al., 2006; Pereira-Rodrigues et al., 2002). d-block MPc (Fe and Co) complexes with macrocyclic extended π-systems allowing them to undergo fast redox processes with minimal re-organisational energies. They have been intensively studied as redox mediators for glucose enzyme electrodes (Hart and Wring, 1997; Wang et al., 2005). GOx catalyses the oxidation of glucose, in which the natural electron-acceptor (oxygen) is converted to H_2O_2. Modification of the electrode surface with highly biocompatible MPc will reduce the voltage requirement for H_2O_2 oxidation (Ozoemena et al., 2005). The group of Arrieta et al. have demonstrated that phthalocyanine based electrodes show rich electrochemical response when they were exposed to flavours (Arrieta et al., 2003). They fabricated an "electronic tongue" device that shows the ability to distinguish the five basic types of taste detected by the human tongue. One of the most key studies using Lanthanides in biology and medical diagnosis was by Bünzli (Bünzli, 2016). He found that Lanthanide luminescent bioprobes (LLBs) have significantly contributed to this field due to their little or no photobleaching and high sensitivity; they have become essential tool in biosciences. Another study stated that due to their stability (redox stability and

photostability), and luminescent properties, lanthanides have led to numerous applicatiuons as cytotoxic agents and inhibitors in biosensing, bioimaging, photodynamic therapy, radiation therapy, and drug/gene delivery (Teo et al., 2016). An electronic tongue based on voltammetric sensor have demonstrated that the electrocatalytic effect of $LuPc_2$ towards glucose is stronger than other non lanthanaide metals such as Zn and Cu (Medina-Plaza et al., 2014).

However lanthanides were known as “rare earth” elements existed in very small amount in the earth's crust, they are today relatively abundant and found as oxides and fluorides (Teo et al., 2016). Among numerous metallophthalocyanine (MPc) families, double-decker lanthanide derivatives (see Figure 2-12) such as lutetium phthalocyanine ($LuPc_2$), Dysprosium phthalocyanine ($DyPc_2$), Europium phthalocyanine ($EuPc_2$), Gadolinium phthalocyanine ($GdPc_2$), Neodymium phthalocyanine ($NdPc_2$), and Samarium phthalocyanine ($SmPc_2$) attract interest due to their high intrinsic conductivity and electrochemical properties (Basova et al., 2008). The electrochromic behaviour of lanthanide phthalocyanine films has been used for the detection of nicotinamide adenine dinucleotide (Galanin and Shaposhnikov, 2012a; Pal et al., 2011). Synthesis and spectral properties of lanthanide double-decker complexes, with tetrabenzoporphyrin and phthalocyanine have also been studied. In the biosensing domain, MPcs as catalysers have significantly developed the biosensing technology through reducing the anodic potential. Thus, integrating bioelectocatalytic electrodes have overcome the required high voltage by enhancing the transfer electrode activity which led to improve the sensitivity of the biosensor (Apetrei et al., 2011; Chaiyo et al., 2018; Fang et al., 2003; Wang et al., 2005).

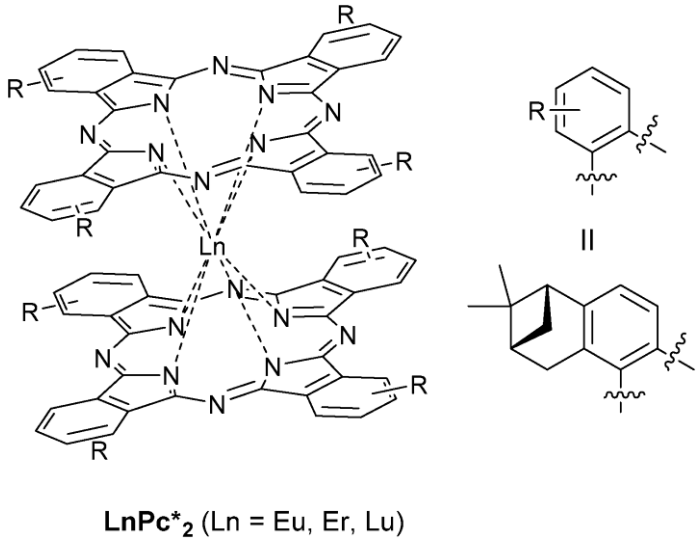

Figure 2-12 Molecular structure of lanthanide phthalocyanines

Chapter: 3 Experimental Methods and Technologies

Chapter Overview

This chapter described in sufficient details the experimental procedures and measurement techniques used to characterise the materials and analytes individually. At the start of the chapter, fundamental electrochemical processes will be presented to illustrate the theoretical vision of the applied electrochemical methods. The rest of the chapter will focus on describing the theory of the instruments employed in the measurements applied in this work.

3.1. Fundamental Electrochemical Processes

There are three principle mechanisms that explain the movement of reacted species which take place on the surface of electrodes; those mechanisms are responsible for electrons transfer from the analyte to the electrode surface (Tobias et al., 1952). The first mechanism is 'diffusion', whereby the molecules move from high to low concentration. The diffusion of chemical species can be described by Fick's first law.

$$J_i = -D_i(\partial C_i/\partial x) \qquad (1)$$

where J_i is the rate of diffusion, $\partial C_i/\partial x$ is the concentration gradient and D_i is the diffusion coefficient for particle *i*.

The transport of charged species under the influence of an electric field represents the second mechanism, which is termed as 'migration'. For instance, anions will be attracted to the electrode surface if it was positive while the cations will be repelled towards the bulk solution and vice versa. 'Convection' is the third principle mechanism which describes the transport of species by hydrodynamic transport mechanisms, such as natural thermal motion and/or stirring (Tobias et al., 1952).

Figure 3-1 illustrates the diffusion and convection mechanisms as described above.

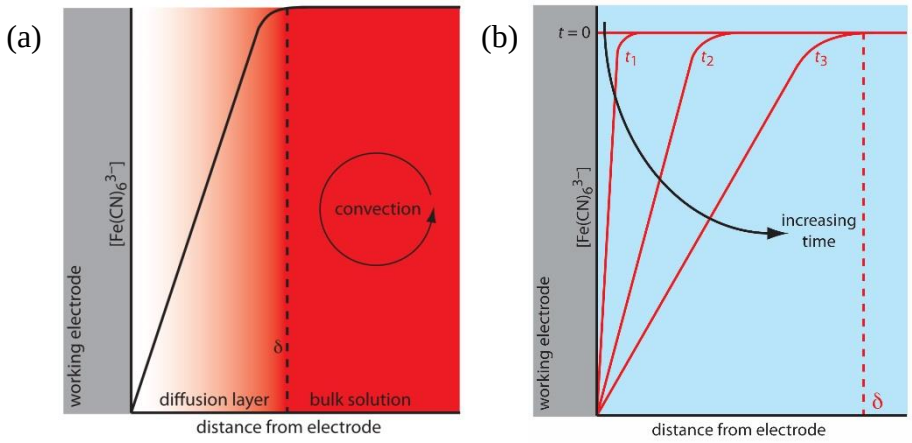

Figure 3-1 (a) the bulk solution as separated from the working electrode via Nernst diffusion layer (δ), (b) the concentration gradient for the electrochemical species (Harvey, 2000)

The number of transported ions at an electrochemical cell can be calculated using the following equation (Sanger, 2017):

$$Trasport\ number\ of\ ion = \frac{I_{ion}}{I} \qquad (2)$$

where I_{ion} is the current carried by the ions while I is the total current.

Redox species in solution travel from the electrode surface to the solution and vice versa through the half-cell reaction which can be either oxidation (anode) or reduction (cathode) reaction.

The electrode potential of reaction (E) is called Nernst potential, which can be obtained from the following equation:

$$E = E^{o\prime} - \frac{RT}{nF}\ln Q \qquad (3)$$

where $E^{o\prime}$ is called the formal potential, R is the universal gas constant (8.3145 J/mol K), T is the absolute temperature, n is the number of electrons transferred in the reaction, F is Faraday's constant (96485 C mol^{-1}) and Q is the reaction quotient, which is a function of the concentration at any chemical reaction.

Nernst equation (Bard and Faulkner, 2001) can be written as,

$$E = E^{o\prime} + \frac{RT}{nF}\ln\frac{C_{ox}}{C_{Red}} \qquad (4)$$

where C_{ox} and C_{Red} represent the bulk concentration of oxidized and reduced species. Typical reaction on the electrode surfaces is illustrated in Figure 3-2.

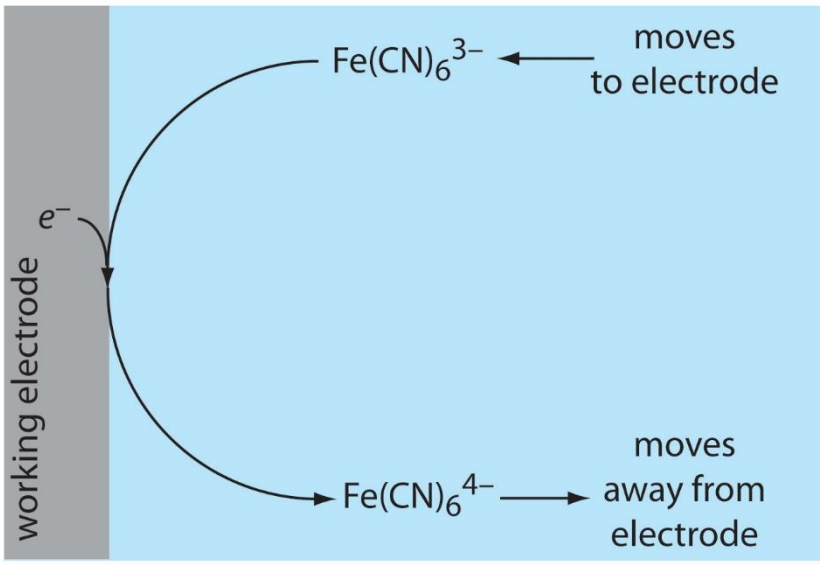

Figure 3-2 Typical reaction of analyte such as ferro-ferricyanides that takes place on the electrode surface (Harvey, 2000)

The fundamental electrochemical processes at an electrode surface can be classified by two processes, capacitive and Faradaic, which are described in the two following sections (Skoog et al., 1988):

3.2. Capacitive Process

Capacitive process is produced through a potential variation or an adsorption process that leads to discharge on the electrode surface. The capacitive current represents charge transfer and it doesn't involve any chemical reactions. It is called non-faradaic or double layer current and it causes removal of electrical charges from the electrode and near the electrode in the electrolyte solution (Conway, 1999).

3.3. Faradaic Process

The current of faradaic process represents the electrochemical reactions at the electrode surface where the nature of species is deduced at the position of the peak potential. These reactions are governed by Faraday's law (defined in section 2.7). In general,

faradaic processes represent electron transfer reactions; this electron transfer takes place between the electrode and the solid or liquid electrolyte in contact with the electrode surface, which donates or accepts electrons. There are two types of electrochemical methods; those are potentiometric and voltammetric methods (Skoog et al., 1988). The potentiometric method does not involve a current or the current flow is negligible and the potential is at equilibrium, while current is measured as a function of applied potential in the voltammetric method. The aim of the potentiometric method is to maintain a constant potential difference between a working electrode (WE) and a reference electrode (RE) (Kissinger and Heineman, 1996). Further illustration of the three-electrode system is shown in Figure 3-3, where the WE is connected to the excitation potential and adjusted with respect to the RE; the current response of the system will be measured between the WE and the counter electrode (CE).

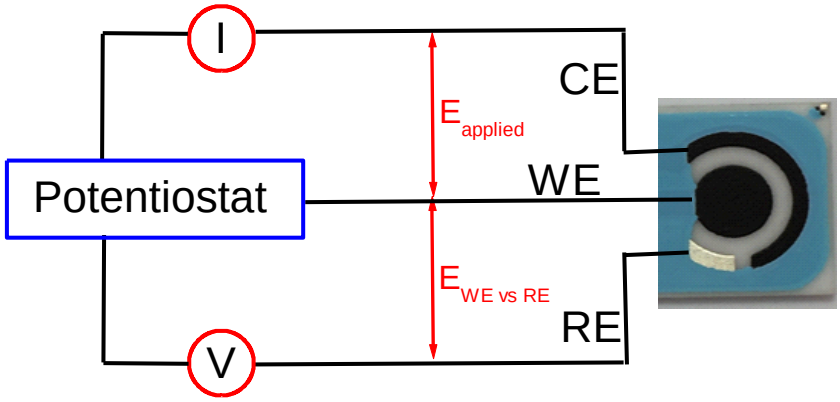

Figure 3-3 The three-electrode system in electrochemical cell with counter (CE), working (WE), and reference (RE) electrodes.

3.4. Cyclic Voltammetry

Cyclic voltammetry (CV) is a widely utilized electrochemical technique that includes studying the electrode processes and redox reactions (Bard and Faulkner, 2001). It is a sensitive technique for the investigation of chemical kinetics (Mundinamani and

Rabinal, 2014). The current is measured as a function of applied voltage and the current contains quantitative mechanistic information. CV system design is simple and economic; three electrodes are preferable for this electrochemical system where the working electrode is measured against a reference electrode that maintains a constant potential. The counter electrode's role is essentially to ensure that current does not run through the reference electrode. The reaction among the system components generates reduction and oxidation peaks when a current is swept in (Rudolph et al., 1994).

The experiment of cyclic voltammetry starts when a voltage is applied to the electrode and swept from V1 to V2 as a triangular waveform as shown in Figure 3-4(a); it is shown that the scan is reversed when the voltage reaches V2. A typical cyclic voltammogram is generated after the current is measured as shown in Figure 3-4 (b).

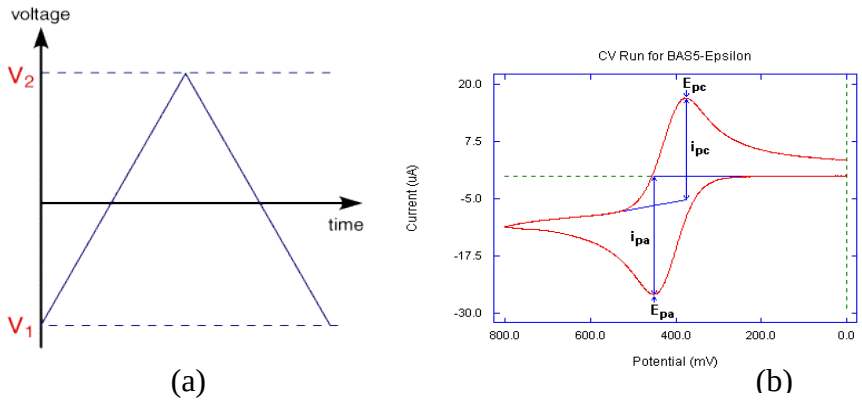

(a) (b)

Figure 3-4 (a) Cyclic voltammetry waveform and (b) current versus potential response for reversible and irreversible electron transfer reactions(Bard and Faulkner, 2001)

From Figure 3-4 (b), E_p^a and E_p^c represent the anode and cathode potentials while i_p^a and i_p^c represent the anode and cathode currents, respectively. The current on both forward and reverse sweep of the redox peaks will have a ratio of one (Bard and Faulkner, 2001). In addition the scan rate has a significant effect on the oxidation and reduction peaks. The redox peak voltage remains in the same position even though the current increases (Scott, 2016). A typical cyclic voltammetry is shown in Figure 3-5.

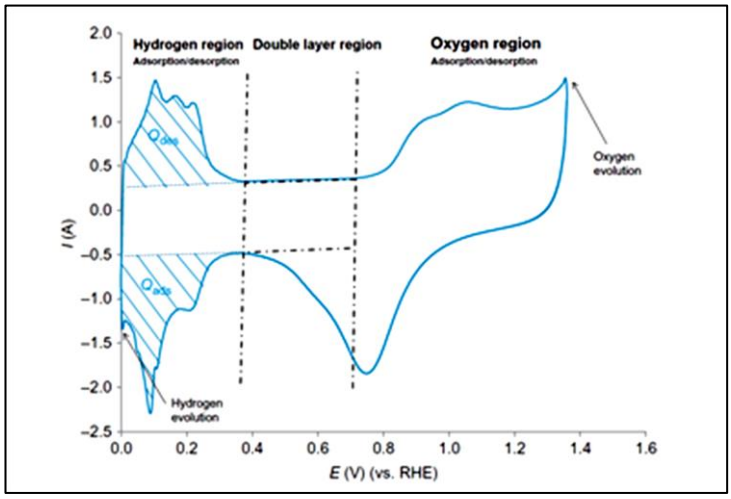

Figure 3-5 Typical cyclic voltammetry diagram (Scott, 2016)

3.5. Chronoamperometry

Chronoamperometry (CA) is a very powerful method for determining diffusion coefficients and on study the kinetics as well as mechanisms of electrochemical reactions (Bard and Faulkner, 2001). When the potential is stepped up in the working electrode it will produce a current from Faradaic processes, which have occurred on the electrode, and that current is measured as a function of time. CA can generate high charging currents that decays exponentially with time which is equivalent to any RC circuit, while the ratio of the peaks of reduction current versus oxidation current in CV give limited information about the electrolyzed species identity (Kissinger and Heineman, 1996; Skoog et al., 1988). The Faradaic current represents the current component of interest and it decays as described by Cottrell equation (Kissinger and Heineman, 1996):

$$i = \frac{nFAD^{0.5}C_b}{(\pi t)^{0.5}} \qquad (5)$$

where D is the diffusion coefficient, F is Faraday's constant (96485 C mol^{-1}), A is the electrode area (cm^2), C_b is the bulk concentration of the electroactive species

($mol\ cm^{-3}$), *n* is the number of electrons involved in the electrode reaction, and *t* is the time (s).

Faradaic current is generated as a result of electron transfer process, which is the movement of an electron from the surface of the working electrode to a species in solution or vice versa. Figure 3-6 illustrates a typical potential excitation waveform and the yield current response (Scott, 2016).

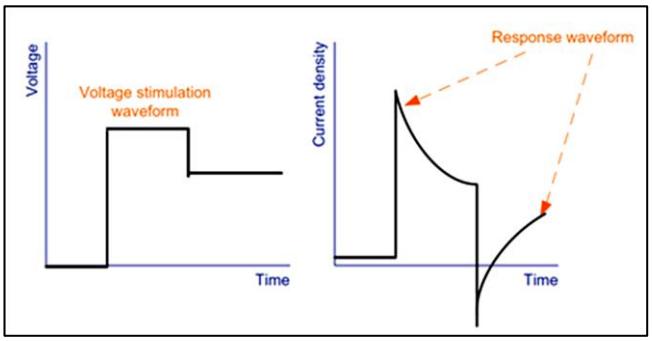

Figure 3-6 Waveform and response for chronoamperometry (Scott, 2016)

3.6. µStat 8000

A potentiostat is a precise electronic instrument which is used to control the potentials and currents measurement capabilities in an electrochemical cell for most electroanalytical techniques (Dryden and Wheeler, 2015). µStat 8000 is a portable multi Potentiostat/Galvanostat which is employed in voltammetric, amperometric or potentiometric electrochemical biosensing applications (DropSens, 2011). µStat 8000 has 8 independent electrochemical nodes/channels which are controlled by a microprocessor; each channel is able to apply potential or current to the electrodes in order to measure the current of potential response. This instrument, (a photograph is shown in figure 3-7), is the world first portable multi Potentiostat/Galvanostat which was produced by DropSens (Spain). The instrument is controlled by a PC with DropView 8400 software. µStat 8000 provides the possibility to be applied using different measurements techniques as illustrated in table 3-1.

Figure 3-7 µStat 8000 potentiostat/galvanostat (DropSens, 2011)

Table 3-1 Possible measuement techniques applied using µStat8000

Voltammetric techniques	Potentiometric techniques:
Linear Sweep Voltammetry LSV	Linear Sweep Potentiometry LSP
Cyclic voltammetry CV	Cyclic Potentiometry CP
Square Wave Voltammetry SWV	Potentiometric Detection POT
Differential Pulse Voltammetry DPV	Zero Current Potentiommetry (OCP) ZCP
Normal Pulse Voltammetry NPV	Fast Potentiometry FP
Differential Normal Pulse Voltammetry NDP	Potentiometric Stripping Analysis (faradaic) PSAF
Alternating Current Voltammetry ACV	Potentiometric Stripping Analysis (galvanostatic) PSAG
Linear Polarization Resistance LPR	
Amperometric techniques:	
Amperometric Detection AD	
Zero Resistance Amperometry ZRA	Pulsed Amperometric Detection PAD
Fast Amperometry FA	Coulometric Detection COUL

3.7. Screen-printed carbon electrodes

Screen-Printed carbon electrodes (SPCEs) are disposable electrodes supplied by DropSense (DRP-C110) with 4 mm diameter carbon working electrodes. The auxiliary and reference electrodes are carbon and silver, respectively, while the träger (carrier) is ceramic as shown in Figure 3-8. In this work, SPCEs have been modified with different sensing platforms, which have been characterised using electrochemical methods in order to investigate their potential for applications in biosensors as in striper for the glucose detection. Toxic component detector in water (Chouler et al., 2018) and antibiotic (thiamphenicol) regulator in milk (Muhammad et al., 2018) are other applications where SPCEs are employed. Figure 3-9 shows the experimental setup where the µStat 8000 was applied using the modified SPCEs under investigation.

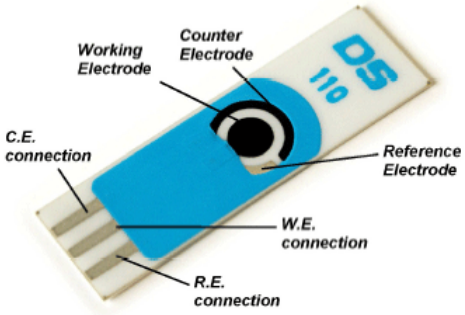

Figure 3-8 Screen-printed carbon electrode (DropSens, 2008)

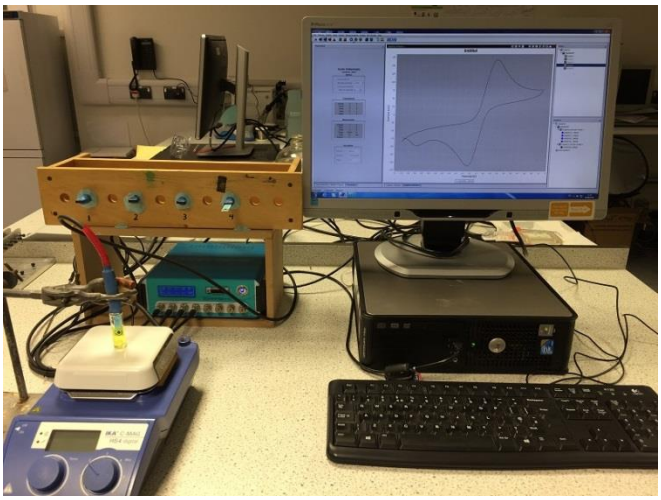

(a)

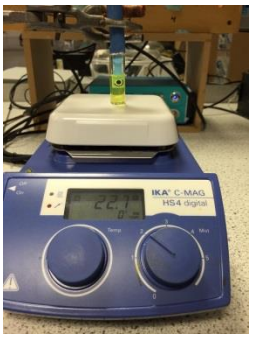

(b)

(c)

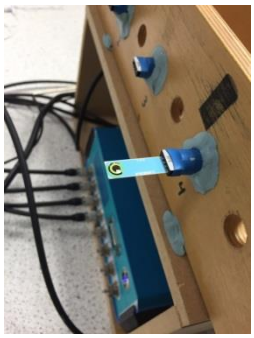

(d)

Figure 3-9 Laboratory setup of the electrochemical experiment for the CV and AD methods, a) the whole experiment setup where the µStat 8000 connected to a PC, b) the investigated sample with the analyte under stirring, c) a blank of SPCE, d) the dropping style of the electrolyte on the modified electrode.

3.8. Electrochemical Impedance Spectroscopy

In 1880s, the concept of electrical impedance was introduced for the first time by Oliver Heaviside and then was developed to be in vector diagrams and complex numbers representation by A. E. Kennelly and C. P. Steinmetz (Lvovich, 2012). Since then the electrical impedance has become attractive method to the researcher in the field of electrochemistry. For instance, the double-layer theory that was developed by Frumkin and Grahame (Frumkin, 1967; Grahame, 1947) led also to the development of equivalent circuit (EC). The EC was presented as the modelling package for the electrochemical impedance spectroscopy (EIS). Figure 3-10 illustrates the electrochemical interface parameters and the equivalent circuit of the common model of

Randles cell which is composed of a resistor and capacitor connected in parallel and connected in series with another resistor (Randles, 1947). Randles proposed that the reaction into the electrochemical cell is due to diffusion, migration, and convection. This achievement has represented a significant achievement in serving to calculate the rate constant from measuring the magnitudes of the components (capacitance and the resistance) of the circuit (Randles, 1947). Understanding the diffusion reaction which is electron transfer reaction, Randles circuit has been employed for several applications. Craven and coworkers have demonstrated the ability of using the Randles circuit analysis to interpret the interfacial effects of electrochemical cell's constituents (Craven et al., 2018). EIS has been employed to device a real-time function-based biosensor to detect the presence of warfare chemical substances such as cytotoxic (Ducote et al., 2016).

Impedance is similar to resistance and it measures the ability of a circuit to resist the flow of electrical current. For any device, impedance can be determined by applying a sinusoidal voltage and current; in electrochemistry, an electrochemical cell is simply an impedance element to an applied small sinusoidal excitation (Bard and Faulkner, 2001). The main purpose of the EIS is eventually to reveal the nature of the electrochemical interface by providing information about the electron transfer and redox behaviour on the surfaces of electrodes (Vanýsek, 1994).

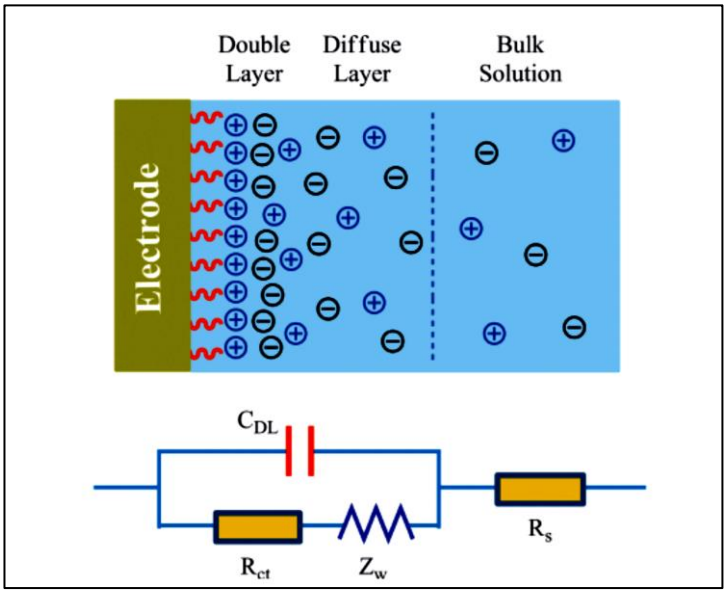

Figure 3-10 Diagram illustrates the electrochemical interfaces between the electrode and the electrolyte and a simplified Randles cell model (Luo and Davis, 2013)

3.9. PARSTAT 4000A Potentiostat Galvanostat

PARASTAT 4000A is a direct current (DC) electrochemical measurements instrument. This tool has been used for many applications, corrosion, batteries and fuel cells, and sensors. The PARASAT 4000A with current range pA and resolution fA, provides current sensitivities for potentiometric sensors such as (ison-selective electrodes and coated wire electrodes) and amperometric sensors (gas sensors, thin film microelectrodes, and chemically modified electrodes) (Metek, 2018).

This technique has improved its accuracy at study the physical electrochemistry and electrochemical sensors through cyclic voltammetry, chronoamperometry, chronopotentiometry, and electrochemical impedance spectroscopy (EIS). In this work, the EIS method has been carried out to characterise the materials and platforms. Figure 3-11 explains the setup of the EIC experiment in the lab.

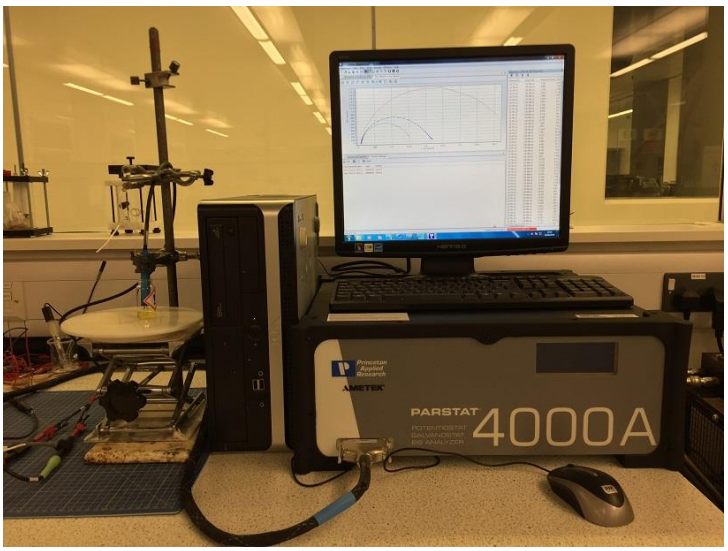

Figure 3-11 Setup of the electrochemical impedance spectroscopy experiment where the potentiostat PARSTAT 4000A connected to a PC and interdigitated sample (modified IDE under infestigation)

3.10. Interdigitated electrodes

Interdigitated electrodes (IDEs) have been effectively used as substrates to study the EIS of composites due to two significant advantages, firstly, it doesn't require polishing and secondly it works with low volumes of sample. Ideally, IDEs are composed of two interdigitated electrodes with two connection tracks, both made of gold, platinum or titanium, on a glass substrate. In this research, interdigitated gold electrodes (IDEAU5) were purchased from DropSens with specific dimensions, with electrode separating gaps of 5 microns, number of digits of 250x2, and digit's length of 6760 µm, as shown in Figure 3-12.

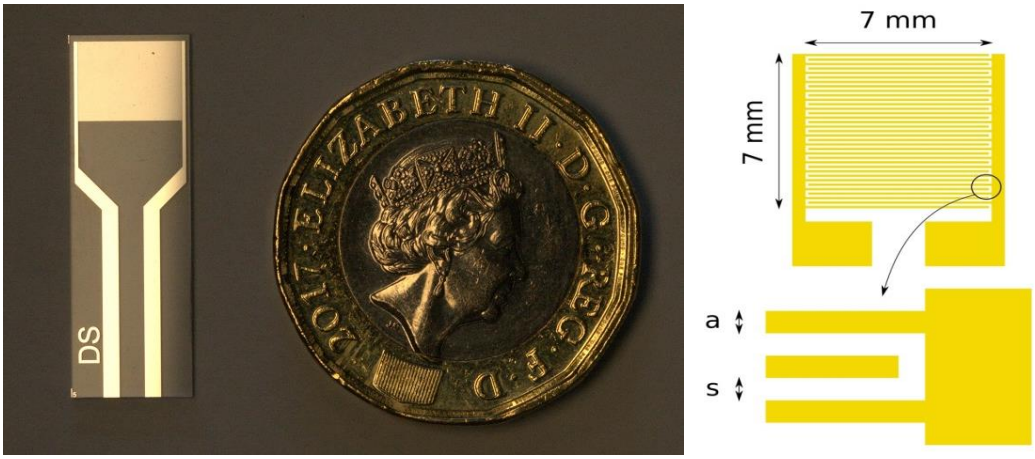

a b

Figure 3-12 a) An image of interdigitated gold electrode (IDEAU5), b) a schematic diagram of IDE

3.11. Brunauer-Emmett-Teller theory and BET measurements

The Brunauer–Emmett–Teller (BET) is an important analysis technique utilised for the measurements of the surface area of materials. It was invented in 1938 by Stephen Brunauer, Paul Hugh Emmett, and Edward Teller when they published their famous paper, Adsorption of Gases in Multimolecular Layers, in the Journal of American Chemical Society (JACS). BET basically works based on the physical adsorption of gas molecules on a solid surface (Brunauer et al., 1938). In the literature, adsorption is defined as a unit operation that deals with utilising the surface forces to reveal information about the active surface of a material. It utilises the Van der Waal's forces, which is not exceeding 80 kJ/mole, to interpret the properties of surfaces in the chemical engineering sense (Webb, 2003). It defines also as the process when atoms, ions, or molecules adhere to and are retained at the surface of a solid or a liquid of the investigated sample.

In this work the surface area of the platform was investigated through nitrogen adsorption−desorption isotherm measurements and performed on a Micromeritics ASAP 2020 M volumetric adsorption analyser at 77.34 K, as shown in Figure 3-13.

Figure 3-13 Micromeritics ASAP 2020 M volumetric adsorption analyser (University of Delaware, 2018)

The following equation describes the BET measurements,

$$v = \frac{v_m c p}{(p_0 - p)\left[1 + (c - 1)\left(\frac{p}{p_0}\right)\right]} \qquad (6)$$

This equation is called S-shaped isotherm equation where v is the adsorbed volume of gas on one square centimetre, v_m is the adsorbed monolayer volume, p is the equilibrium gas pressure, p_o is the saturation pressure and c is the BET constant.

A convenient form of equation (8) is given by the following equation (Brunauer et al., 1938):

$$\frac{p}{v(p_0 - p)} = \frac{1}{v_m c} + \frac{c - 1}{v_m c}\frac{p}{p_0} \qquad (7)$$

where the plot of $\frac{p}{v(p_0-p)}$ against $\frac{p}{p_o}$ should give a straight line; the slope of which is represented in the equation as $\frac{(c-1)}{v_m c}$ while the $\frac{1}{v_m c}$ refers to the intercept line (Figure 3-14). c is BET theory constant and it is related to the ratio of heats of adsorptions, $c = e^{\frac{q1-q2}{RT}}$, where q_1 is the heat of adsorption for the first layer, q_2 for the second and higher layers, R is the gas constant, and T is temperature,

The volume adsorbed is proportional to the pressure. The amount of gas adsorbed depends on the exposed surface and the temperature, gas pressure and the strength of interaction between the gas and solid.

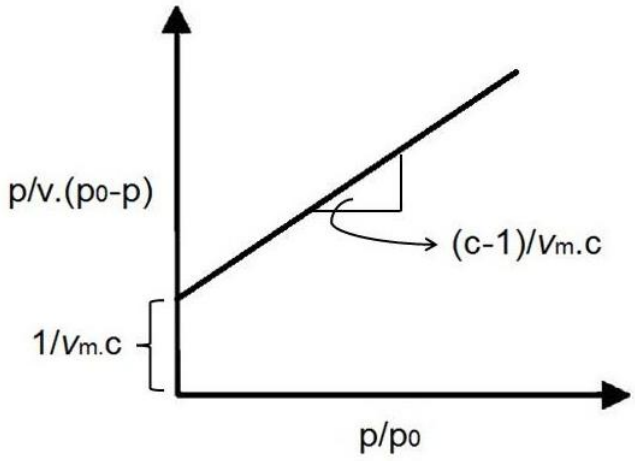

Figure 3-14 BET theory principle

The total surface area can be derived as follows:

$$SA = \frac{v_m N}{M} A_{acs} \qquad (8)$$

where N is the Avagadro's number (6.023×10^{23}), M is the molecular weight of adsorbate, and A_{acs} is the adsorbate cross sectional area (0.162 nm^2 for an absorbed nitrogen molecule) (Hwang and Barron, 2011)

3.12. UV-Visible Spectroscopy

3.12.1. The principle of absorption

The principle of absorption is the interaction of ions or molecules in a sample with incident light; the photons will be absorbed by the sample and its energy will be captured by one or more of the molecules' outer electrons. A number of physico/chemical processes can occur during this interaction, such as reflection, scattering, absorption, fluorescence/phosphorescence (absorption and re-emission), and photochemical reaction (absorbance and bond breaking) (Skoog et al., 1988).

3.12.2. Electronic transitions involve π, σ, and n energy levels:

$\sigma \rightarrow \sigma^*$ Transitions: They are electronic transitions that require large energy as a result of an electron in a bonding **σ** orbital getting excited to the corresponding antibonding orbital. An example of this kind of transition is taking place in methane (which has only C-H bonds, and can only undergo **$\sigma \rightarrow \sigma^*$**transition) which exhibits an absorbance maximum at 125 nm.

$n \rightarrow \sigma^*$ Transitions: These transitions happen to saturated compounds where the atom has lone pair of non-bonding electrons. They can be initiated by the radiation in the wavelength range 150 -250 nm and this area usually is not interested to the organic functional groups.

$n \rightarrow \pi^*$ and $\pi \rightarrow \pi^*$ Transitions: They are the most important transitions that take place in organic compounds where the ***n*** or ***π*** electrons transit to the ***π**** excited state. These transitions require an unsaturated group in the molecule to provide the ***π*** electrons. The absorption peak of these transitions is in the range (200 - 700 nm). All these transition are illustrated in Figure 3-15.

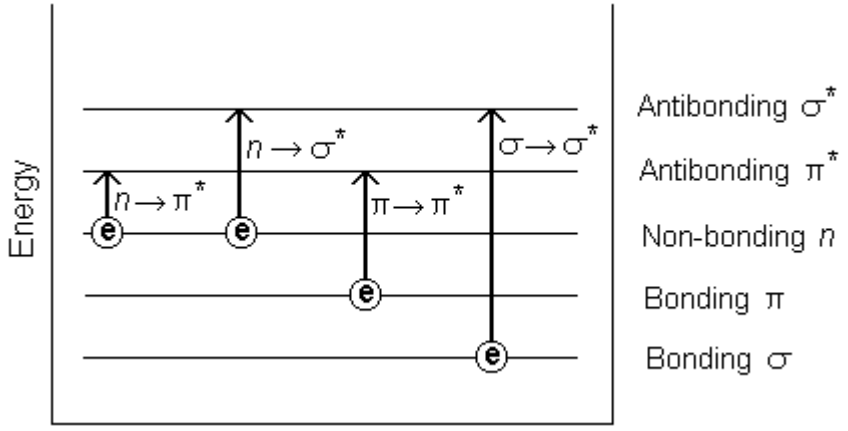

Figure 3-15 Electronic transitions of π, σ, and n electrons

Experimentally and according to Beer's and Lambert's law it is stated that the concentration of a substance in solution is directly proportional to the absorbance *A* of the solution. When a series of wavelengths of monochromatic radiation (light) pass through a solution of a substance the molecules will absorb that light and equation 10 the following equation describes the relationship between absorbance and the concentration of the substance:

$$A = \varepsilon c l = log_{10}\left(\frac{I_0}{I}\right) \qquad (9)$$

where ε is the absorption coefficient (m^2 mol^{-1}), c the concentration (in mole per litre), and l (in cm) is the length of the cell or solution traversed by light.

3.12.3. UV-Visible spectrophotometer

In the current work a Varian Cary 50 UV-Visible spectrophotometer is used which contains a Xenon flash lamp as the source of light, single beam, Czerny-Turner monochromator (Holographic, 27.5 x 35 mm, 1200 lines/mm, blaze angle 8.6° at 240 nm & Beam splitter), and reflecting mirrors as shown in Figure 3-16. The spectral range provided by this instrument is between 190 and 1100 nm.

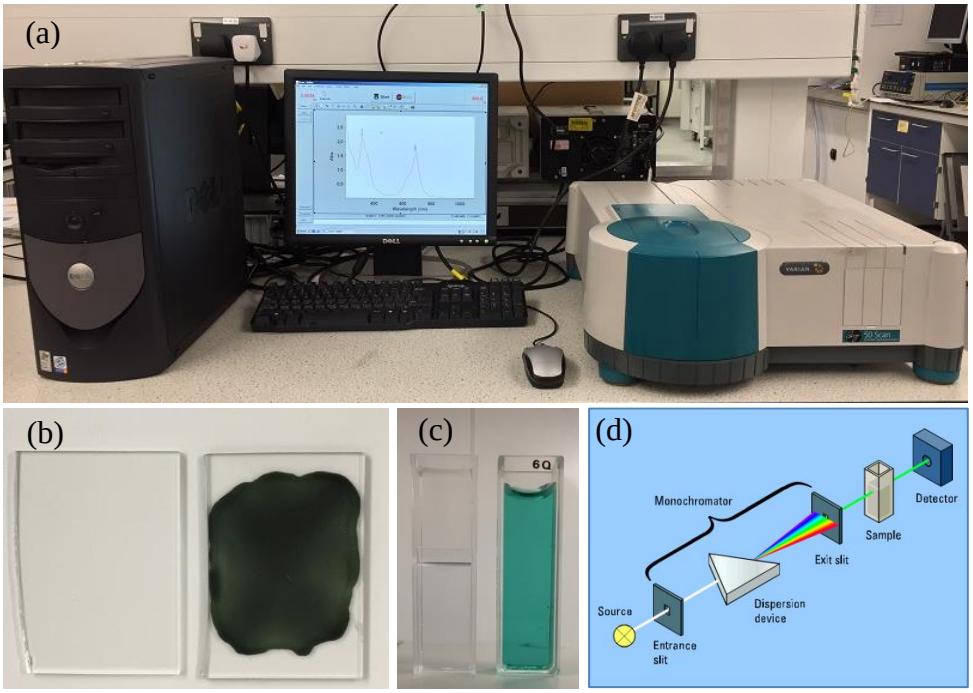

Figure 3-16 a) Cary 50 UV-visible spectroscopy b) prepared films and reference (glass), c) prepared solutions and reference (Deionised Water) in a quartz cell. d) a schematic diagram of the spectroscopy setup

3.13. Fourier-Transform Infrared Spectroscopy

Fourier-transform infrared spectroscopy (FT-IR) is a vibrational spectroscopic technique to study the properties of matters, solids, liquids or gases. In principles, the term "infrared" or IR refers to any electromagnetic radiation in the region 0.7-1000µm however the "mid-IR" region between 2.5 µm and 25 µm which is equivalent to the range (4000 - 40 cm^{-1}). This region is the interesting part for chemical analysis due to the corresponding range of the frequencies in the mid-IR region of the functional groups of organic molecules (Doyle, 1992). FT-IR basically involves an interaction between the infrared radiation and matter; the chemical bonds will be exposed to infrared wavelengths which will cause an asymmetric molecular stretching, vibration, and rotation (Sun, 2009). Figure 3-17 illustrates the Perkin Elmer Spectrum 100 FT-IR spectrophotometer. When the IR radiation passes through a sample, some of that

radiation is absorbed and some transmitted. The molecular absorption and transmission will create a molecular fingerprint of the sample. The obtained results represent the FT-IR spectrum of the sample and provide the following information:

- Identifying the unknown materials.
- Determining the quality or consistency of a sample.
- Determining the amount of components in a mixture.

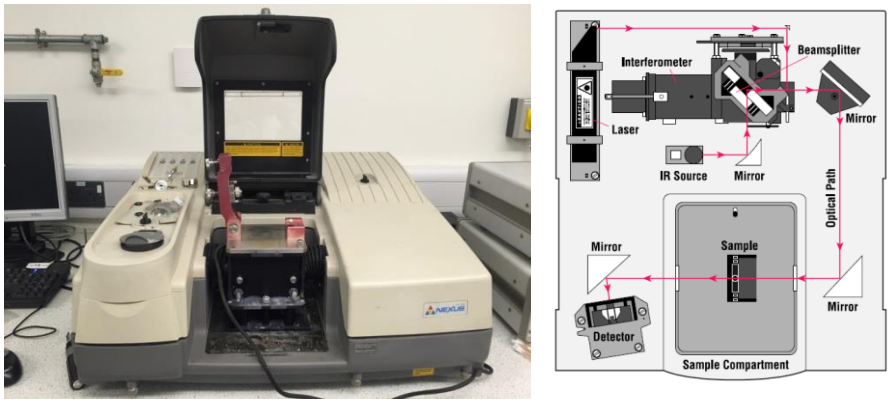

Figure 3-17 FT-IR spectrophotometer and a schematic diagram of the instrument

3.14. X-Ray Diffraction

In the X-ray diffraction (XRD) method, electromagnetic waves (X-rays) interact with electric and magnetic potentials based on Maxwell's equations. XRD is mainly used to provide information about the crystal structure, chemical composition, and physical properties of materials. The method is based on the scattering, emission and absorption of X-radiation. The X-ray diffractometer basically consists of three elements: an X-ray tube, sample holder, and detector. In addition to the XRD, Energy dispersive X-ray spectroscopy (EDX) and X-ray fluorescence (XRF) are the other common techniques that are used for the same purpose of characterising materials. In this work XRD has been used to study the structure of all row materials, including the prepared composites and the fabricated biosensing platforms. When the incident X-ray radiation interacts with the sample a constructive interference between diffracted rays occurs when conditions satisfy Bragg’s law. The Bragg’s law states that a constructive interference is

produced when the path difference between two interfering waves is equal to the whole number (n) of the wavelength (λ). The Bragg's law is given by the following equation:

$$n\lambda = 2d\sin(\theta) \qquad (10)$$

where d is the inter-atomic distance (lattice spacing) and θ is the angle between the incident beam and scattering plane. The XRD characteristics generated in the XRD analysis provides useful information about the crystal phases of the studied sample.

3.14.1. XRD instrument

Precision measurements of the fabricated sensing platform surface were carried out using a computer programmed Philips X-Pert X-ray diffractometer. The instrument employs a Cu K_α radiation source (λ = 0.154056 nm for $K_{\alpha 1}$) working at 40 KV and 40 mA. X-rays measurements were carried out on powdered and thin film materials to analyse their structures as explained in Figure 3-18.

(a)

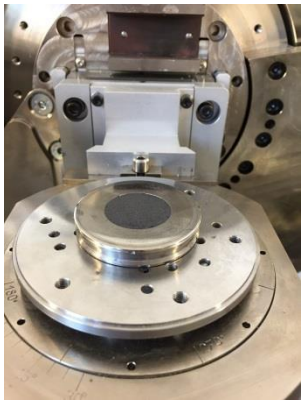

(b)

(c)

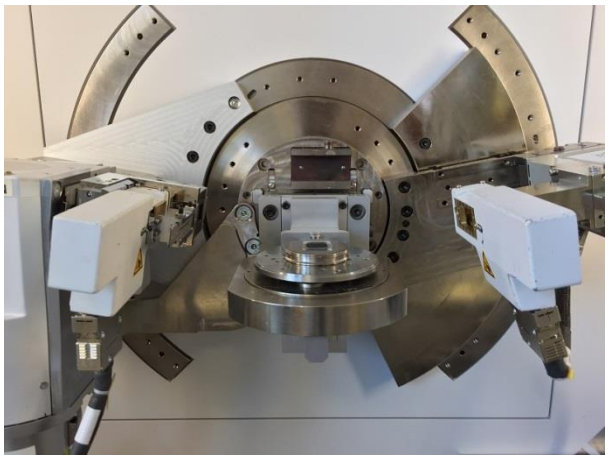

Figure 3-18 a) Philips X-Pert X-ray diffractometer; b) powder sample placed in a special tray and located on the instrument base; c) thin films are placed on a sample holder

3.15. Scanning Electron Microscopy

Scanning Electron Microscopy (SEM) is a technique that is used to characterise objects with size between 1 nanometre to 1 micrometre. The principle of SEM is based onto the scanning of highly focused electron beam of high-energy onto a surface where it can reveal levels of information to explain the morphology of surfaces (Lawes, 1987).

The first Scanning Electron Microscope (SEM) was discovered by Stylizing and Knoll on 1935 in Germany (Nada, 2015). The first SEM was later developed in 1942 by Zworykin from the United States; however the equipment still had problems related to signal to noise ratio. The modern SEM was designed in the United Kingdom by Nixon and Oatly in 1950 which was followed by the first commercial SEM built by Stewart and Snelling in 1965. Lately, a computer was attached to the SEM which has led to

increasing its analysis ability as well as overcoming the signal-to-noise ratio problem (Nada, 2015).

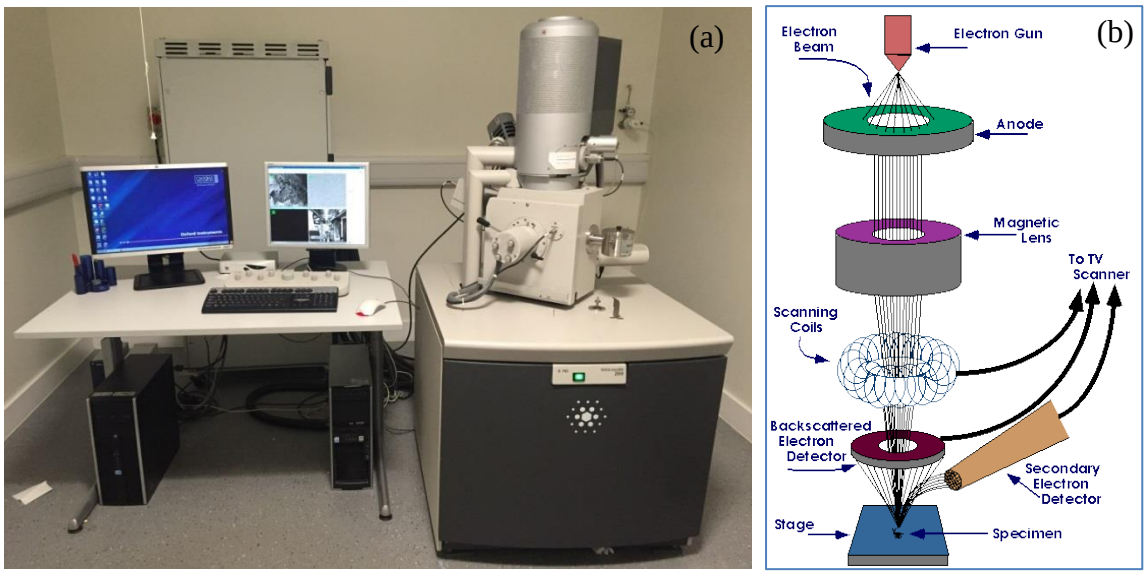

Figure 3-19 a) Scanning Electron Microscopy b) the layout of major parts of SEM

Figure 3-19 shows a photo of the SEM instrument used in this work, as well as a schematic diagram illustrating its operational principles. The instrument involves an electron gun, magnetic lens, scanning coils that facilitate the deflection of the beam in the x and y directions, and detectors for backscattered and secondary electrons. Recently, the SEM has become one of the most powerful techniques for analytical work. Technically, SEM has been used for studying surface topography, elemental composition, and crystallography of samples; however, topographic imaging research and chemical composition studies of a sample were the main purposes of SEM studies (Kaech, 2002; Nada, 2015).

There are two types of SEM; one type is the Field Emission Scanning Electron Microscope (FESEM) which provides topographical and elemental information at magnifications of 10x to 300,000x, with virtually unlimited depth of field. The second type is a conventional scanning electron microscopy (SEM) which provides topographical and elemental information at useful magnifications of 10x to 100,000x,

with virtually unlimited depth of field. FESEM produces clearer and less electrostatically distorted images with spatial resolution down to 1.5 nanometres which is three to six times better than the second type. Both SEM types operate in vacuum chamber with high-energy electron source (2-25 kV).

3.15.1. Materials preparation

Preparation of thin film samples for SEM scan was carried out through using spin coating system in order to produce thin and homogeneous films out of the studied materials solutions. Standard glass slides (1.5 x 2.5 cm) were used as substrates after being subjected to a thorough cleaning and drying; they were placed on the coating system stage of the coating system in order to produce the films (see Figure 3-20(a)). On rotating the coating stage at a certain spin speed the flow of a viscous liquid will spread on the substrate with the effect of centrifugal force (Emslie et al., 1958). Different speeds of the spinner can be controlled via controlling a digital unit, as shown in Figure 3-20(b). The films were left to dry at room temperature condition inside the cupboard. Gold coating system were used as needed to deposit a thin layer of gold on top of the studied films in order to reduce charging effect through enhancing the conductivity of the film, as depicted in Figure 3-20(c). Figure 3-20(d) shows the aluminium mount and carbon conductive tabs that were used as base to the sample to be placed in the SEM instrument for scanning.

(a) (b)

(c) (d)

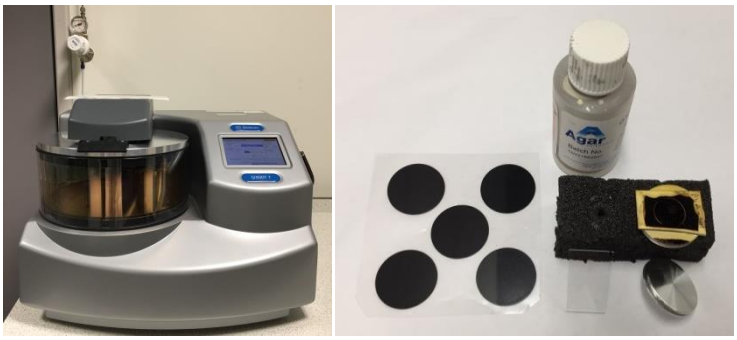

Figure 3-20 SEM samples' preparation, a) spin coating unit, b) the spinner controlling unit manufactured by Electronic Micro Systems (EMS), England, c) Quorum (Q300T T) turbo-pumped coating system, d) Proscitech pin type SEM mount made of aluminium and carbon conductive tabs to fix the specimen inside the chamber of the SEM, agar silver paint

3.16. Energy Dispersive X-ray

Energy dispersive X-ray spectroscopy (EDX) is an analytical technique applied to provide qualitative and quantitative information on the chemical composition of materials. It is used in conjunction with SEM and makes use of the X-ray spectrum emitted by a solid sample bombarded with a focused beam of electrons. Two types of X-rays, directly attributed to the particular elements in the sample, are produced on that inelastic interaction of the electron beam with the specimen atoms of all materials (Inkson, 2016). The first type is characteristic X-rays, which are generated by the interaction between the primary electron beam and the inner shell electron of the atom of investigated sample. Based on Bohr's theory of atomic structure, every electron travels in a specific shell or orbit around the nucleus. Ionisation will take place and inner shell electrons are emitted from the sample's atoms. Following that relaxation of atoms in its neutral state happens when the electrons from the outer shell filled the holes in the inner shell. Characteristic X-rays are suitable to characterise the nanostructured

material and crystal defects. The second type is bremsstrahlung X-rays which are generated due the deceleration of the primary electrons when they pass through atoms. Bremsstrahlung X-rays has continuous range of energies up to the primary electron incident energy. Bremsstrahlung X-rays are suitable to interpret the biomolecular materials that are targeted by the X-ray reaction (Williams and Carter, 2009). Figure 3-21 illustrates the principles of EDX measurements.

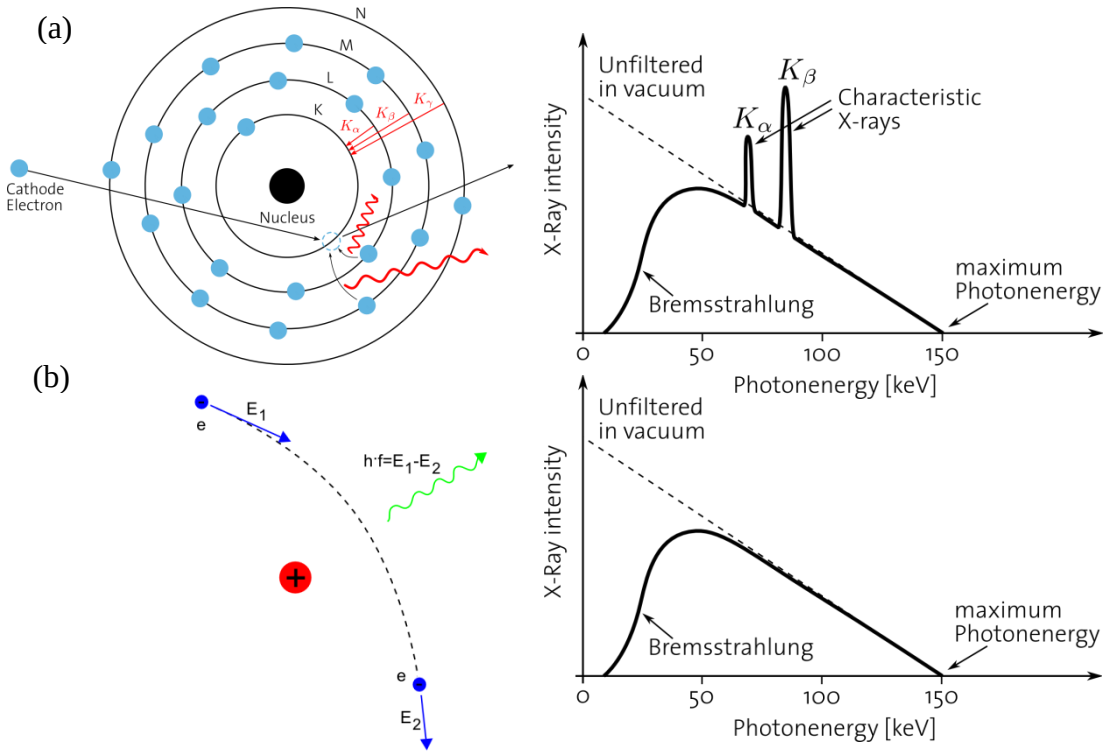

Figure 3-21 a) An illustration of the bermsstrahlung X-rays where the lost energy from the electron emitted as photons; the higher the angle the greater the chance electrons will undergo an inelastic (kinetic energy not conserved) event, b) the characteristic X-rays that are emitted due to the electrons transition to lower atomic energy levels (Cattin, 2016).

3.17. Transmission Electron Microscopy

Transmission electron microscopy (TEM) is a high-resolution microscopy technique, which works on the basis of electrons' ability to be transmitted across thin film specimens. The interaction between the high energy electron beam and thin film will generates a range of signals that could be used for structural and compositional analysis, as illustrated in Figure 3-22.

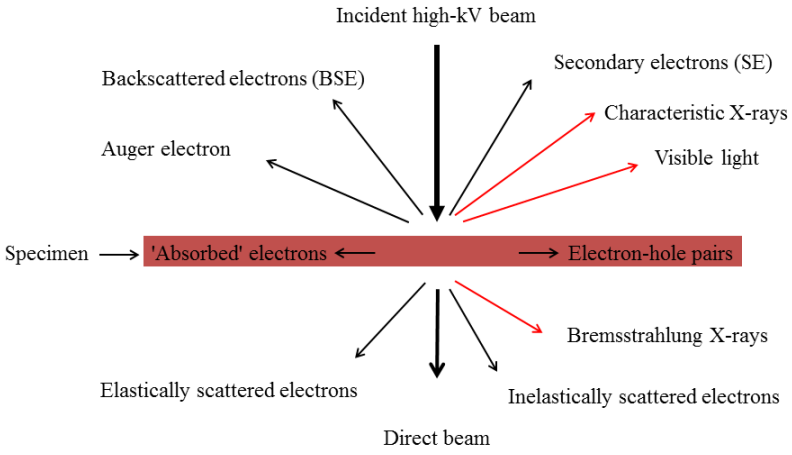

Figure 3-22 Different signals emitted from a thin sample when illuminated with a high energy electron beam. Red arrows represent the photon signals and black arrows represent electron signals

In this study a Philips CM20 transmission electron microscope is used which operates at 200 kV to obtain high-resolution images down to 0.27 nm with maximum magnification of 750,000x. Three stages lensing are responsible for the control of the electron beam between the electron gun and the sample; these are the condenser lenses which are responsible for primary beam formation, the objective lenses which are responsible for focusing the beam that comes through the sample itself, and the projector lenses which are used to expand the beam onto the phosphor screen as shown in Figure 3-23. Figure 3-24 shows the utilised substrate for TEM samples' preparation.

(a)

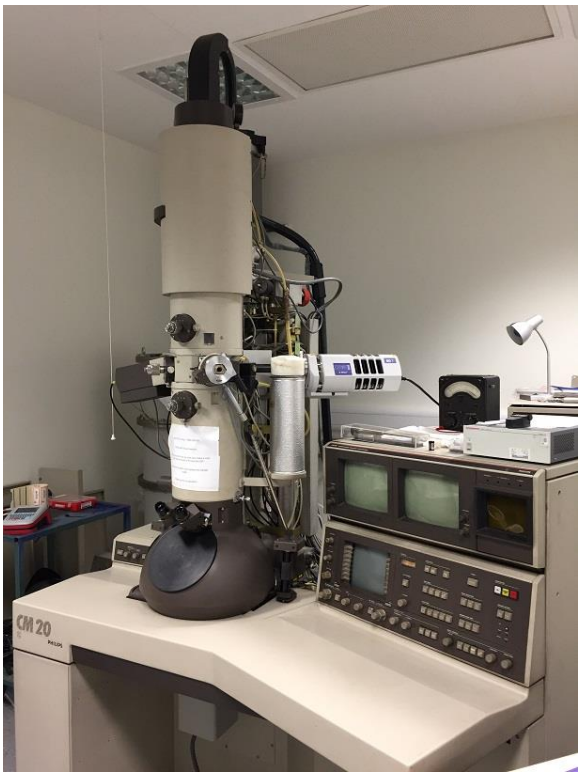

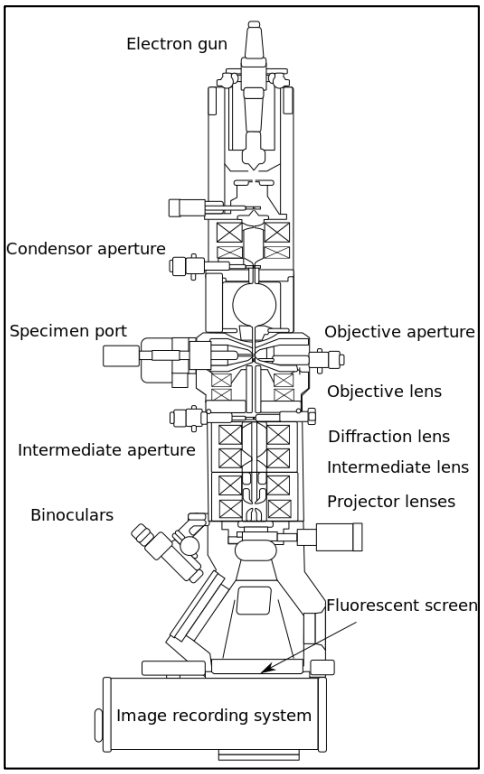

(b)

Figure 3-23 Philips CM20 TEM instrument, b) Layout of optical components in a basic TEM

(a)

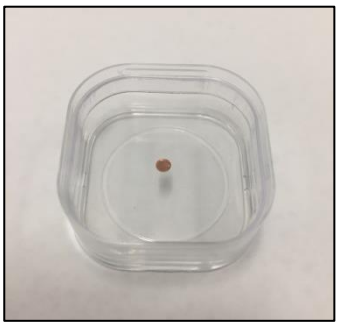

(b)

Figure 3-24 TEM's sample preparation where a) pack of a holey carbon film on 400 mesh copper grids which are used as the substrate of the sample for TEM scan, b) a TEM sample placed inside special storage

3.18. Freeze dry system

Freeze drying is a kind of preservation technique used for the removal of bound water molecules through the process of desorption as well as by the process of sublimation which leads to the removal of the ice of other solvents from a material (Nireesha et al., 2013). In this work, water-rich hydrogel will be first frozen through pouring into a well-

closed vial in a nitrogen gas and then placed in the freeze-dry system. This technique is very convenient to conserve the micro porous structure of the hydrogel sample that was formed earlier. Therefore, getting a dry hydrogel with same structure as formed will enable the SEM analysis to provide good quality images that can reveal the sample structure. Several parameters, such as pore size, depth, and number of pores will be obtained. Furthermore, SEM image analysis will provide information regarding the surface area and porosity of the hydrogel which gives an indication of the conductivity of the gel as well as prospects of enhancing it (O'Brien et al., 2004). The Freeze Dry System equipment comprises vacuum pump, vacuum gauge, vacuum tubing clamps, and glassware (LABCONCO, 2016) as shown in Figure 3-25. Table 3-2 shows a list of an illustration of functions of different instruments that have been utilised in this research.

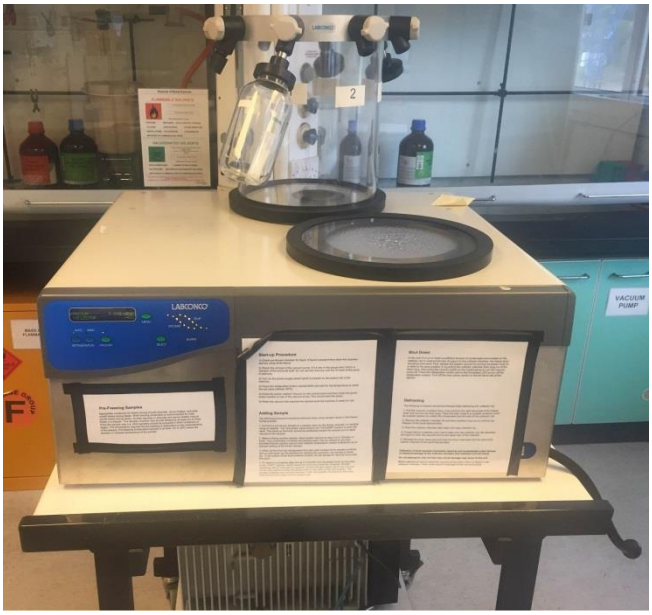

Figure 3-25 Freeze dry system

Table 3-2 Function of utilised instruments

The instrument	Function
Potentiostat (µStat 8000)	To study the electrode processes and redox reactions. By employing the CV or CA electrochemical methods, significant information related to the electrodes surfaces and fabricated platforms could be achieved.
PARSTAT 4000A Potentiostat Galvanostat	To carry out analysis of surfaces or platforms that are fabricated on the typical interdigitated electrodes that have been used in this research in order to measure the conductivity as well as conducting large anodization studies. On the other hand, PARSTAT 4000A has been employed in many applications such as corrosion, batteries and fuel cells, and sensors.
ASAP 2020 M volumetric adsorption analyser	Reveals information about the active surface area, porosity, chemisorption, and physisorption of materials.
Varian Cary 50 UV-Visible spectrophotometer	Studies the absorbance of solutions and thin films of fabricated platforms and raw materials
Perkin Elmer Spectrum 100 FT-IR spectrophotometer	Characterises the molecular structure of scanned samples
Philips X-Pert X-ray diffractometer	Identify the crystallographic structure and grain size of crystalline materials
Scanning Electron Microscope (SEM)	Imaging with high resolution that allows SEM to reveal several information including external morphology, chemical composition, and crystalline structure and orientation of materials. The SEM beams of electrons scan the surface.
Philips CM20 transmission electron microscope (TEM)	Imaging at significantly high resolution to observe the feature of fine specimens such as structure and morphology. The TEM beams of electron transmitted through the sample.
LABCONCO Freeze Dry system	To dry the hydrogel under low temperature and remove of bound water molecules through the process of desorption. It is suitable for lyophilizing aqueous mediums.

Chapter: 4 Multifunctional hydrogel-based lutetium phthalocyanine for glucose detections

Chapter overview

This chapter reports a scalable synthesis of multifunctional conducting polyacrylic acid (PAA) hydrogel (MFH) integrated with reduced graphene oxide (rGO), vinyl substituted polyaniline (VS-PANI) and lutetium phthalocyanine ($LuPc_2$) as three-dimensional robust matrix for glucose oxidase (GOx) immobilisation (PAA-rGO/VS-PANI/$LuPc_2$/GOx-MFH). The role of $LuPc_2$ as dopant to form the multifunctional hydrogel has been discussed in sufficient detail. Full characterisation of the raw materials and the prepared platforms is also presented, and results discussed. The fabrication of a biosensor by immobilising GOx into the multifunctional hydrogel and its use in electrochemical detection of glucose has been fully analysed and conclusions are made. The chapter also provides a thorough analysis of the potential use of the prepared biosensor platform to monitor glucose concentrations over a sufficiently wide range and compares the device sensitivity and lower detection level with the available data in the literature.

4.1. Introduction

Despite many technological advances in biosensor research, the worldwide increase in the prevalence of chronic disease (diabetes mellitus) has been the driving force for the development of glucose sensors (Wang and Lee, 2015). Although several conventional methods are available for the detection of glucose, electrochemical approaches for the detection of glucose show unique advantages such as fast response, sensitive and low cost. Furthermore, electrochemical based sensors do not require skilled labour or large instrumentation for glucose detection (Rahman et al., 2010). Non enzymatic electrochemical sensors exhibit poor performance in selectivity and suffer from

interference from electrochemically active molecules (Toghill and Compton, 2010). Therefore, enzymatic electrochemical sensors as glucose meters have played significant role in monitoring whole blood (Tonyushkina and Nichols, 2009).

However, fewer reports are available on the utilization of a robust three-dimensional multifunctional conducting hydrogel as an enzyme immobilisation matrix and subsequent biosensing of glucose. Hydrogel networks formed from polyacrylic acid (PAA) have the ability to absorb more than hundred times their weight in water and they are classified as super absorbents (Dhodapkar et al., 2009). PAA hydrogel plays an important role as pH stimuli-responsiveness and possesses bioadhesive characteristics because of the presence of −COOH groups in their chain (Arunbabu et al., 2013). However, pristine polymeric hydrogels are mechanically weak and poses insufficient electrical conductivity that limits their application as electrochemical sensors (Mawad et al., 2016). The incorporation of nanomaterials into robust hydrogels generates tailored functionalities feasible to construct sensor and other drug delivery vehicles (Puoci and Curcio, 2013; Gaharwar et al., 2014). Particularly, integration of graphene with polymeric hydrogel offers enhanced actuation performance due to its excellent physico-mechanical properties and facile conjugation reactions (Worsley et al., 2012; Bhattacharjee et al., 2013). The presence of hydroxyl, epoxy and carboxyl end functional groups on the surface of GO provide multiple conjugation avenue and endow electrochemical properties to hydrogel matrices (Bai et al., 2010; Liu et al., 2011).

Metallophthalocyanines (MPcs) are of great interest in electrochemical biosensors due to their excellent electronic properties with rich redox activity (Guillaud et al., 1998; Zhang et al., 2013). Among numerous MPcs, double-decker lanthanide derivatives, such as lutetium phthalocyanine ($LuPc_2$) attract interest due to their high intrinsic conductivity and electrochemical properties (Basova et al., 2008). The electrochromic

behaviour of lanthanide phthalocyanine films has been used for the detection of nicotinamide adenine dinucleotide (Pal et al., 2011; Galanin and Shaposhnikov, 2012a). Synthesis and spectral properties of lanthanide double-decker complexes with tetrabenzoporphyrin and phthalocyanine have also been studied (Galanin and Shaposhnikov, 2012b).

Herein a scalable synthesis of multifunctional conducting PAA hydrogel (MFH) integrated with rGO, VS-PANI and $LuPc_2$ as three-dimensional robust matrix for GOx immobilisation (PAA-rGO/VS-PANI/$LuPc_2$/GOx-MFH). The multicomponents PAA with rGO and VS-PANI have been integrated through free radical polymerization using methylene bis-acrylamide as the cross linker and initiator. The produced hydrogel has been doped with $LuPc_2$ to form multifunctional biosensing platform (PAA-rGO/VS-PANI/$LuPc_2$-MFH). Finally, a biosensor was fabricated by immobilising GOx into PAA-rGO/VS-PANI/$LuPc_2$-MFH and subsequently used for electrochemical detection of glucose.

4.2. Experimental details

4.2.1. Materials

rGO (surface area: 450 m^2/g), poly(ethylene glycol) diamine (NH_2-PEG-NH_2), *N*-(3-dimethylaminopropyl)-*N*′-ethylcarbodiimide hydrochloride (EDC hydrochloride), acrylic acid, 3-vinylaniline (97%), N,N′-methylenebis(acrylamide) (MBA), ammonium persulfate (APS), D-(+)glucose, glucose oxidase from aspergillus niger, Type X-S, lyophilized powder, 100,000-250,000 units/g solid (without added oxygen), glutaraldehyde solution (Grade II, 25% in H_2O), Potassium ferrocyanide, Potassium ferricyanide, potassium chloride (KCl), sodium chloride (NaCl), phosphate buffer solution (PBS, pH 7.0) were all purchased from Sigma Aldrich (UK) and used as received. Synthesis and characterisation of lutetium bis-phthalocyanine ($LuPc_2$) has

appeared in an earlier publication (Gurek et al., 2001). *N*,*N*-Dimethylformamide (DMF) is of analytical grade obtained from Sigma Aldrich.

4.2.2. Measurement instruments and characterisation

The morphologies of the prepared MFH were examined by FEI-Nova scanning electron microscopy (SEM) with a low magnification (160,000×) and high voltage (10 kV). UV–Visible spectrophotometer (Varian 50-scan UV–Visible) in the range 190–1100 nm was used to measure the absorption spectra of MFH. FT-IR spectra were recorded on a Perkin Elmer Spectrum 100 spectrophotometer. The electrochemical measurements of the electrodes were conducted using a portable multi Potentiostat/Galvanostat μStat 8000 and controlled by PC with DropView 8400 software. All the utilised instruments have been described in details in chapter 3. The sensor platforms were disposable screen-printed carbon electrodes DRP-C110 with 4 mm diameter working electrode. The working and auxiliary electrodes were carbon, while silver forms the reference electrode and the träger (carrier) was ceramic. The working electrodes were modified with PAA-rGO/VS-PANI/$LuPc_2$/GOx-MFH or PAA-VS-PANI/$LuPc_2$/GOx-MFH or PAA-$LuPc_2$/GOx-MFH. The electroactivity of MFH modified electrode was evaluated by recording cyclic voltammogram in potassium ferro/ferricyanide solution containing 0.1 M NaCl in the potential range from -0.5V to +0.5V. The biocatalytic activity of PAA-rGO/VS-PANI/$LuPc_2$/GOx-MFH biosensor was evaluated by cyclic voltammetry for a solution of 4 mM glucose in 0.1 M PBS. The amperometric responses of PAA-rGO/VS-PANI/$LuPc_2$/GOx-MFH biosensor towards glucose detection were recorded under stirred conditions in 0.1 M PBS (pH 7.0) by applying a constant potential of +0.3 V at the working electrode.

4.2.3. Preparation of PAA-rGO/VS-PANI/$LuPc_2$/ GOx-MFH biosensor

The preparation of MFH involves three steps: (1) preparation of amine functionalised rGO, (2) formation of PAA-rGO/VS-PANI-MFH, (3) incorporation of LuPc2 and subsequent immobilisation of GOx to form PAA-rGO/VS-PANI/$LuPc_2$/GOx-MFH biosensor.

4.2.3.1. Preparation of amine functionalised rGO

Amine functionalised rGO preparation was carried out according to earlier reports (Lei et al., 2016). Briefly, about 10 mg of rGO was dispersed in 10 mL of water containing NH_2-PEG-NH_2 (0.1 g) and EDC.HCl (0.1 g) under vigorous stirring overnight. rGO-PEG-NH_2 thus obtained were allowed to settle down and filtered through polycarbonate membrane (pore size=200 nm). The samples were dried in vacuum oven at 60^oC for further use.

4.2.3.2. Formation of PAA-rGO/VS-PANI-MFH

5 mg of rGO-PEG-NH_2 was dispersed in 10 mL of HCl (0.1M) containing 10 mg of EDC.HCl under sonication. Subsequently, AA (2.4 mL), MBA (2 M) 3-vinylaniline (0.1 M) and APS (0.2 M) were added into the mixture with continued stirring. The above solution mixture was purged with N_2 gas to remove the dissolved oxygen content and poured into a pre-cleaned vial. The vial was placed in the vacuum oven maintained at 70 °C for about an hour. A solid hydrogel was formed at around 45 min. The solid hydrogel was cooled to room temperature. The colour of the hydrogel turned to green with black spots to form PAA-rGO/VS-PANI-MFH. For comparative purposes, PAA/VS-PANI-MFH and PAA-rGO-MFH were prepared separately. This was achieved by excluding rGO-PEG-NH_2 and 3-vinylaniline respectively in the hydrogel preparation step. It took around 90 min for gelation in the absence of rGO-PEG-NH_2 (PAA/VS-

PANI-MFH) and 60 min in the absence of 3-vinylaniline (PAA-rGO-MFH). The hydrogels thus obtained were systematically analysed by SEM, UV-visible, FTIR spectroscopy to determine the morphology and chemical structure of the hydrogels. In Figure 4-1 the possible formation mechanism starting step by step from the initial to the final expected molecular formula the multifunctional conduction hydrogel.

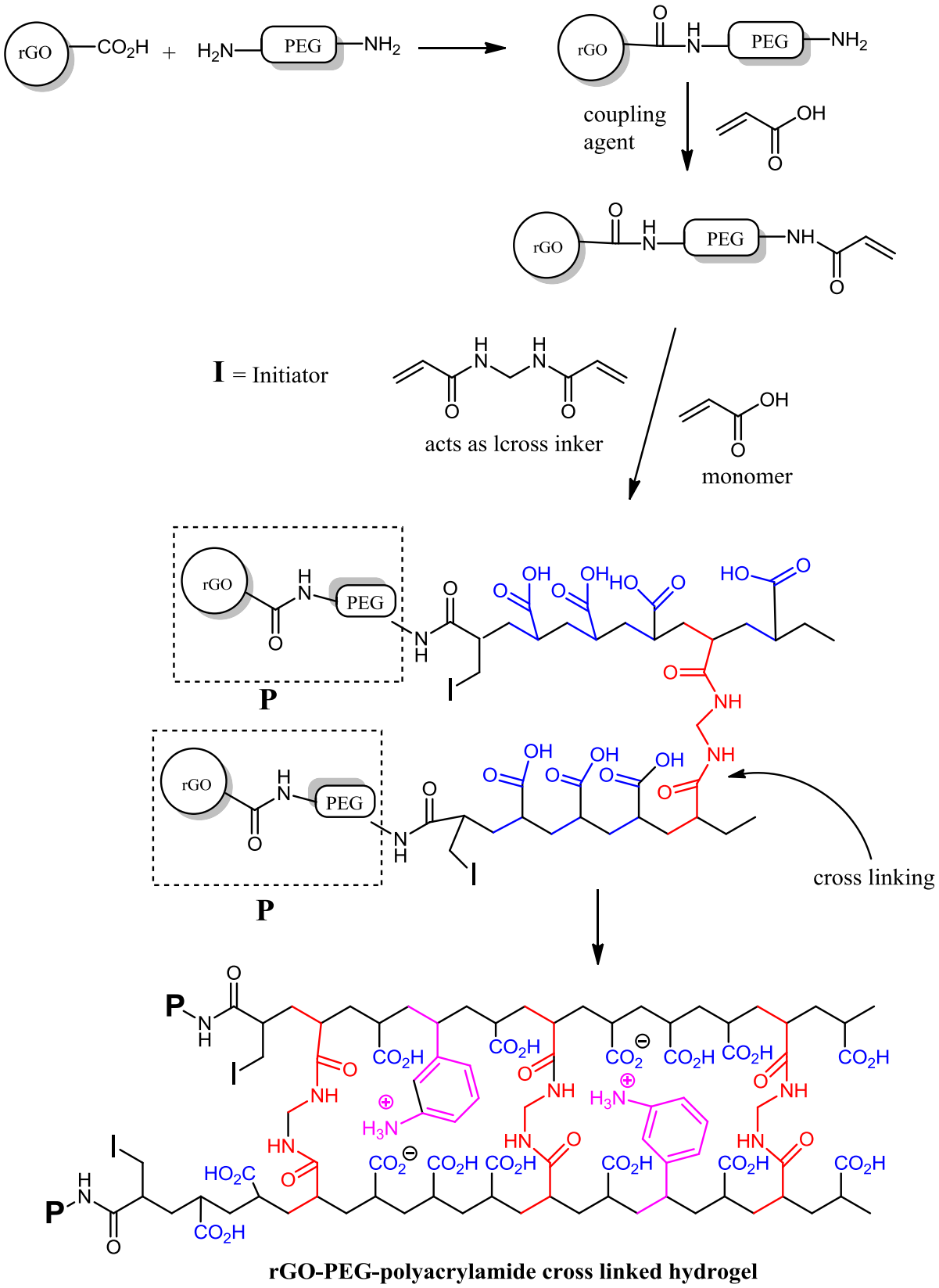

Figure 4-1 Mechanism of the rGO-PEG-polyacrylamide cross linked hydrogel

4.2.3.3. Fabrication of PAA-rGO/VS-PANI/$LuPc_2$/GOx-MFH biosensor

Initially PAA-rGO/VS-PANI-MFH (2 µl) was formed as detailed before on the surface of screen printed electrode (Area = 0.1256 cm_2). Then $LuPc_2$ (2 µl) (5 mg dissolved in 1 mL chloroform) was dropped and allowed to dry in oven at 60^oC for 2 h. The fabrication of PAA-rGO/VS-PANI/$LuPc_2$/GOx-MFH biosensor was achieved by immobilising GOx (1 µl) (10 mg in 1 mL PBS (pH 7.0)) along with glutaraldehyde (1 µl) and dried at room temperature for further analysis. Similarly, the other two PAA/VS-PANI/Pc_2/GOx-MFH biosensor and PAA-rGO/$LuPc_2$/GOx-MFH biosensor were fabricated.

4.3. Results and discussions

4.3.1. Synthesis of PAA-rGO/VS-PANI-MFH

The steps involved in the preparation of the PAA-rGO/VS-PANI/$LuPc_2$/GOx-MFH are illustrated as scheme in Figure 4-2. Initially rGO-PEG-NH_2 was obtained through covalent grafting of PEG diamine chains onto carboxyl sites in the surface of rGO sheets via amidation in aqueous media. PAA-rGO/VS-PANI-MFH was formed through free radical polymerization of AA along with rGO-PEG-NH_2 and 3-vinyl aniline in the presence of MBA and APS (Layek and Nandi, 2013) Figure (4-2). The inclusions of rGO-PEG-NH_2 and VS-PANI in the hydrogel were aimed to improve the binding sites and favourable conditions for loading $LuPc_2$ and GOx immobilisation. PAA containing –COOH groups in MFH protect VS-PANI in its protonated form. Figure 4-3 shows a photograph of the prepared PAA-rGO/VS-PANI-multifunctional hydrogel (MFH). This hydrogel exhibits green colour which is originated from the protonated and doped VS-PANI in MFH with dispersed black spots.

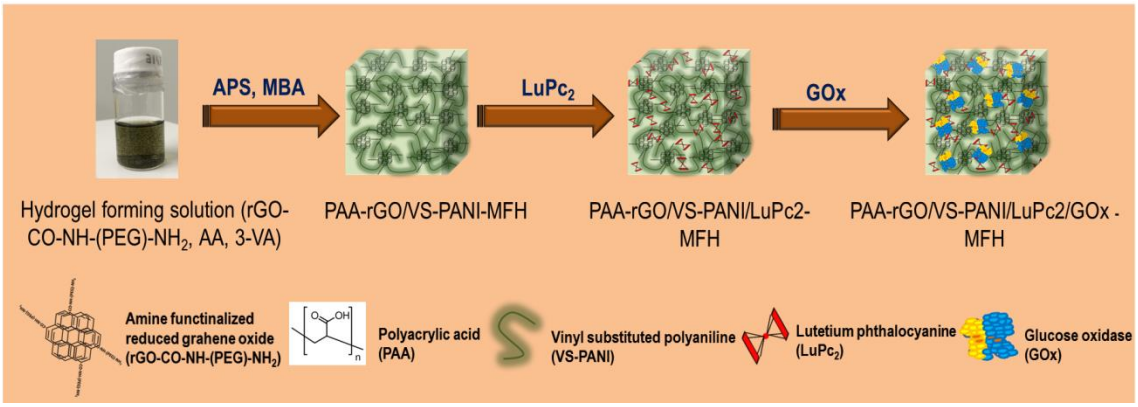

Figure 4-2 Representation of the formation of PAA-rGO/VS-PANI/LuPc$_2$/GOx-MFH

4.3.2. Morphology

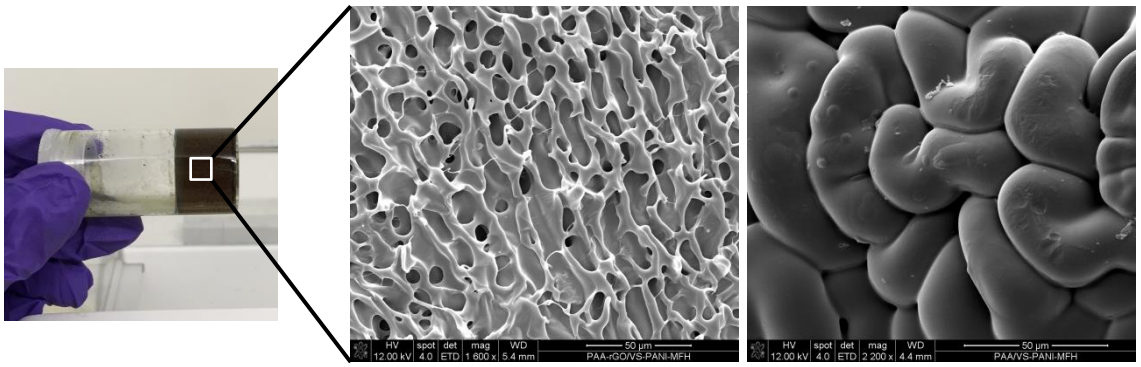

(a) (b)

Figure 4-3 SEM images of (a) PAA-rGO/VS-PANI-MFH, (b) PAA/VS-PANI-MFH

Figure 4-3 (a and b) shows SEM images of PAA-rGO/VS-PANI-MFH and PAA/VS-PANI-MFH respectively. PAA-rGO/VS-PANI-MFH clearly showed randomly distributed micro porous 3D inter-linked network, due to the integration of the components involved (4-3 (a)). The average pore diameter of PAA-rGO/VS-PANI-MFH was estimated to be approximately 7µm. Such 3D interconnected hierarchical porous structure offers greater effective surface areas for LuPc$_2$ and GOx immobilisation. However, the PAA/VS-PANI-MFH showed a layered structure characterised with smooth surface and much smaller pore size as shown in 4-2B (b). This suggests that VS-PANI twists with the PAA component and fills up the existent voids in PAA/VS-PANI-MFH. Further, the surface area of the MFH was also studied

through Brunauer, Emmett and Teller (BET) measurements. From the BET results, the surface area of PAA-rGO/VS-PANI-MFH, PAA-rGO-MFH are calculated to be 1.3653 ± 0.1416 m^2/g and 0.9794 ± 0.1095 m^2/g respectively. We presume that the harsh pretreatment process (degassing condition – 3 h at 120 deg C) before N_2 physisorption has induced a collapse of the pores structure of MFH (Iza et al., 2000). The surface area value is slightly lower than previously reported polyacrylamide–polyacrylic acid copolymer hydrogel (4.9 m^2/g) (Li et al., 2002).

4.3.3. UV-visible analysis

UV-visible spectrum of pristine $LuPc_2$ and hydrogels decorated with $LuPc_2$ (PAA-rGO/VS-PANI/$LuPc_2$, PAA/VS-PANI/$LuPc_2$ and PAA-rGO/$LuPc_2$), were recorded by using Cary 50 UV-Visible Spectrophotometer (190-1100 nm), as shown in Figure 4-4. Thin films of $LuPc_2$ and the hydrogels were formed on the surface of pre-cleaned glass substrate. Main absorption peaks derived from the measured absorption spectra are presented in Table 1. Bis-phthalocyanine complex of $LuPc_2$ thin film exhibited characteristic UV-visible B and Q absorption bands. A strong N-band at 317 nm, Soret B band at 390 nm region and intense visible Q band of the macrocycles at 706 nm can be seen (Figure 4-4inset) (Basova et al., 2008). Also two weak p-radical blue valence (BV)/ red valence (RV) related bands attributed to 2eg–a1u and 1eg–a1u transitions were observed at 510–580 (BV) and 930–970 nm (RV), as reported earlier (Nekelson et al., 2007; Zheng et al., 2015; Pushkarev et al., 2012). In the hydrogels that includes VS-PANI, PAA-rGO/VS-PANI/$LuPc_2$ and PAA/VS-PANI/$LuPc_2$ showed a shoulder peak around 430 nm corresponding to the benzenoid to quinoid transitions of backbone PANI structure (Figure 4-4a,b). Additionally the N band of $LuPc_2$ was coupled with π–π^* absorption peak of VS-PANI. These results demonstrate the presence of interconnected networks of VS-PANI in the hydrogel formed (Ipek et al., 2014). The Q band was shifted bathochromically in the case of PAA-rGO/VS-PANI/$LuPc_2$ to 712 nm (Figure 4-

4a), PAA-rGO/$LuPc_2$ to 718 nm (Figure 4-4c) and hypsochromically in the case of PAA/VS-PANI/$LuPc_2$ to 702 nm (Figure 4-4b). This reveals the perturbance in the electronic states of $LuPc_2$ in MFH due to the electron transfer from rGO to phthalocyanine ring which leads to the formation of π–π stacking interaction between them and thus lower the band gap. This ensures that the studied MFHs were well decorated with double-decker lutetium (III) phthalocyanine moieties (Mani et al., 2015).

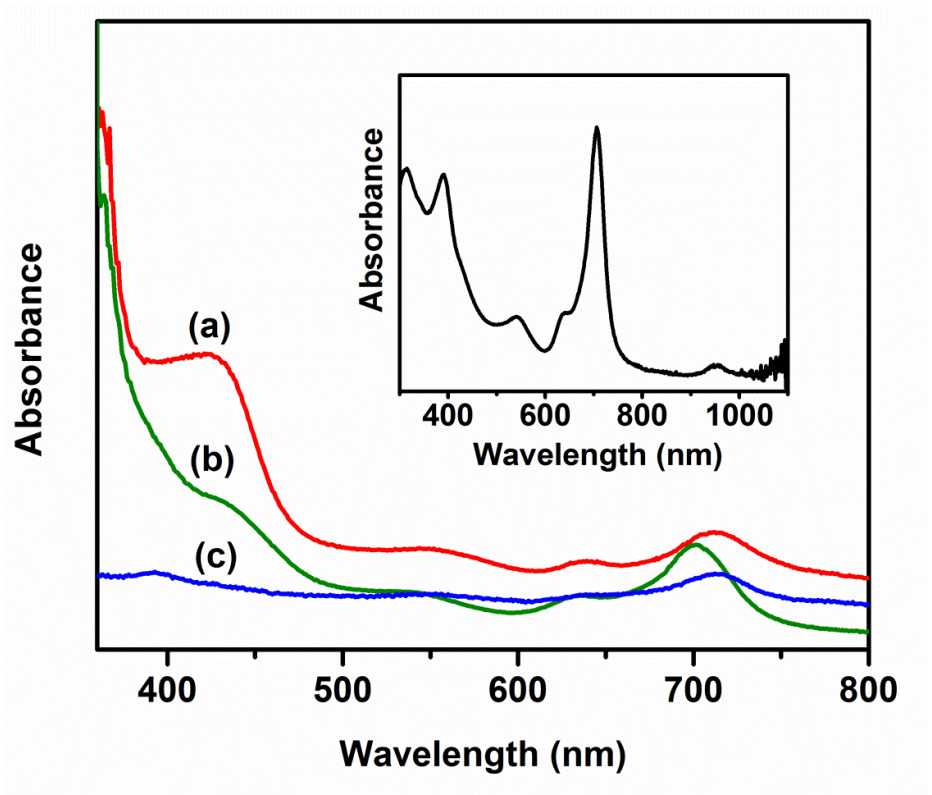

Figure 4-4 UV-visible spectrum of (a) PAA-rGO/VS-PANI/$LuPc_2$-MFH, (b) PAA/VS-PANI/$LuPc_2$-MFH, (c) PAA-rGO/$LuPc_2$ -MFH. Inset UV-visible spectrum of $LuPc_2$ film

Table 4-1 UV-Visible absorption data for MFH and $LuPc_2$ thin films

Sample	N (nm)	B (nm)	Benzenoid to quinoid transitions (nm)	π-radical (nm)	Q (nm)	RV (nm)
$LuPc_2$	317	390	-	543	706	938
PAA-rGO/VS-PANI/$LuPc_2$	-	342	430	546	712	-
PAA/VS-PANI/$LuPc_2$	-	356	432	543	702	-
PAA-rGO/$LuPc_2$	-	385	-	559	718	-

4.3.4. FT-IR analysis

The FT-IR spectra of PAA-rGO/VS-PANI-MFH, PAA/VS-PANI-MFH and PAA-rGO-MFH are shown in Figure 4-5. PAA-rGO/VS-PANI-MFH exhibited the main characteristic absorption peaks of PAA around 2900-3600 cm^{-1} (-OH stretching), 1700 cm^{-1} (C=O stretching) and VS-PANI around 1450 cm^{-1} (benzenoid rings), 1620 cm^{-1} (quinoid rings) (Kennedy and Ratner, 1995; Saravanan et al., 2006; Nabid et al., 2007) curve (a). The absence of 1180 cm^{-1} peak in PAA/VS-PANI/$LuPc_2$ curve (b) and the suppression of 1450 cm^{-1} absorption peak in PAA-rGO/$LuPc_2$ curve (c) can be noticed which illustrates the difference in structure among the three prepared MFH.

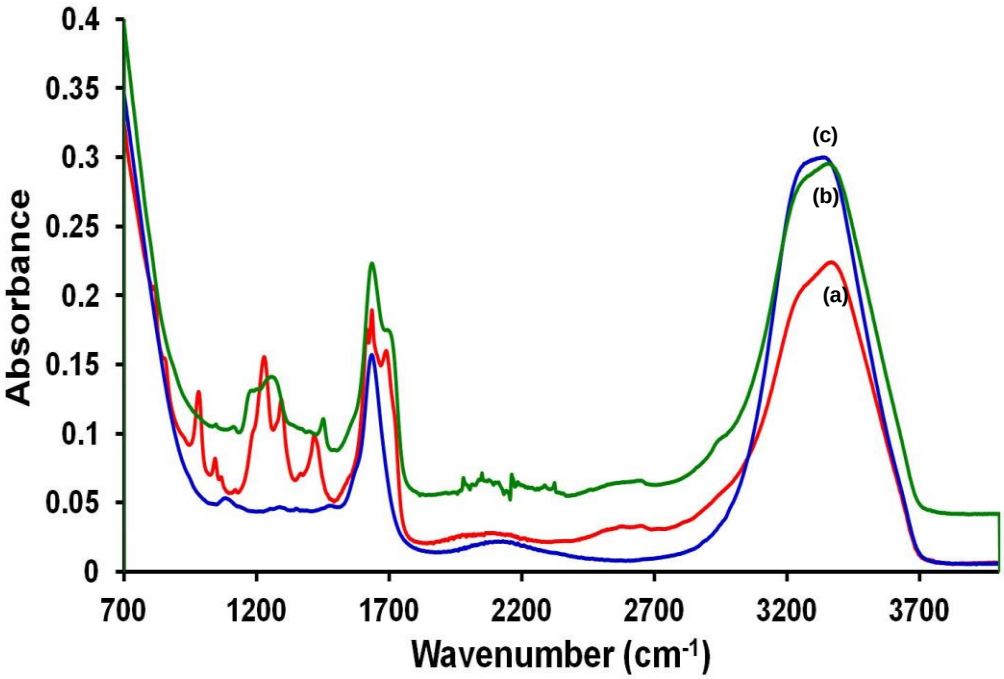

Figure 4-5 FT-IR spectra of (a) PAA-rGO/VS-PANI/$LuPc_2$-MFH, (b) PAA/VS-PANI/$LuPc_2$-MFH, (c) PAA-rGO/$LuPc_2$ -MFH

4.3.5. Electrochemical performance of modified electrodes

Cyclic voltammograms (CVs) were recorded for the PAA-rGO/VS-PANI/$LuPc_2$/GOx-MFH, PAA/VS-PANI/$LuPc_2$/GOx-MFH, and PAA-rGO/$LuPc_2$/GOx-MFH biosensor using 5 mM potassium ferro/ferricyanide solution containing 0.1M NaCl as the bench mark redox system in the potential range from +0.5 to -0.5 V versus silver-silver

chloride electrode (Ag/AgCl) at a scan rate of 0.025 Vs^{-1} , as shown in Figure 4-6. CVs of MFH based biosensor showed well-defined reversible peaks corresponding to the Fe(II)/Fe(III) redox transition process. The efficacy of the electrode was compared in terms of anodic to cathodic peak potential separation (ΔEp = Epa-Epc) and using oxidation or reduction peak currents (I_{pa} or I_{pc}) of the $Fe(CN)_6^{3-/4-}$.

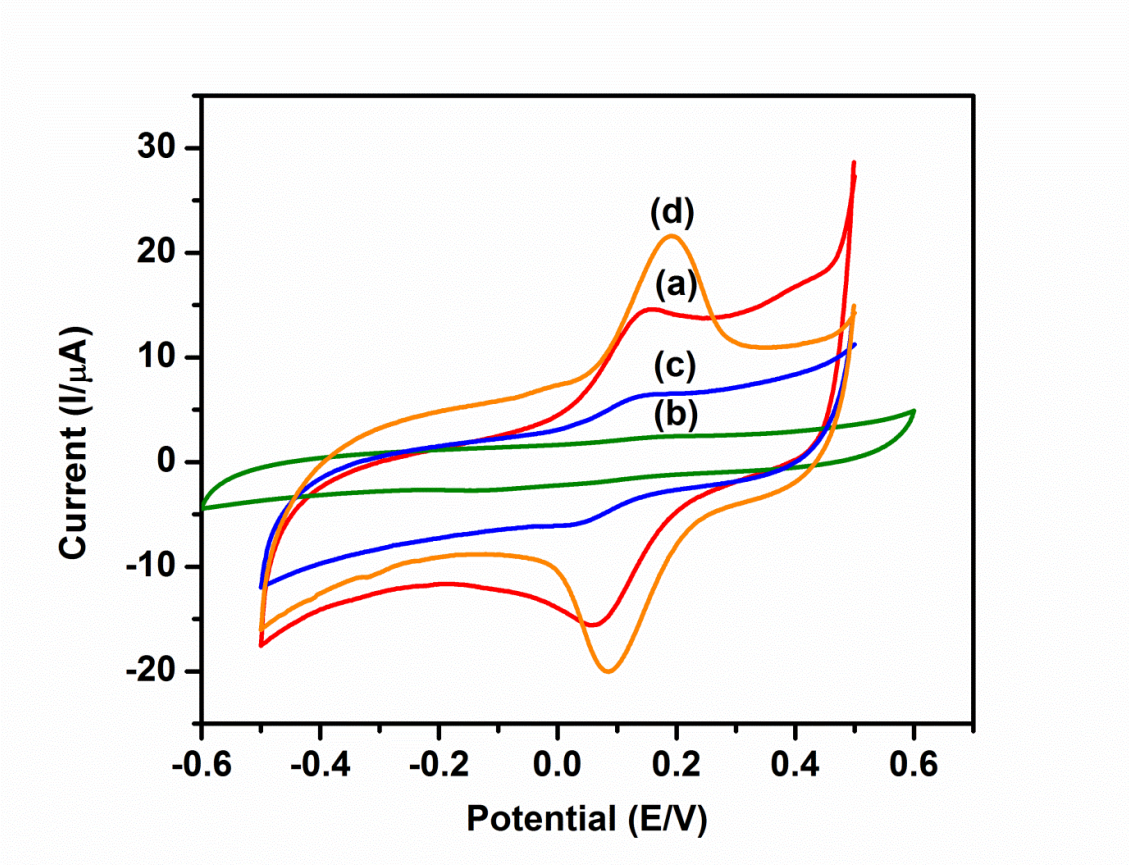

Figure 4-6 Cyclic voltammogram of (a) PAA-rGO/VS-PANI/$LuPc_2$/GOx-MFH, (b) PAA/VS-PANI/$LuPc_2$/GOx-MFH, (c) PAA-rGO/$LuPc_2$/GOx-MFH, (d) PAA-rGO/VS-PANI/$LuPc_2$-MFH recorded in 5 mM Potassium ferro/ferri cyanide solution containing 0.1M NaCl as a supporting electrolyte versus Ag/AgCl; scan rate = 25 mV/s

The I_{pa} of PAA-rGO/VS-PANI/$LuPc_2$/GOx-MFH Figure 4-6 (a) was ~2.32 and ~6.38 times higher than those exhibited by PAA/VS-PANI/$LuPc_2$/GOx-MFH Figure 4-6 (b) and PAA-rGO/$LuPc_2$/GOx-MFH biosensor Figure 4-6 (c). However the I_{pa} of PAA-rGO/VS-PANI/$LuPc_2$/GOx-MFH (14.55 μA) was typically lower than the pristine PAA-rGO/VS-PANI/$LuPc_2$-MFH (21.6 μA) Figure 4-6 (d) prepared in the absence of

GOx. This ensures the effective immobilisation of GOx onto PAA-rGO/VS-PANI/$LuPc_2$-MFH matrix (Hua et al., 2012). Furthermore the ΔE_p value increased from 105 mV for the PAA-rGO/VS-PANI/$LuPc_2$/GOx-MFH to 240 mV for the PAA-rGO/$LuPc_2$/GOx-MFH. The results demonstrates that the presence of VS-PANI as interconnecting network in MFH augment electronic conductivity and promote faster electron transport kinetics at PAA-rGO/VS-PANI/$LuPc_2$/GOx-MFH (Dou et al., 2016). CVs of PAA-rGO/VS-PANI/$LuPc_2$/GOx-MFH were also recorded for different scan rates (10–100 mV/s) Figure 4-7A. A plot of I_{pa} and I_{pc} were linearly proportional to square root υ, which indicates a diffusion controlled process of $Fe(CN)_6^{3-/4-}$ redox reaction at PAA-rGO/VS-PANI/$LuPc_2$/GOx-MFH as explained in Figure 4-7B (Mashazi et al., 2006). From the plot of I_{pa} versus $\upsilon^{1/2}$ a slope of 1.194×10^{-4} A $V^{-1/2}$ $s^{1/2}$ was obtained. For the diffusion controlled reversible process the electrochemical active surface area (A) was determined using Randles–Sevcik equation (Siswana et al., 2006). From the D value for $K_3[Fe(CN)_6] = 6.7 \times 10^{-6}$ cm^2 s^{-1} (Ye et al., 2005), and n = 1, the area ('A') of PAA-rGO/VS-PANI/$LuPc_2$/GOx-MFH was estimated to be 0.244 cm^2. The value of 'A' of PAA-rGO/VS-PANI/$LuPc_2$/GOx-MFH was found to be higher than that of the bare GCE (0.078 cm^2), GOx/PANI microtube/GCE (0.156 cm^2) (L. Zhang et al., 2015) and rGO-C60/GOx (0.12 cm^2) (Thirumalraj et al., 2015) respectively. It is understood that the high value of 'A' results from the porous structure of PAA-rGO/VS-PANI-MFH as seen in Figure 4-3 (a). Furthermore, swelling ratio of PAA-rGO/VS-PANI-MFH is found to be approximately 3 and 1.4 times higher than PAA/VS-PANI -MFH and PAA-rGO-MFH respectively at a fixed time. The higher swelling ratio value results from more pore volume at PAA-rGO/VS-PANI-MFH, where the larger the pore volume leads to lower diffusional resistance.

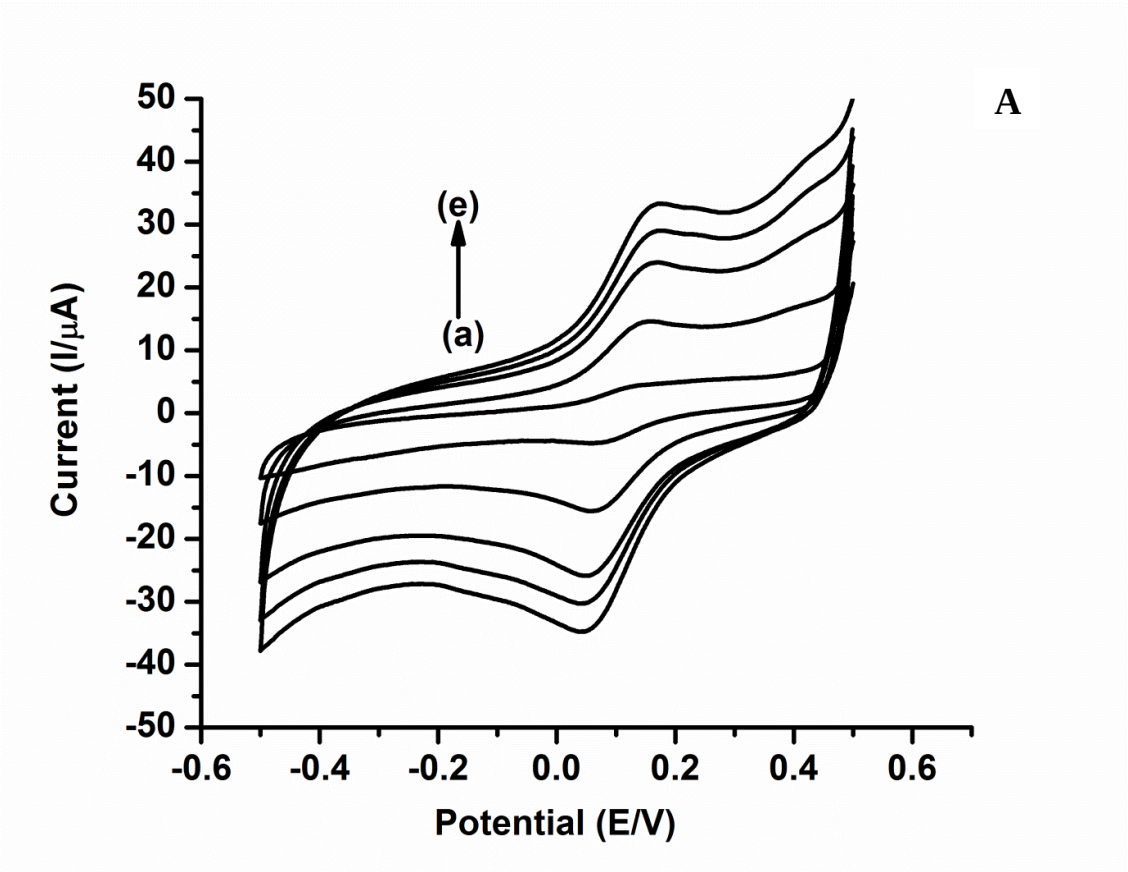

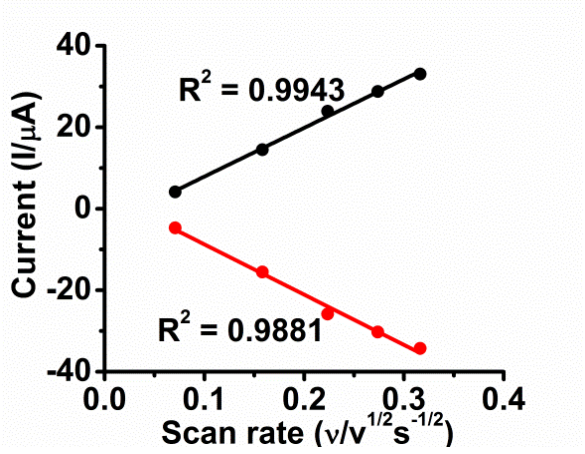

Figure 4-7 (A) Cyclic voltammograms (CVs) of PAA-rGO/VS-PANI/LuPc$_2$/GOx-MFH in 5 mM of Fe(CN)63−/4− containing 0.1 M NaCl versus Ag/AgCl for different scan rates (a–e); 5-100 mVs-1; (B) Dependence of peak current on scan rates

4.3.6. Electrochemical impedance measurements

The electrochemical surface characteristics of the electrodes modified with PAA-rGO/VS-PANI/$LuPc_2$/GOx-MFH (a) and PAA/VS-PANI/$LuPc_2$/GOx-MFH (b) were monitored through electrochemical impedance measurements in PBS containing 0.1M NaCl (Figure 4-8). The immobilisation of GOx enzyme onto the porous sites of the hydrogel alters the interfacial capacitance and electron-transfer resistance of the conductive electrodes (Ding et al., 2005; Katz and Willner, 2003; Pei et al., 2001). The Nyquist plot of PAA-rGO/VS-PANI/$LuPc_2$/GOx-MFH biosensor (a) exhibited a much smaller semicircular diameter ascribed to electron-transfer resistance than those observed on PAA/VS-PANI/$LuPc_2$/GOx-MFH (b). The smaller semicircular diameter indicated faster electron transfer kinetics at high frequency region and the linear part at lower frequency region ensures mixed kinetics and diffusion controlled process. The lower charge transfer resistance (R_{ct}) for PAA-rGO/VS-PANI/$LuPc_2$/GOx-MFH biosensor arises from the inter-connected PAA-rGO/VS-PANI network. The $LuPc_2$ decorated inside PAA-rGO/VS-PANI MFH provides easy electron conduction pathways. The impedance spectra obtained were fitted by a simple Randle circuit made up of electrolyte resistance (R_s), electron transfer resistance (R_{et}), double layer capacitance (C_{dl}) and Warburg coefficient (W). Data fitting was carried out using THALES software with a complex non-linear least-squares method. Based on the model, good agreement was achieved over the frequency range 10 Hz and 2MHz between the simulated and experimental results. An equivalent circuit model is presented in (Figure 4-9)

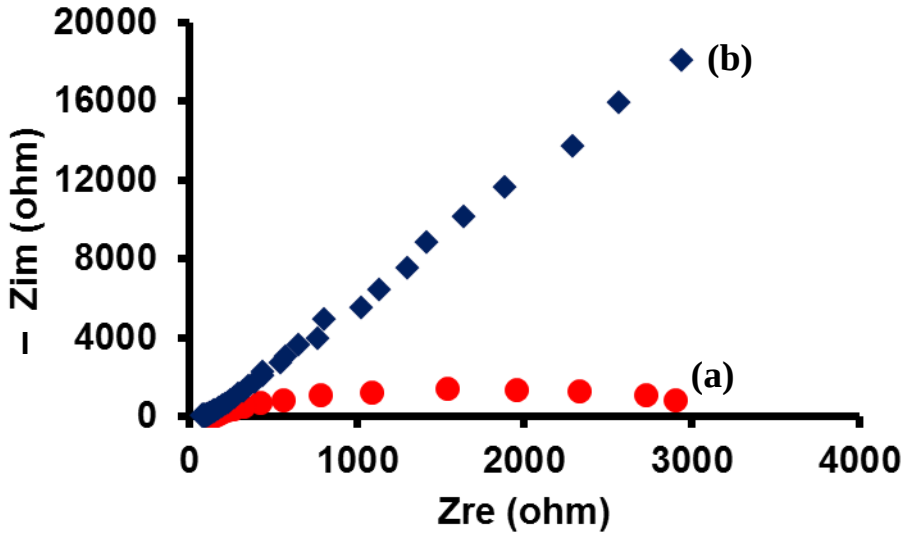

Figure 4-8 Nyquist plots (Z_{im} vs. Z_{re}) of PAA-rGO/VS-PANI/$LuPc_2$/GOx-MFH (a) and PAA/VS-PANI/$LuPc_2$/GOx-MFH (b) in the presence of PBS containing 0.1M NaCl

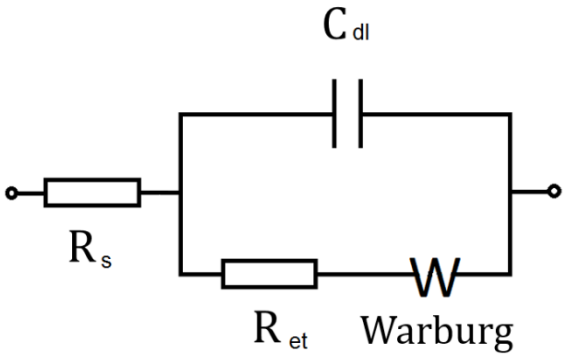

Figure 4-9 Equivalent circuit model for the fabricated biosensor where R_s: the uncompensated solution resistance; R_{et} is the electron transfer resistance; Warburg diffusion element (W) and C_{dl} is the double layer capacitance

4.3.7. Electrochemical detection of glucose

Figure 4-10 shows the CV of PAA-rGO/VS-PANI/$LuPc_2$/GOx-MFH biosensor; Figure 4-10 (red curve) in bare PBS (pH 7.0) and in the presence of glucose (4mM) Figure 4-10 (black curve). At PAA-rGO/VS-PANI/$LuPc_2$/GOx-MFH a reversible redox peak which corresponds to Lu(II)Pc_2/ Lu(III)Pc_2 was observed at -0.05 V/0.1 V under our experimental conditions, and this result is similar to results reported by Kadish et al.

(2001). In the latter reference only one reduction and oxidation peak of $Lu(Pc)_2$ have been reported in a cast film in aqueous media (0.5 M KCl). For further confirmation, CV was also recorded for PAA-rGO/VS-PANI/$LuPc_2$-MFH in the absence of GOx, where a sharp redox couple at -0.12/ 0.1 V was obtained under identical conditions (Figure 4-10 inset). Figure 4-10 (black curve) shows the electrocatalytic oxidation of glucose (4 mM) at PAA-rGO/VS-PANI/$LuPc_2$/GOx-MFH. With the addition of glucose a large increase in anodic current, starting above 0.2 V was observed. This suggests that Lu(III)Pc_2 mediates electron transfer between the immobilised GOx and the electrode through oxidation of the reduced form of the enzyme. The plausible mechanism is as follows,

$$GOx(FAD) + Glucose + O_2 \rightarrow GOx(FADH_2) + Gluconolactone + H_2O_2 \quad (1)$$

$$GOx(FADH_2) + 2[Lu(III)Pc_2] + H_2O_2 \rightarrow GOx(FAD) + 2[Lu(II)Pc_2] + O_2 + 2H^+ \quad (2)$$

$$2[Lu(II)Pc_2] + 2H^+ \rightarrow 2[Lu(III)Pc_2] + 2e^- \quad (3)$$

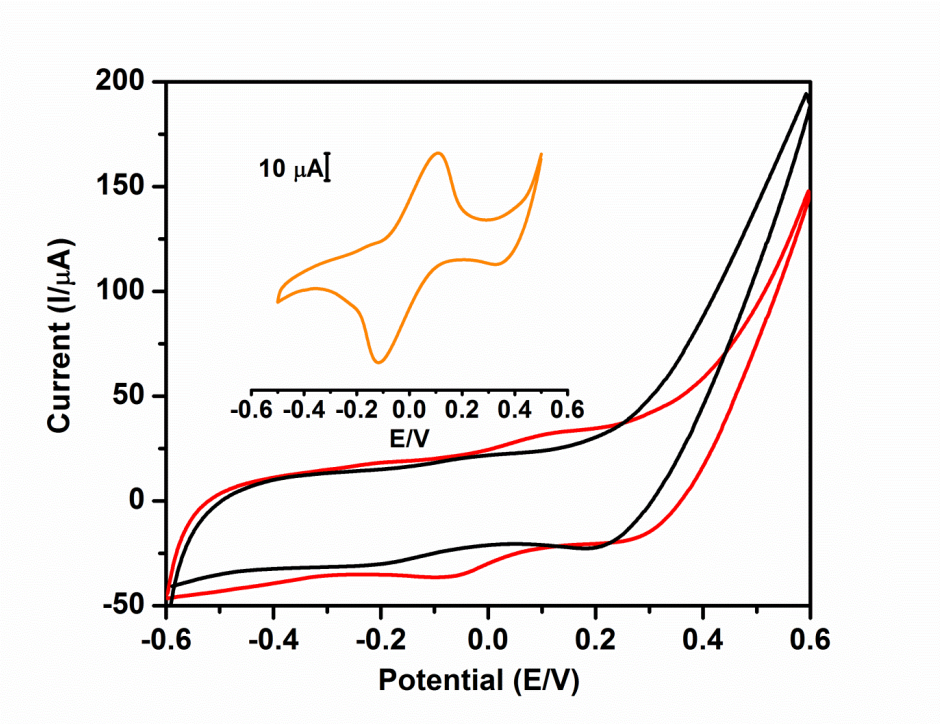

Figure 4-10 Cyclic voltammogram of PAA-rGO/VS-PANI/LuPc$_2$/GOx-MFH (red line) 0 mM glucose and (black line) 4 mM glucose in 0.1M PBS (pH 7.0) versus Ag/AgCl. Inset, Cyclic voltammogram of PAA-rGO/VS-PANI/LuPc$_2$-MFH in 0.1M PBS (pH 7.0)

Glucose is transferred from bulk solution to the PAA-rGO/VS-PANI/LuPc$_2$/GOx-MFH biosensor through diffusion. The enzyme GOx(FAD) in the presence of the natural co-substrate O_2, converts glucose to gluconic acid and O_2 to H_2O_2. The reduced GOx($FADH_2$) will be reoxidized by Lu(III)Pc_2 which exists in the MFH. The reduced mediator, Lu(II)Pc_2 which remains intact inside the MFH, is completely oxidized back to Lu(III)Pc_2 when the anodic potential is applied, resulting in high currents. A similar mechanism was reported for the electrochemical determination of glucose by GOx and the mediator by the Mn(III)-M(IV) tetra(o-aminophenyl)rphyrin couple (Rishpon et al., 1991), cobalt(II) phthalocyanine–cobalt(II) tetra(5-phenoxy-10,15,20-triphenylporphyrin), (CoPc–$(CoTPP)_4$) pentamer (Ozoemena and Nyokong, 2006) and Au-ME-CoTCAPc SAM (Mashazi et al., 2006). However electrocatalytic oxidation of glucose at PAA/VS-PANI/LuPc$_2$/GOx-MFH and PAA-rGO/LuPc$_2$/GOx-MFH showed only a marginal increase in the anodic current value (Figure 4-11). This confirms the

importance of individual component (PAA, rGO, and VS-PANI) as interconnected network in the hydrogel. To ascertain the importance of $LuPc_2$ and GOx in MFH for glucose sensing, a similar MFH biosensor was fabricated without loading $LuPc_2$ and GOx immobilisation. MFH biosensor in the absence of GOx does not show glucose response in the applied potential region. However, for MFH biosensor in the absence of $LuPc_2$, the oxidation glucose response current was feeble. This further ensures the significance of combined presence of $LuPc_2$ and GOx in MFH for good electrochemical glucose determination.

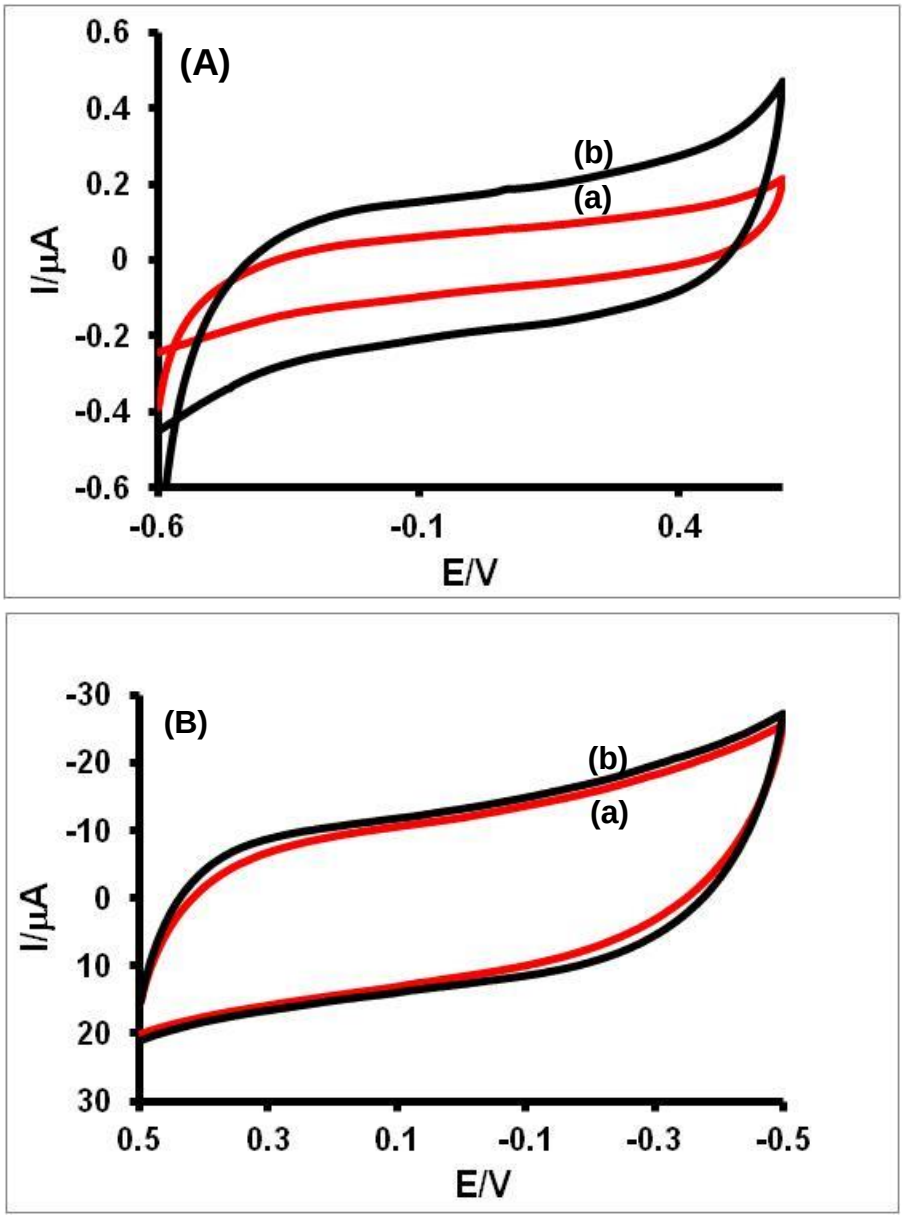

Figure 4-11 Cyclic voltammogram of (A) PAA/VS-PANI/$LuPc_2$/GOx-MFH, (B) PAA-rGO/$LuPc_2$/GOx-MFH for (a) 0 mM glucose (b) 4 mM glucose in 0.1M PBS (pH 7.0) versus Ag/AgCl

4.3.8. Amperometric response of glucose at PAA-rGO/VS-PANI/$LuPc_2$/GOx-MFH biosensor

To demonstrate the functioning of PAA-rGO/VS-PANI/$LuPc_2$/GOx-MFH as a potential glucose biosensor, amperometric measurements were recorded for varied glucose concentration as shown in Figure 4-12.

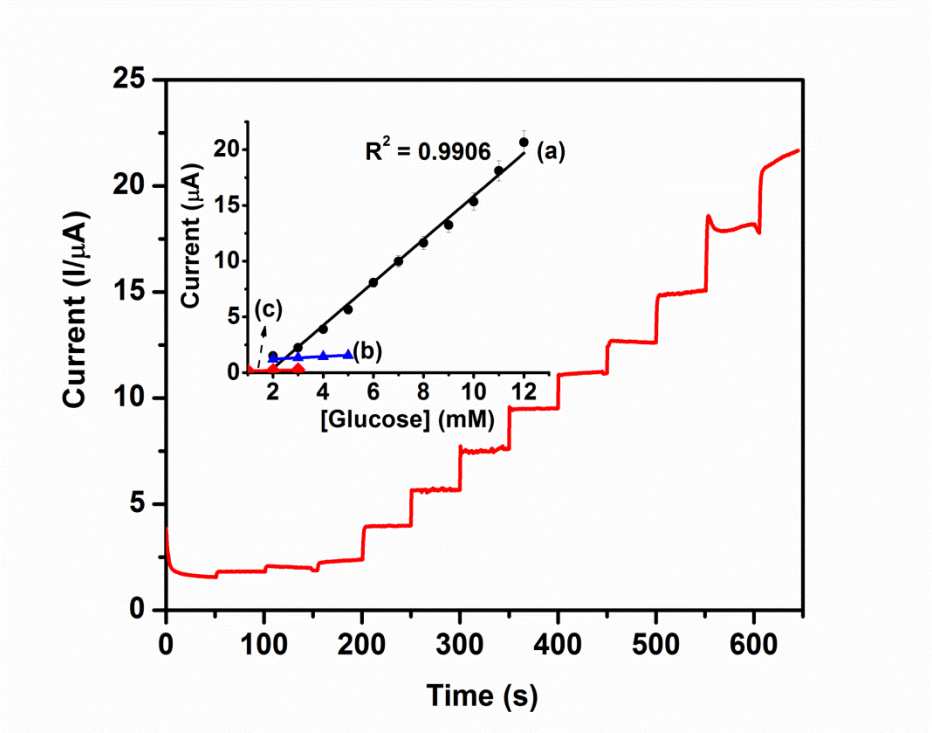

Figure 4-12 Amperometry of PAA-rGO/VS-PANI/$LuPc_2$/GOx-MFH for successive addition of glucose in 0.1M PBS (pH 7.0). Inset: calibration plot peak current versus [glucose]

The bioelectrocatalytic current response for the successive additions of 1 mM glucose was monitored amperometrically under stirred condition. The PAA-rGO/VS-PANI/$LuPc_2$/GOx-MFH biosensor showed a rapid response to the changes in glucose concentration and the steady-state response current reached within 1s. The response time is much lower than PANI incorporated silica particles (Manesh et al., 2010), MWNT-g–SPAN-NW GOx based biosensors (Kwang Pill Lee et al., 2010), GOx/PtNP/PAni hydrogel/Pt (Zhai et al., 2013), and GOx/GNp/CS/GOx/GNp/PAA/Pt (Wu et al., 2007). The reduced amperometric response time observed here is attributed

to the faster diffusion of glucose into the porous three-dimensional PAA-rGO/VS-PANI MFH. The rapid response to glucose was also achieved due to the existence of $LuPc_2$ that transfers electrons at a fast pace from GOx to MFH (Koide and Yokoyama, 1999; Dervisevic et al., 2014). The amperometric *i–t* response current of the biosensor is linear in the range of 2–12 mM concentration of glucose (R^2 = 0.9903) as shown in Figure 4-12(Inset, line (a)) with the sensitivity of 15.31 μA mM^{-1} cm^{-2} calculated from the slope of the calibration plot. The sensitivity is higher than those of 5.2 μA cm^{-2} mM^{-1} for GOD immobilised in an osmium-based three-dimensional redox hydrogel (Ohara et al., 1994), 1.7 μA cm^{-2} mM^{-1} for GOD formed upon cross-linking with the copolymer hydrogels (Lumley-Woodyear et al., 1995). To illustrate the importance of $LuPc_2$ and GOx in the fabrication of glucose biosensor, the amperometric *i-t* response for glucose was also observed for electrodes PAA-rGO/VS-PANI/$LuPc_2$-MFH and pristine PAA-rGO/VS-PANI-MFH (both fabricated without GOx). Typically, the electrodes exhibited a linear range from 2-5 mM (PAA-rGO/VS-PANI/$LuPc_2$-MFH) as shown in Figure 4-12(Inset, line (b)) and 1-3 mM (pristine PAA-rGO/VS-PANI-MFH) as shown in Figure 4-12(Inset, line (c)) of glucose respectively. The linear range of glucose detection for pristine PAA-rGO/VS-PANI-MFH and PAA-rGO/VS-PANI/$LuPc_2$-MFH are relatively lower than PAA-rGO/VS-PANI/$LuPc_2$/GOx-MFH biosensor. Furthermore, the sensitivity of PAA-rGO/VS-PANI/$LuPc_2$-MFH (0.912 μA mM^{-1} cm^{-2}) and pristine PAA-rGO/VS-PANI-MFH (0.455 μA mM^{-1} cm^{-2}) are ~16.8 and ~33.6 times lower than PAA-rGO/VS-PANI/$LuPc_2$/GOx-MFH biosensor. The smaller linear range along with lowered sensitivity value in the case of PAA-rGO/VS-PANI/$LuPc_2$-MFH and pristine PAA-rGO/VS-PANI-MFH might be due the blockage of pores in the hydrogel structures by the oxidised products of glucose which in-turn hampered the diffusion of glucose molecules to the electrode surface. However, the obtained longer linear response of PAA-rGO/VS-PANI/$LuPc_2$/GOx-MFH biosensor (2-12 mM) to glucose is

suitable for glucose detection in human blood samples (normal glucose range in human blood is 4.4–6.6 mM). The wide linear range with high sensitivity of PAA-rGO/VS-PANI/$LuPc_2$/GOx-MFH biosensor for the amperometric detection of glucose may be due to the following facts. The porous three dimensional PAA-rGO/VS-PANI MFH matrices offer low diffusional resistance to glucose and hence reduces the mass transport barrier. rGO and VS-PANI as interconnected network within hydrogel provide electronic conductivity to achieve fast electron transport. PAA based hydrogel creates favourable environment for loading $LuPc_2$ and GOx enzyme immobilisation (Y. Zhao et al., 2013). The results obtained from the amperometric current response of glucose at PAA-rGO/VS-PANI/$LuPc_2$-MFH and pristine PAA-rGO/VS-PANI-MFH electrodes illustrate that GOx plays the key component in the detection of glucose and $LuPc_2$ effectively transfers electrons from GOx to the electronically conducting hydrogel matrix.

Optimisation studies were performed with the PAA-rGO/VS-PANI/$LuPc_2$/GOx-MFH biosensor in stirred solution was found to be dependent on pH. Figure 4-13 shows the effect of pH on the oxidation current of glucose at the PAA-rGO/VS-PANI/$LuPc_2$/GOx-MFH biosensor. Initially the current value rises at pH 2.0 and then found to be decreased; later at around pH 7.0, the oxidation current increases steeply, then reaches a maximum value. Hence 0.1 M PBS (pH 7.0) is chosen as a medium buffer for further determination of glucose.

The effect of potential on the steady-state current for the PAA-rGO/VS-PANI/$LuPc_2$/GOx-MFH biosensor is studied. The applied potential of +0.3 V to +0.6 V in 0.1 M PBS (pH 7.0) does not show significant variation in the response current of glucose and hence +0.3 V is chosen as the applied potential for amperometric detection of glucose concentration.

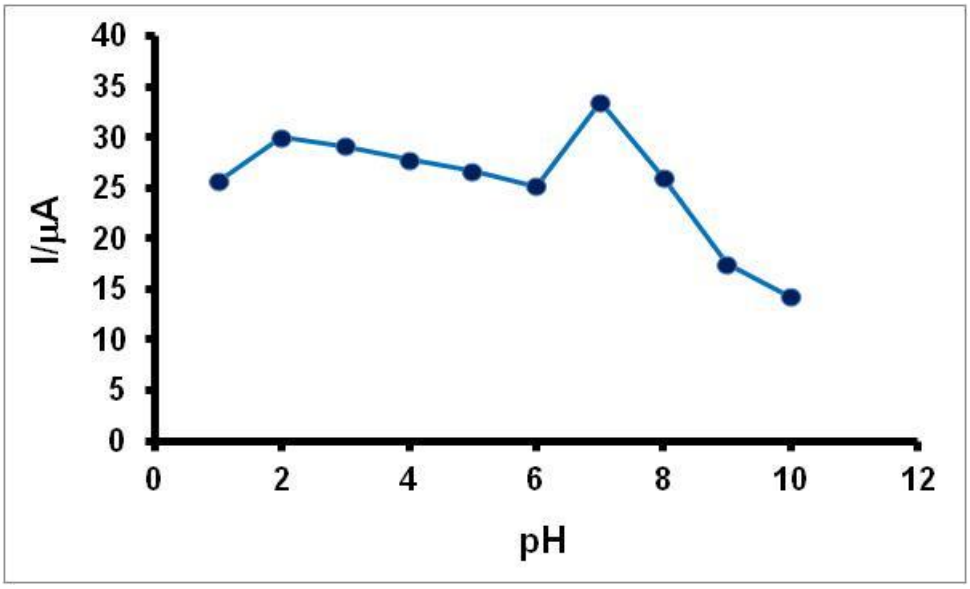

Figure 4-13 Effect of pH on the current response of glucose at PAA-rGO/VS-PANI/LuPc$_2$/GOx-MFH biosensor

The apparent Michaelis–Menten constant (K_M) was calculated as 17.05 mM using the slope and intercept values from Lineweaver–Burk plot for PAA-rGO/VS-PANI/LuPc$_2$/GOx-MFH biosensor (Iwuoha and Smyth, 1997). The K_M value obtained for this biosensor is higher than other GOx-mediator based glucose sensors (Ghica and Brett, 2005). The high value of K_M informs that the GOx in the PAA-rGO/VS-PANI/LuPc$_2$/GOx-MFH biosensor possesses higher affinity for glucose. The limit of detection (LOD) for glucose at PAA-rGO/VS-PANI/LuPc$_2$/GOx-MFH biosensor was calculated as 25 μM (signal to noise ratio = 3). The detection limit is estimated as three times of the standard deviation of the background. The LOD value was lower than Ru mediator attached PVPAA copolymer/GOx biosensor (Deng, et al, 2014). In enzymless detection of glucose a LOD in the nano mole range has been found for Cu/3D graphene hybrid-based electrode (Hussain et al., 2015).

The analytical performance of the proposed sensor are compared with similar enzyme/mediator based glucose biosensors and presented in Table 4-2. From the Table

4-2 values it is understood that the proposed PAA-rGO/VS-PANI/$LuPc_2$/GOx-MFH biosensor exhibits wide linear range response to glucose, high sensitivity and low LOD.

Table 4-2 Comparison of analytical performance of some glucose biosensors

Electrode	Response time (s)	Iinear range (mM)	Sensitivity ($\mu A\ mM^{-1}\ cm^{-2}$)	LOD (μM)	Ref.
Au-MPS-OsPVP-GOx	5	0.1–10	-	50	(Hou et al., 1998)
SPCE/CoPC/GOD	60	0.2–5	1.12	-	(Crouch et al., 2005)
GCE–CoPc–$(CoTPP)_4$–GOx	~5	up to 11	0.024	10	(Ozoemena and Nyokong, 2006)
{GOx/Au-(SH)PANI-g-MWNT}*n*/ITO	~8	1–9	3.97	0.06	(Komathi et al., 2009a)
GOx-nanoPANi/Pt	3	0.01-5.5	97.18±4.62	0.3±0.1	(Wang et al., 2009)
GOx-PANI nanowire	10	0–8	2.5	0.05	(Horng et al., 2009)
GOD/ERGO/PLL/GC	-	0.25 - 5	-	-	(Hua et al., 2012)
Nafion-GOx-ordered mesoporous carbon	9±1	5-15	0.053	156.52	(Zhou et al., 2008)
Os(2,2′bpy)2-RP/GOx	<5	0-10	16.5	-	(Deng et al., 2013)
poly(GMA-co-VFc)-GOx	1	1-17	0.27	33	(Dervisevic et al., 2014)
Au/CA/(GOx/TFGn)n	6	1-13 mM	19.9	-	(Ren et al., 2016)
Hedgehog-like NiO nanostructures	-	0.1–5.0 μM	1052.8	1.2	(Soomro et al., 2015)
PAA-rGO/VS-PANI/$LuPc_2$/GOx-MFH	~1	2-12	15.31	25	Our present work

4.3.9. Repeatability, Reproducibility and stability of PAA-rGO/VS-PANI/$LuPc_2$/GOx-MFH biosensor

Different aspects concerning the utility of PAA-rGO/VS-PANI/$LuPc_2$/GOx-MFH as sensible glucose biosensor were evaluated. The repeatability of PAA-rGO/VS-PANI/$LuPc_2$/GOx-MFH as sensible glucose biosensor was tested through amperometric measurements for two different concentrations of glucose, 4 mM and 6 mM Figure 4-14.

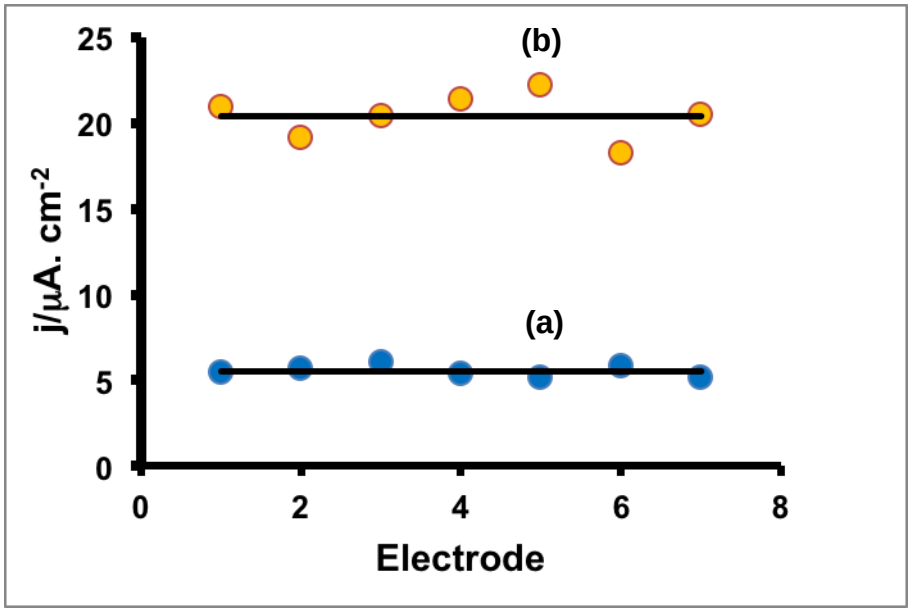

Figure 4-14 Amperometric response of (a) 4 mM (b) 6 mM at PAA/VS-PANI/$LuPc_2$/GOx-MFH biosensor

Seven repetitive measurements of a single PAA-rGO/VS-PANI/$LuPc_2$/GOx-MFH biosensor (washed with 0.1M PBS between individual measurements) yielded a relative standard deviation (RSD) value of 6.1% (4 mM) and 6.5% (6 mM) of glucose. To demonstrate the stability of fabricated PAA-rGO/VS-PANI/$LuPc_2$/GOx-MFH biosensor, amperometric response to 4 mM glucose solution was periodically registered for a period of 3 months keeping the electrodes stored at 4 °C refrigerated condition. It has been found that the PAA-rGO/VS-PANI/$LuPc_2$/GOx-MFH biosensor retained > 98% of current response which indicates that the functioning of GOx well protected

within the new MFH without leaching under ideal conditions. The leaching effect of $LuPc_2$ from the fabricated PAA-rGO/VS-PANI/$LuPc_2$-MFH was investigated by recording UV-visible spectrum before and after immersion into 0.1M PBS for a time period of 30 minutes (time taken to record amperometry). From the characteristic B and Q band absorption peaks of $LuPc_2$ it is confirmed that there is no leaching of $LuPc_2$ from PAA-rGO/VS-PANI/$LuPc_2$-MFH electrode. This may be due to the π-π interaction between the rGO, VS-PANI with double ducker $LuPc_2$ (Fukuda et al., 2012). The reproducibility of PAA-rGO/VS-PANI/$LuPc_2$/GOx-MFH biosensor was estimated with ten similarly fabricated sensor assemblies. The results revealed that the biosensor has a satisfactory reproducibility (RSD = 2.2%, n = 10). Under the applied potential of +0.3 V, the addition of interfering substances such as ascorbic acid and uric acid hardly affects the amperometric response current of glucose (4 mM) Figure 4-15.

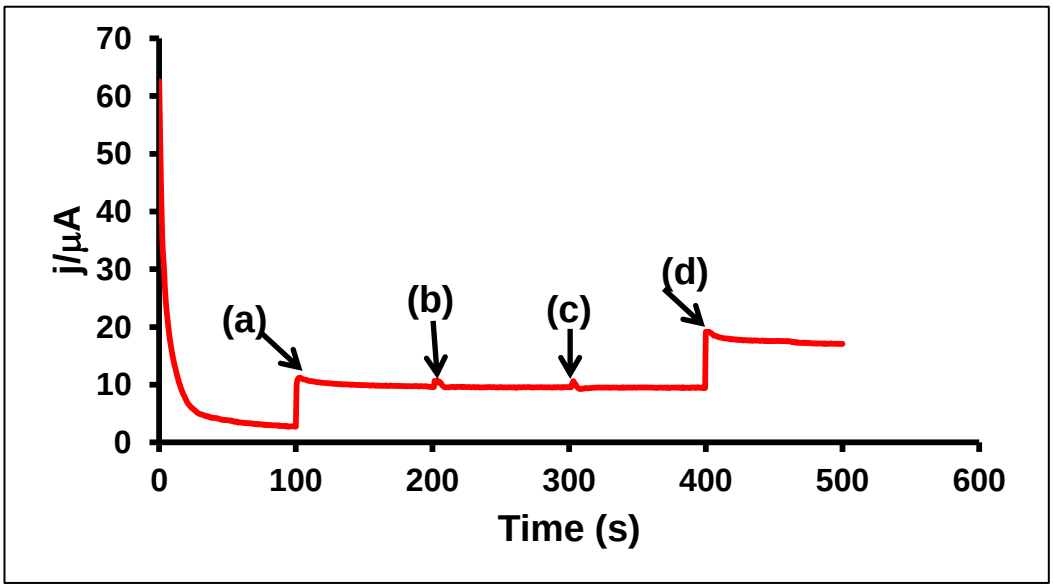

Figure 4-15 Amperometric response of (a) glucose (4 mM); (b) ascorbic acid (0.1 mM); (c) uric acid (0.5 mM); (d) glucose (4 mM) at PAA/VS-PANI/$LuPc_2$/GOx-MFH biosensor

With three repetitive measurements of glucose (4 mM) along-with interfering substances in a single PAA-rGO/VS-PANI/$LuPc_2$/GOx-MFH biosensor, the coefficient of variation (COV) was found to be 10.03%. Also the COV was calculated for the

reproducibility test results of glucose (4 mM) in the presence of interference and was found to be 11.36% (n=5). This shows that PAA-rGO/VS-PANI/$LuPc_2$-MFH biosensor exhibit selective detection of glucose even in the presence of electrochemically active substances.

4.3.10. Glucose determination in real samples at PAA-rGO/VS-PANI/$LuPc_2$/GOx-MFH biosensor

To illustrate the feasibility of PAA-rGO/VS-PANI/$LuPc_2$/GOx-MFH as a potential biosensor in industrial as well in clinical diagnosis, real sample analysis was carried out. In our work, commercial glucose samples and human serum obtained from Biomolecular Sciences Research Centre at Sheffield Hallam University were suitably diluted using 0.1 M PBS (pH 7.0) to obtain required concentration sample solutions. A continuous amperometry was recorded for varied additions of real samples under identical experimental conditions as similar to Figure 4-12. PAA-rGO/VS-PANI/$LuPc_2$/GOx-MFH biosensor exhibited response to all the real samples added. The data obtained from analysis are summarized in Figure 4-16 and table 4-3. The results obtained are satisfactory with an error percentage of +3.0. The satisfactory results demonstrate good practical applicability of the proposed biosensor.

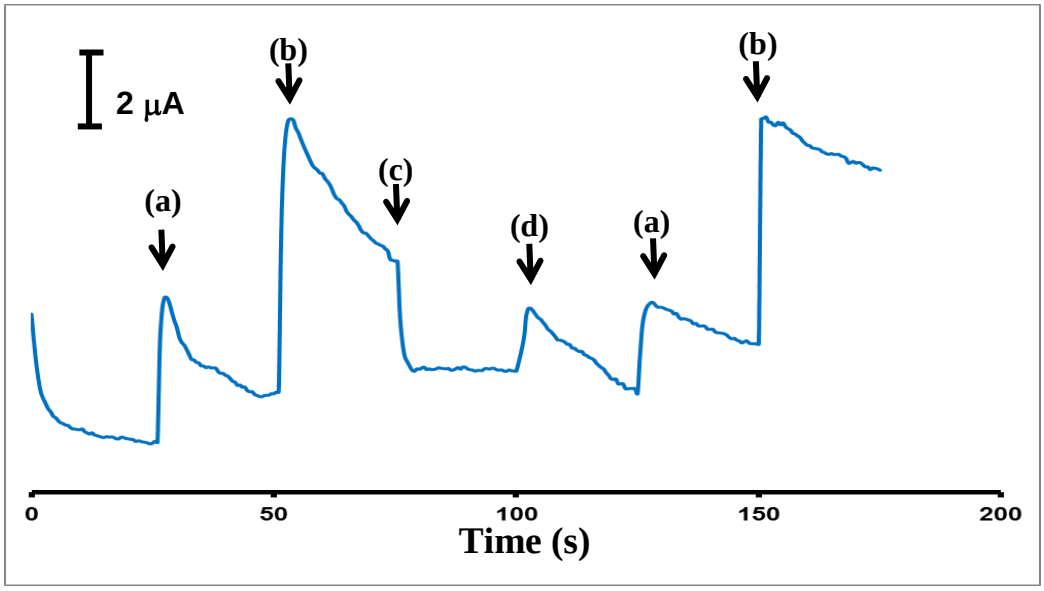

Figure 4-16 Amperometric responses of real samples (a) glucose, (b) juice 1, (c) juice 2, (d) human serum, at PAA/VS-PANI/LuPc$_2$/GOx-MFH biosensor at an applied potential of +0.3 V

Table 4-3 Amperometric responses of real samples

Real samples	Added (according to specification in the label) (mM)	Found (mM)	Recovery (%)
Glucose	4	4.13	103.25
Juice 1	7.5	7.78	103.76
Juice 2	2.5	2.44	97.6
Human serum	-	3.86	-

4.4. Conclusions

In this work, we demonstrate the synthesis of multifunctional conducting polyacrylic acid (PAA) hydrogel (MFH) integrated with reduced grapheme oxide (rGO) and vinyl substituted polyaniline (VS-PANI) (PAA-rGO/VS-PANI-MFH). A redox mediator based glucose biosensor was constructed by loading lutetium phthalocyanine ($LuPc_2$) and glucose oxidase (GOx) into PAA-rGO/VS-PANI-MFH matrix (PAA-rGO/VS-PANI/$LuPc_2$/GOx-MFH). The structural stability and hierarchical porosity of PAA-rGO/VS-PANI-MFH resulted in large surface area for GOx immobilisation. The high electrical conductivity is achieved through interconnected VS-PANI network for rapid mass/charge transport. $LuPc_2$ functions as an excellent redox mediator and reduces the amperometric glucose detection potential to +0.3 V. The present work demonstrates that the multi-components (rGO,VS-PANI, and $LuPc_2$) have synergistic influences on the performance of biosensor. The PAA-rGO/VS-PANI/$LuPc_2$/GOx-MFH biosensor exhibits wide linear range and high sensitivity to glucose with a low detection limit. PAA-rGO/VS-PANI/$LuPc_2$/GOx-MFH could be effectively used as an electrochemical biosensor in industrial as well clinical diagnosis. Further, the MFH provides scope for loading of other redox enzymes to fabricate high performance biosensors.

Chapter: 5 Water processable iron phthalocyanine-based conducting hydrogel for glucose biosensing

Chapter overview

This chapter introduces a new glucose biosensor platform based on water processable iron phthalocyanine (FePc) functionalised graphene nanoplatelets (GPL) dispersed polyacrylic acid (PAA)-based three-dimensional conducting hydrogel (PAA-CP/GPL-FePc/GOx-CH). The processability of FePc was achieved through the quaternized cationic 5-(trifluoromethyl)-2-N-methylmercaptopyridine substituents onto FePc moieties. The water-soluble FePc was non-covalently functionalised to the graphene platelets to control aggregation in the formed hydrogel. The FePc role into the structure of the conducting hydrogel has been discussed in sufficient detail. Full characterisation of the raw materials and the prepared platforms is also presented, and results are discussed. The fabrication of the biosensor platform by immobilising GOx into the conducting hydrogel and its use in electrochemical detection of glucose has been fully analysed and conclusions are made. The chapter also provides a thorough analysis of the potential use of the prepared biosensor platform to monitor glucose concentrations over a sufficiently wide range and compares the device sensitivity and lower detection level with the available data in the literature.

5.1. Introduction

Metallophthalocyanines (MPcs) has frequently been linked to the development of devices employed in bio-detection and chemical sensing. They have been utilised in many applications, for instance, as a tumor-targeting in photodynamic therapy (Carrión, 2018), dopamine's detection as important neurotransmitter (Martin et al., 2016), and polyphenol determination in tea samples (Maximino et al., 2016). Iron phthalocyanine (FePc) complexes like many other phthalocyanines family members have been applied

in different applications; FePc is used in the catalytic oxidation of phenols by *tert*-butyl hydroperoxide in the presence of water soluble iron(III) tetra-(4-carboxyphenoxy)phthalocyanine and iron(III) tetra-(8-quinolineoxy-5-sulfonicacid)phthalocyanine (Gong et al., 2014). Metallophthalocyanines (MPcs) are known to exhibit good electrocatalytic activities toward hydrogen peroxide (Mashazi et al., 2006) especially the first transition metals, Fe, Co, Cu, and Ni (J. Han et al., 2017). Modification the MPcs with four sulfuric group (SO_4) allows solubility in water and other solvents which significantly improve their deposition for catalysis applications (Zagal et al., 1980). These water-soluble metallophthalocyanines have attracted interest in a wide range of applications; for instance, Muckley and coworkers have utilised water-soluble copper phthalocyanine to develop a multi-mode humidity sensor (Muckley et al., 2017). High catalytic activity has been the most significant effective feature that has been invested to produce sensing devices based MPcs (Han et al., 2016; Mashazi et al., 2006; Ndiaye et al., 2016; Wang et al., 2005). Therefore, MPcs were found to be a suitable element to establish the basis of electrochemical reaction devices (Chaiyo et al., 2018; Zagal, 1992). Due to the need for neutral and alkaline media at the catalysed redox reactions, the metal macrocyclic catalysts, such as FePc has shown promising catalyst for O_2 reduction in the biological fuel cell applications (Yu et al., 2009). In addition to the biocompatibility (Jia et al., 2017), FePc has shown ability in enhancing hydrogen peroxide (H_2O_2) control (Han et al., 2016), which basically represents the significant outcome in the glucose sensor reactions . Thus, water-soluble FePc is a strong candidate for glucose biodetection and is sought to improve the stability and sensitivity of the bioanalytical sensors as in electrochemical biosensing devices.

Graphene derivatives on the other hand have been used as suitable support materials in the electrochemical biosensing applications (Al-Sagur et al., 2017; Buber et al., 2017;

Chaiyo et al., 2018; Cui et al., 2015; Liu and Long, 2015; Mani et al., 2014). Graphene and its derivatives have become extremely attractive materials in the bioanalytical field for electrodes-based biosensors design due to the unique properties they possess. High surface area, biocompatibility, electrical conductivity, thermal, mechanical, and electrochemical stability are graphene derivatives major properties that make them so special in various applications (Geim and Novoselov, 2007; Liu et al., 2010; Pandey et al., 2017; Zhu et al., 2012). Graphene nanoplatelets (GPL) are one of the ideal graphene derivatives that are employed in chemical sensing, biosensing, and energy storage applications (Martin, 2009). Yue and coworkers have utilised single-layer graphene nanoplatelets (SLGnP) for the fabrication of new nitrite biosensor based on heme protein myoglobin immobilisation. The sensing platform has shown biocompatibility, high conductivity, and high sensitivity (Yue et al., 2011). Graphene nanosheets have covalently conjugated to GOx modified polypyrrole (Ppy) to form stable matrix in the fabrication of electrochemical sensing platform for glucose monitoring purposes (Alwarappan et al., 2010). Extensive research has been carried out to produce stable matrix for enzymes immobilisation with good environmental conditions for applications in the field of electrochemical sensing reactions (Dugas et al., 2010; Lai et al., 2016; Ramanavičius et al., 2006; Singh et al., 2009). Conducting polymers such as hydrogels have been employed as an attractive materials for the purpose of producing three dimensional (3D) structure that provides good biocompatibility and permeability to biochemical solutions such as glucose (Gerard et al., 2002; Guo et al., 2015; Liu et al., 2018).

In our earlier work, PAA-CP hydrogel was employed to form biosensor platform for glucose sensor studies (Al-Sagur et al., 2017). However, $LuPc_2$ was used as mediator in that study where it was introduced into the PAA-CP platform after the formation of the hydrogel. In order to simplify the bioplatform preparation and further improve the

dispersibility of graphene into the hydrogel, the preparation of a new platform was planned with the same PAA-CP gelation polymer but with graphene nanoplates (GPL) non-covalently functionalised with water-soluble iron phthalocyanine (FePc). These substitutions were thought to sufficiently enhance the sensing performance of the formed hydrogel. Although sufficient work has been carried out using metallophthalocyanines as mediators in sensor studies, the use of water processable GPL-FePc into conducting hydrogel platform has not yet been reported.

The aim of the work carried out in this chapter is to produce a new glucose biosensor platform based on water processable iron phthalocyanine (FePc) functionalised graphene nanoplatelets (GPL) dispersed polyacrylic acid (PAA) 3D conducting hydrogel (PAA-CP/GPL-FePc/GOx-CH). The high dispersibility was achieved through the cationic quaternized 5-(trifluoromethyl)-2-N-methylmercaptopyridine substituents on the phthalocyanine macrocycle. The water-soluble FePc was non-covalently functionalised with graphene platelets to control aggregation in the formed hydrogel, PAA-CP/GPL-FePc-CH. The biosensor was fabricated by immobilising GOx onto the conducting hydrogel (PAA-CP/GPL-FePc-CH) and used for electrochemical detection of glucose.

5.2. Experimental details

5.2.1. Materials

Graphene nanoplatelets (GPL) (surface area: an anionic surfactant, sheet resistance 10 (± 5) Ω/sq (for a 25 μm film) and the sheet has been packed at around 5-7 atomic layers), poly(ethylene glycol) diamine (NH_2-PEG-NH_2), N-(3-dimethylaminopropyl)-N′-ethylcarbodiimide hydrochloride (EDC hydrochloride), acrylic acid, 3-vinylaniline (97%), N,N'-methylenebis(acrylamide) (MBA), ammonium persulfate (APS), D-(+)glucose, glucose oxidase from aspergillus niger, Type X-S, lyophilized powder,

100,000–250,000 units/g solid (without added oxygen), glutaraldehyde solution (Grade II, 25% in H_2O), Potassium ferrocyanide, Potassium ferricyanide, potassium chloride (KCl), sodium chloride (NaCl), phosphate buffer solution (PBS, pH 7.0), hydrochloric acid (HCl, 37% solution in water), ascorbic acid, uric acid and human serum were all purchased from Sigma Aldrich (UK) and used as received. FePc was produced by research partners in Gebze Technical University, Turkey; it was synthesised from the precursors 4,5-dichlorophthalonitrile which was synthesised and purified according to reported procedure (Wöhrle et al., 1993). All reaction solvents were dried and purified as described by Perrin and Armarego (Perrin and Armarego, 1989). All other reagents were obtained from commercial suppliers. The purity of the products was tested in each step using thin layer chromatography (TLC) (silica gel).

5.2.2. Measurement instruments and characterisation

The morphologies of the prepared conducting hydrogel were examined by FEI-Nova scanning electron microscopy (SEM) with a low magnification (160,000×) and high voltage (10 kV). UV–visible spectrophotometer (Varian 50-scan UV–Visible) in the range 190–1100 nm was used to measure the absorption spectra of the hydrogel as well as all compounds used in this study. FT-IR spectra were recorded on a Perkin Elmer Spectrum 100 spectrophotometer. The electrochemical measurements of the electrodes were conducted using a portable multi Potentiostat/Galvanostat μStat 8000 and controlled by PC with DropView 8400 software. All the utilised instruments have been described in details in chapter 3. The sensor platforms were disposable screen-printed carbon electrodes DRP-C110 with 4 mm diameter working electrode. The working and auxiliary electrodes are carbon, while silver forms the reference electrode and the träger (carrier) is ceramic. The working electrodes were modified with PAA-CP/GPL-FePc/GOx-CH or PAA-CP/GPL-CH or PAA-CP/FePc-CH. The electroactivity of MFH modified electrode was evaluated by recording cyclic voltammogram in potassium

ferro/ferricyanide solution containing 0.1 M NaCl in the potential range from -0.5V to +0.5V. The biocatalytic activity of PAA-CP/GPL-FePc/GOx-CH biosensor was evaluated by cyclic voltammetry for a solution of 4 mM glucose in 0.1 M PBS. The amperometric responses of PAA-CP/GPL-FePc/GOx-CH biosensor towards glucose detection were recorded under stirred conditions in 0.1 M PBS (pH 7.0) by applying a constant potential of +0.3 V at the working electrode.

5.2.3. Preparation of PAA-CP/GPL-FePc/ GOx-CH biosensor

The preparation of the conducting hydrogel (CH) involves three steps: (1) preparation of FePc functionalised GPL, (2) formation of PAA-CP/GPL-FePc-CH, (3) immobilisation of GOx to form PAA-CP/GPL-FePc/GOx-CH biosensor.

5.2.3.1. Preparation of FePc non-covalently functionalised GPL

Briefly, about 1 mg of FePc was dispersed in 10 mL of dionised water, followed by dispersing 10 mg of GPL in the FePc solution under ultra-sonication for 30 minutes. NH_2-PEG-NH_2 (0.1 g) and EDC.HCl (0.1 g) were then added under vigorous stirring overnight. FePc/GPL-PEG-NH_2 thus obtained were allowed to settle down and filtered through polycarbonate membrane (pore size=200 nm). The samples were dried in vacuum oven at 60^{o}C for further use.

5.2.3.2. Formation of PAA-CP/GPL-FePc-CH

5 mg of FePc/GPL-PEG-NH_2 was dispersed in 10 mL of HCl (0.1M) containing 10 mg of EDC.HCl under sonication. Subsequently, AA (2.4 mL), MBA (2 M), 3-vinylaniline (0.1 M) and APS (0.2 M) were added into the mixture with continued stirring. The above solution mixture was purged with N_2 gas to remove the dissolved oxygen content and poured into a pre-cleaned vial. The vial was placed in vacuum oven maintained at 70 °C for about an hour. A solid hydrogel was formed after about 38 min. The solid hydrogel was cooled to room temperature. The colour of the hydrogel has turned to

green with black spots to form PAA-CP/GPL-FePc-CH. The formation of hydrogels has been controlled through the exclusion or inclusion of FePc and 3-vinylaniline or without both; the formed hydrogels are PAA-CP/GPL-CH, PAA-GPL-FePc-CH, and PAA-GPL-CH, respectively, where they were prepared separately for comparative purposes. The forming time of every prepared hydrogel was different; it took around 45 minutes to form PAA-CP/GPL-CH when the gelation carried out in the absence of FePc. Separately, it took around 75 minutes to form PAA-GPL-FePc-CH when the gelation carried out in the absence of 3-vinylaniline. On the other hand PAA-GPL-CH was formed in about 85 minutes in the absence of both FePc and 3-vinylaniline. The hydrogels thus obtained were systematically analysed using SEM, and UV-visible and FTIR spectroscopies to determine the morphology and the chemical structure of the hydrogels.

5.2.3.3. Fabrication of PAA-CP/GPL-FePc/GOx-CH

Initially PAA-CP/GPL-FePc-CH (2 µl) was deposited on the surface of screen-printed electrode (Area = 0.1256 cm^2), where the coated electrode was allowed to dry in oven at 60^oC for 2 hours. The fabrication of PAA-CP/GPL-FePc/GOx-CH biosensor electrode was completed by immobilising GOx (1 µl) (10 mg in 1 mL PBS (pH 7.0)) along with glutaraldehyde (1 µl) as cross-linking and dried at room temperature for further analysis. The other coatings (PAA-CP/GPL-CH, PAA-GPL-FePc-CH, and PAA-GPL-CH) were treated in a similar manner in order to complete the fabrication process of the biosensor electrodes, which are examined for glucose detection for the sake of comparison.

5.3. Results and discussions

5.3.1. Synthesis of PAA-CP/GPL-FePc-CH

Figure 5-1 shows the scheme followed in the fabrication of PAA-CP/GPL-FePc/GOx-CH coating. FePc/GPL-PEG-NH_2 has been obtained through effective ultra-sonication approach to non-covalent functionalisation of FePc with GPL. Non-covalent interactions is found preferable for catalyst support applications (Zhong et al., 2013). To the best of our knowledge, water-soluble FePc functionalised graphene derivatives have not been reported as electrochemical glucose sensor applications. PAA-CP/GPL-FePc-CH was formed through organic free radical polymerisation, which is termed as conductive polymer. The purpose of including FePc/GPL-PEG-NH_2 was to improve the binding sites and provide suitable conditions for GOx immobilisation. The 3-vinylaniline has been utilised as monomer to construct this fabricated conducting polymer; the PAA containing –COOH groups in CH is to protect CP in its protonated form. A photograph of the prepared PAA-CP/GPL-FePc-conducting hydrogel (CH) could be seen in Figure 5-1. This hydrogel exhibits green colour which is originated from the protonated and doped CP in CH with dispersed black spots.

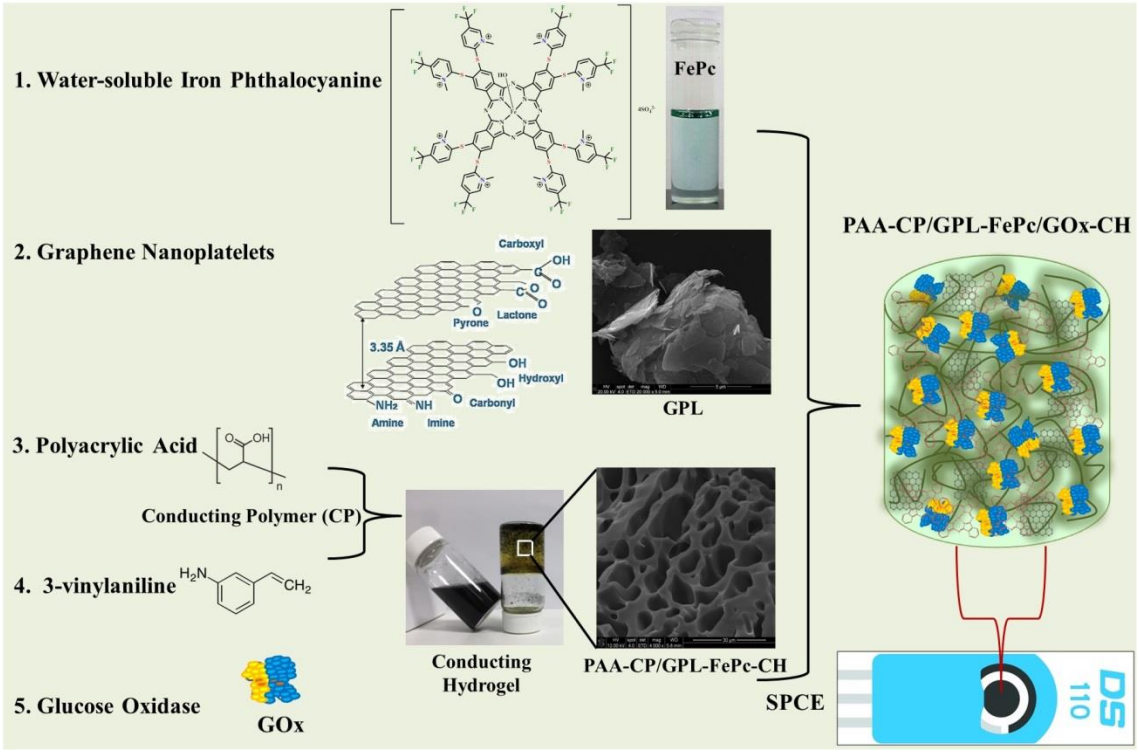

Figure 5-1 The procedure of formation PAA-CP/GPL-FePc/GOx-CH

5.3.2. Morphology

SEM images of PAA-CP/GPL-FePc-CH and PAA-CP-FePc-CH are shown in Figure 5-2(a) and 5-2(b), respecively. PAA-CP/GPL-FePc-CH has shown micro porous 3D inter-linked network due to the 3D integration of the components involved (Figure 5-2(a)).

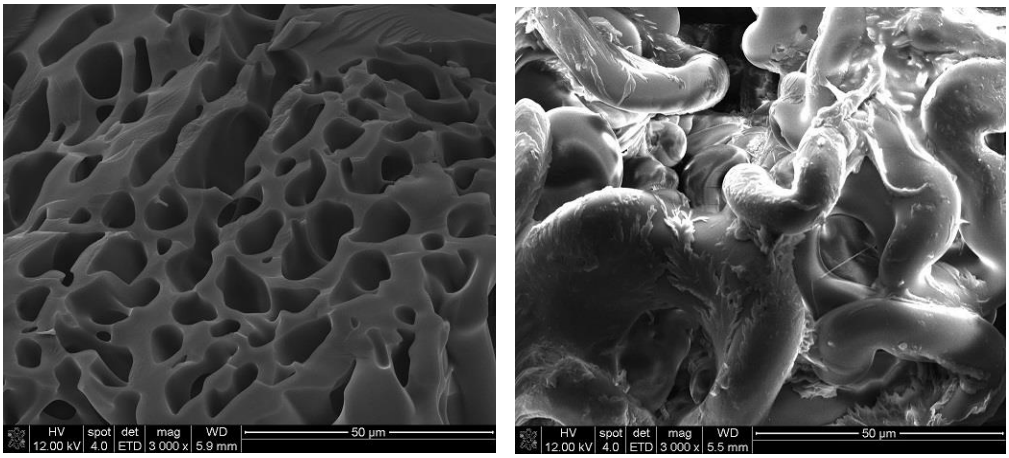

(a) (b)

Figure 5-2 SEM images of (a) PAA-CP/GPL-FePc-CH, (b) PAA-CP/FePc-CH

The average pore diameter of PAA-CP/GPL-FePc-CH was estimated to be approximately 19 μm. The 3D interconnected hierarchical porous structure of the conducting hydrogel offers greater effective surface areas for GOx immobilisation. However, the PAA-CP/FePc-CH showed a smooth surface and much smaller pore size as shown in Figure 5-2(b). This illustrates the role of GPL in the hydrogel matrix in the self-assembly of monomer and the cross-linker to form the polymer (Chirani et al., 2015). The semi-smooth surface might refers to the random interconnection between the cross-linker and the monomer.

5.3.3. UV- visible analysis

UV-visible spectra of FePc and the conducting hydrogels PAA-CP/GPL-FePc-CH and PAA-CP/GPL-FePc-CH have been studied using Cary 50 UV-visible spectrophotometer operating in the range 190-1100 nm. 1 cm path-length cuvettes have been used to measure the solution spectra, while pre-cleaned glass substrate were used for films spectral measurements. Table 5-1 illustrates the main absorption peaks in the measured absorption spectra of FePc and the conducting hydrogels. Iron phthalocyanine solution which was prepared by dissolving 1 mg of FePc in 1mL deionised water, exhibited sharp absorption band in the visible region (Q band) centred at 689 nm as well as a strong band in the UV region (B band or Soret band) at 316 nm (Figure 5-3 (red curve)). The two bands have been assigned to the π–π^* transitions which represent the electronic transition from the highest occupied molecular orbital (HOMO) to the lowest unoccupied molecular orbital (LUMO) (de la Torre et al., 2004). In addition, two shoulders at 432-490 and 614-637 probably refer to the transitions of the ligand-to-metal charge transfer (LMCT) (Arıcı et al., 2013; Han et al., 2016). Figure 5-3 (black curve) shows absorption spectrum of FePc thin film, which was deposited onto microscopic glass slides using spin coating method; the Q band was red-shifted from 689 nm to 705 nm and the B band from 316 nm to 323 nm. These red shifts could be

referred to self-aggregation of free base prophyrins of FePc molecules in the thin films (Andrade et al., 2008; Volpati et al., 2008).

The conducting hydrogels, PAA-CP/GPL-FePc-CH and PAA-CP/GPL-CH have shown two shoulders at 445 and 440 nm, and two peaks, 627 and 608 nm of CP, respectively (Figure 5-4). These absorption spectra are ascribed to the π–π^* transition of benzenoid ring and n–π^* transition of benzenoid to quinoid, respectively (Chaiyo et al., 2018; Muckley et al., 2017). The Q band in the PAA-CP/GPL-FePc-CH spectrum is shifted bathochromically to 699 nm. For comparison, the exclusion of 3-vinylaniline from the hydrogel has produced PAA-GPL-CH and PAA-GPL-FePc-CH; their spectra indicate the absence of CP from the structures of the prepared platform. No peaks representing CP have appeared while the Q and B bands of the FePc are clearly apparent in the PAA-GPL-FePc-CH spectrum with less intensity due to the GPL influence.

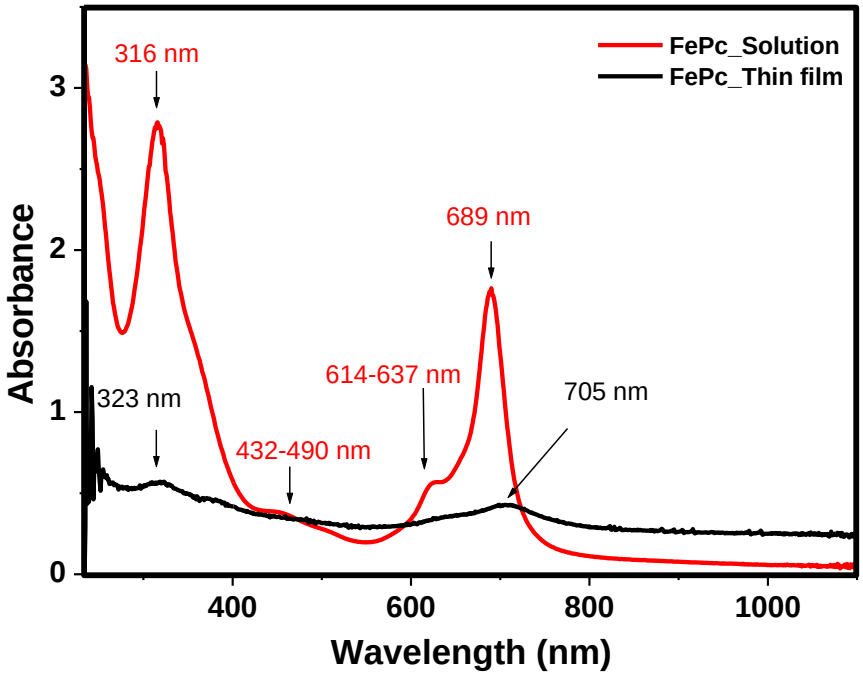

Figure 5-3 UV-visible spectra of FePc solution in deionised water and as thin film

Table 5-1 UV-visible absorption data for thin films of FePc and CHs

Sample	π–π^* λ_B (nm)	π–π^* λ_B (nm)	LMCT	n–π^* λ_Q (nm)	n–π^* λ_Q (nm)
FePc_solution	316	432-490		614-637	689
FePc_thin film	323				705
GPL	-	-	-	-	-
PAA-GPL-CH	-	-	-	-	-
PAA-CP/GPL- CH		440	534	608	
PAA-GPL-FePc-CH	316				699
PAA-CP/GPL-FePc-CH		445	557	627	699

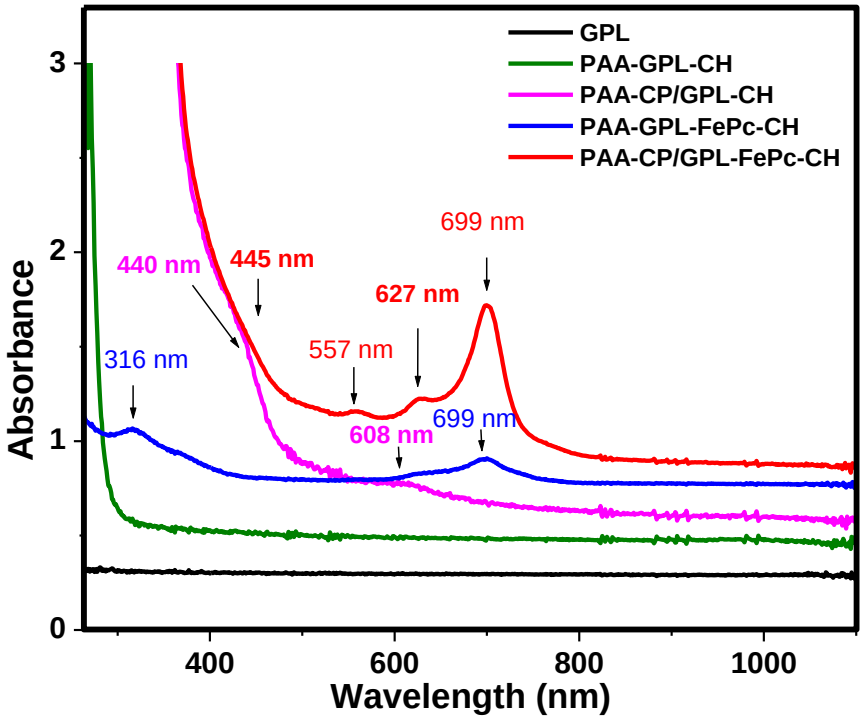

Figure 5-4 UV-visible spectra of the sensing platforms as shown in the legends

5.3.4. FT-IR analysis

The investigation of the molecular structure of the row materials and prepared composites has been carried out using FT-IR in absorption mode. Figure 5-5 shows the expected FTIR spectra of the studied composites; no characteristic peaks have been observed for the powder of GPL indicating its expected free-oxygen structure which confirms its hydrophilic nature (Kazi et al., 2015; Mani et al., 2013; F. Wang et al., 2012). FT-IR spectra of FePc have shown the main phthalocyanine characteristic peaks at 1030, 1110, 1150 and 1330 cm^{-1} (Bata et al., 2015; Kluson et al., 2009). The CHs

have exhibited the typical peaks of PAA in each of the conducting polymer-based platforms (PAA-GPL-CH, PAA-GPL-FePc-CH, PAA-CP/GPL-CH, and PAA-CP/GPL-FePc-CH) at around 2900-3700 cm^{-1} (-OH stretching), 1700 cm^{-1} (C=O stretching), 1410 cm^{-1} (benzenoid rings) and 1600 cm^{-1} (quinoid rings) (Choudhary et al., 2014). The spectrum of PAA-CP/GPL-FePc-CH has clearly exhibited the typical sharp peaks at 1030, 1110, 1150, and 1330 cm^{-1} of the FePc, which indicates its existence and incorporation into the structure. However, the PAA-GPL-FePc-CH, which has been modified with FePc, exhibits noticeable suppression of the phthalocyanine sharp peaks; this is attributed to the different structure of PAA-GPL-FePc-CH compared to PAA-CP/GPL-FePc-CH. The only peak at 1330 cm^{-1} which appeared in the spectrum of PAA-GPL-FePc-CH clearly indicated the presence of FePc in this conducting hydrogel as shown in Figure 5-5 and summarised in table 5-2. Figure 5-6 shows the molecular structure of the water-soluble iron phthalocyanine.

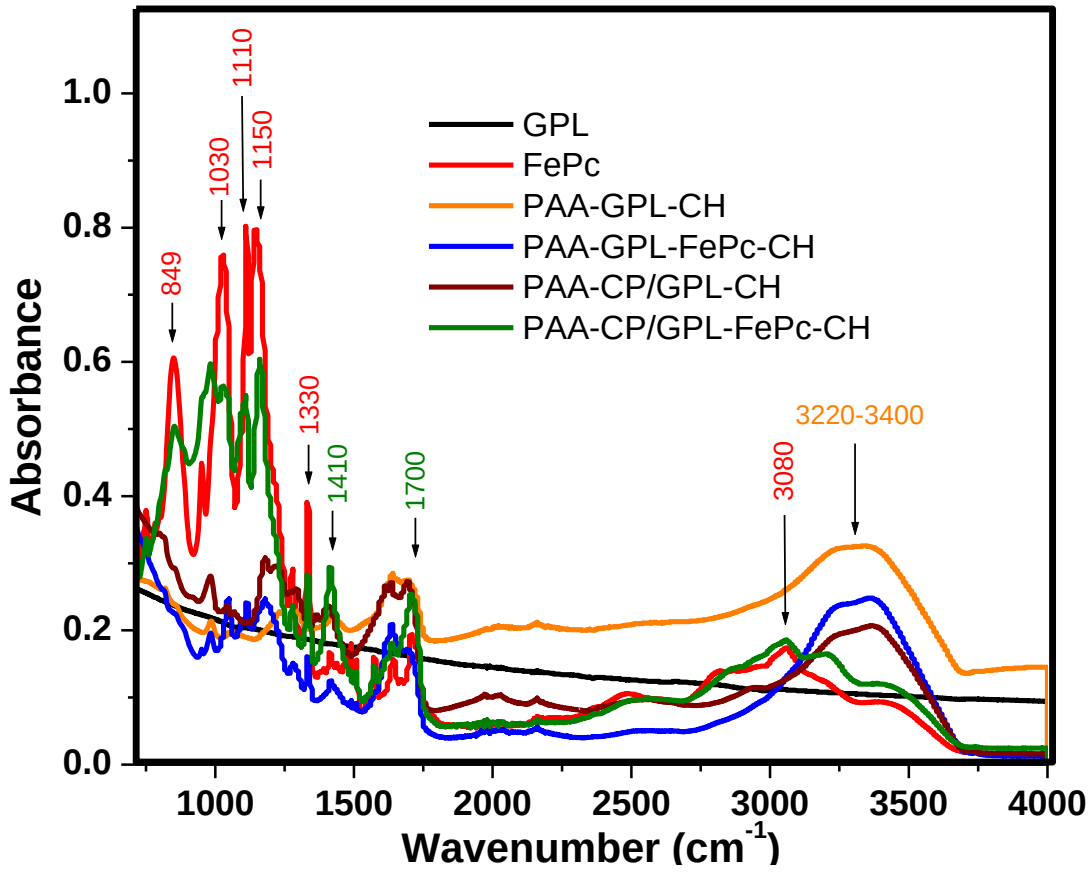

Figure 5-5 FTIR spectra of all studied materials

Table 5-2 FTIR absorption data of all studied materials

Sample	Pc (cm^{-1})	benzenoid rings (cm^{-1})	quinoid rings (cm^{-1})	C=O stretching (cm^{-1})	-OH stretching (cm^{-1})
GPL					
FePc powder	1030-1330				3080
PAA-GPL-CH		1410	1600	1700	
PAA-GPL-FePc-CH		1410	1600		2900-3700
PAA-CP/GPL-CH		1410	1600	1700	2900-3700
PAA-CP/GPL-FePc-CH	1030-1330	1410	1600	1700	3080

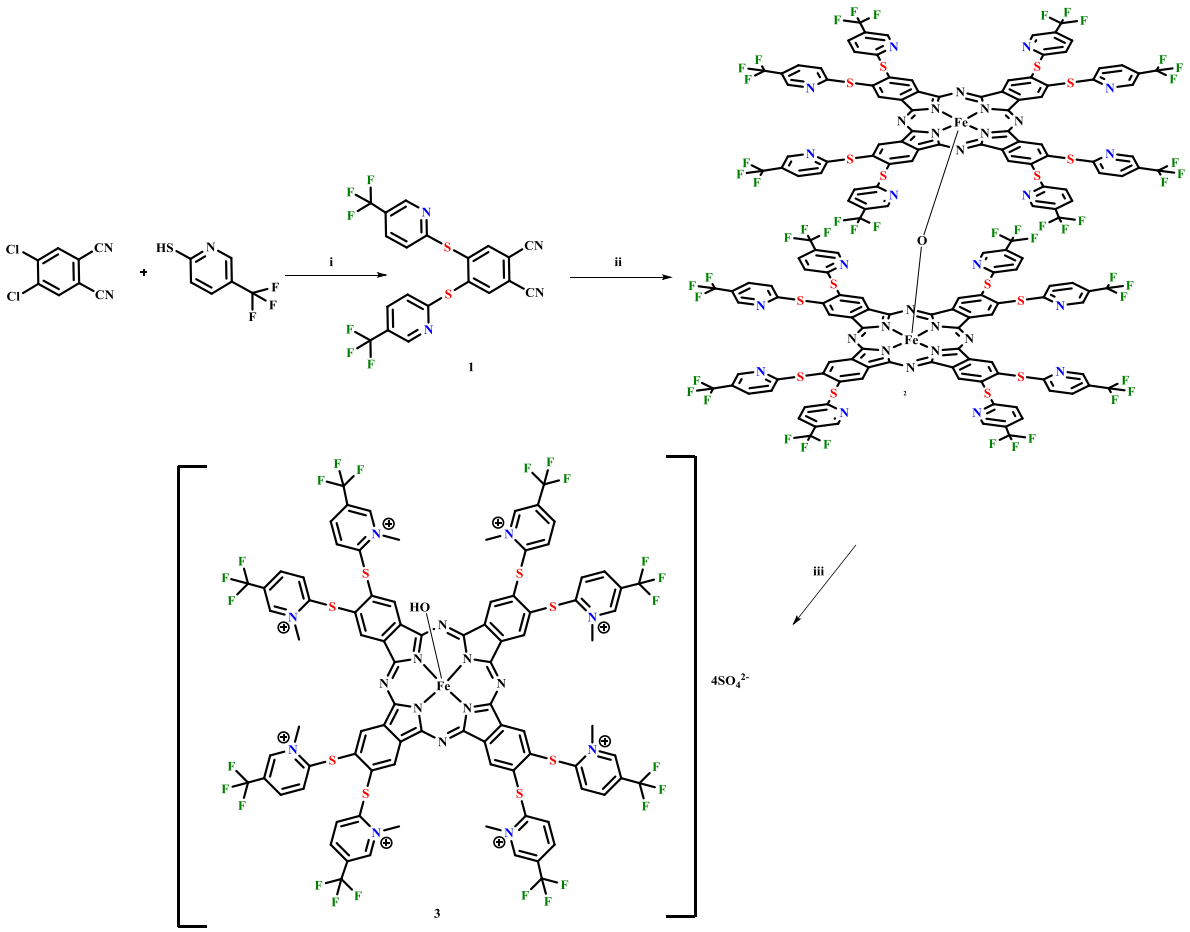

Figure 5-6 Molecular structure of the water-soluble iron phthalocyanine

5.3.5. Electrochemical performance of modified electrodes

Cyclic voltammograms (CVs) were recorded for the modified electrodes to study the interfacial electrochemical properties through measuring the voltammetric response in 5 mM of $Fe(CN)_6^{-3/-4}$ solution containing 0.1M NaCl versus silver-silver chloride electrode (Ag/AgCl) as the bench mark redox system. Water-soluble FePc-modified electrode was scanned in the potential range from −1 to +1 V. As shown in Figure 5-7 three redox processes can be identified (Arslan and Yilmaz, 2007). Process I shows first redox where in the beginning of the positive scan a small anodic peak for FePc at −0.62 V which is attributed to ring oxidation $[Fe^{I}Pc^{3-}]^{-2} \rightarrow [Fe^{I}Pc^{2-}]^{-1} + e-$, with corresponding reverse cathodic peak at −0.66 V in the first cycle. Process II shows sharp redox at the FePc due to metal centre $[Fe^{I}Pc^{2-}]^{-1} \rightarrow [Fe^{II}Pc^{2-}] + e-$. The anodic

peak appears at +0.17 with corresponding reverse cathodic peaks at −0.01(Arıcı et al., 2013; Martin et al., 2016) however a reversible behaviour in aqueous media corresponding to the Fe(II)/Fe(III) redox transition process of the $Fe(CN)_6^{-3/-4}$ as shown in the case of bare electrode in Figure 5-7 (blue curve). Process III represents weak cathodic peak and anodic peak at +0.78 V assigned to metal-based redox (Akinbulu and Nyokong, 2010). Irreversible peak (as pointed via an arrow) marked at +0.37 V refers to monomer cation radical formation (Martin et al., 2016). Increasing polarisation effect might refers to the lack of reversibility (Arslan and Yilmaz, 2007). For comparison, the GPL modified electrode was scanned and showed expected increasing in the current of the Fe(II)/Fe(III) redox which illustrates the enhanced in conductivity that is contributed by GPL. Dong and coworkers have improved the reduction catalyst activity and thus considerably produced excellent chemical stability for electrocatalyst in alkaline media when they employed a noncovalent binding between FePc and single-walled carbon nanotubes (SWCNTs) (Dong et al., 2012).

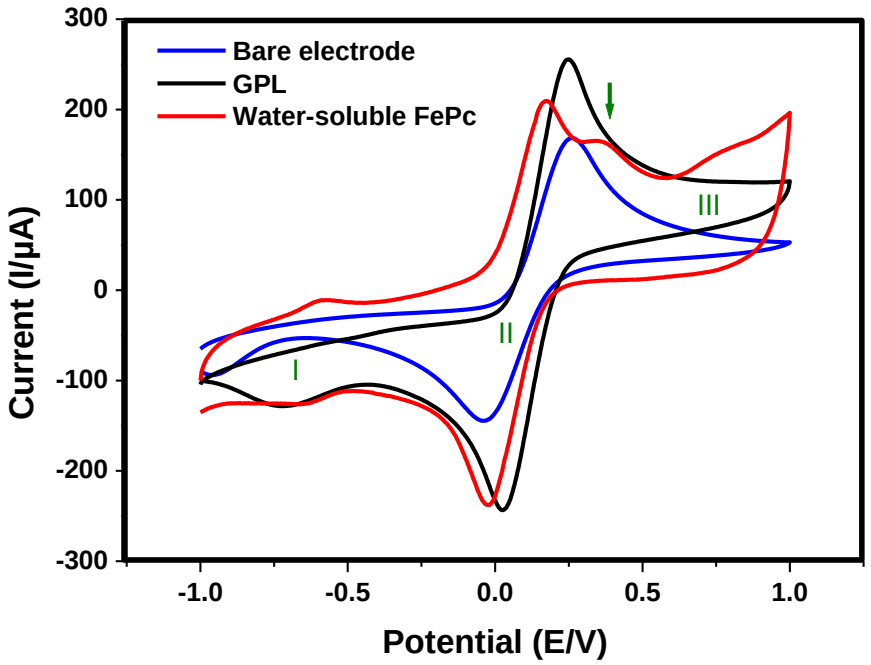

Figure 5-7 Cyclic voltammogram of modified electrodes as shown in the legeneds; recorded in 5 mM of $Fe(CN)_6^{-3/-4}$ solution containing 0.1M NaCl as a supporting electrolyte versus Ag/AgCl at scan rate = 100 mV/s

CVs for the PAA-CP/GPL-FePc/GOx-CH biosensor have been recorded using 5 mM of the bench mark redox system, $Fe(CN)_6^{-3/-4}$ in the potential range from -0.5 to +0.5 V. The efficacy of the electrode was studied through calculating anodic to cathodic peak potential separation ($\Delta E_p = E_{pa}-E_{pc}$) as well as oxidation or reduction peak currents (I_{pa} or I_{pc}) at the $Fe(CN)_6^{-3/-4}$. The I_{pa} of PAA-CP/GPL-FePc/GOx-CH, Figure 5-8(red), was ~1.96 time higher than currents exhibited by PAA-CP/GPL/GOx-CH biosensor (Figure 5-8(blue)). The I_{pa} of the PAA-CP/GPL-FePc/GOx-CH biosensor (174.94 µA) is even higher than the pristine PAA-CP/GPL-FePc-CH biosensor (173.60 µA) (Figure 5-8(green)), which explains the higher current of the new based water-soluble FePc in the herein developed biosensor. Basically, the different response of the modified electrodes interprets the different interfacial structures within the constructed biosensors (Buber et al., 2017).

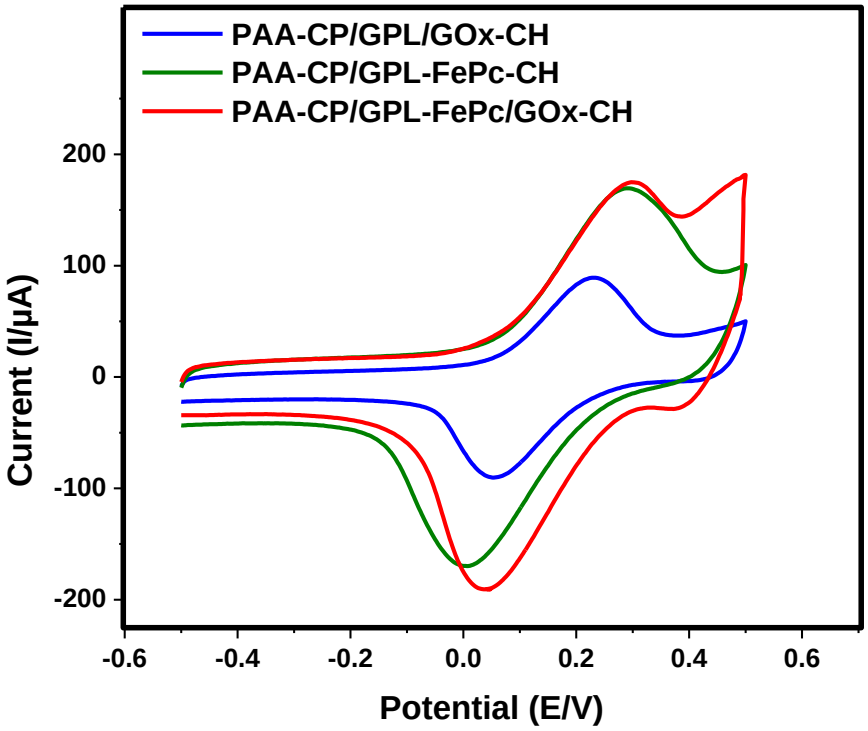

Figure 5-8 CVs of (blue) PAA-CP/GPL/GOx-CH, (green) PAA-CP/GPL-FePc/GOx-CH, and (red) PAA-CP/GPL-FePc/GOx-CH recorded in 5 mM of $Fe(CN)_6^{-3/-4}$ solution containing 0.1M NaCl as a supporting electrolyte versus Ag/AgCl; scan rate = 100 mV/s

The ΔE_p value of the PAA-CP/GPL-FePc/GOx-CH biosensor was 262 mV while that for the PAA-CP/GPL-FePc-CH biosensor was 316 mV. The results demonstrate the faster electron rate at the PAA-CP/GPL-FePc-CH biosensor electrode that was facilitated by GPL and FePc due to their large effective area and high conductivity (Muckley et al., 2017; Zagal et al., 1980). On immobilisation of GOx, the PAA-CP/GPL-FePc/GOx-CH biosensor electrode shows smaller ΔE_p value indicates fast electron tansfer rate during the reaction (Liu et al., 2018). The PAA-CP/GPL/GOx-CH biosensor exhibited low reversable redox in the abcense of FePc which was employed to enhance the electrocatalytic activity of the biosensor (Costa de Oliveira et al., 2017).

Figure 5-9 shows the CVs of PAA-CP/GPL-FePc/GOx-CH biosensor electrode recorded for different scan rates (10–100 mV/s) which explain the diffusion behaviour of the modified electrode.

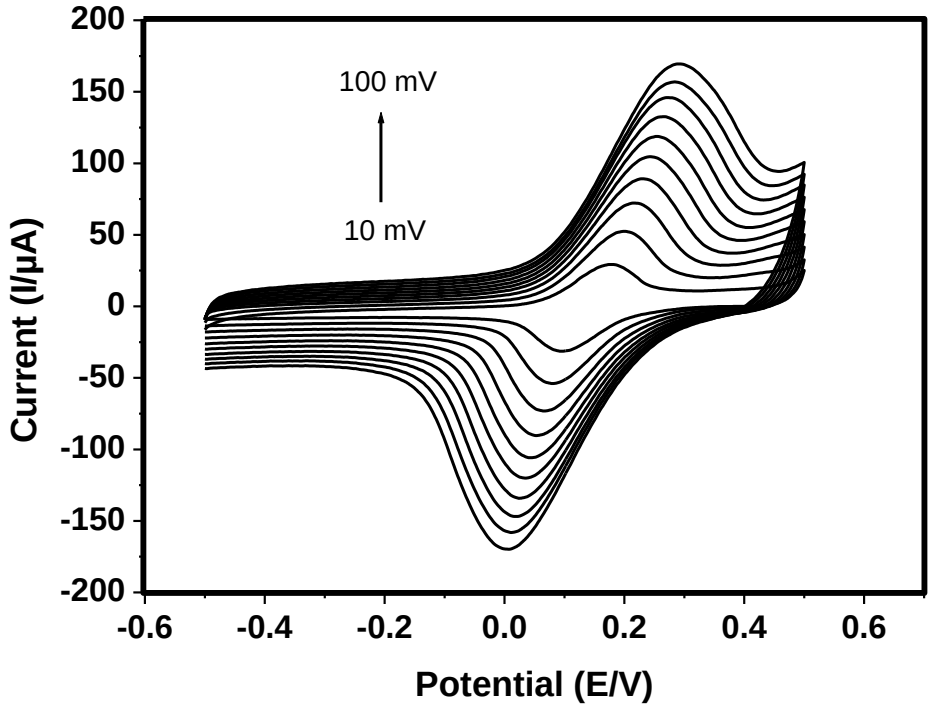

Figure 5-9 CVs of PAA-CP/GPL-FePc/GOx-CH platform in 5 mM of $Fe(CN)_6^{-3/-4}$ containing 0.1 M NaCl versus Ag/AgCl for different scan rates in the range 10-100 mV/s

To study the stability of the fabricated enzymatic biosensor, CV cycle applied for 50 times to the PAA-CP/GPL-FePc/GOx-CH biosensor in 5 mM of $Fe(CN)_6^{-3/-4}$ containing 0.1 M NaCl versus Ag/AgCl at scan rate of 100 mV/s. Figure 5-10 shows good long-term stability of the new conducting hydrogel coating which demonstrates the robust structure of the matrix. Even at the end of 50 cycles, the PAA-CP/GPL-FePc/GOx-CH exhibited redox peaks of $Fe(CN)_6^{-3/-4}$ with small shift in ΔE_p value. This clearly shows that the GOx immobilized onto the hydrogel has strong interaction with the hydrogel platform.

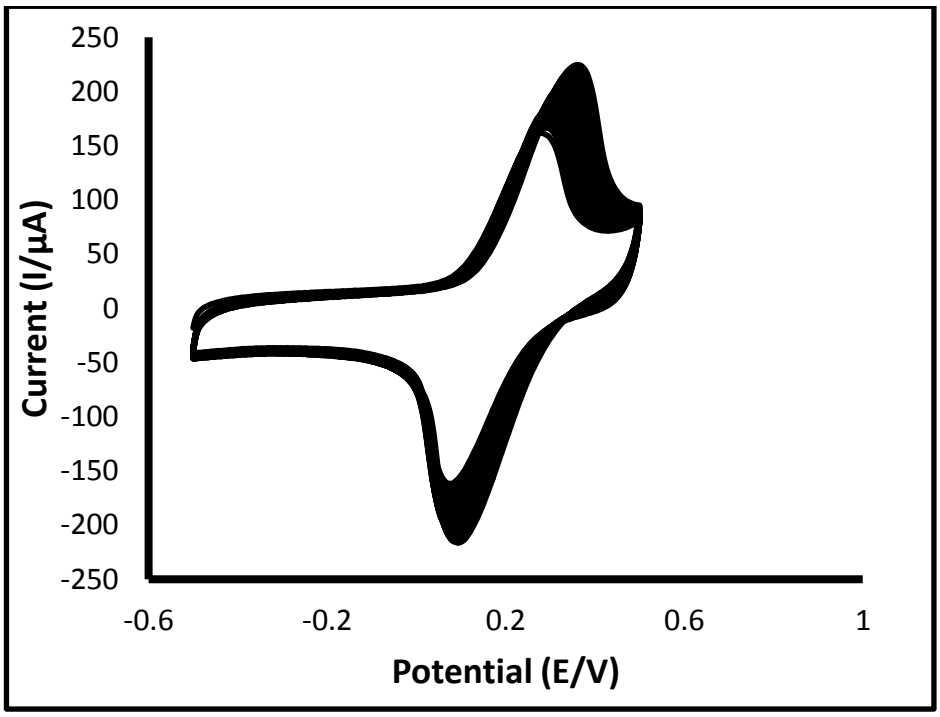

Figure 5-10 CV cycle applied for 50 times to the PAA-CP/GPL-FePc/GOx-CH biosensor in 5 mM of $Fe(CN)_6^{-3/-4}$ containing 0.1 M NaCl versus Ag/AgCl at scan rate = 100 mV/s

5.3.6. Electrochemical impedance measurements

Electrochemical impedance spectroscopy (EIS) measurements have been carried out to study the nature of the electrochemical interface on the modified electrodes, PAA-CP/GPL-FePc/GOx-CH and PAA-CP/FePc/GOx-CH in PBS containing 0.1M NaCl, and the results are shown in Figure 5-11. The biocatalytic activity of the immobilised GOx onto the porous site of the hydrogel-based electrode has changed the interfacial capacitance and charge transfer resistance (Ding et al., 2005; Katz and Willner, 2003). As demonstrated in Figure 5-11, the Nyquist plot exhibited small semicircular diameter for the PAA-CP/GPL-FePc/GOx-CH-modified electrodes (curve (c)), which refers to smaller charge transfer resistance in comparison with the PAA-CP-FePc/GOx-CH-coated electrode (curve (b)), which has exhibited larger semicircular diameter, as shown in Figure 5-11. The PAA-CP/GPL-FePc/GOx-CH exhibited low R_{ct} of 27.978 Ω compared to that exhibited by PAA-CP-FePc/GOx-CH hydrogel with the value of approximately 37.611 Ω. The smaller semicircular diameter is attributed to faster

electron transfer kinetics at high frequency region while the linear part at lower frequency region ensures mixed kinetics and diffusion-controlled process. The large semicircular curve suggests the catalytic activity role of the conductive hydrogel when GPL is excluded from the biosensor coating (Costa de Oliveira et al., 2017). Fitting of the experimental data has carried out using ZSimpWin software and apply Randle's model. Equivalent circuit for the PAA-CP/GPL-FePc/GOx-CH biosensor is presented in Figure 5-12. Based on the model, good agreement was achieved over the frequency range 10 Hz-2 MHz between the simulated and experimental results when Randle's model, R(Q(R(QR))) was applied in ZSimpWin software.

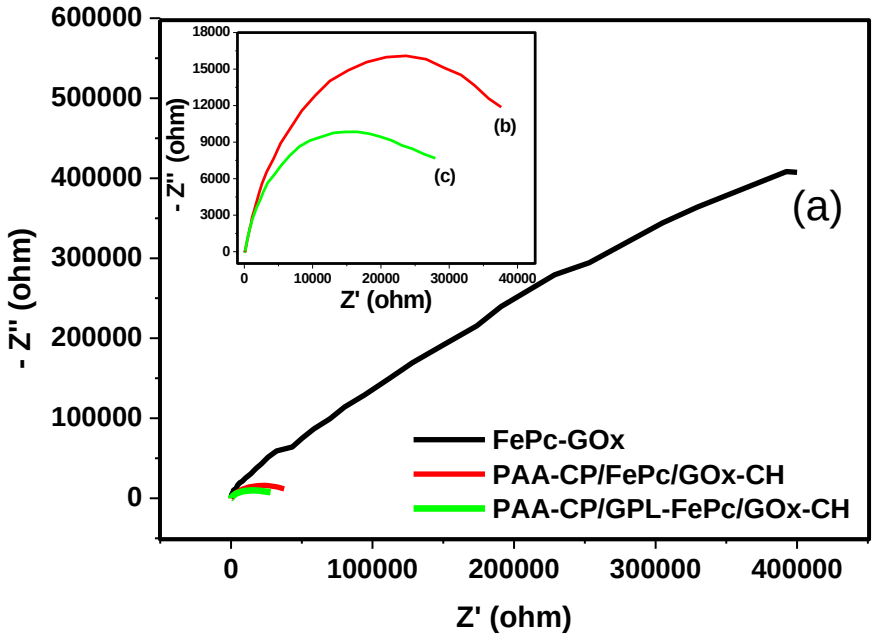

Figure 5-11 Nyquist plots (Zim vs. Zre) of (a) FePc-GOx, (b) PAA-CP/FePc/GOx-CH and (c) PAA-CP/GPL-FePc/GOx-CH in the presence of PBS containing 0.1M NaCl. Inset: Zoomed-in of b and c

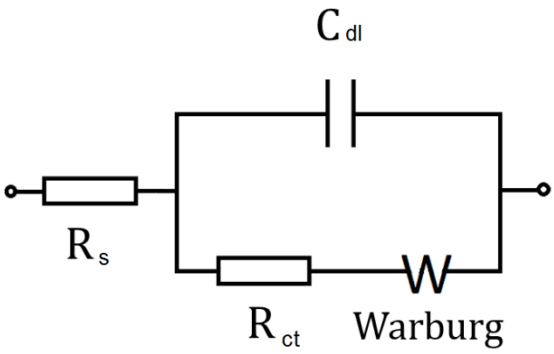

Figure 5-12 Equivalent circuit model R(Q(R(QR))) for the PAA-CP/GPL-FePc/GOx-CH biosensor

5.3.7. Swelling ratio

The swelling ratio of the prepared conducting hydrogels has been studied; the welling ration of PAA-CP/GPL-FePc-CH is found to be approximately 3.2, 1.7 and 1.2 times higher than PAA-GPL-FePc-CH, PAA-CP/GPL-CH, and PAA-GPL-CH, respectively (Figure 5-13). The four prepared conducting hydrogels were examined by adding same amount of DI-water to the samples of dry hydrogels for certain amount of time, individually. The pore volume has significant impact on the swelling ratio of a hydrogel, where the larger pore volume is the higher swelling ratio as have been noticed in PAA-CP/GPL-FePc-CH. The diffusional resistance decreases as the pore volume increases. The swelling ratio has been calculated based using the following equation (Sun et al., 2013):

$$Swelling\ Ratio\ (\%) = \frac{W_S - W_d}{W_d} \times 100 \qquad (1)$$

where,

W_s: the weight of swollen sample

W_d: the weight of dry sample

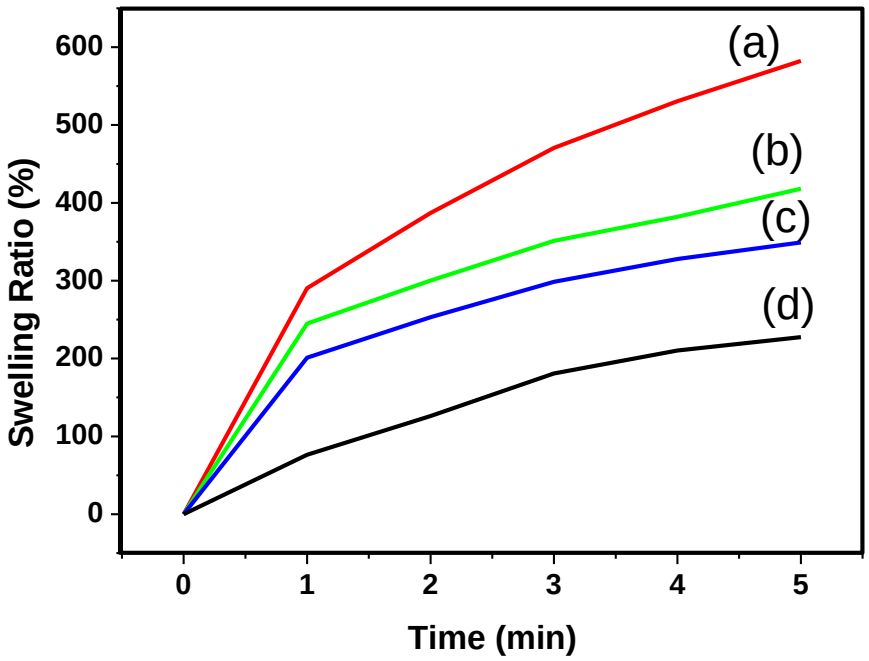

Figure 5-13 The swelling ratio of (a) PAA-CP/GPL-FePc-CH, (b) PAA-GPL-FePc-CH, (c) PAA-CP/GPL-CH, and (d) PAA-GPL-CH

5.3.8. Electrochemical detection of glucose

PAA-CP/GPL-FePc/GOx-CH biosensor has been employed to study the catalytic reaction on the electrode surface with glucose in the presence of the GOx enzyme. Figure 5-14 shows the CVs of the enzymatic electrode (PAA-CP/GPL-FePc/GOx-CH) where the red curve demonstrates the behaviour of the electrode in bare PBS (pH 7.0), while the black curve displays its behaviour in the presence of glucose (4mM). PAA-CP/GPL-FePc/GOx-CH electrode has clearly exhibited a reversible redox peak, which corresponds to the redox of the Pc ring with the electron shuttled via the Fe(II)/Fe(I) redox transition of the Fe center (Alsudairi et al., 2017). The black curve in Figure 5-14 shows the electrocatalytic oxidation of the 4 mM glucose at the PAA-CP/GPL-FePc/GOx-CH. Large increase in the anodic current strating above 0.3 V was noticed with the addition of glucose. This suggests oxidation to the reduced form of the enzyme took place due to the electron transfer between Fe(III)Pc and the immobilised GOx.

The glucose transfers from the solution to the PAA-CP/GPL-FePc/GOx-CH biosensor via diffusion; this mechanism has been discussed in sufficient details in chapter 4.

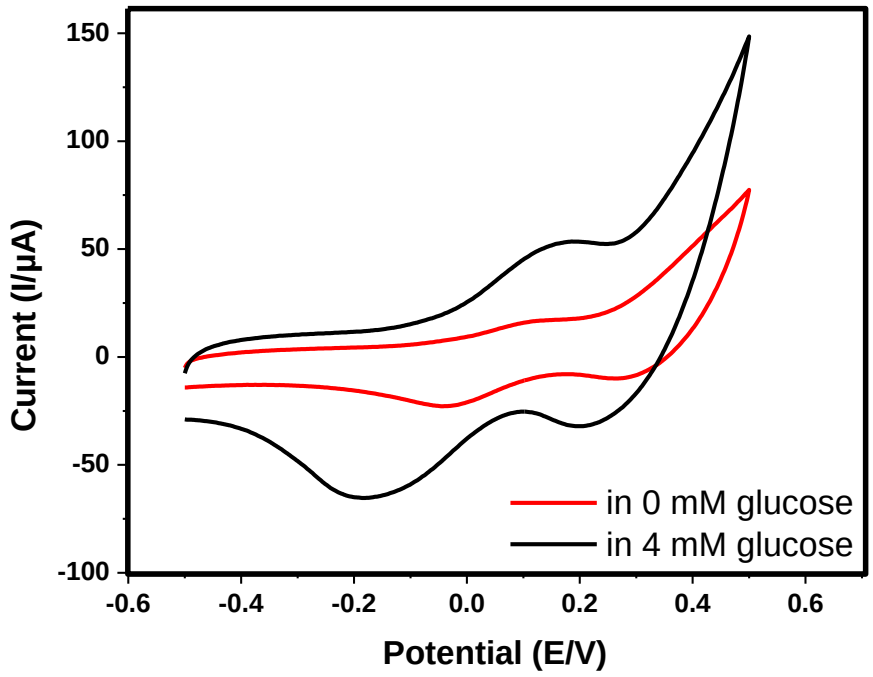

Figure 5-14 CVs of PAA-CP/GPL-FePc/GOx-CH at 0 Mm glucose and 4 mM glucose both in 0.1M PBS in PBS (pH 7.0) as shown in the legends: versus Ag/AgCl and scan rate (100 mV/s)

5.3.9. Amperometric response of glucose of PAA-CP/GPL-FePc/GOx-CH-based biosensor

Amperometric measurements were recorded over a varied concentration range of glucose in order to examine the functioning potential of PAA-CP/GPL-FePc/GOx-CH as a glucose biosensor, and the results are demonstarted in Figure 5-15.

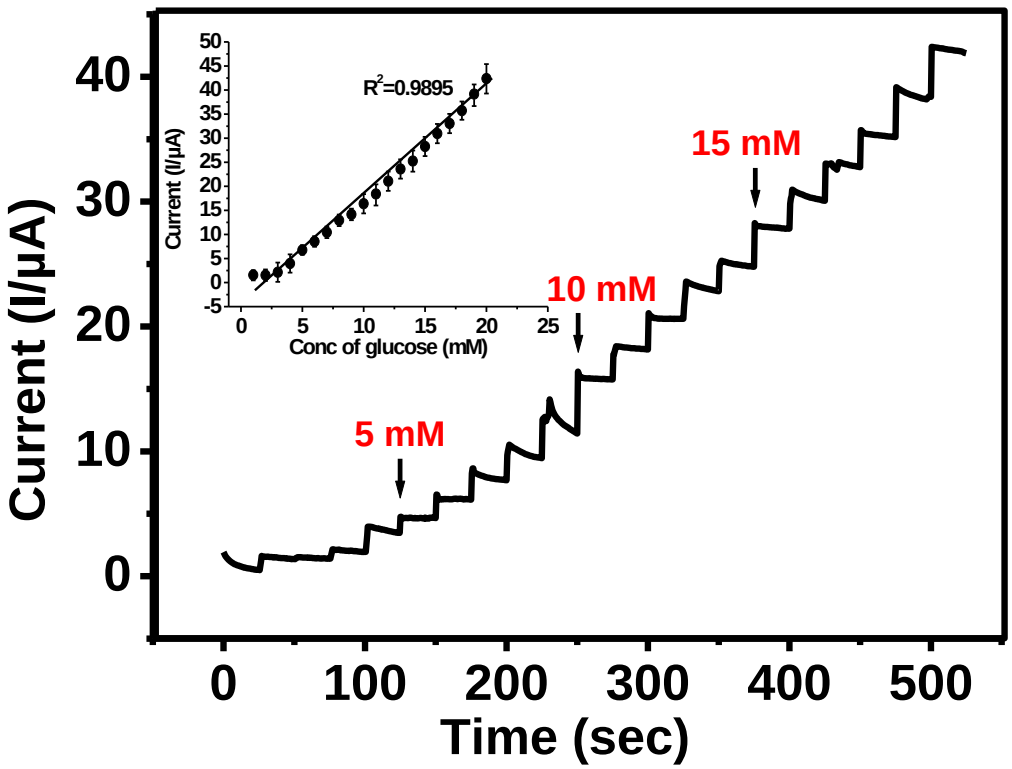

Figure 5-15 Amperometry of PAA-CP/GPL-FePc/GOx-CH for successive addition of glucose in 0.1M PBS (pH 7.0). Inset: calibration plot peak current versus [glucose]

Linear current response was achieved for the glucose in the concentration range 1-20 mM with correlation coefficient R^2 of 0.9895 as shown in the inset of Figure 5-15. The correlation coefficient measures the strength and direction of a linear relationship between two variables. The sensor has exhibited a sensitivity of 18.11 μA mM^{-1} cm^{-2}; limit of detection (LOD) of the biosensor was calculated as 1.1503 ng/mL based on the equation $LOD = 3\sigma/S$ (Yang et al., 2004) at signal to noise ratio of 3. The PAA-CP/GPL-FePc/GOx-CH biosensor has shown a rapid response against glucose with response time of 1 second. This fast response indicates the fast diffusion of glucose which takes place on the surface of the fabricated electrode as was discussed in section 4.3.8. This short response time indicates the compatibility structure of the fabricated biosensor compared to recent fabricated biosensors, which exhibited longer response time. Sode and coworkers have presented glucose enzymatic sensor strips with current time reponse of 5 seconds (Sode et al., 2017). An in-vitro glucose detection study which

was found to be minimally invasive compared to the biosensors-based stripers, has demonstrated a very long response time, 32(± 22) min when the biosensor was placed on pig ear skin membrane (Ullah et al., 2018).

Optimisation of the performance of glucose biosensors has been carried out through study of the pH effect where the current response of PAA-CP/GPL-FePc/GOx-CH was found to be in its highest at pH 7.0. The effect of applied potential to the amperometric detection has been studied also and +0.3 V was chosen for the current glucose detection study.

5.3.10. Repeatability, reproducibility, and stability of PAA-CP/GPL-FePc/GOx-CH

The repeatability of PAA-CP/GPL-FePc/GOx-CH biosensor was tested through amperometric measurements for three different concentrations of glucose, 5 mM, 10 mM, and 15 mM as shown in Figure 5-16.

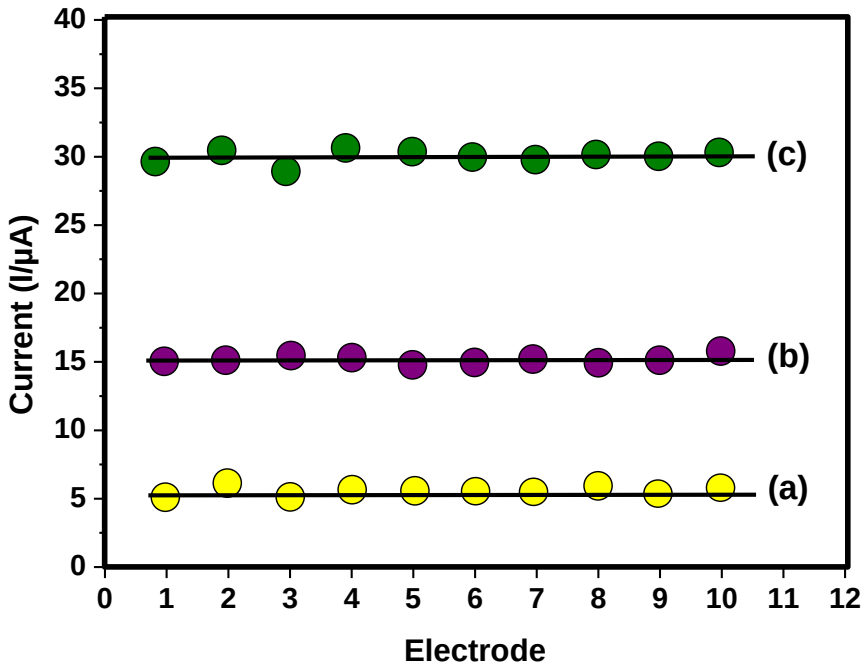

Figure 5-16 Amperometric response of (a) 5 mM, (b) 10 mM, and (c) 15 mM glucose conentration of PAA-CP/GPL-FePc/GOx-CH-based biosensor (repetitive measurements) at +0.3 V

Ten repetitive measurement of a single PAA-CP/GPL-FePc/GOx-CH biosensor electrode has produced a relative standard deviation (RSD) value of 0.29 (5 mM), 0.18 (10 mM), and 0.55 (15 mM) of glucose under identical conditions. The reproducibility of PAA-CP/GPL-FePc/GOx-CH biosensor was examined by fabricating ten similarly fabricated electrodes. The results have shown a satisfactory reproducibility where the relative standard deviation for ten electrodes was; RSD = 0.05 for n=10.

To demonstrate the stability of PAA-CP/GPL-FePc/GOx-CH biosensor, amperometric response to 4mM glucose was recorded over a period of 4 months keeping the electrodes at 4 °C refrigerated condition. PAA-CP/GPL-FePc/GOx-CH biosensor has retained 99% of its current response. This result clearly indicates that the used enzyme (GOx) was well protected by the conducting hydrogel, a result that suggests the suitability of the new developed hydrogel for practical application in blood sugar detection.

5.3.11. Specificity and interference

The selectivity of the PAA-CP/GPL-FePc/GOx-CH-based glucose biosensor has been investigated by examining the biosensor on exposure to whole blood with interfering substances such as ascorbic acid and uric acid. Figure 5-17 shows that the amperometric response current to 4 mM glucose was hardly affected by other interfering blood components; the applied potential was + 0.3 V.

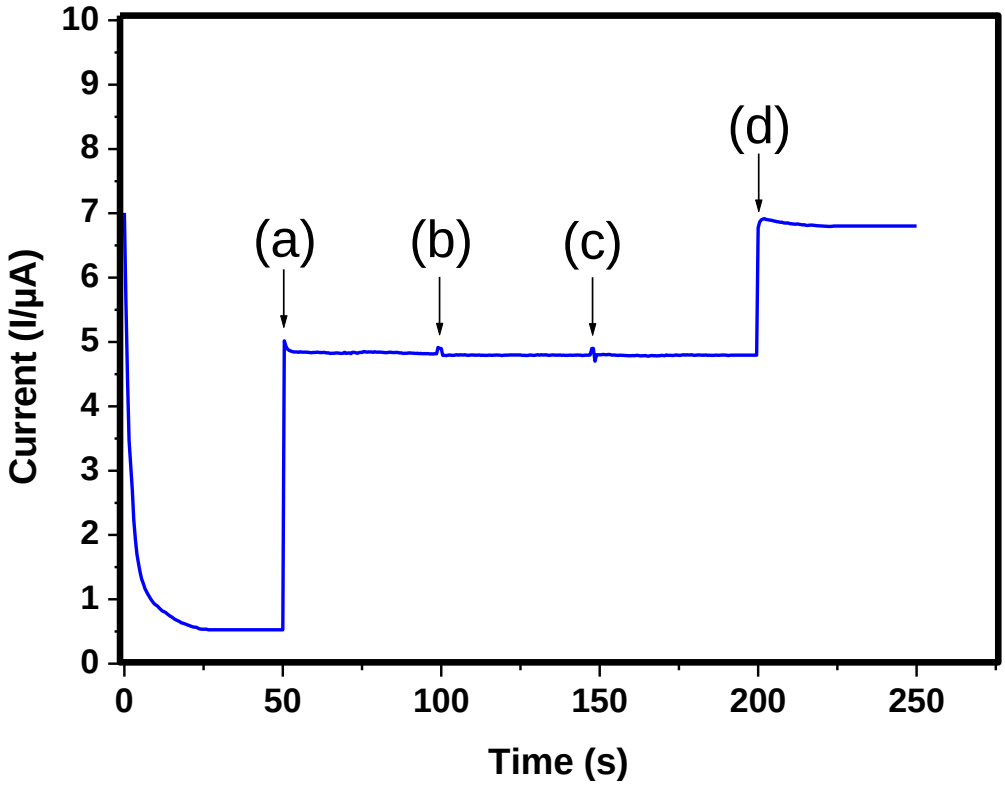

Figure 5-17 Amperometric response of PAA-CP/GPL-FePc/GOx-CH biosensor to (a) glucose (4 mM); (b) ascorbic acid (0.1 mM); (c) uric acid (0.5 mM); (d) glucose (5 mM)

5.3.12. Glucose determination in real samples at PAA-CP/GPL-FePc/GOx-CH biosensor

To demonstrate the feasibility of PAA-CP/GPL-FePc/GOx-CH as viable biosensor in industrial applications, as well in clinical diagnosis, glucose concentration in real samples (different types of fruit juice as well as human serum) were examined. A continuous amperometry scan was recorded for varied additions of these samples under identical experimental conditions, as applied in the results shown in Figure 5-15. PAA-CP/GPL-FePc/GOx-CH biosensor exhibited response to all the real samples added. The results obtained are summarised in Figure 5-18 and Table 5-3; a satisfactory performance is clearly shown with an error margin of 3%, which demonstrates the viability of the CH platform-based biosensor for practical application in diabetes testing.

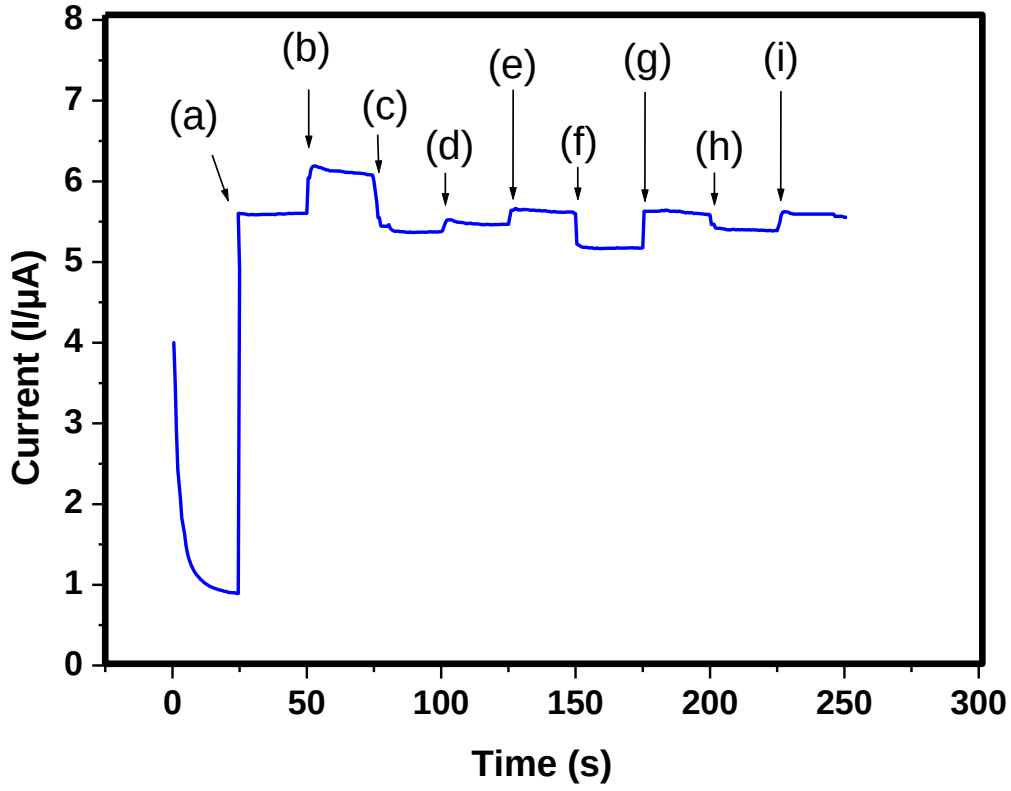

Figure 5-18 Amperometric responses to real samples (a) glucose, (b) mango juice, (c) pineapple juice, (d) energy drink, (e) glucose, (f) apple juice, (g) human serum, (h) pineapple juice, (i) human serum, at PAA-CP/GPL-FePc/GOx-CH biosensor at an applied potential of +0.3 V

Table 5-3 Amperometric responses of real samples

	Real samples	Added (according to specification in the label) (mM)	Found (mM)	Recovery (%)
a	Glucose	5.5	5.4	101.71
b	Mango	6.5	6.35	102.76
c	Pineapple	5.3	5.15	97.6
d	Energy drink	5.4	5.2	97.02
e	Glucose	5.5	5.4	101.75
f	Apple juice	5.1	5.0	98.35
g	Human serum	5.6	5.51	98.83
h	Pineapple	5.3	5.15	97.75
i	Human serum	5.6	5.51	98.93

5.4.Conclusion

In this chapter the synthesis of a new conducting hydrogel has been demonstrated; this hydrogel is based water processable iron phthalocyanine (FePc) functionalised graphene nanoplatelets (GPL) dispersed polyacrylic acid (PAA) in 3D matrix (PAA-CP/GPL-FePc/GOx-CH). The high dispersibility was achieved through the cationic quaternized 5-(trifluoromethyl)-2-N-methylmercaptopyridine substituents on the phthalocyanine macrocycle. Functionalising the water-soluble FePc with graphene platelets through non-covalent interaction was the key to controlling aggregation in the formed hydrogel. The exceptional structure stability and hierarchical porosity of PAA-CP/GPL-FePc-CH provided a large surface area for good immobilisation to the GOx enzyme. The hydrogel has exhibited excellent performance due to its high conductivity compared to the one discussed in chapter 4; this has been achieved through the initial interconnection between the water-soluble FePc structure and GPL. This interconnection has enhanced the catalytic activity, and thus reduced the amperometric glucose detection potential to +0.3 V. The work has demonstrated the significant role of every element (FePc, GPL, and PAA) in the performance of the fabricated platform. The proposed PAA-CP/GPL-FePc/GOx-CH biosensor exhibited wide linear range and good sensitivity (18.11 μA mM^{-1} cm^{-2}) and low detection limit for glucose detection (1.1503 ng/mL).

Chapter: 6 Silica nanoparticles-based water-soluble phthalocyanine as glucose biosensing probe

Chapter overview

This chapter introduces facile preparation of highly sensitive electrochemical bioprobe based on water-soluble lutetium phthalocyanine incorporated into silica nanoparticles ($SiO_2(LuPc_2)$) grafted with Poly(vinyl alcohol-vinyl acetate) itaconic acid (PANI(PVIA)) doped polyaniline conducting nanobeads (CNB), ($SiO_2(LuPc_2)$PANI(PVIA)-CNB). The CNB are employed as host to immobilise GOx enzyme and used as sensitive electrochemical bioprobe for glucose detection. Physico-chemical characteristics of all materials used are studied and results are discussed in sufficient detail. The fabrication procedures of the nanostructural probe are described in detail and the immobilisation of GOx into the conducting nanobeads is explained. The standard electrochemical methods have been applied using the new sensing platform for the selective detection of glucose and probe sensitivity is determined under optimized conditions. Finally, the chapter reports the high potential of using the new biosensor platform for real-time monitoring of glucose.

6.1. Introduction

Diabetes mellitus is a major global public health problem and has become one of the death causes and disability in addition to the heavy economical cost (Dhand et al., 2015; Tabish, 2007; Zhu et al., 2012). There is no known cure for diabetes, however postponing or may be preventing the associated serious complication could be possible with early diagnosis (Salek-Maghsoudi et al., 2018). Factors that limit hospitalisations of diabetic patients include regular/continuous monitoring and control of the glucose level in the body (Shafiee et al., 2012). A variety of unambiguous methods for detecting

and quantifying glucose in assorted biological fluids and food matrices exist which include spectrophotometric, calorimetric, chromatographic and electrochemical approaches (Galant et al., 2015). Electrochemical biosensors have gained immense acceptance in the field of medical diagnostics due to their attributes of simple, real-time, rapid and economical systems. The device comprises of a synergistic combination of biological recognition element (biotechnology) and a compatible transducer (microelectronics) (Singh et al., 2009). To achieve reliable and sensitive electrochemical biosensors, many nanomaterials with large surface area have been used to develop the sensing part of the these devices such as graphene nanosheets, carbon nanotube, gold nanoparticles, and silica nanoparticles (Wei et al., 2013b; Wu et al., 2007; Zhang et al., 2013). Silica nanoparticles have gained much research attention due to the wide range of application and low cost (Zou et al., 2008b).

Silica nanoparticles have expressed the ability to work as an excellent sensing inorganic probe due to the tunable size, large surface area, biocompatibility (Sun et al., 2016). Developing the sensing activity of electrochemical enzymatic sensors have been studied widely by employing different materials, for instance, 8000 published papers between 2015 and 2017 have used the term "Chemical Sensing", according to the citation index Web of Science (Carvalho et al., 2018). Different studies have been carried out silica-dispersed glucose oxidase have been applied to monitor the whole blood (Harris et al., 2012), and recently, a novel matrix GOx/silica-based for biosensors have been presented as an amperometric glucose biosensor (Jędrzak et al., 2018). However the significant improvement in the mechanical and electrical properties to the silica nanoparticles doped polymers for the sensing domain purposes, phthalocyanine has been used as an efficient redox catalyst to enhance the electron transfer activity within reactions (Bata et al., 2015).

Phthalocyanines (Pcs) are planar 18 π-electron aromatic compounds with a considerably large π-delocalized surface; and are promising functional materials for diverse applications (Binnemans, 2005). Owing to their excellent electronic properties, rich redox chemistry and high physico-electrochemical stability metal Pc (MPcs) derivatives are widely employed as molecular wires in biosensor applications (Cui et al., 2015; Mani et al., 2014). Nanocomposites of d-block (Co, Cu and Zn) Pcs incorporated graphene/carbon nanotubes have been employed for amperometric glucose biosensor construction (Zhang et al., 2013; Wang et al., 2015; Cui et al., 2013; Devasenathipathy et al., 2015). Olgac et al. reported ZnPc mediated detection of glucose in real samples (Olgac et al., 2017). Double decker lutetium phthalocyanine ($LuPc_2$) in particular is attractive due to its high intrinsic conductivity redox properties, and chemical stability compared to several other MPcs (Basova et al., 2008a; Basova et al., 2008b). Recently Al-Sagur and coworkers reported on glucose biosensor construction using $LuPc_2$ as redox mediator decorated in conducting polymer hydrogel (Al-Sagur et al., 2017). Thin films of $LuPc_2$ have been used for the detection of nicotinamide adenine dinucleotide and volatile organic compounds (Açikbaş et al., 2009; Galanin and Shaposhnikov, 2012a; Pal et al., 2011). Physico-chemical properties of $LuPc_2$ complexes are utilized for the photoconversion of 4-nitrophenol (Zugle and Nyokong, 2012). Literature reports reveal that incorporation of MPcs onto a silica support improves the efficacy of its catalytic performance (Armengol et al., 1999). Also MPcs grafted silica gel displayed antibactericidal activity (Kuznetsova et al., 2011). However MPcs incorporated onto silica matrix for electrocatalytic glucose biosensor application has been less studied. To further impart conductivity in bio-sensor construction, conducting polymers especially polyaniline (PANI) as electron transducers due to its excellent conductivity in its doped state, has been employed (Yanmin Wang et al., 2014). Doping with poly(vinyl alcohol-vinyl acetate) itaconic acid (PVIA) may largely improve the processability, stability and

cytocompatibility for biomedical application (Yin et al., 2017; Zeghioud et al., 2015). In this context, we intend to integrate the beneficial properties of silica, MPcs and PANI(PVIA) in the construction of a biosensor for effective GOx immobilisation. Bearing in mind the challenges in the preparation of multicomponent based biosensing platforms, a new strategy has been employed for the integration of multicomponents (silica, $LuPc_2$ and PANI(PVIA)) into a conducting nanobead (CNB) formation. The objective is achieved through the preparation of water soluble $LuPc_2$; one-step incorporation of $LuPc_2$ into the porous SiO_2 nanocages ($SiO_2(LuPc_2)$) during its synthesis; instigating grafting approach for tagging ($SiO_2(LuPc_2)$) with PANI(PVIA) to obtain $SiO_2(LuPc_2)$-PANI(PVIA)-CNB. We also evaluated the GOx immobilised CNB as a high sensitive glucose biosensor.

Herein, we report on a facile preparation of $SiO_2(LuPc_2)$-PANI(PVIA)-CNB as an electrochemical probe for the application of glucose biosensor. Nanoparticles of $SiO_2(LuPc_2)$ were obtained by the Stöber method using TEOS and APTES as a precursor. PANI(PVIA) was obtained by oxidative polymerization of aniline followed by doping it with PVIA in THF. $SiO_2(LuPc_2)$ nanoparticles were grafted with PANI(PVIA) through EDC/NHS chemistry to obtain $SiO_2(LuPc_2)$-PANI(PVIA)-CNB. The surface morphologies and other physico-chemical characteristics of $SiO_2(LuPc_2)$-PANI(PVIA)-CNB were investigated. An amperometric glucose biosensor was constructed by immobilisation of GOx onto $SiO_2(LuPc_2)$-PANI(PVIA)-CNB coated screen printed carbon electrode.

6.2. Experimental details

6.2.1. Materials

Tetraethyl orthosilicate (TEOS, 99.9%), 3-Aminopropyltriethoxysilane (APTES, 99%), ammonium hydroxide solution (NH_4OH) (28.0–30.0 wt% ammonia), Ethanol (≥99.9%), Poly(vinyl alcohol-vinyl acetate) itaconic acid (PVIA), aniline, *N*-(3-dimethylaminopropyl)-*N′*-ethylcarbodiimide hydrochloride (EDC hydrochloride), NHS (N-hydroxysuccinimide), ammonium persulfate (APS), D-(+)glucose, glucose oxidase from aspergillus niger, Type X-S, lyophilized powder, 100,000-250,000 units/g solid (without added oxygen), glutaraldehyde solution (Grade II, 25% in H_2O), Potassium ferrocyanide, Potassium ferricyanide, potassium chloride (KCl), sodium chloride (NaCl), phosphate buffer saline (PBS, pH 7.0), ascorbic acid, uric acid, horse serum and human serum were all purchased from Sigma Aldrich (UK) and used as received. Polyethoxy substituted water soluble $LuPc_2$ was prepared following a previous method (Ayhan et al., 2013) but with a few modifications. To brief the double decker lutetium (III) compound was synthesised by the reaction of the dinitrile derivative with lutetium acetate in n-pentanol in the presence of *1,8-diazabicyclo [5.4.0] undec-7-ene* (DBU) as a strong base.

6.2.2. Measurement instruments and characterisation

The morphologies of the as prepared $SiO_2(LuPc_2)$, PANI(PVIA) and $SiO_2(LuPc_2)$-PANI(PVIA)-CNB were examined by FEI-Nova scanning electron microscopy (SEM) with a low magnification (200,000×) and high voltage (20 kV). A Philips CM20 transmission electron microscopy (TEM) was used to obtain high resolution images operating at a voltage of 200kV. UV–Visible spectrophotometer (Varian 50-scan UV–Visible) was used to measure the absorption spectra of the platform. FT-IR spectra of pristine and integrated CNB were recorded on a Perkin Elmer Spectrum 100

spectrophotometer. The Brunauer–Emmett–Teller (BET) surface area of the platform was investigated through nitrogen adsorption−desorption isotherm measurements and performed on a Micromeritics ASAP 2020 M volumetric adsorption analyser at 77.34 K. A precision measurement to the platform surface was carried out by using a computer programmed Philips X-Pert X-ray diffractometer to be employed for the X-ray diffraction (XRD) work, using a Cu Kα radiation source (λ = 0.154056 nm for Kα1) working at 40 KV and 40 mA. Electrochemical measurements were performed using a portable multi Potentiostat µStat 8000/8 channels purchased from DropSens (Spain) and controlled by PC with DropView 8400 software. Disposable screen-printed carbon electrodes (DRP-C110) from DropSens with 4 mm diameter working electrode (carbon) were used for modification. The auxiliary and reference electrodes are carbon and silver, respectively, while the träger (carrier) is ceramic. The basal carbon working electrodes were modified with pristine $SiO_2(LuPc_2)$ or PANI(PVIA) or $SiO_2(LuPc_2)$-PANI(PVIA)-CNB for electrochemical purpose. The electroactivity of $SiO_2(LuPc_2)$-PANI(PVIA)-CNB modified electrode was evaluated by recording cyclic voltammogram (CV) in potassium ferro/ferricyanide solution containing 0.1 M NaCl in the potential range from -0.5 V to +0.5 V. Electrochemical impedance spectroscopy (EIS) measurements were carried out in the frequency range between 10 and 2000000 Hz. The amperometric responses of the fabricated $SiO_2(LuPc_2)$-PANI(PVIA)/GOx-CNB biosensor towards glucose detection were recorded under stirred conditions in 0.1 M PBS (pH 7.0) containing 0.1M NaCl by applying a constant potential of +0.2 V at the working electrode. The electrolyte solution was saturated with N_2 gas to remove dissolved oxygen prior to individual measurements. All electrochemical experiments were carried out at room temperature

6.2.3. Preparation of $SiO_2(LuPc_2)$-PANI(PVIA)-CNB

The preparation of $SiO_2(LuPc_2)$-PANI(PVIA)-CNB involves three stages: (1) synthesis of $SiO_2(LuPc_2)$ nanoparticles (2) synthesis of PANI(PVIA), and (3) formation of CNB.

6.2.3.1. Synthesis of $SiO_2(LuPc_2)$ nanoparticles

Monodispersed $LuPc_2$ incorporated SiO_2-NH_2 nanoparticles ($SiO_2(LuPc_2)$) was produced using modified Stöber method (Y. Han et al., 2017). Briefly, water soluble $LuPc_2$ (10% V/V) was added to TEOS (3 mL) in NH_4OH/ethanol mixture (7:100 V/V). The mixture solution was allowed to stir for about 12 h followed by quick addition of 4 mL of APTES to the above mixture under continued stirring for another 12 h at room temperature. The resultant colloidal $LuPc_2$ incorporated SiO_2-NH_2 ($SiO_2(LuPc_2)$) was obtained by centrifugation and washed with ethanol for three times.

6.2.3.2. Synthesis of PANI(PVIA)

PANI(PVIA) was prepared by doping PANI-EB onto PVIA backbone. PANI-EB was prepared as reported in the literature (Nobrega et al., 2012). Doping was achieved by mixing 1 g of PANI-EB in a THF dispersion with appropriate quantity of PVIA (0.1 M) solution. The suspension was sonicated for about 2 h followed by electromagnetic stirring (6 h) at room temperature to make the dispersion homogeneous. The resultant PANI-PVIA dispersant was filtered through polycarbonate membrane (pore size: 0.2 mm) and washed several times with deionized water till the filtrate became colorless. The precipitate was dried in vacuum oven at 60 ^oC for 24 h to obtain PANI(PVIA) powder.

6.2.3.3. Formation of CNB:

Conducting nanobeads (CNB) structure of $SiO_2(LuPc_2)$-PANI(PVIA) was obtained through covalent grafting of COOH groups in PANI(PVIA) with NH_2 groups in $SiO_2(LuPc_2)$ nanoparticles. About 0.05 g of dispersed PANI(PVIA) and 0.05 g of $SiO_2(LuPc_2)$ were redispersed in 80 mL of 0.1M PBS solution (pH 7.0). 20 mL of EDC and NHS solutions (each 25 mM) were added and stirred for about 30 min. The dispersant solution was kept undisturbed at 25 °C for 24 h. The residue ($SiO_2(LuPc_2)$-PANI(PVIA)) was separated by centrifugation, washed with deionized water and dried at room temperature.

6.2.4. Fabrication of $SiO_2(LuPc_2)$-PANI(PVIA)/GOx-CNB biosensor

About 10 mg of as prepared $SiO_2(LuPc_2)$-PANI(PVIA) was dispersed in 1 mL of isopropyl alcohol/nafion mixture (7:3 V/V). 2 µl from the above stock solution was drop casted onto pre-cleaned screen-printed carbon electrode and dried at room temperature. $SiO_2(LuPc_2)$-PANI(PVIA)/GOx-CNB biosensor was fabricated by simultaneous drop casting GOx (1 µl) (10 mg in 1 mL PBS (pH 7.0)) and glutaraldehyde (1 µl) solution. The modified electrodes were dried at room temperature under N_2 atmosphere for further analysis. Similarly, the other two $SiO_2(LuPc_2)$/GOx and PANI(PVIA)/GOx biosensors were fabricated.

6.3. Results and discussions

6.3.1. Preparation of $SiO_2(LuPc_2)$-PANI(PVIA)/GOx-CNB

The various stages in the formation of $SiO_2(LuPc_2)$-PANI(PVIA)/GOx-CNB are presented in Figure 6-1 (Stage 1(i)) that involves synthesis of $SiO_2(LuPc_2)$ nanoparticles and Figure 6-1 (Stage 1(ii)) PANI(PVIA). $SiO_2(LuPc_2)$ nanoparticles were obtained by synthesis of water soluble $LuPc_2$ as described in 6.2.3.1 and subsequent incorporation

into SiO_2 nanoparticle through mixed hydrolysis/polycondensation of TEOS and APTES in NH_4OH/ethanol medium. The incorporation of $LuPc_2$ was achieved through direct encapsulation into SiO_2 nanoparticles through Lu-O-Si bond formation during silanisation process (Sorokin et al., 2001; Zhao et al., 2009a). The colour of the $SiO_2(LuPc_2)$ nanoparticles turns slightly yellow after 24 h of gelation time in contrast to misty white observed in pristine SiO_2 nanoparticle synthesis. This confirms the presence of $LuPc_2$ in the synthesized $SiO_2(LuPc_2)$ nanoparticles. To further demonstrate the presence of $LuPc_2$ in the SiO_2 nanoparticles UV-visible spectra were recorded. Stage 1(ii): Synthesis of PANI(PVIA) was achieved by polymeric acid doping method (Taşdelen, 2017). The itaconic acid/acetate doping onto the PANI structure was confirmed by the slow colour change of PANI-EB from blue to green (Figure 6-1, see: photograph of PANI(PVIA)). Doping was further confirmed by the change in the viscosity of the PANI-PVIA mixture solution. The –COOH/acetate groups of PVIA doped onto nitrogen atoms of PANI are connected to both benzene and quinone rings. It is to be noted that upon PVIA doping the solubility of PANI greatly enhanced (verified by dissolving PANI(PVIA) and PANI-EB in water). The PANI(PVIA) in water remains unsettled over a period of 48 hrs. Stage 2 involves formation of CNB structure from the above synthesized $SiO_2(LuPc_2)$ nanoparticles and PANI(PVIA).

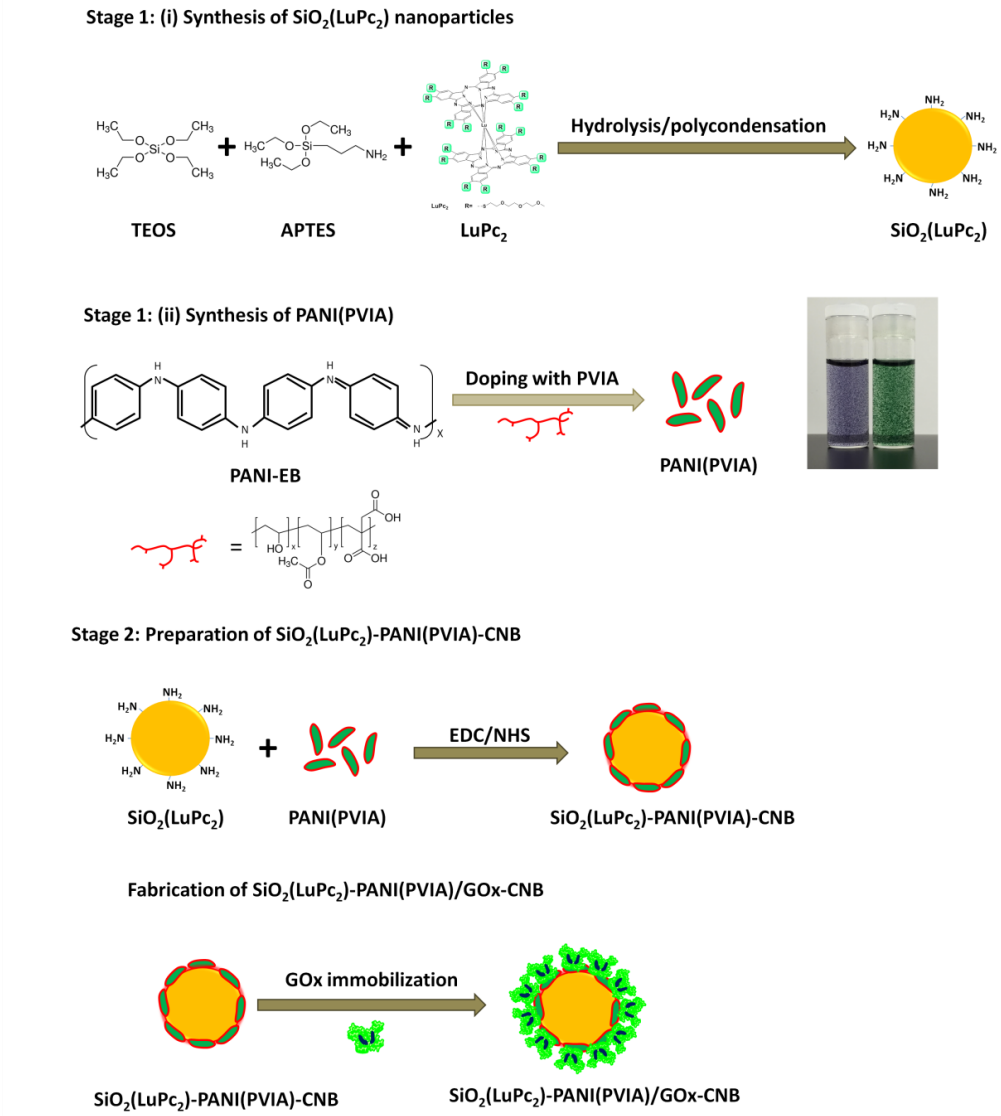

Figure 6-1 Schematic representation of the formation of SiO2(LuPc2)-PANI(PVIA)/GOx-CNB

The CNB formation was achieved through amide bond formation (amidation) via EDC/NHS chemistry (Booth et al., 2015; Qu et al., 2015). The excess –COOH group in PANI(PVIA) was covalently linked to $–NH_2$ sites in $SiO_2(LuPc_2)$ by carbodiimide activation with the assistance of NHS, leading to conjugation (Olde Damink et al., 1996; Pattabiraman and Bode, 2011). In this work, the SiO_2, $LuPc_2$, PANI, and PVIA were chosen to form CNB due to the following reasons; the simultaneous incorporation of $LuPc_2$ during SiO_2 synthesis leads to the formation of porous cage over $LuPc_2$ particles. The SiO_2 cage formation over $LuPc_2$ protects it from leaching and maintains

the functionalities under diverse environments. The SiO_2 cage was made conductive by grafting it with PANI(PVIA). The multiple functional groups in PVIA assist grafting PANI onto $SiO_2(LuPc_2)$ nanoparticle. Furthermore PVIA also offers biocompatibility/stability of CNB at different pH (Mishra et al., 2011). Thus, $SiO_2(LuPc_2)$-PANI(PVIA)-CNB can have the beneficial characteristics of an electron conductive PANI backbone, the electron mediating property of $LuPc_2$, while SiO_2 to protect leaching of catalyst and PVIA to offer biocompatibility to the CNB structures. The final product was greenish white resulted from the covalent grafting of PANI(PVIA) onto the surface of $SiO_2(LuPc_2)$ nanoparticles.

6.3.2. Morphology

$SiO_2(LuPc_2)$ nanoparticles exhibited similar spherical morphology (Figure 6-2(a)) as that of pristine SiO_2 nanoparticles (Figure 6-2(d)), except with the change in the size of the nanoparticles. Figure 6-2(a) shows spherical particles of $SiO_2(LuPc_2)$ in different size distribution. The particle size ranges from 150 to 200 nm. However, the as prepared pristine SiO_2 nanoparticles are uniform with an average size of 140 nm (Figure 6-2(d)). The variation in the size distribution of $SiO_2(LuPc_2)$ exemplifies the incorporation of $LuPc_2$ into SiO_2 nanoparticles during the mode of synthesis. Furthermore it could be seen that the particles are slightly tilted to accommodate $LuPc_2$ in its interior porous structure. The presence of $LuPc_2$ in $SiO_2(LuPc_2)$ nanoparticles was further confirmed through EDX measurements. The elemental test results confirmed the presence of

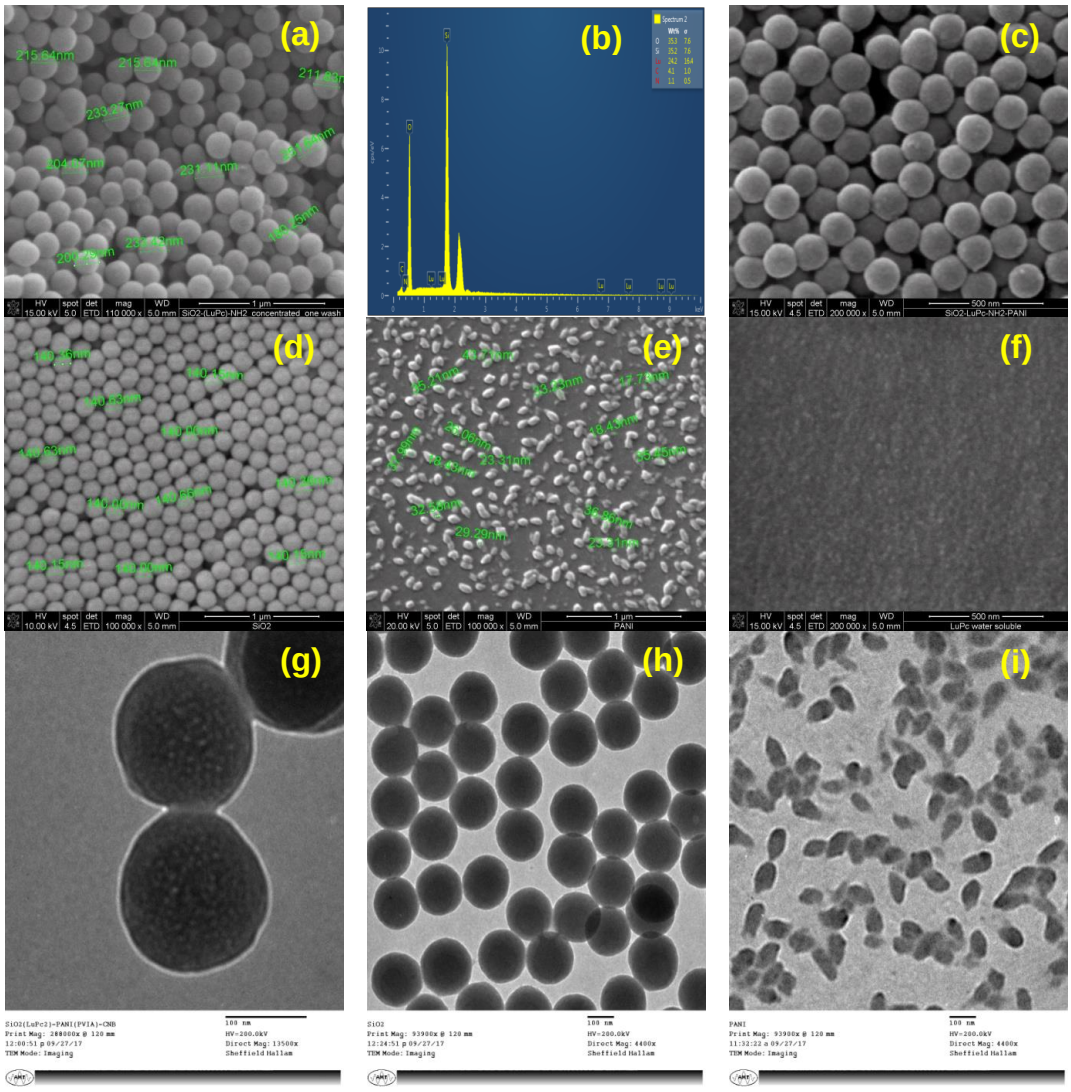

Figure 6-2 SEM images of (a) $SiO_2(LuPc_2)$, (b) EDX image of $SiO_2(LuPc_2)$, (c) $SiO_2(LuPc_2)$-PANI(PVIA)-CNB, (d) SiO_2, (e) PANI(PVIA), (f) $LuPc_2$; TEM images of (g) $SiO_2(LuPc_2)$-PANI(PVIA)-CNB, (h) SiO_2, (i) PANI(PVIA)

inorganic ion Lu (24.2 wt%) in the ratio of 1:3 with SiO_2 (Figure 6-2(b)) within $SiO_2(LuPc_2)$ nanoparticles. Figure 6-2(c) shows the morphology of $SiO_2(LuPc_2)$-PANI(PVIA)-CNB. Upon PANI(PVIA) grafting onto $SiO_2(LuPc_2)$, the size of the nanoparticles transformed between 180 to 220 nm. This ensures the successive grafting of PANI(PVIA) onto the surface of $SiO_2(LuPc_2)$ nanoparticles (Roosz et al., 2017). For further confirmation TEM image of $SiO_2(LuPc_2)$-PANI(PVIA)-CNB is recorded (Figure 6-2(g)). The dark spots noticed within the SiO_2 nanoparticles ensure the incorporation of $LuPc_2$ inside the nanocages of SiO_2. However, the TEM image of

pristine SiO_2 nanoparticle showed smooth and uniform size distribution of particles (Figure 6-2(h)). On closer analysis, we could notice that the surface becomes coarse due to PANI(PVIA) grafting. For reference the SEM images of PANI(PVIA) and $LuPc_2$ are shown in Figure 6-2(e) and Figure 6-2(f), respectively. TEM image of PANI(PVIA) exhibited nanobead-like structure with average particle size around 30 nm (Figure 6-2(i)).

The surface area of pristine SiO_2 and $SiO_2(LuPc_2)$ are studied through Brunauer, Emmett and Teller (BET) measurements. The surface area of pristine SiO_2 and $SiO_2(LuPc_2)$ are found to be 48.2889 ± 0.8737 m^2/g and 20.4619 ± 0.5225 m^2/g respectively. The reduction in the surface area ~57% addresses the incorporation of $LuPc_2$ well within porous nanocage of SiO_2 nanoparticles. The results are analogous to the significant decrease in the specific surface area noticed in palladium immobilised nanocages of SBA-16 compared to parent SBA-16 (Wang et al., 2013).

6.3.3. UV-visible analysis

The UV-visible absorption spectra of $SiO_2(LuPc_2)$ (Figure 6-3a) show characteristic N, B, and Q bands of $LuPc_2$ around λ = 315 nm, sharp band around λ = 390 nm, and an intensive Q absorption band of the macrocycles at λ = 702 nm (Basova et al., 2008a; 2008b). This features the incorporation of $LuPc_2$ inside SiO_2 nanoparticles. However the observed variation in peak intensity in addition to small shift in absorption bands compared to pristine $LuPc_2$ (Figure 6-3,inset) may arise due to the interaction of $LuPc_2$ with host walls of SiO_2 and dimerization of larger aggregates during the gellation process (Holland et al., 1998).

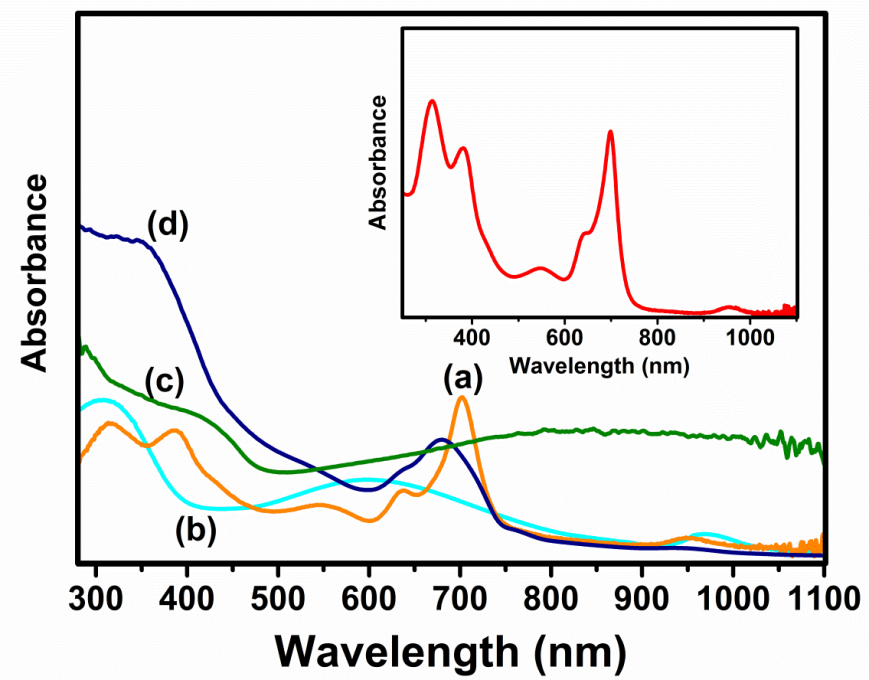

Figure 6-3 UV-visible spectrum of (a) $SiO_2(LuPc_2)$, (b) PANI-EB (dedoped), (c) PANI(PVIA), (d) $SiO_2(LuPc_2)$-PANI(PVIA)-CNB. Inset UV-visible spectrum of $LuPc_2$

Figure 6-3 b,c shows the absorption spectra of PANI-EB and PANI(PVIA), respectively. The undoped PANI-EB (Figure 6-3b) showed absorption bands corresponding to π-π* transition of benzene ring (310 nm) and excitation of the imine segment on the PANI chain (around 600 nm) (Rahy et al., 2011). Moreover for PANI(PVIA) (Figure 6-3c), the disappearance of the band around 600 nm indicates that

the doping occurs at the imine segment of the emeraldine chain (Yanmin Wang et al., 2014). The observed bathochromic (red) shift of π-polaron to > 750 nm illustrates that PANI backbone was well doped with –COOH/acetate functional groups in PVIA (Taşdelen, 2017). Additionally, the appearance of the band at 420 nm results from the polaron phenomenon of PANI(PVIA) (Dominis et al., 2002). In the case of $SiO_2(LuPc_2)$-PANI(PVIA), the polaronic band of PANI(PVIA) exhibits hypsochromic shift to around 360 nm (Figure 6-3d) with broadening of the Q band around 700 nm. This ensures that PANI(PVIA) grafting over $SiO_2(LuPc_2)$ (~30 nm thickness calculated from SEM) does insignificantly affect the electronic properties of $LuPc_2$ (Zhuang et al., 2011).

6.3.4. FT-RI analysis

The FTIR spectrum of PANI(PVIA), $SiO_2(LuPc_2)$ and $SiO_2(LuPc_2)$-PANI(PVIA)-CNB is shown in Figure 6-4. Curve a shows the predominant peaks of PANI around 1610 cm^{-1} and 1520 cm^{-1} that can be referred to the stretching vibrations of quinone and benzene rings, respectively (Komathi et al., 2017b). Further, absorption bands associated with PVIA doping were also observed. A strong hydroxyl bands for hydrogen-bonded alcohol between (ν=3100-3570 cm^{-1}) was clearly observed. The saturated aliphatic esters (acetate) and carboxylic acid have also been noticed around 1650 cm^{-1} (C=O stretching band) and the other C-O peak corresponding to stretching alcohol, ester, and carboxylic acid groups of PVIA was identified by an absorption band around 1220 cm^{-1} (Anis et al., 2007). The presence of a strong peak around 1088 cm^{-1} in $SiO_2(LuPc_2)$ (curve b) confirms the formation of Si–O–Si linkages (Komathi et al., 2009b). The FTIR spectra of $SiO_2(LuPc_2)$-PANI(PVIA)-CNB (curve c) exhibited the signature peaks of both SiO_2 and PANI(PVIA) however with a minor shift in its corresponding peak position as compared to pristine materials.

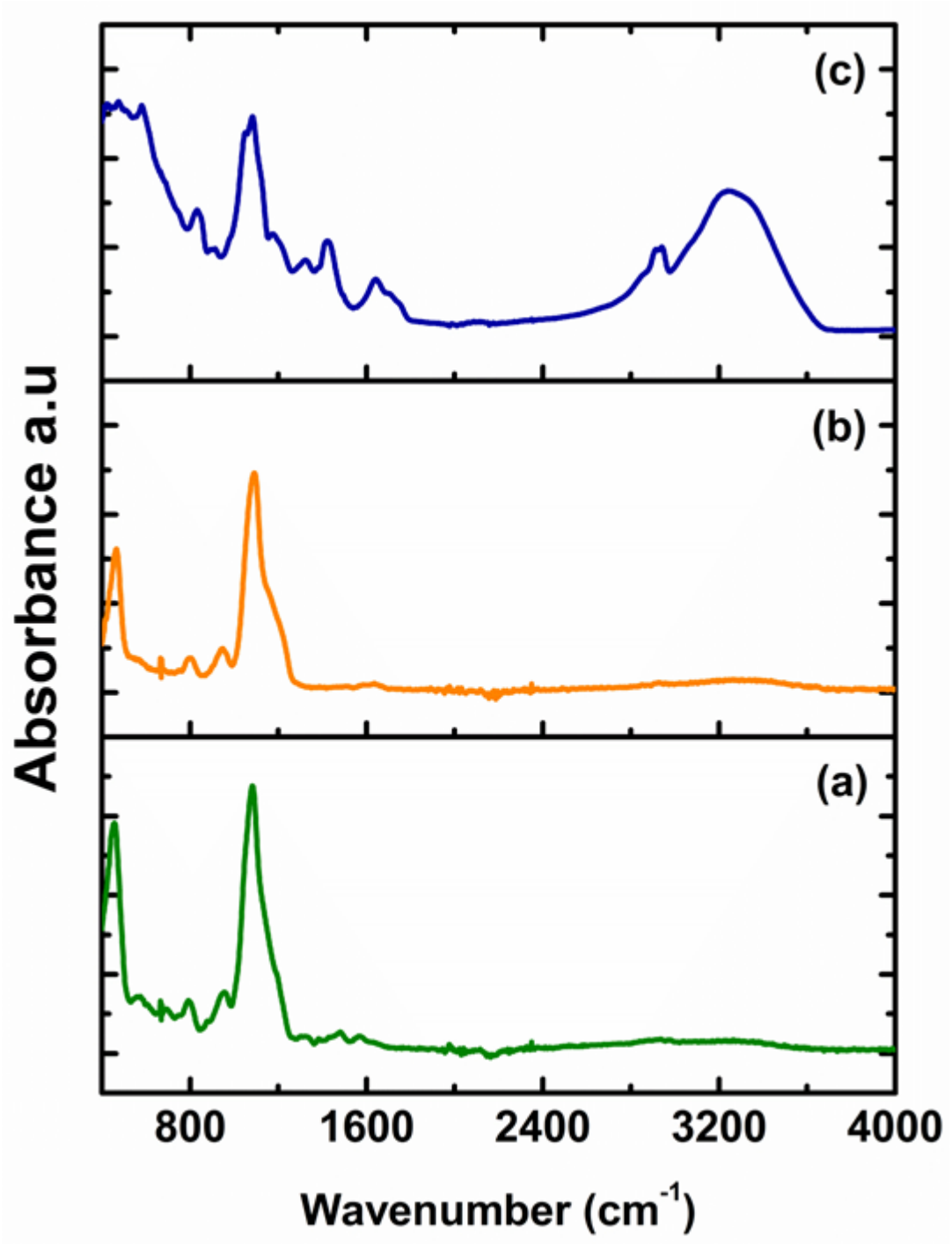

Figure 6-4 FTIR spectra of (a) PANI(PVIA), (b) $SiO_2(LuPc_2)$, (c) $SiO_2(LuPc_2)$-PANI(PVIA)-CNB

6.3.5. XRD analysis

To investigate the structure of PANI(PVIA), $SiO_2(LuPc_2)$ and $SiO_2(LuPc_2)$-PANI(PVIA)-CNB, XRD analysis was carried out. The diffractogram of PANI(PVIA) powder (Figure 6-5) showed two peaks centered at 22.81° and the other at 46.91° representing the crystal planes of (100) and (110) respectively. The high peak intensity

illustrates that the chains of PANI(PVIA) were more ordered as witnessed from the TEM images of PANI(PVIA) (Figure 6-2(i)). However, the diffractograms of $SiO_2(LuPc_2)$ and $SiO_2(LuPc_2)$-PANI(PVIA)-CNB (Figure 6-5 inset) showed broad peak around 2theta = 23° illustrating that these materials were amorphous or non-periodic. It reveals that grafting PANI(PVIA) onto the surface of $SiO_2(LuPc_2)$ insignificantly affects the crystal structure of $SiO_2(LuPc_2)$ (Sharma and Gulati, 2012).

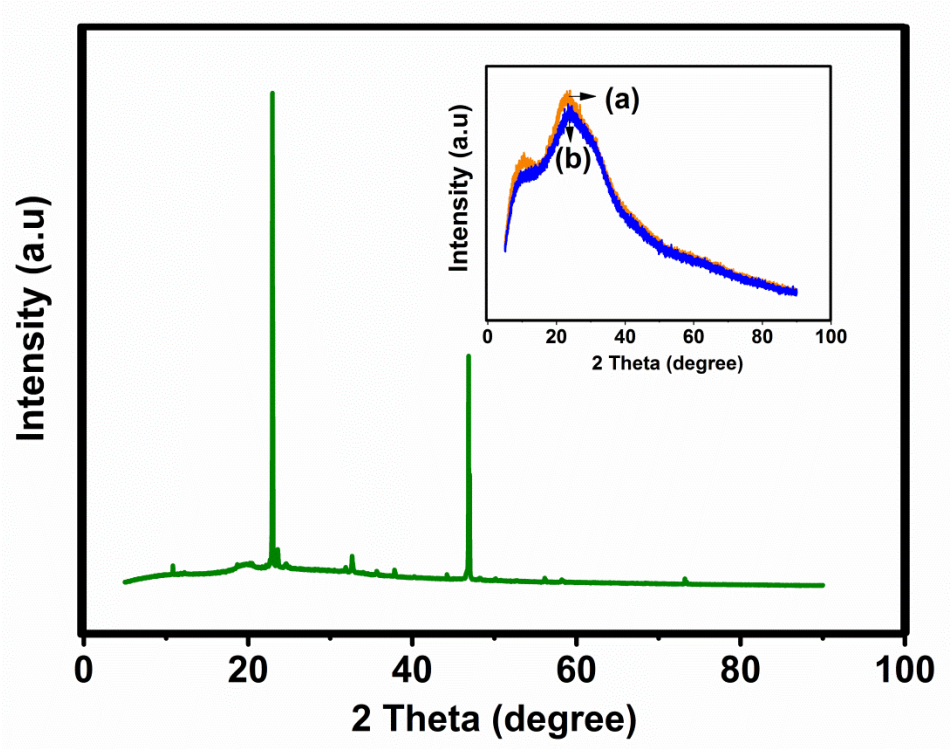

Figure 6-5 XRD patterns of PANI(PVIA) (Inset: XRD patterns where curve (a) represents $SiO_2(LuPc_2)$ and curve (b) is $SiO_2(LuPc_2)$-PANI(PVIA)-CNB

6.3.6. Electrochemical impedance measurements

Electrochemical impedance spectroscopy is a powerful tool to study interfacial characteristics of surface modified electrodes as well as gaining information about charge transfer properties of the various compounds incorporated in the electrode to support the function of the modifiers. Figure 6-6A shows the impedance measurements (Nyquist plot) of $SiO_2(LuPc_2)$, PANI(PVIA) and $SiO_2(LuPc_2)$-PANI(PVIA) GOx-CNB respectively carried out at the open circuit potential in 5 mM $K_3[Fe(CN)_6]/K_4[Fe(CN)_6]$

containing g 0.1 M NaCl. One could observe distinct differences in the impedance spectra. The charge transfer resistance (R_{ct}) was calculated from the obtained semicircular part at the high frequency region.

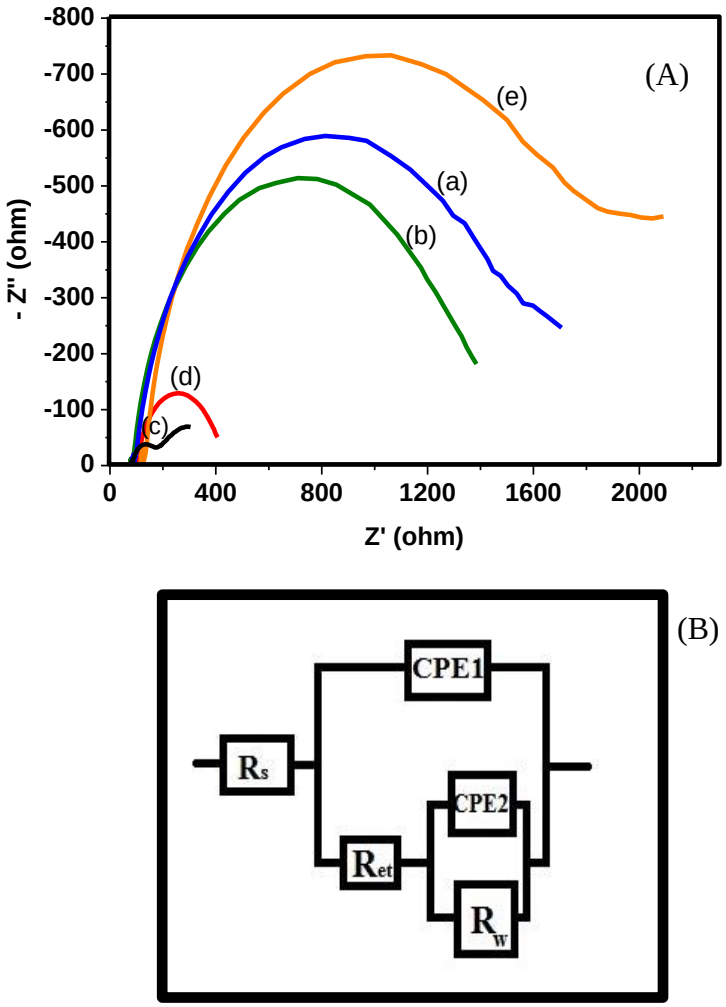

Figure 6-6 (A) Nyquist plots (Z_{im} vs. Z_{re}) of (a) PANI(PVIA), (b) $SiO_2(LuPc_2)$, (c) $SiO_2(LuPc_2)$-PANI(PVIA)/GOx-CNB, (d) $LuPc_2$, and (e) SiO_2 at 5 mM $K_3[Fe(CN)_6]/K_4[Fe(CN)_6]$ containing g 0.1 M NaCl; (B) Equivalent circuit model of the fabricated biosensor, $SiO_2(LuPc_2)$-PANI(PVIA)/GOx-CNB

The results showed that $SiO_2(LuPc_2)$-PANI(PVIA) GOx-CNB exhibits much lower R_{ct} value (180 Ω) compared to $SiO_2(LuPc_2)$ (1380 Ω) and PANI(PVIA) (1710 Ω) modified electrodes. The electron transfer rate at $SiO_2(LuPc_2)$-PANI(PVIA)-CNB biosensor was approximately 7.6 and 9.5 higher than that at $SiO_2(LuPc_2)$ and PANI(PVIA) electrodes,

respectively. The reduction in the resistance to charge transfer in the electrode is possibly accomplished by the $LuPc_2$, as clearly indicated in Figure 6-6A curve (d). The linear part at low frequency region ensures a mixed kinetic and diffusion controlled process at $SiO_2(LuPc_2)$-PANI(PVIA)-CNB biosensor while surface controlled process prevails at pristine $SiO_2(LuPc_2)$ and PANI(PVIA) modified electrodes (based on tail length). The fast electron transfer rate at $SiO_2(LuPc_2)$-PANI(PVIA)-CNB informs that the grafted PANI(PVIA) chains electronically wires the electron from the surface through $LuPc_2$ to the underlying electrode. For comparison the Nyquist plot of $LuPc_2$ and SiO_2 is also presented. Equivalent circuit model R(Q(R(QR))) for the fabricated biosensor, $SiO_2(LuPc_2)$–PANI(PVIA)/GOx-CNB, where R_s is the uncompensated solution resistance; R_{et} is the electron transfer resistance; R_W is Warburg diffusion element (W) and CPE_1 & CPE_2 standing for the double layer capacitance on the electrode/electrolyte interface and the pseudocapacitance in the polymer film, respectively, is shown in Figure 6-6B.

6.3.7. Electrochemical behaviour of $SiO_2(LuPc_2)$-PANI(PVIA)-CNB modified electrode

The electrochemical behavior of the modified electrodes was investigated by recording cyclic voltammograms (CVs) of modified electrodes using $Fe(CN)_6^{3-/4-}$ as a redox marker. CV obtained at pristine SiO_2 (curve a), $SiO_2(LuPc_2)$ (curve b), PANI(PVIA) (curve c) and $SiO_2(LuPc_2)$-PANI(PVIA)-CNB (curve d) in $Fe(CN)_6^{3-/4-}$ (5 mM) containing 0.1M NaCl versus silver-silver chloride electrode (Ag/AgCl) is shown in

Figure 6-7. A pair of one electron quasi-reversible redox peaks corresponding to

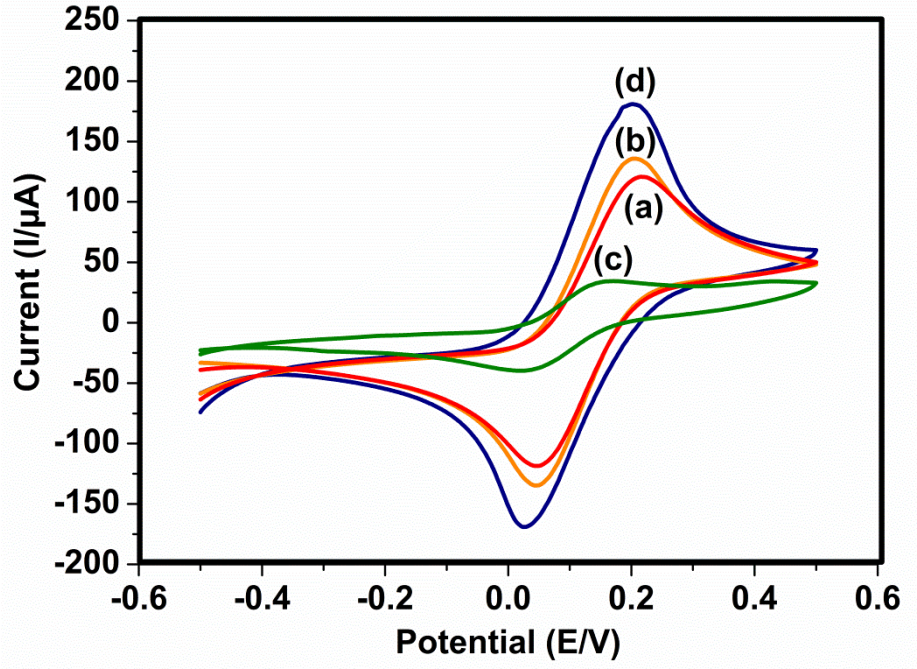

Figure 6-7 Cyclic voltammogram of (a) SiO_2, (b) $SiO_2(LuPc_2)$, (c) PANI(PVIA), (d) $SiO_2(LuPc_2)$-PANI(PVIA)-CNB recorded in 5 mM Potassium ferro/ferri cyanide solution containing 0.1 M NaCl as a supporting electrolyte versus Ag/AgCl; scan rate = 100 mV/s

Fe(II)/Fe(III) transition process was observed at all electrodes. However, the redox peak current (I_{pa}/I_{pc}) and the peak potential separation between anodic (E_{pa}) and cathodic (E_{pc}) wave (ΔE_p) differ between the individual electrodes. It is observed that the I_{pa}/I_{pc} value of $SiO_2(LuPc_2)$ increases by ~1.2 times than that of pristine SiO_2 modified electrode. This ensures that the incorporated $LuPc_2$ within SiO_2 cage enhances the electrochemical activity of SiO_2 (García-Sánchez et al., 2013). Moreover the Ipa/Ipc redox peak current further increases to 181.4 µA /-168.4 µA (I_{pa}/I_{pc}) at $SiO_2(LuPc_2)$-PANI(PVIA)-CNB modified electrode (curve d). It should be noted that the Fe(II)/Fe(III) redox peak current is found to be highest at $SiO_2(LuPc_2)$-PANI(PVIA)-CNB which is ~1.3 and ~1.5 times higher than at $SiO_2(LuPc_2)$ and pristine SiO_2 nanoparticles modified electrodes. The result demonstrates that the presence of PANI(PVIA) as a grafted network onto $SiO_2(LuPc_2)$ augments the electronic conductivity (Gopalan et al., 2010), in addition to the presence of $LuPc_2$ and SiO_2 that

provide three dimensional pathway for the adequate percolation of ions to the electrode surface and facilitate the electron transfer process (Al-Sagur et al., 2017; Gopalan et al., 2009). The I_{pa}/I_{pc} redox peaks of pristine PANI(PVIA) are ~5.1 times lower than that in the case of $SiO_2(LuPc_2)$-PANI(PVIA)-CNB modified electrode. The ΔE_p value was found to increase in the following order: PANI (PVIA) (145 mV) < $SiO_2(LuPc_2)$-PANI(PVIA)-CNB (170 mV) < $SiO_2(LuPc_2)$ (172 mV) < SiO_2 (175 mV).

CVs of $SiO_2(LuPc_2)$-PANI(PVIA)-CNB were also recorded for different scan rates (10–100 mV/s) (Figure 6-8A); Figure 6-8B represents the dependence of scan rates on peak current. The calibration of $v^{1/2}$ *vs* Ipa or Ipc showed linearity with the correlation coefficient of 0.999 (n=10), which confers the diffusion controlled process of $Fe(CN)_6^{3-/4-}$ redox reaction at $SiO_2(LuPc_2)$-PANI(PVIA)-CNB (Siswana et al., 2006). The diffusional coefficient (D) was calculated to be 8.106×10^{-6} cm^2/s using Randles–Sevcik equation (Nagarale et al., 2009). With the known value of D and n=1 for reversible redox process, the electrochemical active surface area (A) of the electrode was determined to be 1.184 cm^2. The value of 'A' results from the three dimensional porous structures of $SiO_2(LuPc_2)$-PANI(PVIA)-CNB. The results from electrochemical activity (CV) demonstrate the importance of individual components (SiO_2, $LuPc_2$, PANI(PVIA)) in its fabrication design for the further immobilisation of GOx for the determination of glucose.

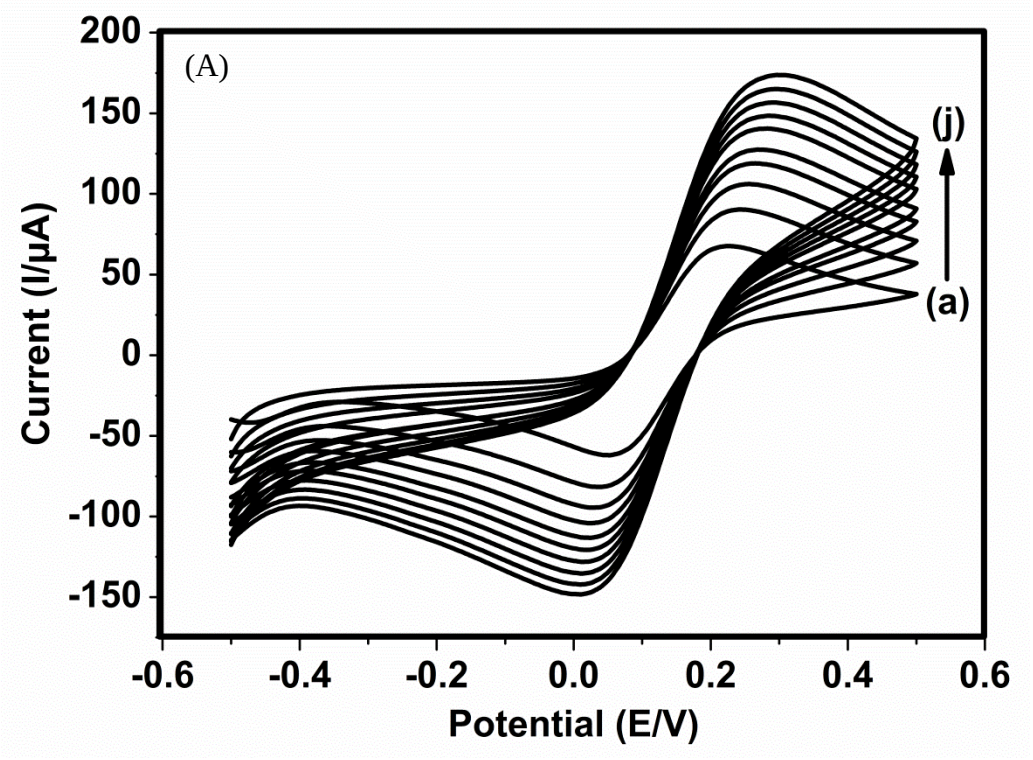

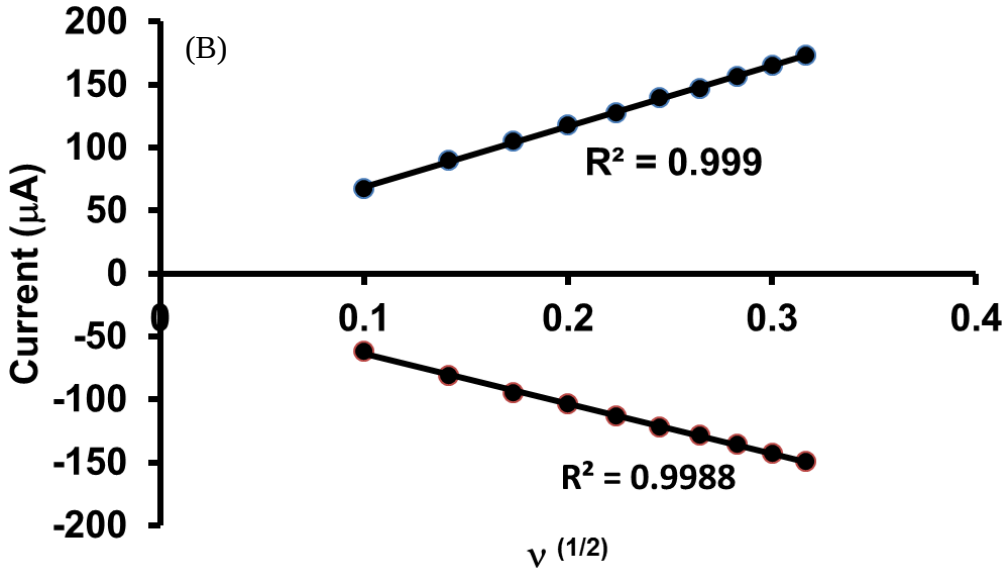

Figure 6-8 (A) Cyclic voltamograms (CVs) of $SiO_2(LuPc_2)$-PANI(PVIA)-CNB in 5 mM of Fe(CN)63−/4− containing 0.1 M NaCl versus Ag/AgCl for different scan rates (a–j); 10-100 mVs-1; (B) Dependence of scan rates on peak current

6.3.8. Electrochemical behavior of $SiO_2(LuPc_2)$-PANI(PVIA)/GOx-CNB biosensor

CV response of the GOx immobilised $SiO_2(LuPc_2)$-PANI(PVIA)-CNB modified electrode in N_2-saturated PBS solution (pH 7.0) containing 0.1M NaCl is shown in Figure 6-9.

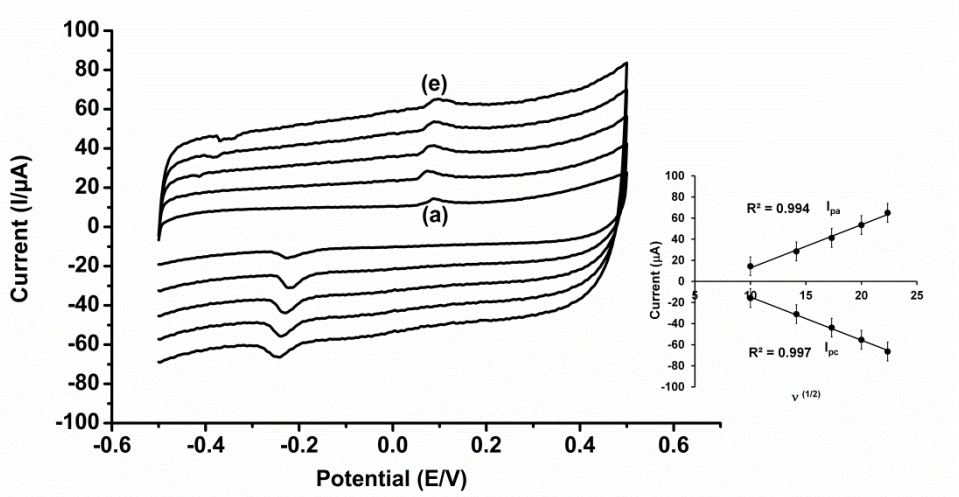

Figure 6-9 Cyclic voltammogram of $SiO_2(LuPc_2)$-PANI(PVIA)/GOx-CNB in N_2 saturated 0.1 M PBS (pH 7.0) containing 0.1 M NaCl versus Ag/AgCl for different scan rate 100-500 mV/s (a-e); inset: plot of $\nu^{1/2}$ vs I_p

A well-defined symmetrical redox peaks (0.074 V anodic; -0.212 V cathodic) corresponding to immobilised GOx at scan rate = 100 mV/s could be noticed. The effect of scan rate on the CV response of redox peaks was also studied by varying the scan rate from 100-500 mV/s. It should be noted that even at the higher scan rate of 500 mV/s, the $SiO_2(LuPc_2)$-PANI(PVIA)/GOx-CNB biosensor showed redox behavior with a slight shift in its ΔE_p. This ensures the stable immobilisation of GOx onto $SiO_2(LuPc_2)$-PANI(PVIA)-CNB in its native configuration (Gopalan et al., 2009). The redox peak current linearly increased with $\nu^{1/2}$ in the range of 100–500 mV s ($R^2 \approx 0.999$), indicating a diffusion-controlled electrochemical process. The plot of log $\nu^{1/2}$ vs E_{pa} and E_{pc} (inset Figure 6-9) showed straight lines with the correlation coefficient of R^2

= 0.994 (anodic) and R^2 = 0.997 (cathodic). The diffusion coefficient (D) of charge transfer was estimated to be $1.47x10^{-6}$ cm^2/s using Randles–Sevcik equation (Nagarale et al., 2009). The surface coverage of the modified electrode is calculated to be $7.13x10^{-7}$ mol/cm^2 which is typically higher than GOx immobilised on SAM modified electrode ($4.80x10^{-12}$ mol/cm^2) (Fang et al., 2003). The higher value of surface coverage admits the increased loading of GOx onto $SiO_2(LuPc_2)$-PANI(PVIA)-CNB surface. Moreover the immobilised GOx enzymes are well bound on the surface observed from the redox peaks at scan rate = 500 mV/s in 0.1 M PBS. Thus the higher and native loading of GOx could be achieved by the excess functional groups (from PVIA&PANI) and biocompatible environment provided by PVIA for the guest enzymes. For comparison CVs of pristine $SiO_2(LuPc_2)$/GOx and PANI(PVIA)/GOx were also recorded in 0.1M PBS and presented in Figure 6-10.

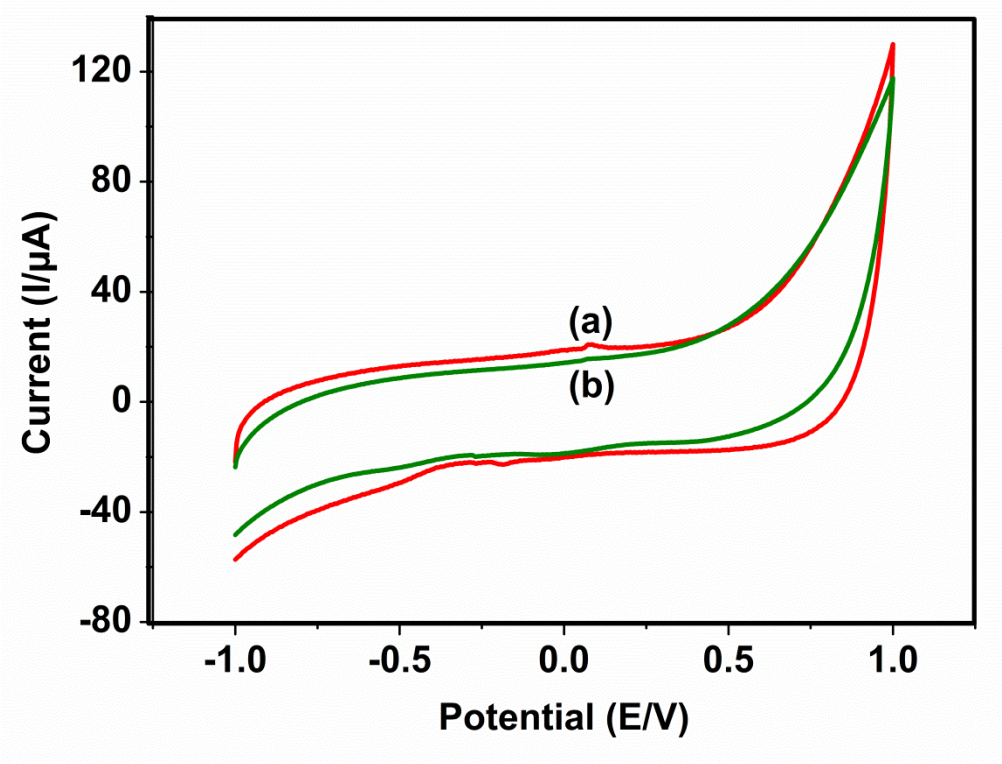

Figure 6-10 Cyclic voltamograms (CVs) of (a) $SiO_2(LuPc_2)$/GOx and (b) PANI(PVIA)/GOx in N_2 saturated 0.1M PBS (pH 7.0) containing 0.1 M NaCl versus Ag/AgCl

6.3.9. Amperometric response of glucose at $SiO_2(LuPc_2)$-PANI(PVIA)/GOx-CNB biosensor

Amperometric measurements were recorded for varied concentrations of glucose to demonstrate the functioning of $SiO_2(LuPc_2)$-PANI(PVIA)/GOx-CNB as a potential glucose biosensor and the results are shown in Figure 6-11. Upon successive injection of glucose (1 mM) at regular intervals, a rapid and prominent increase in the bioelectrocatalytic amperometric current (E = +0.2 V) was observed under stirred condition.

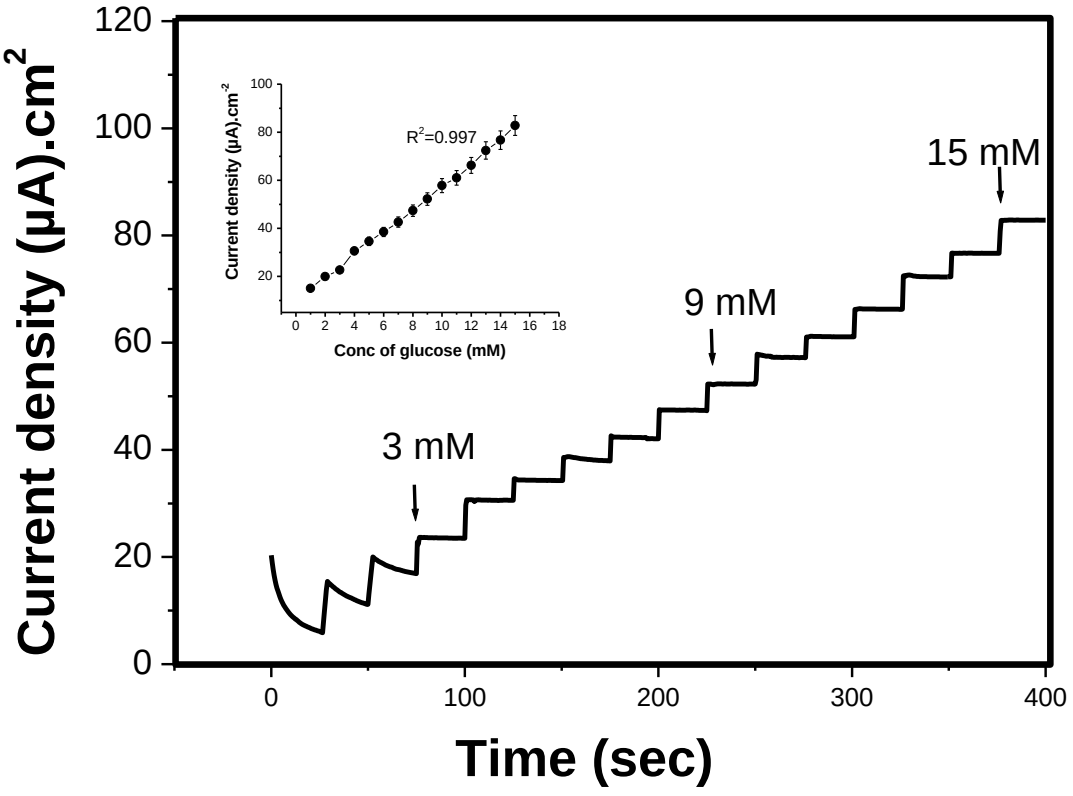

Figure 6-11 Amperometry response for successive addition of glucose in 0.1 M PBS (pH 7.0) at $SiO_2(LuPc_2)$-PANI(PVIA)/GOx-CNB. Inset: calibration plot [glucose] vs peak current density

The operating principle is based on the enzymatic oxidation of glucose catalyzed by GOx immobilised onto $SiO_2(LuPc_2)$-PANI(PVIA)-CNB. The injected glucose are first enzymatically oxidized to gluconolactone, while GOx(FAD) reduced to GOx($FADH_2$).

Thereafter GOx(Red) will be regenerated to GOx(FAD) by electrooxidized $SiO_2(LuPc_2)$-PANI(PVIA)-CNB. The plausible mechanism is as follows

$$Glucose + GOx(FAD) \rightarrow Gluconolactone + GOx(FADH_2) \quad (1)$$

$$GOx(FADH_2) + SiO_2\left(Lu^{(III)}Pc_2\right) - PANI(PVIA) - CNB \rightarrow GOx(FAD) + SiO_2\left(Lu^{(II)}Pc_2\right) + 2H^+ \quad (2)$$

$$2SiO_2\left(Lu^{(II)}(II)Pc_2\right) - PANI(PVIA) - CNB \rightarrow 2SiO_2\left(Lu^{(III)}(III)Pc_2\right) - PANI(PVIA) - CNB + 2e^- \ (+0.2\,V) \quad (3)$$

The current response was linear for glucose concentration in the range of 1–16 mM (correlation coefficient, $R = 0.997$) (Figure 6-11 inset). The responses were saturated when glucose concentrations were higher than 16 mM that could be attributed to enzyme saturation (Li et al., 2009). The sensitivity of the $SiO_2(LuPc_2)$-PANI(PVIA)/GOx-CNB biosensor is calculated to be 38.53 μA/mM/cm^2 from the slope of the calibration plot with a RSD of 5.8%. The sensitivity of the $SiO_2(LuPc_2)$-PANI(PVIA)/GOx-CNB biosensor is superior than reported for the glucose biosensor fabricated with other SiO_2 composites for GOx immobilisation. Sol–gel/GOx/copolymer (0.6 μA/mM) (Wang et al., 1998), PEDOT/PB/MWNT (2.67 μA/mM) (Chiu et al., 2009), Silica/GOx/CNTs (approximately 0.2 μA/mM) (Salimi et al., 2004), and GOx-SWCNT conjugates/PVI-Os bilayers (32 μA/mM/cm^2) (Gao et al., 2011) are typical examples as reported in the literature. The superior sensitivity results from the judicious design of the fabricated electrode. The presence of thin grafted PANI(PVIA) layer provides excess functional groups (-OH/ -CH_3COO-/ –COOH from PVIA and NH_2 sites from PANI) for the bonding of GOx. Also PVIA provides biocompatible environment for the immobilised (GOx) enzyme (biocompatibility of poly itaconic acid for biomolecules). While SiO_2 provides three dimensional porous surface for the grafting process, $LuPc_2$ in SiO_2 nanoparticles mediates/transfers electrons to the electrode surface. The $SiO_2(LuPc_2)$-

PANI(PVIA)/GOx-CNB biosensor showed a fast response to the changes in glucose concentration and the steady-state response current reached within 2 s. The response time is much lower than in the case of pristine PANI incorporated silica particles (Manesh et al., 2010), SiO_2 grafted with PVA+PVP (Wang et al., 1998), and mesacellular carbon foam (Wang et al., 1998). The instant amperometric current response upon the addition of glucose is attributed to the faster diffusion of glucose at $SiO_2(LuPc_2)$-PANI(PVIA)/GOx-CNB. The rapid response to glucose was achieved due to the integrated presence of PANI(PVIA) that electronically wires the electron from GOx through $LuPc_2$ to underlying electrode (Tiwari et al., 2015). The wide linear range (1-16 mM) and high sensitivity (38.53 μA/mM/cm^2) of $SiO_2(LuPc_2)$-PANI(PVIA)/GOx-CNB biosensor made it suitable for human blood glucose detection.

The apparent Michaelis–Menten constant (K_M) was calculated as 10.36 mM using the slope and intercept values from the Lineweaver–Burk plot for $SiO_2(LuPc_2)$-PANI(PVIA)/GOx-CNB biosensor (Mobin et al., 2010). The value is close to that reported for the free GOx enzyme (12.4 mM) (Swoboda and Massey, 1965). This demonstrates that non-denaturated characteristics of GOx immobilised onto $SiO_2(LuPc_2)$-PANI(PVIA)-CNB. The limit of detection (LOD) for glucose at $SiO_2(LuPc_2)$-PANI(PVIA)/GOx-CNB biosensor was calculated as 0.1 mM (signal to noise ratio=3). The detection limit is estimated as three times of the standard deviation of the background. Comparison of analytical performances of some glucose biosensors based on GOx immobilised onto PANI/phthalocyanine/silica as one of the component in the matrix is presented in Table 6-1.

Table 6-1 Comparison of the oxidation of glucose performance at different modified electrodes

Electrode	Linear range (mM)	Sensitivity ($\mu A\ cm^{2}\ mM^{-1}$)	Ref
$PyCO_2$/Ppy-Fc/GOx	1.0-4.0	1.796	(Şenel, 2011)
FC-20/Chi/GOx	1.0-6.0	0.86	(Nagarale et al., 2009)
PAA-rGO/VS-PANI/$LuPc_2$/GOx-MFH	2-12	15.31	(Al-Sagur et al., 2017)
Ru-RP/GOx	0-10	24.3	(Deng et al., 2014)
Os-complex/GOx	0-0.7	28.24	(Jiang et al., 2008)
(GOx/Au-(SH)PANI-g-MWNT)$_n$/ITO	1-9	3.97	(Komathi et al., 2009a)
Au-ME-CoTCAPc-GOx-SAM	0.3-25	$7.5x10^{-3}$	(Mashazi et al., 2006)
MWNT-g-SPAN-NW/GOx	0-9	4.34	(Kwang Pill Lee et al., 2010)
Os(2,2'Bpy)2-RP/GOx	0-10	16.5	(Deng et al., 2013)
Ferrocene/GOx	0.1-10	12.42	(Nien et al., 2006)
GOx/mesoFe/C-Nafion	0.2-10	27	(Yu et al., 2010)
GOx/CoPc/SPCE	0.2-5	-	(Crouch et al., 2005)
SiO_2($LuPc_2$)-PANI(PVIA)/GOx-CNB	1-16	38.53	Our present work

6.3.10. Optimisation of SiO_2($LuPc_2$)-PANI(PVIA)/GOx-CNB biosensor performance

6.3.10.1. Effect of pH

The pH effect on the biosensor performance of SiO_2($LuPc_2$)-PANI(PVIA)/GOx-CNB was investigated by measuring the amperometric current response to 1 mM glucose at +0.2 V. So we have varied the pH from 2 to 10 to in order to determine the optimum value for the immobilised GOx enzyme (Figure 6-12). Depending on the pH of the environment, the charges on the functional groups on the external surface of enzymes will vary. The catalytic performance of the enzyme strongly depends on environmental pH and is usually "bell-shaped" maximum at optimum pH (Zheng et al., 2002). In case of of SiO_2($LuPc_2$)-PANI(PVIA)/GOx-CNB biosensor the maximum current response occurs at pH 7.0. the current response for glucose at SiO_2($LuPc_2$)-PANI(PVIA)/GOx-CNB biosensor gradually increases till pH 7 and the demise of the current response at pH > 8 may be due partial destruction of cystine residues (Zheng et al., 2002). Hence

pH 7 is chosen for the further amperometric determination of glucose at $SiO_2(LuPc_2)$-PANI(PVIA)/GOx-CNB biosensor.

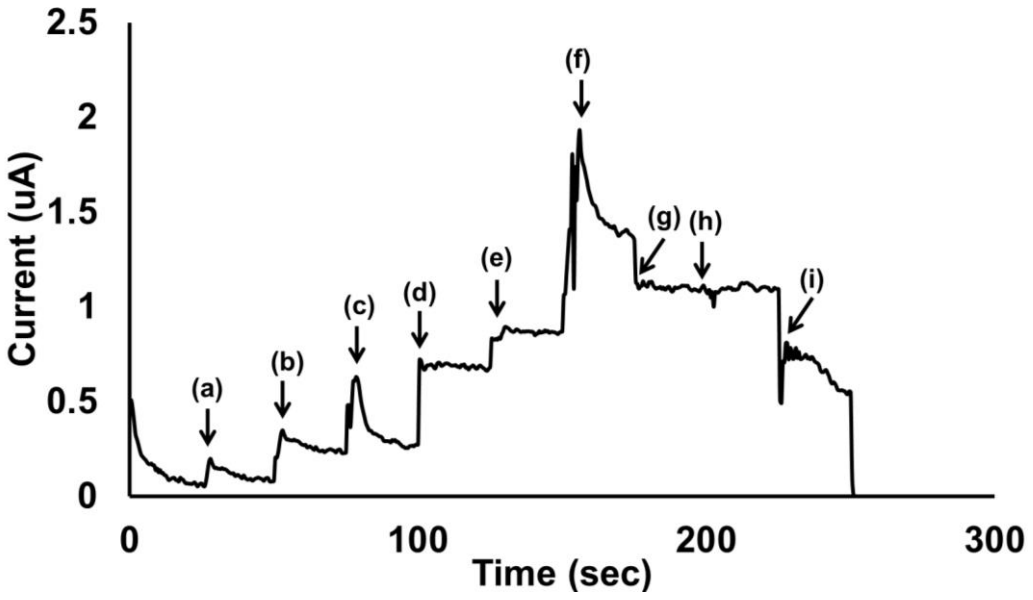

Figure 6-12 Effect of pH (a) 2, (b) 3, (c) 4, (d) 5, (e) 6, (f) 7, (g) 8, (h) 9, (i) 10 on the current response of glucose by $SiO_2(LuPc_2)$-PANI(PVIA)/GOx-CNB biosensor

6.3.10.2. Effect of GOx concentration

The variation of immobilised GOx in the performance of $SiO_2(LuPc_2)$-PANI(PVIA)/GOx-CNB biosensor was monitored. $SiO_2(LuPc_2)$-PANI(VIA) was fixed as 2 μL (10 mg/1mL) and GOx concentration varied between 0.25 to 2 μL (10 mg GOx dissoved in 1 mL PBS). The results were presented in Figure 6-13. As can be seen the current response increases with increasing enzyme concentration and reaches maximum at 1 μL and thereafter no significant improvement could be observed.

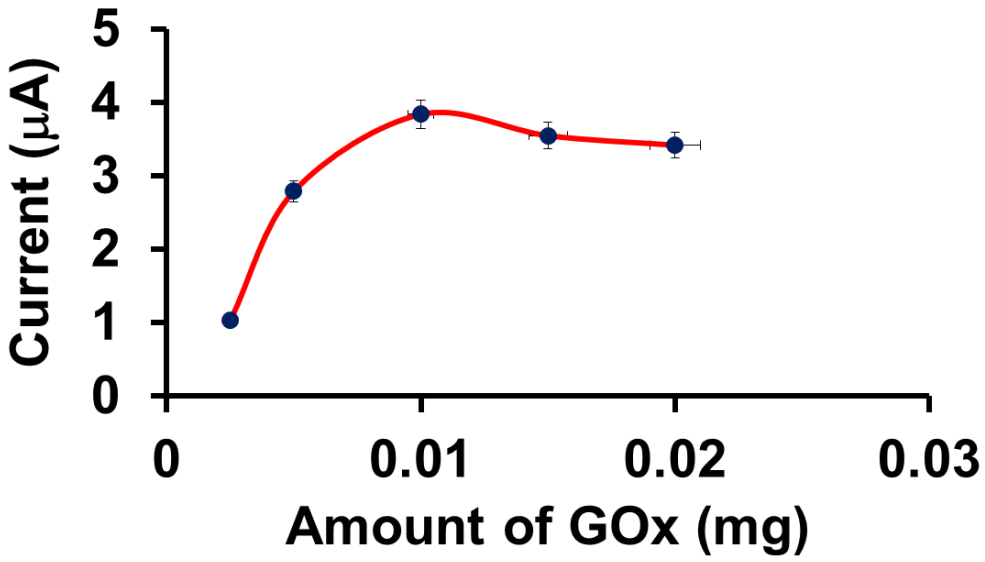

Figure 6-13 Effect of amount of GOx immobilised on the current response of glucose at SiO2($LuPc_2$)-PANI(PVIA)/GOx-CNB biosensor

6.3.10.3. Effect of applied voltage

To ascertain the optimal working electrode potential of $SiO_2(LuPc_2)$-PANI(PVIA)/GOx-CNB biosensor for 1 mM glucose determination, the amperometric potential was varied between -0.1 V to 0.3 V (Figure 6-14). A constant increase in response current was observed with a maximum value at +0.2 V. Based on the above observations, the following conditions pH-7.0; applied potential-+0.2 V; GOx concentration-2 micro litre; operating conditions-25^{o}C (room temperature) was set for the further amperometric determination of glucose at $SiO_2(LuPc_2)$- PANI(PVIA)/GOx-CNB biosensor. Room temperature (25 °C) was chosen for this work due to ease of operations and having in mind the application of biosensor for determination of glucose in biological liquids and food samples tested mostly at room temperature (Kong et al., 2009).

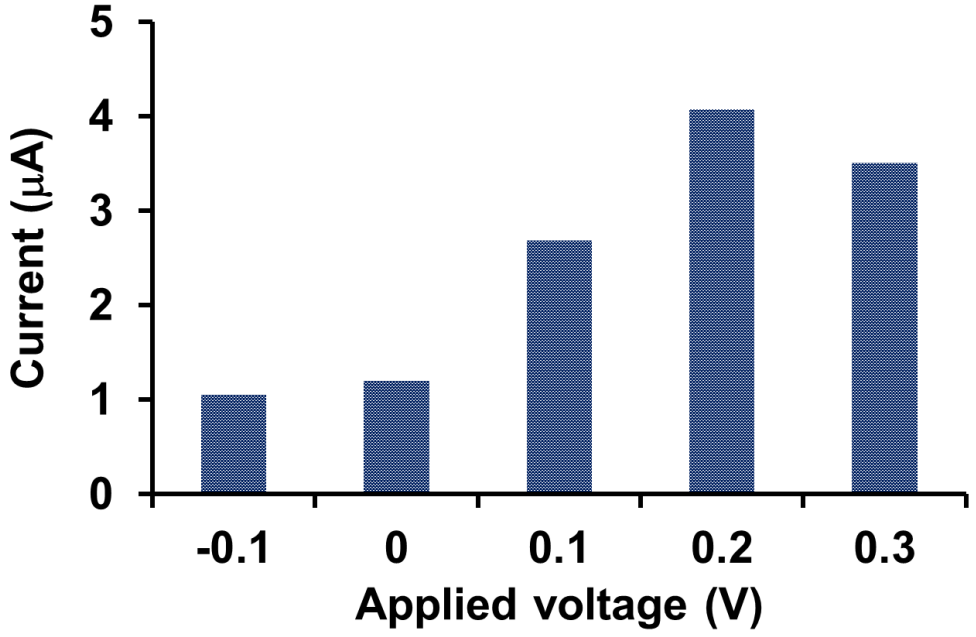

Figure 6-14 Effect of applied voltage on the current response of glucose at $SiO_2(LuPc_2)$-PANI(PVIA)/GOx-CNB biosensor

6.3.11. Repeatability, Reproducibility and stability of $SiO_2(LuPc_2)$-PANI(PVIA)/GOx biosensor

To investigate the stability of the $SiO_2(LuPc_2)$-PANI(PVIA)/GOx biosensor, (preserved in 0.1M PBS at 4 °C), amperometric current response was recorded at regular intervals for a period of 45 days (Figure 6-15). After two week time the $SiO_2(LuPc_2)$-PANI(PVIA)/GOx biosensor retained 98.7% of its initial current response (glucose 4mM). By the end of 45 days, 96.4% of the initial current response was restored. These results confirmed that the functioning of GOx immobilised onto $SiO_2(LuPc_2)$-PANI(PVIA)-CNB was well protected because of the co-presence of PVIA and SiO_2 nanoparticles in the fabricated biosensor (Işiklan et al., 2009). The leaching effect of immobilised GOx from the fabricated $SiO_2(LuPc_2)$-PANI(PVIA)-CNB/GOx biosensor was investigated by recording cyclic voltammetry after immersion of the test electrode in 0.1M PBS for a period of 1h. From the characteristic redox peaks of GOx, it is

confirmed that there is insignificant leaching of GOx from the fabricated biosensor. Also the leaching effect of $LuPc_2$ in the pristine $SiO_2(LuPc_2)$ electrode was also tested after immersion in $Fe(CN)_6^{3-/4-}$ (5 mM) for the time period of 30 min. It was observed from CV (recorded at the scan rate of 50 mV/s) that the redox peak current does not vary before and after immersion. This confirms that $LuPc_2$ is well incorporated within the host SiO_2 porous cage and hence protected from leaching to the background solution that is usually observed in many mediator based biosensor electrodes (Wang et al., 2015).

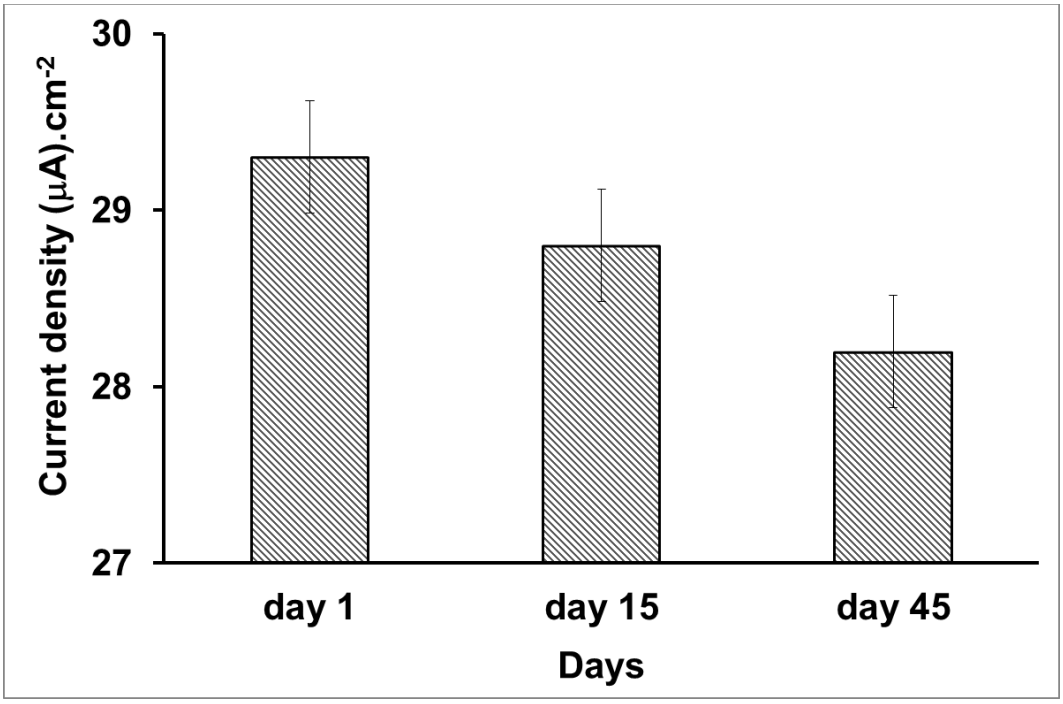

Figure 6-15 Stability test - Current response of glucose (4mM) at $SiO_2(LuPc_2)$-PANI(PVIA)/GOx-CNB biosensor from day 1 to day 45

To examine the reproducibility of $SiO_2(LuPc_2)$-PANI(PVIA)-CNB/GOx biosensor, seven electrodes were prepared under identical conditions and stored at 4^oC. Amperometric current response was recorded in optimized conditions for three different concentrations of glucose (low (a), normal (b) and high (c)) (Figure 6-16A). The relative standard deviations (RSD) for glucose were 2.8 % (2mM), 1.3% (4mM) and 4.9% (9 mM). The relatively low RSD value indicated that $SiO_2(LuPc_2)$-PANI(PVIA)-

CNB/GOx biosensor exhibited good reproducibility in all levels of glucose. The repeatability of $SiO_2(LuPc_2)$-PANI(PVIA)-CNB/GOx biosensor for 5 consecutive measurements of glucose (4 mM) was estimated to RSD = 1.4% under ideal conditions (Figure 6-16B).

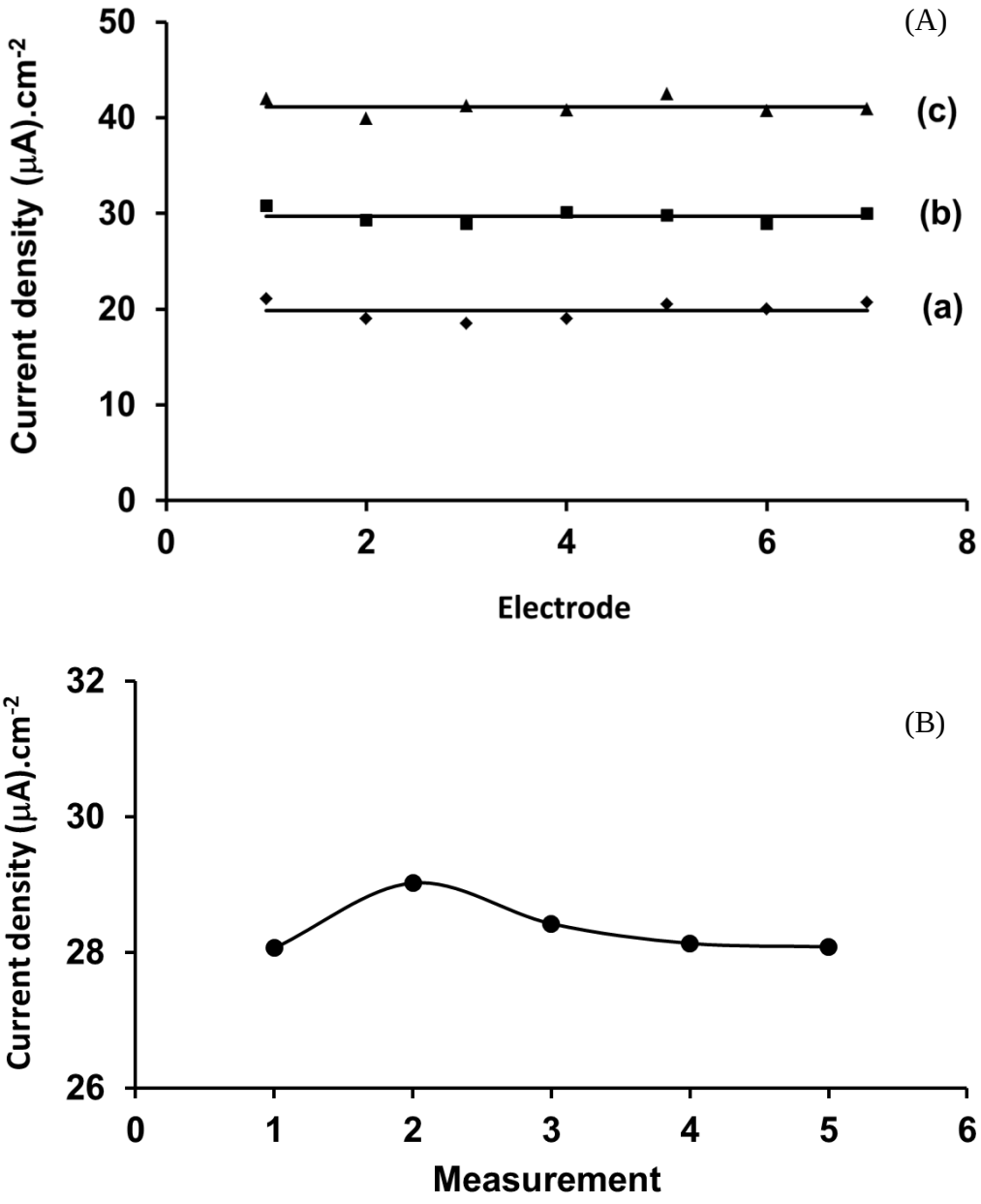

Figure 6-16 (A) Reproducibility on the current response of glucose (a) 2 mM, (b) 4 mM, (c) 8 mM at different $SiO_2(LuPc_2)$-PANI(PVIA)/GOx-CNB biosensor electrodes; (B) Repeatability measurement on the current response of glucose (4 mM) at $SiO_2(LuPc_2)$-PANI(PVIA)/GOx-CNB biosensor

6.3.12. Specificity and interference

The selectivity of the fabricated electrode is an important criterion for biosensor application. Under the applied potential of +0.2 V, the presence of interfering substances hardly affects the amperometric current response of glucose at $SiO_2(LuPc_2)$-PANI(PVIA)-CNB/GOx biosensor. Repetitive measurements of glucose (4 mM) in the presence of interfering substances such as dopamine (DA), lactic acid (LA), ascorbic acid (AA) and uric acid (UA) (2 mM each), are shown in Figure 6-17. DA and UA at the concentration of 2 mM produced the relative low response of ~ 2.2% and ~ 5.0%, indicating that these species coexisting in the sample matrix did not affect the determination of glucose. This informs that $SiO_2(LuPc_2)$-PANI(PVIA)-CNB/GOx biosensor exhibits relatively selective detection of glucose and can be potentially applied for serum samples even in the presence of higher concentration of electrochemically active substances.

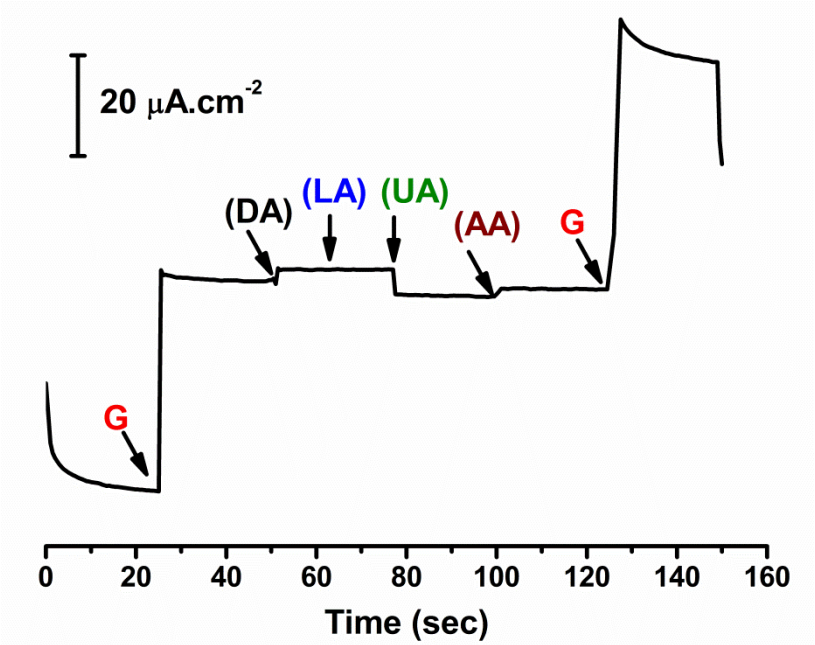

Figure 6-17 Amperometric current of glucose (G = 4 mM) in the presence of interference substances such as dopamine (DA), lactic acid (LA), ascorbic acid (AA) and uric acid (UA) (2 mM) each at $SiO_2(LuPc_2)$-PANI(PVIA)/GOx-CNB biosensor

6.3.13. Glucose determination in real samples at $SiO_2(LuPc_2)$-PANI(PVIA)/GOx-CNB biosensor

The suitability of the $SiO_2(LuPc_2)$-PANI(PVIA)/GOx-CNB biosensor in the determination of glucose in real samples was examined. A continuous amperometry was recorded as shown in Figure 6-18 at optimised conditions (E= +0.2V) in the presence of diluted (using 0.1M PBS to obtain required concentration) fruit juices and horse serum sample. The results obtained for a typical determination of glucose by standard additions method are presented in Table 6-2. The results in Table 6-2, indicate that the percentage recovery ranged from 89.72 to 105 %, which agrees with other standard spectrophotometric method. The satisfactory results demonstrate the practical usage of the fabricated biosensor. Direct determination of glucose in human and horse serum samples at $SiO_2(LuPc_2)$-PANI(PVIA)/GOx-CNB biosensor was also carried out at optimized condition (Figure 6-19). From the amperometric response, it could be

understood that the fabricated $SiO_2(LuPc_2)$-PANI(PVIA)/GOx-CNB biosensor responded well for real samples.

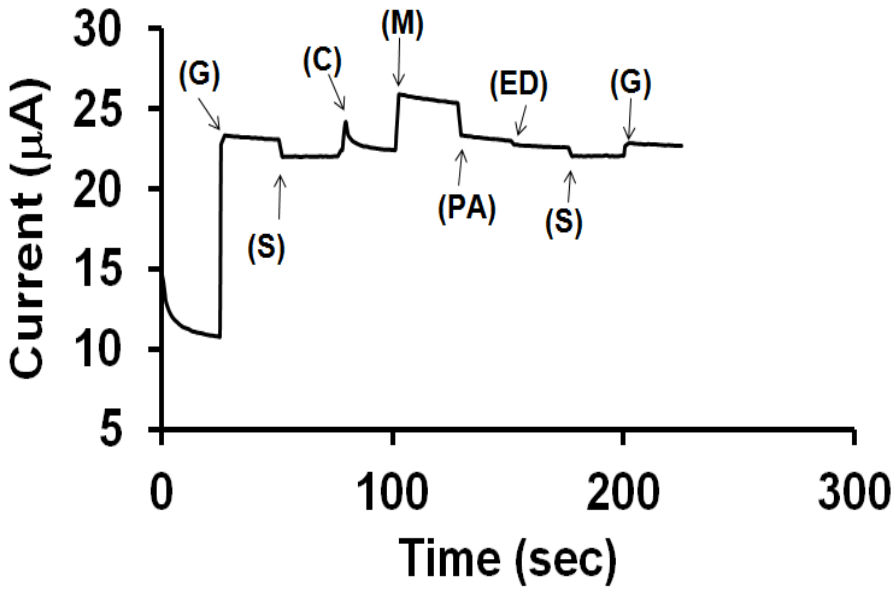

Figure 6-18 Amperometric responses of real samples (G) glucose, (S) Serum, (C) Coke, (M) Mango, (PA) pineapple, (ED) Energy drink at $SiO_2(LuPc_2)$-PANI(PVIA)/GOx-CNB biosensor at an applied potential of +0.2 V

Table 6-2 Amperometric responses of real samples

Real samples	Glucose (3 mM)+real sample [Added after dilution for specific conc. according to label)] (mM)	Found (mM)	Recovery (%)
Mango	3.14	2.92	89.72
Pineapple	3.101	3.03	103.5
Energy drink	3.11	2.96	92.89
Coke zero	3.0	3.12	105
Horse serum	3.16	3.08	96.42

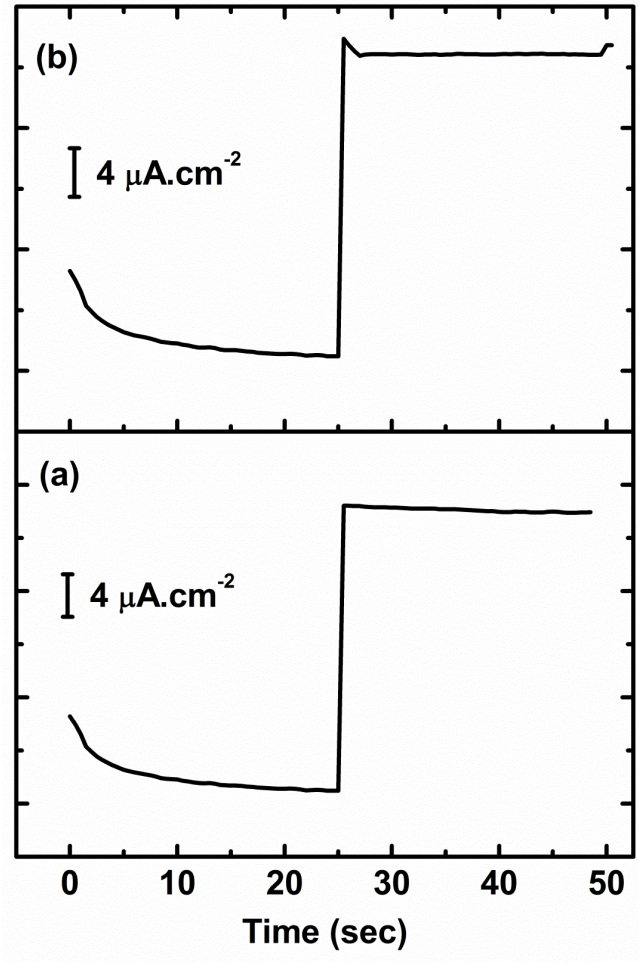

Figure 6-19 Amperometric responses of real samples (a) Human serum, (b) Horse serum at $SiO_2(LuPc_2)$-PANI(PVIA)/GOx-CNB biosensor at an applied potential of +0.2 V

6.4. Conclusions

In this chapter, a multicomponent based conducting nanobead (CNB) has been successfully prepared comprising lutetium phthalocyanine ($LuPc_2$), SiO_2 nanoparticle, polyaniline (PANI) and poly (vinyl alcohol-vinyl acetate-itaconic acid) (PVIA). The prepared CNB was utilized as the platform for the immobilisation of glucose oxidase (GOx). The new fabricated $SiO_2(LuPc_2)$PANI(PVIA)/GOx-CNB biosensor has shown good sensitivity (38.53 $\mu A.mM^{-1}cm^2$) with wide linear range (1-16 mM) for the amperometric detection of glucose. The $SiO_2(LuPc_2)$-PANI(PVIA)/GOx-CNB biosensor has exhibited a specific and fast response (~2s) on addition of glucose. The proposed $SiO_2(LuPc_2)$-PANI(PVIA)/GOx-CNB biosensor showed good accuracy for

both juice and serum samples, providing the potential possibility for its use in Industrial & Clinical analysis. In addition to its use as a glucose sensor, the CNB can be utilised as a platform for the construction of other biosensors in future.

Chapter: 7 Summary and future work

7.1.Conclusions

In this thesis, the synthesis and preparation of novel biosensing platforms for the detection of glucose in whole blood have been undertaken. Multifunctional hydrogels and conducting nanobeads have constituted the fundamental frame work of metallophthalocyanine-based platforms which are used for the detection of glucose in blood samples. The use of graphene derivatives, metallophthalocyanices, and silica nanoparticles have shown excellent enhancement to the sensitivity of the enzymatic glucose biosensors. Several objectives have been achieved during the course of this work which can be summarised in the following points:

- 3D platforms of interconnected hierarchical porous structure of multifunctional and conducting hydrogels are found to offer superior effective surface area and biocompatibility to host GOx.
- $LuPc_2$ as redox mediator has been shown to exhibit excellent redox activity which reduced the amperometric glucose detection potential to +0.3 V.
- High electrical conductivity is achieved through interconnection of VS-PANI network for rapid mass/charge transport during the electrochemical reactions on the electrode surfaces.
- Water-processable iron phthalocyanine (FePc) has improved the processability and formation of the hydrogel and enhanced the redox activity reactions. It is found to be a suitable element to establish the basis of electrochemical reaction devices.

- Functionalising the water-soluble FePc with graphene nanoplatelets through non-covalent interaction was the key to controlling aggregation in the formed hydrogel.
- Multicomponent based conducting nanobead (CNB) structure has been successfully produced comprising $LuPc_2$ and SiO_2.
- The novel-based biosensors could be effectively used as an electrochemical biosensor in industrial as well in clinical diagnosis.

Enzymatic detection of glucose using biosensing platforms made of the above described materials has demonstrated good performance. The sensitivity of MFH biosensor in the range 2-12 mM found to fall in the region of 15.31 μA mM^{-1} cm^{-2} with low detection limit of 25 μM. Biosensing platform based on CH structure exhibited a broad linear behaviour when glucose measured in the range 1-20 mM, with sensitivity in the region of 18.11 μA mM^{-1} cm^{-2} and low detection limit of 1.1503 ng/mL. The conducting nanobeads-based biosensor (CNB) has led to a further improvement the sensitivity of glucose detection (38.53 μA mM^{-1} cm^{-2}) with a linear behaviour in the range of 1-16 mM and detection limit of 0.1 mM. All three biosensing platforms have exhibited excellent selectivity when examined against whole blood components.

7.2.Future work

Further work will be carried out utilising different water-soluble substituted metal phthalocyanines and explore the effect of including these derivatives as a component of the MFH and examine their response to glucose as well as other analytes.

Study of size-effect of the silica nanoparticles on the bioactivity of the developed bioprobes features one of the main objectives to broaden the scope of the current research.

Non-enzymatic electrodes will also be examined through the use of new synthesisezed Carbon nanotube-Cumarin (CNT-CUM) 3D hybrid and Carbon nanotube-Pyrene (CNT-Pyrene) 3D Hybrid. These structures are part of future collaborative work with our research partners in Gebze Technical University.

Further work will be carried out using similar modified electrodes with different recognition elements such as antibodies, RNA/DNA aptamers or whole-cell in order to obtain functional information for monitoring purposes. The modified electrodes could be utilised as electrochemical analysis devices to:

- Monitor low concentrations of antineoplastic (anticancer) drugs to reduce the toxicity level which is produced due the chemotherapy treatment.
- Monitor antimicrobial drug residues in animal-derived food.
- Monitor alcohol consumption through the detection of a metabolite of ethanol in the human sweat.
- Measure low concentrations of some substances, which are placed on the International Olympic Committee's list of banned substances such as Erythropoietin and Testosterones.

The research programme will also look into the viability of the proposed biosensors matrix with its perspective feature to be employed as a wearable sensor in the near future for health and medical services. Wearable sensors are considered as important devices to monitor low amount of samples such as human sweat in addition to their flexible and stretchable features. They could be urgently used to monitor individual health status of different categories of people such as premature infants, children, psychiatric patients, elderly, and athletes.

REFERENCES

Açikbaş, Y., Evyapan, M., Ceyhan, T., Çapan, R., Bekaroğlu, Ö., 2009. Characterization and organic vapor sensing properties of Langmuir-Blodgett film using a new three oxygen-linked phthalocyanine incorporating lutetium. Sensors Actuators, B Chem. 135, 426–429. doi:10.1016/j.snb.2008.09.031

Ahmed, E.M., 2015. Hydrogel: Preparation, characterization, and applications: A review. J. Adv. Res. 6, 105–121. doi:10.1016/j.jare.2013.07.006

Akinbulu, A.I., Nyokong, T., 2010. Fabrication and characterization of single walled carbon nanotubes-iron phthalocyanine nano-composite: surface properties and electron transport dynamics of its self assembled monolayer film. New J. Chem. 34, 2875. doi:10.1039/c0nj00395f

Al-Sagur, H., Komathi, S., Karakaş, H., Atilla, D., Gürek, A.G., Basova, T., Farmilo, N., Hassan, A.K., 2018. A glucose biosensor based on novel Lutetium bis-phthalocyanine incorporated silica-polyaniline conducting nanobeads. Biosens. Bioelectron. 102, 637–645. doi:10.1016/j.bios.2017.12.004

Al-Sagur, H., Komathi, S., Khan, M.A., Gurek, A.G., Hassan, A., 2017. A novel glucose sensor using lutetium phthalocyanine as redox mediator in reduced graphene oxide conducting polymer multifunctional hydrogel. Biosens. Bioelectron. 92, 638–645. doi:10.1016/j.bios.2016.10.038

Ali, S., Hassan, A., Hassan, G., Eun, C., Bae, J., 2018. Disposable all-printed electronic biosensor for instantaneous detection and classification of pathogens. Sci. Rep. 1–11. doi:10.1038/s41598-018-24208-2

Alocilja, E.C., Radke, S.M., 2003. Market analysis of biosensors for food safety. Biosens. Bioelectron. 18, 841–846. doi:10.1016/S0956-5663(03)00009-5

Alsudairi, A., Li, J., Ramaswamy, N., Mukerjee, S., Abraham, K.M., Jia, Q., 2017. Resolving the Iron Phthalocyanine Redox Transitions for ORR Catalysis in Aqueous Media. J. Phys. Chem. Lett. 8, 2881–2886. doi:10.1021/acs.jpclett.7b01126

Alwarappan, S., Liu, C., Kumar, A., Li, C.Z., 2010. Enzyme-doped graphene nanosheets for enhanced glucose biosensing. J. Phys. Chem. C 114, 12920–12924. doi:10.1021/jp103273z

American Diabetes Association, 2010. Diagnosis and classification of diabetes mellitus. Diabetes Care 33, S62–S69. doi:10.2337/dc10-S062

Andrade, S.M., Teixeira, R., Costa, S.M.B., Sobral, A.J.F.N., 2008. Self-aggregation of free base porphyrins in aqueous solution and in DMPC vesicles. Biophys. Chem. 133, 1–10. doi:10.1016/j.bpc.2007.11.007

Anis, A., Banthia, A.K., Bandyopadhyay, S., 2007. Synthesis and characterization of polyvinyl alcohol copolymer/phosphomolybdic acid-based crosslinked composite polymer electrolyte membranes. J. Power Sources 179, 69–80.

Apetrei, C., Alessio, P., Constantino, C.J.L., de Saja, J.A., Rodriguez-Mendez, M.L., Pavinatto, F.J., Fernandes, G.R., Zucolotto, V., Oliveira, O.N., 2011. Biomimetic biosensor based on lipidic layers containing tyrosinase and lutetium bisphthalocyanine for the detection of antioxidants. Biosens. Bioelectron. 26, 2513–2519. doi:10.1016/j.bios.2010.10.047

Appleby, A.J., 1971. Electrocatalysis and Fuel Cells. Catal. Rev. 4, 221–244. doi:10.1080/01614947108075490

Arıcı, M., Arıcan, D., Uğur, A.L., Erdoğmuş, A., Koca, A., 2013. Electrochemical and spectroelectrochemical characterization of newly synthesized manganese, cobalt,

iron and copper phthalocyanines. Electrochim. Acta. doi:10.1016/j.electacta.2012.09.045

Armengol, E., Corma, A., Forne, V., Garcõ, H., Primo, J., 1999. inside Y faujasite and mesoporous MCM-41 as heterogeneous catalysts for the oxidation of cyclohexane. Appl. Catal. A Gen. 181, 305–312.

Aronoff, S., Berkowitz, K., Shreiner, B., Want, L., 2004. Glucose Metabolism and Regulation: Beyond Insulin and Glucagon. Diabetes Spectr. 17, 183–190. doi:10.2337/diaspect.17.3.183

Arrieta, A., Rodriguez-Mendez, M.L., De Saja, J.A., 2003. Langmuir-Blodgett film and carbon paste electrodes based on phthalocyanines as sensing units for taste. Sensors Actuators, B Chem. 95, 357–365. doi:10.1016/S0925-4005(03)00438-6

Arslan, S., Yilmaz, I., 2007. A new water-soluble metal-free phthalocyanine substituted with naphthoxy-4-sulfonic acid sodium salt. Synthesis, aggregation, electrochemistry and in situ spectroelectrochemistry. Polyhedron 26, 2387–2394. doi:10.1016/j.poly.2006.11.047

Arunbabu, D., Shahsavan, H., Zhang, W., Zhao, B., 2013. Poly (AAc - co - MBA) Hydrogel Films : Adhesive and Mechanical Properties in Aqueous Medium. doi:10.1021/jp3101688

Åsberg, P., Inganäs, O., 2003. Hydrogels of a conducting conjugated polymer as 3-D enzyme electrode. Biosens. Bioelectron. 19, 199–207. doi:10.1016/S0956-5663(03)00220-3

Ayhan, M.M., Altınbaş Özpınar, G., Durmuş, M., Gürek, A.G., 2013. Effects of position (α or β) and linker heteroatom (O or S) of substituent on the photophysicochemical behavior of poly(oxyethylene) substituted ZnPcs and

assessment of J-aggregation or protonation using TD-DFT computations. Dalt. Trans. 42, 14892.

Azioune, A., Ben Slimane, A., Ait Hamou, L., Pleuvy, A., Chehimi, M.M., Perruchot, C., Armes, S.P., 2004. Synthesis and Characterization of Active Ester-Functionalized Polypyrrole−Silica Nanoparticles: Application to the Covalent Attachment of Proteins. Langmuir 20, 3350–3356. doi:10.1021/la030407s

Bahadir, E., Sezgintürk, M., 2015. Applications of electrochemical immunosensors for early clinical diagnostics. Talanta 132, 162–174. doi:10.1016/j.talanta.2014.08.063

Bai, H., Li, C., Wang, X., Shi, G., 2010. A pH-sensitive graphene oxide composite hydrogel. Chem. Commun. (Camb). 46, 2376–2378. doi:10.1039/c000051e

Balandin, A.A., Ghosh, S., Bao, W., Calizo, I., Teweldebrhan, D., Miao, F., Lau, C.N., 2008. Superior thermal conductivity of single-layer graphene. Nano Lett. 8, 902–907. doi:10.1021/nl0731872

Barakat, M.A., Sahiner, N., 2008. Cationic hydrogels for toxic arsenate removal from aqueous environment. J. Environ. Manage. 88, 955–961. doi:10.1016/j.jenvman.2007.05.003

Bard, A.J., Faulkner, L.R., 2001. ELECTROCHEMICAL METHODS Fundamentals and Applications, Electrochemistry. I. Faulkner, Larry R. doi:10.1016/B978-0-12-381373-2.00056-9

Barrera, C., Zhukov, I., Villagra, E., Bedioui, F., Páez, M.A., Costamagna, J., Zagal, J.H., 2006. Trends in reactivity of unsubstituted and substituted cobalt-phthalocyanines for the electrocatalysis of glucose oxidation. J. Electroanal. Chem. 589, 212–218. doi:10.1016/j.jelechem.2006.02.009

Barsan, M.M., Klinčar, J., Batič, M., Brett, C.M.A., 2007. Design and application of a flow cell for carbon-film based electrochemical enzyme biosensors. Talanta 71, 1893–1900. doi:10.1016/j.talanta.2006.08.032

Basova, T., Jushina, I., Gürek, A.G., Ahsen, V., Ray, A.K., 2008. Use of the electrochromic behaviour of lanthanide phthalocyanine films for nicotinamide adenine dinucleotide detection. J. R. Soc. Interface 5, 801–6.

Basova, T., Plyashkevich, V., Hassan, A., 2008. Spectral characterization of thin films of vanadyl hexadecafluorophthalocyanine VOPcF16. Surf. Sci. 602, 2368–2372.

Basu, S., Hazra, S., 2017. Graphene–Noble Metal Nano-Composites and Applications for Hydrogen Sensors. C 3, 29. doi:10.3390/c3040029

Bata, P., Notheisz, F., Kluson, P., Zsigmond, Á., 2015. Iron phthalocyanine as new efficient catalyst for catalytic transfer hydrogenation of simple aldehydes and ketones. Appl. Organomet. Chem. 29, 45–49. doi:10.1002/aoc.3247

Besteman, K., Lee, J.O., Wiertz, F.G.M., Heering, H.A., Dekker, C., 2003. Enzyme-coated carbon nanotubes as single-molecule biosensors. Nano Lett. 3, 727–730. doi:10.1021/nl034139u

Bharathi, S., Lev, O., 2000. Sol-gel-derived prussian blue-silicate amperometric glucose biosensor. Appl. Biochem. Biotechnol. - Part A Enzym. Eng. Biotechnol. 89, 209–216. doi:10.1385/ABAB:89:2-3:209

Bhattacharjee, P., Paul, S., Banerjee, M., Patra, D., Banerjee, P., Ghoshal, N., Bandyopadhyay, A., Giri, A.K., 2013. Functional compensation of glutathione S-transferase M1 (GSTM1) null by another GST superfamily member, GSTM2. Sci. Rep. 3, 2704. doi:10.1038/srep02704

Binnemans, K., 2005. Rare-earth beta-diketonates. Handb. Phys. Chem. Rare Earths 35, 107–272.

Bitar, A., Ahmad, N.M., Fessi, H., Elaissari, A., 2012. Silica-based nanoparticles for biomedical applications. Drug Discov. Today 17, 1147–1154. doi:10.1016/j.drudis.2012.06.014

Bohunicky, B., Mousa, S.A., 2011. Biosensors: The new wave in cancer diagnosis. Nanotechnol. Sci. Appl. 4, 1–10. doi:10.2147/NSA.S13465

Booth, M.A., Kannappan, K., Hosseini, A., Partridge, A., 2015. In-Depth Electrochemical Investigation of Surface Attachment Chemistry via Carbodiimide Coupling. Langmuir 31, 8033–8041.

Braik, M., Barsan, M.M., Dridi, C., Ben Ali, M., Brett, C.M.A., 2016. Highly sensitive amperometric enzyme biosensor for detection of superoxide based on conducting polymer/CNT modified electrodes and superoxide dismutase. Sensors Actuators B Chem. 236, 574–582. doi:10.1016/j.snb.2016.06.032

Braun, A. v., Tcherniac, J., 1907. Über die Produkte der Einwirkung von Acetanhydrid auf Phthalamid. Ber. Dtsch. Chem. Ges.(Resumed) 40, 2709–2714.

Brian T. Holland, Chad Walkup, A., Stein*, A., 1998. Encapsulation, Stabilization, and Catalytic Properties of Flexible Metal Porphyrin Complexes in MCM-41 with Minimal Electronic Perturbation by the Environment. J. Phys. Chem. B 102, 4301–4309.

Brunauer, S., Emmett, P.H., Teller, E., 1938. Adsorption of Gases in Multimolecular Layers. J. Am. Chem. Soc. 60, 309–319. doi:10.1021/ja01269a023

Buber, E., Yuzer, A., Soylemez, S., Kesik, M., Ince, M., Toppare, L., 2017.

Construction and amperometric biosensing performance of a novel platform containing carbon nanotubes-zinc phthalocyanine and a conducting polymer. Int. J. Biol. Macromol. 96, 61–69.

Bünzli, J.C.G., 2016. Lanthanide light for biology and medical diagnosis. J. Lumin. 170, 866–878. doi:10.1016/j.jlumin.2015.07.033

Canadian Diabetes Association, 2008. Canadian Diabetes Association 2008 clinical practice guidelines for the prevention and management of diabetes in Canada. Can. J. Diabetes 32, S1–S201. doi:10.1503/cmaj.080554

Carpani, I., Scavetta, E., Tonelli, D., 2008. Amperometric Glucose Biosensors Based on Glassy Carbon and SWCNT-Modified Glassy Carbon Electrodes 84–90. doi:10.1002/elan.200704054

Carrión, E.N., 2018. Tumor-Targeting Fluorinated Phthalocyanines for Theranostic Applications. Seton Hall University Dissertations and Theses (ETDs). 2524.

Carvalho, W.S.P., Wei, M., Ikpo, N., Gao, Y., Serpe, M.J., 2018. Polymer-Based Technologies for Sensing Applications. Anal. Chem. 90, 459–479. doi:10.1021/acs.analchem.7b04751

Cash, K.J., Clark, H.A., 2010. Nanosensors and nanomaterials for monitoring glucose in diabetes. Trends Mol. Med. 16, 584–593. doi:10.1016/j.molmed.2010.08.002

Cass, A.E.G., Davis, G., Francis, G.D., Hill, H.A.O., Aston, W.J., Higgins, I.J., Plotkin, E. V., Scott, L.D.L., Turner, A.P.F., 1984. Ferrocene-mediated enzyme electrode for amperometric determination of glucose. Anal. Chem. 56, 667–671. doi:10.1021/ac00268a018

Cattin, P.C., 2016. Basics of X-ray [WWW Document]. MIAC, Univ. Basel. URL

https://miac.unibas.ch/PMI/01-BasicsOfXray.html#(16) (accessed 7.29.18).

Chaiyo, S., Mehmeti, E., Siangproh, W., Hoang, T.L., Nguyen, H.P., Chailapakul, O., Kalcher, K., 2018. Non-enzymatic electrochemical detection of glucose with a disposable paper-based sensor using a cobalt phthalocyanine–ionic liquid–graphene composite. Biosens. Bioelectron. 102, 113–120. doi:10.1016/j.bios.2017.11.015

Chambers, J.P., Arulanandam, B.P., Matta, L.L., Weis, A., Valdes, J.J., 2002. Biosensor recognition elements 1–12.

Chen, C., Jiang, Y., Kan, J., 2006. A noninterference polypyrrole glucose biosensor. Biosens. Bioelectron. 22, 639–643. doi:10.1016/j.bios.2006.01.023

Chen, H., Müller, M.B., Gilmore, K.J., Wallace, G.G., Li, D., 2008. Mechanically strong, electrically conductive, and biocompatible graphene paper. Adv. Mater. 20, 3557–3561. doi:10.1002/adma.200800757

Cherevko, S., Chung, C.H., 2009. Gold nanowire array electrode for non-enzymatic voltammetric and amperometric glucose detection. Sensors Actuators, B Chem. 142, 216–223. doi:10.1016/j.snb.2009.07.023

Chirani, N., Yahia, L., Gritsch, L., Motta, F.L., Chirani, S., Faré, S., 2015. History and Applications of Hydrogels. J. Biomed. Sci. 4, 1–23. doi:10.4172/2254-609X.100013

Chiu, J.Y., Yu, C.M., Yen, M.J., Chen, L.C., 2009. Glucose sensing electrodes based on a poly(3,4-ethylenedioxythiophene)/Prussian blue bilayer and multi-walled carbon nanotubes. Biosens. Bioelectron. 24, 2015–2020.

Choudhary, M., Shukla, S.K., Taher, A., Siwal, S., Mallick, K., 2014. Organic-

inorganic hybrid supramolecular assembly: An efficient platform for nonenzymatic glucose sensor. ACS Sustain. Chem. Eng. 2, 2852–2858. doi:10.1021/sc500613q

Chouler, J., Cruz-Izquierdo, Á., Rengaraj, S., Scott, J.L., Di Lorenzo, M., 2018. A screen-printed paper microbial fuel cell biosensor for detection of toxic compounds in water. Biosens. Bioelectron. 102, 49–56. doi:10.1016/j.bios.2017.11.018

Chung, Y., Ahn, Y., Christwardana, M., Kim, H., Kwon, Y., 2016. Development of a glucose oxidase-based biocatalyst adopting both physical entrapment and crosslinking, and its use in biofuel cells. Nanoscale 8, 9201–9210. doi:10.1039/C6NR00902F

Clark, L.C., 1956. Monitor and control of blood tissue O2 tensions. Trans. Am. Soc. Artif. Intern. Organs 41–48.

Clark, L.C., Lyons, C., 1962. Electrode Systems for Continuous Monitoring in Cardiovascular Surgery. Ann. N. Y. Acad. Sci. 102, 29–45. doi:10.1111/j.1749-6632.1962.tb13623.x

Clarke, S.F., Foster, J.R., 2012. A history of blood glucose meters and their role in self-monitoring of diabetes mellitus. Br. J. Biomed. Sci. 69, 83–93. doi:10.3310/hta13150

Claussen, J.C., Kumar, A., Jaroch, D.B., Khawaja, M.H., Hibbard, A.B., Porterfield, D.M., Fisher, T.S., 2012. Nanostructuring platinum nanoparticles on multilayered graphene petal nanosheets for electrochemical biosensing. Adv. Funct. Mater. 22, 3399–3405. doi:10.1002/adfm.201200551

Conway, B.E., 1999. Electrochemical Supercapacitors Scientific Fundamentals and Technological Applications, Electrochemical Technologies for Energy Storage and Conversion. doi:10.1002/9783527639496.ch8

Costa de Oliveira, M.A., Mecheri, B., D'Epifanio, A., Placidi, E., Arciprete, F., Valentini, F., Perandini, A., Valentini, V., Licoccia, S., 2017. Graphene oxide nanoplatforms to enhance catalytic performance of iron phthalocyanine for oxygen reduction reaction in bioelectrochemical systems. J. Power Sources 356, 381–388. doi:10.1016/j.jpowsour.2017.02.009

Craven, J.E., Kinnamon, D.S., Prasad, S., 2018. Randles Circuit Analysis Toward Investigating Interfacial Effects on Microchannel Electrodes. IEEE Sensors Lett. 2, 1–4. doi:10.1109/LSENS.2018.2803519

Crouch, E., Cowell, D.C., Hoskins, S., Pittson, R.W., Hart, J.P., 2005. Amperometric, screen-printed, glucose biosensor for analysis of human plasma samples using a biocomposite water-based carbon ink incorporating glucose oxidase. Anal. Biochem. 347, 17–23.

Cui, L., Lv, G., He, X., 2015. Enhanced oxygen reduction performance by novel pyridine substituent groups of iron (II) phthalocyanine with graphene composite. J. Power Sources 282, 9–18.

DATA BRIDGE, 2018. Global Glucometer Market – Industry Trends and Forecast to 2024 [WWW Document]. URL https://databridgemarketresearch.com/reports/global-glucometer-market/ (accessed 7.30.18).

Davis, F., Higson, S.P.J., 2009. Glucose Biosensors-Recent Advances in the Field of Diabetes Management, Micro Fuel Cells. Elsevier Inc. doi:10.1016/B978-0-12-374713-6.00006-8

de la Torre, G., Vázquez, P., Agulló-López, F., Torres, T., 2004. Role of structural factors in the nonlinear optical properties of phthalocyanines and related

compounds. Chem. Rev. 104, 3723–3750. doi:10.1021/cr030206t

De Saja, J.A., Rodríguez-Méndez, M.L., 2005. Sensors based on double-decker rare earth phthalocyanines. Adv. Colloid Interface Sci. 116, 1–11. doi:10.1016/j.cis.2005.03.004

Deng, H., Shen, W., Gao, Z., 2013. An interference-free glucose biosensor based on an anionic redox polymer-mediated enzymatic oxidation of glucose. ChemPhysChem 14, 2343–2347.

Deng, H., Teo, A.K.L., Gao, Z., 2014. An interference-free glucose biosensor based on a novel low potential redox polymer mediator. Sensors Actuators, B Chem. 191, 522–528.

Deoim, P., Moller, V., 2018. Causes, consequences, solutions to sport's anti-doping crisis [WWW Document]. URL http://www.sportsintegrityinitiative.com/causes-consequences-solutions-sports-anti-doping-crisis/ (accessed 7.17.18).

Dervisevic, M., Cvika, E.C., Senel, M., 2014. Development of glucose biosensor based on reconstitution of glucose oxidase onto polymeric redox mediator coated pencil graphite electrodes. Enzyme Microb. Technol. 68, 69–76. doi:10.1016/j.enzmictec.2014.09.007

Desai, D., Kumar, A., Bose, D., Datta, M., 2018. Ultrasensitive sensor for detection of early stage chronic kidney disease in human. Biosens. Bioelectron. 105, 90–94. doi:10.1016/j.bios.2018.01.031

Dhand, C., Dwivedi, N., Mishra, S., Solanki, P.R., Mayandi, V., Beuerman, R.W., Ramakrishna, S., Lakshminarayanan, R., Malhotra, B.D., 2015. Polyaniline-based biosensors. Nanobiosensors Dis. Diagnosis 25. doi:10.2147/NDD.S64841

Diabetes UK, 2015. Number of people living with diabetes doubles in twenty years [WWW Document]. URL https://www.diabetes.org.uk/about_us/news/39-million-people-now-living-with-diabetes (accessed 7.25.18).

Diabetes UK, 2012. Key statistics on diabetes [WWW Document]. URL https://www.diabetes.org.uk/professionals/position-statements-reports/statistics/diabetes-in-the-uk-2012 (accessed 6.15.18).

Diabeteshealth, 2015. The link between diabetes and hormones [WWW Document]. URL https://www.diabeteshealth.com/the-link-between-diabetes-and-hormones/ (accessed 5.31.18).

Ding, H., Zhong, M., Kim, Y.J., Pholpabu, P., Balasubramanian, A., Hui, C.M., He, H., Yang, H., Matyjaszewski, K., Bettinger, C.J., Science, M., Beijing, T., Road, X., Avenue, F., States, U., Engineering, B., Engineering, C., Avenue, M., 2014. Biologically Derived Soft Conducting Hydrogels Using Heparin-Doped Polymer Networks. ACS Nano 8, 4348–4357.

Ding, S.J., Chang, B.W., Wu, C.C., Lai, M.F., Chang, H.C., 2005. Impedance spectral studies of self-assembly of alkanethiols with different chain lengths using different immobilization strategies on Au electrodes. Anal. Chim. Acta 554, 43–51. doi:10.1016/j.aca.2005.08.046

Dominis, A.J., Spinks, G.M., Kane-Maguire, L.A.P., Wallace, G.G., 2002. A de-doping/re-doping study of organic soluble polyaniline. Synth. Met. 129, 165–172.

Dong, G., Huang, M., Guan, L., 2012. Iron phthalocyanine coated on single-walled carbon nanotubes composite for the oxygen reduction reaction in alkaline media. Phys. Chem. Chem. Phys. 14, 2557–2559. doi:10.1039/c2cp23718k

Dou, P., Liu, Z., Cao, Z., Zheng, J., Wang, C., Xu, X., 2016. Rapid synthesis of

hierarchical nanostructured Polyaniline hydrogel for high power density energy storage application and three-dimensional multilayers printing. J. Mater. Sci. 51, 4274–4282. doi:10.1007/s10853-016-9727-8

Doyle, W.M., 1992. Principles and Applications of Fourier Transform Infra- red (FTIR) Process Analysis. Process Control Qual 2.

DropSens, 2011. DropView 8400 Software.

DropSens, 2008. Screen-printed electrodes [WWW Document]. URL http://www.dropsens.com/en/screen_printed_electrodes_pag.html (accessed 7.2.18).

Dryden, M.D.M., Wheeler, A.R., 2015. DStat: A versatile, open-source potentiostat for electroanalysis and integration. PLoS One 10, 1–17. doi:10.1371/journal.pone.0140349

Ducote, M., Vinson, B., Hogquist, S., 2016. Electrochemical Impedance Spectroscopy (EIS) as a Tool for Pathogen Detection. J. Biosens. Bioelectron. 7. doi:10.4172/2155-6210.1000224

Dugas, V., Elaissari, A., Chevalier, Y., 2010. Surface Sensitization Techniques and Recognition Receptors Immobilization on Biosensors and Microarrays, Recognition Receptors in Biosensors. doi:10.1007/978-1-4419-0919-0

Dutta, D., Sharma, R., 2003. Regulation of Hepatic Glucocorticoid Receptors in Mice During Dietary Restriction.

Eggins, B.R., 2002. Chemical sensors and biosensors. Jhon Wiley Sons 28. doi:10.1021/a1980010w

Ekhlaspour, L., Mondesir, D., Lautsch, N., Balliro, C., Hillard, M., Magyar, K.,

Radocchia, L.G., Esmaeili, A., Sinha, M., Russell, S.J., 2017. Comparative Accuracy of 17 Point-of-Care Glucose Meters. J. Diabetes Sci. Technol. 11, 558–566. doi:10.1177/1932296816672237

Emslie, A.G., Bonner, F.T., Peck, L.G., 1958. Flow of a viscous liquid on a rotating disk. J. Appl. Phys. 29, 858–862. doi:10.1063/1.1723300

Erdem, A., Pabuccuoglu, A., Meric, B., Kerman, K., Ozsoz, M., 2000. Electrochemical biosensor based on horseradish peroxidase for the determination of oxidizable drugs. Turkish J. Med. Sci. 30, 349–354.

Etchenique, R.A., Calvo, E.J., 1997. Electrochemical quartz crystal impedance study of redox hydrogel mediators for amperometric enzyme electrodes. Anal. Chem. 69, 4833–41. doi:10.1021/ac970413r

Fang, A., Ng, H.T., Li, S.F.Y., 2003. A high-performance glucose biosensor based on monomolecular layer of glucose oxidase covalently immobilised on indium-tin oxide surface. Biosens. Bioelectron. 19, 43–49.

Fang, Y.-S., Huang, X.-J., Wang, L.-S., Wang, J.-F., 2015. An enhanced sensitive electrochemical immunosensor based on efficient encapsulation of enzyme in silica matrix for the detection of human immunodeficiency virus p24. Biosens. Bioelectron. 64, 324–32.

Fávaro, W.J., Cagnon, V.H.A., 2010. Effect of combined hormonal and insulin therapy on the steroid hormone receptors and growth factors signalling in diabetic mice prostate. Int. J. Exp. Pathol. 91, 537–545. doi:10.1111/j.1365-2613.2010.00739.x

Felix, F.S., Angnes, L., 2018. Electrochemical immunosensors – A powerful tool for analytical applications. Biosens. Bioelectron. 102, 470–478. doi:10.1016/j.bios.2017.11.029

Feng, X., Cheng, H., Pan, Y., Zheng, H., 2015. Development of glucose biosensors based on nanostructured graphene-conducting polyaniline composite. Biosens. Bioelectron. 70, 411–417. doi:10.1016/j.bios.2015.03.046

Fernandes, E.G.R., Brazaca, L.C., Rodríguez-Mendez, M.L., Saja, J.A. de, Zucolotto, V., 2011. Immobilization of lutetium bisphthalocyanine in nanostructured biomimetic sensors using the LbL technique for phenol detection. Biosens. Bioelectron. 26, 4715–4719. doi:10.1016/j.bios.2011.05.032

Ferri, S., Kojima, K., Sode, K., 2011. Review of Glucose Oxidases and Glucose Dehydrogenases: A Bird's Eye View of Glucose Sensing Enzymes. J. Diabetes Sci. Technol. 5, 1068–1076. doi:10.1177/193229681100500507

Fitzpatrick, D., 2015. Glucose Biosensors. Implant. Electron. Med. Devices 37–51. doi:10.1016/B978-0-12-416556-4.00004-8

Free, A.H., Free, H.M., 1984. Self testing, an emerging component of clinical chemistry. Clin. Chem. 30, 829–838.

Freire, R.S., Pessoa, C.A., Mello, L.D., Kubota, L.T., 2003. Direct electron transfer: An approach for electrochemical biosensors with higher selectivity and sensitivity. J. Braz. Chem. Soc. 14, 230–243. doi:10.1590/S0103-50532003000200008

Frumkin, A.N., 1967. THE DEPENDENCE OF THE DOUBLE LAYER STRUCTURE ON THE NATURE OF THE METAL SURFACE *). J. Res. Inst. Catal. 15, 61–83.

Fu, J., Reinhold, J., Woodbury, N.W., 2011. Peptide-modified surfaces for enzyme immobilization. PLoS One 6, 2–7. doi:10.1371/journal.pone.0018692

Fu, Y., Liang, F., Tian, H., Hu, J., 2014. Nonenzymatic glucose sensor based on ITO

electrode modified with gold nanoparticles by ion implantation. Electrochim. Acta 120, 314–318. doi:10.1016/j.electacta.2013.12.082

Gaharwar, A.K., Peppas, N.A., Khademhosseini, A., 2014. Nanocomposite hydrogels for biomedical applications. Biotechnol. Bioeng. 111, 441–453. doi:10.1002/bit.25160

Galanin, N.E., Shaposhnikov, G.P., 2012a. Synthesis and spectral properties of unsymmetrical phthalocyanines from 3,6-dioctyloxyphthalonitrile and 3,4,5,6-tetrachlorophthalonitrile. Russ. J. Gen. Chem. 82, 1734–1739. doi:10.1134/S1070363212100179

Galanin, N.E., Shaposhnikov, G.P., 2012b. Synthesis and spectral properties of lanthanide double-decker complexes with tetrabenzoporphyrin and phthalocyanine. Russ. J. Org. Chem. 48, 851–857. doi:10.1134/S1070428012060176

Galant, A.L., Kaufman, R.C., Wilson, J.D., 2015. Glucose: Detection and analysis. Food Chem. 188, 149–160.

Gao, Q., Guo, Y., Zhang, W., Qi, H., Zhang, C., 2011. An amperometric glucose biosensor based on layer-by-layer GOx-SWCNT conjugate/redox polymer multilayer on a screen-printed carbon electrode. Sensors Actuators, B Chem. 153, 219–225.

García-Sánchez, M.A., Rojas-González, F., Menchaca-Campos, E.C., Tello-Solís, S.R., Quiroz-Segoviano, R.I.Y., Diaz-Alejo, L.A., Salas-Bañales, E., Campero, A., 2013. Crossed and linked histories of tetrapyrrolic macrocycles and their use for engineering pores within sol-gel matrices. Molecules 18, 588–653.

Garingarao, C.J.P.-A., Buenaluz-Sedurante, M., Jimeno, C.A., 2014. Accuracy of point-of-care blood glucose measurements in critically ill patients in shock. J. Diabetes

Sci. Technol. 8, 937–944. doi:10.1177/1932296814538608

Garjonyte, R., Malinauskas, A., 1999. Amperometric glucose biosensor based on glucose oxidase immobilized in poly ž o -phenylenediamine / layer. Sensors Actuators B Chem. 56, 85–92.

Geim, A.K., Novoselov, K.S., 2007. The rise of graphene. Nat. Mater. 6, 183–191. doi:10.1038/nmat1849

Gerard, M., Chaubey, A., Malhotra, B.D., 2002. Application of conducting polymers to biosensors. Biosens. Bioelectron. 17, 345–359. doi:10.1016/S0956-5663(01)00312-8

Ghadimi, H., Ab Ghani, S., Amiri, I., 2017. Introduction, in: Electrochemistry of Dihydroxybenzene Compounds: Carbon Based Electrodes and Their Uses in Synthesis and Sensors. Elsevier, pp. 1–30. doi:10.1016/B978-0-12-813222-7.00001-2

Ghibaudi, M., Lorenzati, M., Pasini, G., 2017. DigitCult | Scientific Journal on Digital Cultures Current and Novel Strategies for Biomarkers Detection in Neurodegenerative Diseases : Future Graphene - Based Applications. DigitCult 2, 51–71. doi:10.4399/97888255088955

Gong, J., Li, D., Huang, J., Ding, L., Tong, Y., Li, K., Zhang, C., 2014. Synthesis of two novel water-soluble iron phthalocyanines and their application in fast chromogenic identification of phenolic pollutants. Catal. Letters 144, 487–497. doi:10.1007/s10562-013-1178-0

González-Pérez, S., Arellano, J.B., 2009. Vegetable protein isolates. Handb. Hydrocoll. Second Ed. 383–419. doi:10.1533/9781845695873.383

Gopalan, A.I., Lee, K.P., Komathi, S., 2010. Bioelectrocatalytic determination of nitrite ions based on polyaniline grafted nanodiamond. Biosens. Bioelectron. 26, 1638–1643. doi:10.1016/j.bios.2010.08.042

Gopalan, A.I., Lee, K.P., Ragupathy, D., Lee, S.H., Lee, J.W., 2009. An electrochemical glucose biosensor exploiting a polyaniline grafted multiwalled carbon nanotube/perfluorosulfonate ionomer-silica nanocomposite. Biomaterials 30, 5999–6005.

Grahame, D.C., 1947. The electrical double layer and the theory of electrocapillarity. Chem. Rev. 41, 441–501. doi:10.1021/cr60130a002

Guillaud, G., Simon, J., Germain, J.P., 1998. Metallophthalocyanines. Coord. Chem. Rev. 178–180, 1433–1484. doi:10.1016/S0010-8545(98)00177-5

Guiseppi-Elie, A., 2010. Electroconductive hydrogels: Synthesis, characterization and biomedical applications. Biomaterials 31, 2701–2716. doi:10.1016/j.biomaterials.2009.12.052

Gulrez, S.K.H., Al-Assaf, S., Phillips, G.O., 2011. Hydrogels : Methods of Preparation , Characterisation and Applications. Prog. Mol. Environ. Bioeng. 51, 117–150. doi:10.1016/j.jvs.2009.12.028

Guo, H., He, W., Lu, Y., Zhang, X., 2015. Self-crosslinked polyaniline hydrogel electrodes for electrochemical energy storage. Carbon N. Y. 92, 133–141. doi:10.1016/j.carbon.2015.03.062

Han, J., Zhang, F., You, J., Hiroaki, Y., Yamada, S., Morifuji, T., Wang, S., Li, X., 2017. The first transition metal phthalocyanines: Sensitizing rubrene emission based on triplet-triplet annihilation. Photochem. Photobiol. Sci. 16, 1384–1390. doi:10.1039/c6pp00464d

Han, J., Zhuo, Y., Chai, Y.Q., Xiang, Y., Yuan, R., 2015. New type of redox nanoprobe: C60-based nanomaterial and its application in electrochemical immunoassay for doping detection. Anal. Chem. 87, 1669–1675. doi:10.1021/ac503406p

Han, Y., Lu, Z., Teng, Z., Liang, J., Guo, Z., Wang, D., Han, M.Y., Yang, W., 2017. Unraveling the growth mechanism of silica particles in the stöber method: In situ seeded growth model. Langmuir 33, 5879–5890.

Han, Z., Han, X., Zhao, X., Yu, J., Xu, H., 2016. Iron phthalocyanine supported on amidoximated PAN fiber as effective catalyst for controllable hydrogen peroxide activation in oxidizing organic dyes. J. Hazard. Mater. 320, 27–35. doi:10.1016/j.jhazmat.2016.08.004

Harris, J.M., Lopez, G.P., Reichert, W.M., 2012. Silica-dispersed glucose oxidase for glucose sensing: In vitro testing in serum and blood and the effect of condensation pH. Sensors Actuators, B Chem. 174, 373–379. doi:10.1016/j.snb.2012.08.046

Hart, J.P., Wring, S.A., 1997. Recent developments in the design and application of screen-printed electrochemical sensors for biomedical, environmental and industrial analyses. TrAC - Trends Anal. Chem. 16, 89–103. doi:10.1016/S0165-9936(96)00097-0

Hartmann, M., Kostrov, X., 2013. Immobilization of enzymes on porous silicas – benefits and challenges. Chem. Soc. Rev. 42, 6277. doi:10.1039/c3cs60021a

Harvey, D., 2000. Modern Analytical Chemistry 1–1133.

Hasanzadeh, M., Shadjou, N., de la Guardia, M., Eskandani, M., Sheikhzadeh, P., 2012. Mesoporous silica-based materials for use in biosensors. TrAC - Trends Anal. Chem. 33, 117–129. doi:10.1016/j.trac.2011.10.011

He, Q., Zhang, J., Shi, J., Zhu, Z., Zhang, L., Bu, W., Guo, L., Chen, Y., 2010. The effect of PEGylation of mesoporous silica nanoparticles on nonspecific binding of serum proteins and cellular responses. Biomaterials 31, 1085–1092.

Hecht, H.J., Schomburg, D., Kalisz, H. and Schmid, R.D., 1993. The 3d Structure of Glucose-Oxidase from Aspergillus-Niger - Implications for the Use of God as a Biosensor Enzyme. Biosens. Bioelectron. 8, 197–203. doi:10.1016/0956-5663(93)85033-K

Heller, A., 2006. Electron-conducting redox hydrogels: design, characteristics and synthesis. Curr. Opin. Chem. Biol. 10, 664–672. doi:10.1016/j.cbpa.2006.09.018

Heller, A., 1996. Amperometric Biosensors. Curr. Opin. Biotechnol. 7, 50–54.

Heller, A., Feldman, B., 2008. Electrochemical Glucose Sensors and Their Applications in Diabetes Management. Chem. Rev. (Washington, DC, United States) 108, 2482–2505. doi:10.1021/cr068069y

Hernandez-Vargas, G., Sosa-Hernández, J.E., Saldarriaga-Hernandez, S., Villalba-Rodríguez, A.M., Parra-Saldivar, R., Iqbal, H.M.N., 2018. Electrochemical biosensors: A solution to pollution detection with reference to environmental contaminants. Biosensors 8, 1–21. doi:10.3390/bios8020029

Higson, S., 2012. Biosensors for Medical Applications, Woodhead Publishing Limited. Cambridge, United Kingdom.

Holford, T.R.J., Davis, F., Higson, S.P.J., 2012. Recent trends in antibody based sensors. Biosens. Bioelectron. 34, 12–24. doi:10.1016/j.bios.2011.10.023

Homaei, A.A., Sariri, R., Vianello, F., Stevanato, R., 2013. Enzyme immobilization: An update. J. Chem. Biol. 6, 185–205. doi:10.1007/s12154-013-0102-9

Horng, Y.Y., Hsu, Y.K., Ganguly, A., Chen, C.C., Chen, L.C., Chen, K.H., 2009. Direct-growth of polyaniline nanowires for enzyme-immobilization and glucose detection. Electrochem. commun. 11, 850–853. doi:10.1016/j.elecom.2009.02.010

Hou, S.F., Yang, K.S., Fang, H.Q., Chen, H.Y., 1998. Amperometric glucose enzyme electrode by immobilizing glucose oxidase in multilayers on self-assembled monolayers surface. Talanta 47, 561–567. doi:10.1016/S0039-9140(98)00081-2

Hu, Z., Kang, Z., Yu, C., Wang, B., Jiao, S., Peng, R., 2017. Direct electron transfer of glucose oxidase in carbon paper for biofuel cells and biosensors. Int. J. Electrochem. Sci. 12, 7103–7120. doi:10.20964/2017.08.24

Hua, L., Wu, X., Wang, R., 2012. Glucose sensor based on an electrochemical reduced graphene oxide-poly(l-lysine) composite film modified GC electrode. Analyst 137, 5716–5719. doi:10.1039/c2an35612k

Huang, X., Zeng, Z., Fan, Z., Liu, J., Zhang, H., 2012. Graphene-based electrodes. Adv. Mater. 24, 5979–6004. doi:10.1002/adma.201201587

Hussain, S., Akbar, K., Vikraman, D., Choi, D.-C., Kim, S.J., An, K.-S., Jung, S., Jung, J., 2015. A highly sensitive enzymeless glucose sensor based on 3D graphene-Cu hybrid electrodes. New J. Chem. 39, 7481–7487. doi:10.1039/c5nj01512j

Hwang, N., Barron, A.R., 2011. BET surface area analysis of nanoparticles. Connexions Proj. 1–11.

Inkson, B.J., 2016. Scanning Electron Microscopy (SEM) and Transmission Electron Microscopy (TEM) for Materials Characterization, Materials Characterization Using Nondestructive Evaluation (NDE) Methods. Elsevier Ltd. doi:10.1016/B978-0-08-100040-3.00002-X

International Diabetes Federation, 2017. IDF Diabetes Atlas Eighth Edition 2017, International Diabetes Federation.

International Diabetes Federation, 2013. Sixth Edition.

International Diabetes Federation, 2006. Diabetes Atlas - third edition, Journal of Chemical Information and Modeling.

Inzelt, G., Pineri, M., Schultze, J.W., Vorotyntsev, M.A., 2000. Electron and proton conducting polymers: Recent developments and prospects. Electrochim. Acta 45, 2403–2421. doi:10.1016/S0013-4686(00)00329-7

Ipek, Y., Dinçer, H., Koca, A., 2014. Electrode modification based on "click electrochemistry" between terminal-alkynyl substituted cobalt phthalocyanine and 4-azidoaniline. Sensors Actuators, B Chem. 193, 830–837. doi:10.1016/j.snb.2013.12.031

Işiklan, N., Kurşun, F., Inal, M., 2009. Graft copolymerization of itaconic acid onto sodium alginate using ceric ammonium nitrate as initiator. J. Appl. Polym. Sci. 114, 40–48.

Ivnitski, D., Artyushkova, K., Rincón, R.A., Atanassov, P., Luckarift, H.R., Johnson, G.R., 2008. Entrapment of enzymes and carbon nanotubes in biologically synthesized silica: Glucose oxidase-catalyzed direct electron transfer. Small 4, 357–364. doi:10.1002/smll.200700725

Jaganathan, H., Godin, B., 2012. Biocompatibility assessment of Si-based nano- and micro-particles. Adv. Drug Deliv. Rev. 64, 1800–1819. doi:10.1016/j.addr.2012.05.008

Jędrzak, A., Rębiś, T., Klapiszewski, Ł., Zdarta, J., Milczarek, G., Jesionowski, T.,

2018. Carbon paste electrode based on functional GOx/silica-lignin system to prepare an amperometric glucose biosensor. Sensors Actuators, B Chem. 256, 176–185. doi:10.1016/j.snb.2017.10.079

Jia, Q., Ge, J., Liu, W., Zheng, X., Wang, M., Zhang, H., Wang, P., 2017. Biocompatible Iron Phthalocyanine-Albumin Assemblies as Photoacoustic and Thermal Theranostics in Living Mice. ACS Appl. Mater. Interfaces 9, 21124–21132. doi:10.1021/acsami.7b04360

Jiang, L., Liu, H., Liu, J., Yang, Q., Cai, X., 2008. A sensitive biosensor based on Os-complex mediator and glucose oxidase for low concentration glucose determination. J. Electroanal. Chem. 619–620, 11–16.

Joshi, S.R., Parikh, R.M., Das, A.K., 2007. Insulin--history, biochemistry, physiology and pharmacology. J. Assoc. Physicians India 55 Suppl, 19–25.

Kadish, K.M., Nakanishi, T., Gürek, A., Ahsen, V., Yilmaz, I., 2001. Electrochemistry of a double-decker lutetium(III) phthalocyanine in aqueous media. The first evidence for five reductions. J. Phys. Chem. B 105, 9817–9821. doi:10.1021/jp012636y

Kaech, A., 2002. An introduction to electron microscopy instrumentation, imaging and preparation. Cent. Microsc. Image Anal. 1–26.

Kalhotka, L., Hrdinová, Z., Kořínková, R., Přichastalová, J., Konečná, M., Kubáč, L., Lev, J., 2012. Test of Phthalocyanines Antimicrobial Activity 6–11.

Kang, Z., Jiao, K., Cheng, J., Peng, R., Jiao, S., Hu, Z., 2018. A novel three-dimensional carbonized PANI 1600 @CNTs network for enhanced enzymatic biofuel cell. Biosens. Bioelectron. 101, 60–65. doi:10.1016/j.bios.2017.10.008

Karalliedde, J., Gnudi, L., 2016. Diabetes mellitus, a complex and heterogeneous disease, and the role of insulin resistance as a determinant of diabetic kidney disease. Nephrol. Dial. Transplant. 31, 206–213. doi:10.1093/ndt/gfu405

Karamitsos, D.T., 2011. The story of insulin discovery. Diabetes Res. Clin. Pract. 93, S2–S8. doi:10.1016/S0168-8227(11)70007-9

Karunakaran, C., Rajkumar, R., Bhargava, K., 2015. Introduction to Biosensors, Biosensors and Bioelectronics. Elsevier Inc. doi:10.1016/B978-0-12-803100-1.00001-3

Katz, E., Willner, I., 2003. Probing Biomolecular Interactions at Conductive and Semiconductive Surfaces by Impedance Spectroscopy: Routes to Impedimetric Immunosensors, DNA-Sensors, and Enzyme Biosensors. Electroanalysis 15, 913–947. doi:10.1002/elan.200390114

Kazi, S.N., Badarudin, A., Zubir, M.N.M., Ming, H.N., Misran, M., Sadeghinezhad, E., Mehrali, M., Syuhada, N.I., 2015. Investigation on the use of graphene oxide as novel surfactant to stabilize weakly charged graphene nanoplatelets. Nanoscale Res. Lett. 10, 16–18. doi:10.1186/s11671-015-0882-7

Kempahanumakkagari, S., Deep, A., Kim, K.H., Kumar Kailasa, S., Yoon, H.O., 2017. Nanomaterial-based electrochemical sensors for arsenic - A review. Biosens. Bioelectron. 95, 106–116. doi:10.1016/j.bios.2017.04.013

Kennedy, J.P., Ratner, B.D., 1995. Amphiphilic Networks. 9. Surface Characterization. Macromolecues 28, 2595.

Kim, B.C., 1999. The synthesis and characterisation of hydrogel and polypyrrole blends. Res. Online.

Kim, D.-M., Moon, J.-M., Lee, W.-C., Yoon, J.-H., Choi, C.S., Shim, Y.-B., 2017. A potentiometric non-enzymatic glucose sensor using a molecularly imprinted layer bonded on a conducting polymer. Biosens. Bioelectron. 91, 276–283. doi:10.1016/j.bios.2016.12.046

Kissinger, P.T., Heineman, W.R., 1996. Laboratory Techniques in Electroanalytical Chemistry, Second. ed. CRC press.

Klonoff, D.C., Ahn, D., Drincic, A., 2017. Continuous glucose monitoring: A review of the technology and clinical use. Diabetes Res. Clin. Pract. 133, 178–192. doi:10.1016/j.diabres.2017.08.005

Kluson, P., Drobek, M., Zsigmond, A., Baranyi, J., Bata, P., Zarubova, S., Kalaji, A., 2009. Environmentally friendly phthalocyanine catalysts for water decontamination-Non-photocatalytic systems. Appl. Catal. B Environ. 91, 605–609. doi:10.1016/j.apcatb.2009.06.033

Knopp RH, Bergelin RO, Wahl PW, Walden CE, 1985. No TitleRelationships of infant birth size to maternal lipoproteins, apoproteins, fuels, hormones, clinical chemistries, and body weight at 36 weeks gestation. Diabetes 34.

Komathi, S., Gopalan, A.I., Lee, K.P., 2009a. Fabrication of a novel layer-by-layer film based glucose biosensor with compact arrangement of multi-components and glucose oxidase. Biosens. Bioelectron. 24, 3131–3134.

Komathi, S., Gopalan, A.I., Lee, K.P., 2009b. Covalently linked silica-multiwall carbon nanotube-polyaniline network: An electroactive matrix for ultrasensitive biosensor. Biosens. Bioelectron. 25, 944–947.

Komathi, S., Gopalan, A.I., Muthuchamy, N., Lee, K.P., 2017a. Polyaniline nanoflowers grafted onto nanodiamonds via a soft template-guided secondary

nucleation process for high-performance glucose sensing. RSC Adv. 7, 15342–15351. doi:10.1039/C6RA24760A

Komathi, S., Gopalan, A.I., Muthuchamy, N., Lee, K.P., 2017b. Polyaniline nanoflowers grafted onto nanodiamonds via a soft template-guided secondary nucleation process for high-performance glucose sensing. RSC Adv. 7, 15342–15351.

Kong, T., Chen, Y., Ye, Y., Zhang, K., Wang, Z., Wang, X., 2009. An amperometric glucose biosensor based on the immobilization of glucose oxidase on the ZnO nanotubes. Sensors Actuators, B Chem. 138, 344–350.

Kowalewska, B., Jakubow, K., 2017. The impact of immobilization process on the electrochemical performance, bioactivity and conformation of glucose oxidase enzyme. Sensors Actuators, B Chem. 238, 852–861. doi:10.1016/j.snb.2016.07.138

Kuila, T., Bose, S., Khanra, P., Mishra, A.K., Kim, N.H., Lee, J.H., 2011. Recent advances in graphene-based biosensors. Biosens. Bioelectron. 26, 4637–4648. doi:10.1016/j.bios.2011.05.039

Kuznetsova, N. a., Yuzhakova, O. a., Strakhovskaya, M.G., Shumarina, A.O., Kozlov, A.S., Krasnovsky, A. a., Kaliya, O.L., 2011. New heterogeneous photosensitizers with phthalocyanine molecules covalently linked to aminopropyl silica gel. J. Porphyr. Phthalocyanines 15, 718–726.

LABCONCO, 2016. Benchtop Freeze Dry System [WWW Document]. LABCONO. URL http://www.labconco.com/product/freezone-105c-45-liter-benchtop-freeze-dry-system-with-ptfe-coated-co/92

Laczka, O., Campo, F.J., Munoz-Pascual, F.X., Baldrich, E., 2011. Electrochemical Detection of Testosterone by Use of. Anal. Chem. 83, 4037–4044.

Lai, J., Yi, Y., Zhu, P., Shen, J., Wu, K., Zhang, L., Liu, J., 2016. Polyaniline-based glucose biosensor: A review. J. Electroanal. Chem. 782, 138–153. doi:10.1016/j.jelechem.2016.10.033

Laschi, S., Fránek, M., Mascini, M., 2000. Screen-printed electrochemical immunosensors for PCB detection. Electroanalysis 12, 1293–1298. doi:10.1002/1521-4109(200011)12:16<1293::AID-ELAN1293>3.0.CO;2-5

Lawes, G., 1987. Scanning electron microscopy and X-ray microanalysis.

Lee, C.S., Kyu Kim, S., Kim, M., 2009. Ion-sensitive field-effect transistor for biological sensing. Sensors 9, 7111–7131. doi:10.3390/s90907111

Lee, K.P., Gopalan, A., Komathi, S., Raghupathy, D., 2010. Polyaniline-based nanocomposites: preparation, properties and applications. Phys. Prop. Appl. Polym. Nanocomposites 187–243. doi:10.1533/9780857090249.1.187

Lee, K.P., Komathi, S., Nam, N.J., Gopalan, A.I., 2010. Sulfonated polyaniline network grafted multi-wall carbon nanotubes for enzyme immobilization, direct electrochemistry and biosensing of glucose. Microchem. J. 95, 74–79.

Lei, L., Xia, Z., Zhang, L., Zhang, Y., Zhong, L., 2016. Preparation and properties of amino-functional reduced graphene oxide/waterborne polyurethane hybrid emulsions. Prog. Org. Coatings 97, 19–27. doi:10.1016/j.porgcoat.2016.03.011

Leznoff, C.C., Lever, A.B.P., 1993. Phthalocyanines: Properties and Applications, Volume 4 Edited by C. C. Leznoff and A. B. P. Lever (York University, Canada). VCH: New York, 1996, (York University, Canada), VCH(LSK), New York. doi:10.1021/ja965771a

Li, H., Wang, D.Q., Liu, B.L., Gao, L.Z., 2004. Synthesis of a novel gelatin-carbon

nanotubes hybrid hydrogel. Colloids Surfaces B Biointerfaces 33, 85–88. doi:10.1016/j.colsurfb.2003.08.014

Li, J., Wei, X., Yuan, Y., 2009. Synthesis of magnetic nanoparticles composed by Prussian blue and glucose oxidase for preparing highly sensitive and selective glucose biosensor. Sensors Actuators, B Chem. 139, 400–406.

Li, Q., Luo, G., Wang, Y., Zhang, X., 2000. Immobilization of glucose oxidase in sol-gel matrix and its application to fabricate chemiluminescent glucose sensor. Mater. Sci. Eng. C 11, 67–70.

Li, X., Zou, R., Niu, Y., Sun, W., Shao, T., Chen, X., 2018. Gold Nanocage-Based Electrochemical Sensing Platform for Sensitive Detection of Luteolin. Sensors 18, 2309. doi:10.3390/s18072309

Liu, D., Long, Y.T., 2015. Superior Catalytic Activity of Electrochemically Reduced Graphene Oxide Supported Iron Phthalocyanines toward Oxygen Reduction Reaction. ACS Appl. Mater. Interfaces 7, 24063–24068. doi:10.1021/acsami.5b07068

Liu, J., Chen, G., Jiang, M., 2011. Supramolecular hybrid hydrogels from noncovalently functionalized graphene with block copolymers. Macromolecules 44, 7682–7691. doi:10.1021/ma201620w

Liu, M., Chen, S., Zhao, X., Ye, Y., Li, J., Zhu, Q., Zhao, B., Zhao, W., Huang, X., Shen, J., 2013. Biocompatible phosphonic acid-functionalized silica nanoparticles for sensitive detection of hypoxanthine in real samples. Talanta 117, 536–542. doi:10.1016/j.talanta.2013.08.061

Liu, Y., Turner, A.P.F., Zhao, M., Mak, W.C., 2018. Processable enzyme-hybrid conductive polymer composites for electrochemical biosensing. Biosens.

Bioelectron. 100, 374–381. doi:10.1016/j.bios.2017.09.021

Liu, Y., Yu, D., Zeng, C., Miao, Z., Dai, L., 2010. Biocompatible graphene oxide-based glucose biosensors. Langmuir 26, 6158–6160. doi:10.1021/la100886x

Liu, Y., Yu, T., 1997. Polymers and Enzyme Biosensors. Polym. Rev. 37, 459–500. doi:10.1080/15321799708018372

Lomax, S.Q., 2005. Phthalocyanine and quinacridone pigments: their history, properties and use. Stud. Conserv. 50, 19–29. doi:10.1179/sic.2005.50.Supplement-1.19

Lourencao, B.C., Medeiros, R.A., Fatibello-Filho, O., 2015. Simultaneous determination of antihypertensive drugs by flow injection analysis using multiple pulse amperometric detection with a cathodically pretreated boron-doped diamond electrode. J. Electroanal. Chem. 754, 154–159. doi:10.1016/j.jelechem.2015.06.022

Luo, X., Davis, J.J., 2013. Electrical biosensors and the label free detection of protein disease biomarkers. Chem. Soc. Rev. 42, 5944–5962. doi:10.1039/c3cs60077g

Luong, J.H.T., Male, K.B., Glennon, J.D., 2008. Biosensor technology: Technology push versus market pull. Biotechnol. Adv. 26, 492–500. doi:10.1016/j.biotechadv.2008.05.007

Lv, M., Liu, Y., Geng, J., Kou, X., Xin, Z., Yang, D., 2018. Engineering nanomaterials-based biosensors for food safety detection. Biosens. Bioelectron. 106, 122–128. doi:10.1016/j.bios.2018.01.049

Lvovich, V.F., 2012. Impedance Spectroscopy : Applications to Electrochemical and Dielectric Phenomena. John Wiley & Sons, Incorporated.

Ma, Q., Li, Y., Su, X., 2015. Silica-nanobead-based sensors for analytical and

bioanalytical applications. TrAC Trends Anal. Chem. 74, 130–145. doi:10.1016/j.trac.2015.06.006

Maduraiveeran, G., Sasidharan, M., Ganesan, V., 2018. Electrochemical sensor and biosensor platforms based on advanced nanomaterials for biological and biomedical applications. Biosens. Bioelectron. 103, 113–129. doi:10.1016/j.bios.2017.12.031

Mamaeva, V., Sahlgren, C., Lindén, M., 2013. Mesoporous silica nanoparticles in medicine-Recent advances. Adv. Drug Deliv. Rev. 65, 689–702. doi:10.1016/j.addr.2012.07.018

Manesh, K.M., Santhosh, P., Uthayakumar, S., Gopalan, A.I., Lee, K.P., 2010. One-pot construction of mediatorless bi-enzymatic glucose biosensor based on organic-inorganic hybrid. Biosens. Bioelectron. 25, 1579–1586.

Mani, V., Devadas, B., Chen, S.M., 2013. Direct electrochemistry of glucose oxidase at electrochemically reduced graphene oxide-multiwalled carbon nanotubes hybrid material modified electrode for glucose biosensor. Biosens. Bioelectron. 41, 309–315. doi:10.1016/j.bios.2012.08.045

Mani, V., Devasenathipathy, R., Chen, S.M., Gu, J.A., Huang, S.T., 2015. Synthesis and characterization of graphene-cobalt phthalocyanines and graphene-iron phthalocyanine composites and their enzymatic fuel cell application. Renew. Energy 74, 867–874.

Mani, V., Devasenathipathy, R., Chen, S.M., Huang, S.T., Vasantha, V.S., 2014. Immobilization of glucose oxidase on graphene and cobalt phthalocyanine composite and its application for the determination of glucose. Enzyme Microb. Technol. 66, 60–66.

Martin, C.S., Gouveia-Caridade, C., Crespilho, F.N., Constantino, C.J.L., Brett, C.M.A., 2016. Iron Phthalocyanine Electrodeposited Films: Characterization and Influence on Dopamine Oxidation. J. Phys. Chem. C 120, 15698–15706. doi:10.1021/acs.jpcc.5b09707

Martin, P., 2009. Electrochemistry of gaphene: New horizons for sensing and energy storage. Chem. Rec. 9, 211–223. doi:10.1002/tcr.200900008

Mashazi, P.N., Ozoemena, K.I., Nyokong, T., 2006. Tetracarboxylic acid cobalt phthalocyanine SAM on gold: Potential applications as amperometric sensor for H2O2 and fabrication of glucose biosensor. Electrochim. Acta 52, 177–186.

Mawad, D., Lauto, A., Wallace, G.G., 2016. Conductive Polymer Hydrogels. Springer International Publishing Switzerland, Switzerland. doi:10.1007/978-3-319-25322-0

Maximino, M.D., Martin, C.S., Paulovich, F.V., Alessio, P., 2016. Layer-by-Layer Thin Film of Iron Phthalocyanine as a Simple and Fast Sensor for Polyphenol Determination in Tea Samples. J. Food Sci. 81, C2344–C2351. doi:10.1111/1750-3841.13394

Mcmillin, J.M., 1990. Blood Glucose. Clin. Methods Hist. Phys. Lab. Exam. 662–665. doi:10.1185/03007995.2011.626760

Medina-Plaza, C., Revilla, G., Muñoz, R., Fernández-Escudero, J.A., Barajas, E., Medrano, G., de Saja, J.A., Rodriguez-Mendez, M.L., 2014. Electronic tongue formed by sensors and biosensors containing phthalocyanines as electron mediators: Application to the analysis of red grapes. J. Porphyr. Phthalocyanines 18, 76–86. doi:10.1142/S1088424613501137

Mei, L., Zhang, P., Chen, J., Chen, D., Quan, Y., Gu, N., Zhang, G., Cui, R., 2016. Non-enzymatic sensing of glucose and hydrogen peroxide using a glassy carbon

electrode modified with a nanocomposite consisting of nanoporous copper, carbon black and nafion. Microchim. Acta 183, 1359–1365. doi:10.1007/s00604-016-1764-0

Mercante, L.A., Scagion, V.P., Migliorini, F.L., Mattoso, L.H.C., Correa, D.S., 2017. Electrospinning-based (bio)sensors for food and agricultural applications: A review. TrAC - Trends Anal. Chem. 91, 91–103. doi:10.1016/j.trac.2017.04.004

Mergenthaler, P., Lindauer, U., Dienel, G.A., Meisel, A., 2013. Sugar for the brain: the role of glucose in physiological and pathological brain function. Trends Neurosci. 36, 587–597. doi:10.1016/j.tins.2013.07.001.Sugar

Metek, 2018. PARSTAT 4000 Potentiostat/Galvanostat/EIS Analyzer.

Minunni, M., Scarano, S., Mascini, M., 2008. Affinity-based biosensors as promising tools for gene doping detection. Trends Biotechnol. 26, 236–243. doi:10.1016/j.tibtech.2008.02.005

Mishra, R.K., Majeed, A.B.A., Banthia, A.K., 2011. Fabrication and characterization of Chitosan/Poly (vinyl alcohol)-co-(vinyl acetate)-co-(itaconic acid) hydrogel membranes. Int. J. Plast. Technol. 15, 21–32.

Mobin, S.M., Sanghavi, B.J., Srivastava, A.K., Mathur, P., Lahiri, G.K., 2010. Biomimetic sensor for certain phenols employing a copper(II) complex. Anal. Chem. 82, 5983–5992.

Mohamad, N.R., Marzuki, N.H.C., Buang, N.A., Huyop, F., Wahab, R.A., 2015. An overview of technologies for immobilization of enzymes and surface analysis techniques for immobilized enzymes. Biotechnol. Biotechnol. Equip. 29, 205–220. doi:10.1080/13102818.2015.1008192

Mohanraj, V., Chen, Y., Chen, M.&, 2006. Nanoparticles – A Review. Trop. J. Pharm. Res. Trop J Pharm Res 5, 561–573. doi:10.4314/tjpr.v5i1.14634

Muckley, E.S., Jacobs, C.B., Vidal, K., Lavrik, N. V., Sumpter, B.G., Ivanov, I.N., 2017. Multi-mode humidity sensing with water-soluble copper phthalocyanine for increased sensitivity and dynamic range. Sci. Rep. 7, 1–11. doi:10.1038/s41598-017-10401-2

Muhammad, A., Hajian, R., Yusof, N.A., Shams, N., Abdullah, J., Woi, P.M., Garmestani, H., 2018. A screen printed carbon electrode modified with carbon nanotubes and gold nanoparticles as a sensitive electrochemical sensor for determination of thiamphenicol residue in milk. RSC Adv. 8, 2714–2722. doi:10.1039/c7ra07544h

Mulchandani, P., Chen, W., Mulchandani, A., 2001. Flow injection amperometric enzyme biosensor for direct determination of organophosphate nerve agents. Environ. Sci. Technol. 35, 2562–2565. doi:10.1021/es001773q

Mundinamani, S.P., Rabinal, M.K., 2014. Cyclic Voltammetric Studies on the Role of Electrode , Electrode Surface Modification and Electrolyte Solution of an Electrochemical Cell 7, 45–52.

Murugaboopathi, G., Parthasarathy, V., Chellaram, C., Anand, T.P., Vinurajkumar, S., 2013. Applications of biosensors in food industry. Biosci. Biotechnol. Res. Asia 10, 711–714. doi:10.13005/bbra/1185

Nabid, M.R., Sedghi, R., Jamaat, P.R., Safari, N., Entezami, A.A., 2007. Catalytic oxidative polymerization of aniline by using transition-metal tetrasulfonated phthalocyanine. Appl. Catal. A Gen. 328, 52–57. doi:10.1016/j.apcata.2007.05.017

Nada, M.H., 2015. Scanning electron microscopy. BAOJ Microbio 1, 1–8.

Nagarale, R.K., Lee, J.M., Shin, W., 2009. Electrochemical properties of ferrocene modified polysiloxane/chitosan nanocomposite and its application to glucose sensor. Electrochim. Acta 54, 6508–6514.

Nath, B.C., Gogoi, B., Boruah, M., Sharma, S., Khannam, M., Ahmed, G.A., Dolui, S.K., 2014. High performance polyvinyl alcohol/multi walled carbon nanotube/polyaniline hydrogel (PVA/MWCNT/PAni) based dye sensitized solar cells. Electrochim. Acta 146, 106–111. doi:10.1016/j.electacta.2014.08.134

Ndiaye, A.L., Delile, S., Brunet, J., Varenne, C., Pauly, A., 2016. Electrochemical sensors based on screen-printed electrodes: The use of phthalocyanine derivatives for application in VFA Detection. Biosensors 6. doi:10.3390/bios6030046

Nekelson, F., Monobe, H., Shiro, M., Shimizu, Y., 2007. Liquid crystalline and charge transport properties of double-decker cerium phthalocyanine complexes. J. Mater. Chem. 17, 2607. doi:10.1039/b616848p

Newman, J.D., Turner, A.P.F., 2005. Home blood glucose biosensors: A commercial perspective. Biosens. Bioelectron. 20, 2435–2453. doi:10.1016/j.bios.2004.11.012

Nguyen, D.N., Yoon, H., 2016. Recent Advances in Nanostructured Conducting Polymers : from Synthesis to Practical Applications. doi:10.3390/polym8040118

Nien, P.C., Tung, T.S., Ho, K.C., 2006. Amperometric glucose biosensor based on entrapment of glucose oxidase in a poly(3,4-ethylenedioxythiophene) film. Electroanalysis 18, 1408–1415.

Nigam, V.K., Shukla, P., 2015. Enzyme based biosensors for detection of environmental pollutants-A review. J. Microbiol. Biotechnol. 25, 1773–1781. doi:10.4014/jmb.1504.04010

Nireesha, G., Divya, L., Sowmya, C., Venkateshan, N., Niranjan Babu, M., Lavakumar, V., 2013. Lyophilization/Freeze Drying -An Review. Ijntps 3, 87–98.

Nobrega, M.M., Silva, C.H.B., Constantino, V.R.L., Temperini, M.L.A., 2012. Spectroscopic study on the structural differences of thermally induced cross-linking segments in emeraldine salt and base forms of polyaniline. J. Phys. Chem. B 116, 14191–14200.

Nouri, E., Mohammadi, M.R., Xu, Z.X., Dracopoulos, V., Lianos, P., 2018. Improvement of the photovoltaic parameters of perovskite solar cells using a reduced-graphene-oxide-modified titania layer and soluble copper phthalocyanine as a hole transporter. Phys. Chem. Chem. Phys. 20, 2388–2395. doi:10.1039/c7cp04538g

Novoselov, K.S., Geim, A.K., Morozov, S.V., Jiang, D., Zhang, Y., Dubonos, S. V., Grigorieva, I. V., Firsov, A.A., 2004. Electric Field Effect in Atomically Thin Carbon Films. Science (80-.). 306, 666–669. doi:10.1126/science.1102896

O'Brien, F.J., Harley, B.A., Yannas, I. V., Gibson, L., 2004. Influence of freezing rate on pore structure in freeze-dried collagen-GAG scaffolds. Biomaterials 25, 1077–1086.

O'Hare, D., 2014. Body Sensor Networks. doi:10.1007/978-1-4471-6374-9

Olde Damink, L.H.H., Dijkstra, P.J., Van Luyn, M.J.A., Van Wachem, P.B., Nieuwenhuis, P., Feijen, J., 1996. Cross-linking of dermal sheep collagen using a water-soluble carbodiimide. Biomaterials 17, 765–773.

Olgac, R., Soganci, T., Baygu, Y., Gök, Y., Ak, M., 2017. Zinc(II) phthalocyanine fused in peripheral positions octa-substituted with alkyl linked carbazole: Synthesis, electropolymerization and its electro-optic and biosensor applications.

Biosens. Bioelectron. 98, 202–209.

Overbye, M., 2016. Doping control in sport: An investigation of how elite athletes perceive and trust the functioning of the doping testing system in their sport. Sport Manag. Rev. 19, 6–22. doi:10.1016/j.smr.2015.10.002

Ozoemena, K.I., Nyokong, T., 2006. Novel amperometric glucose biosensor based on an ether-linked cobalt(II) phthalocyanine-cobalt(II) tetraphenylporphyrin pentamer as a redox mediator. Electrochim. Acta 51, 5131–5136. doi:10.1016/j.electacta.2006.03.055

Ozoemena, K.I., Zhao, Z., Nyokong, T., 2005. Immobilized cobalt(II) phthalocyanine-cobalt(II) porphyrin pentamer at a glassy carbon electrode: Applications to efficient amperometric sensing of hydrogen peroxide in neutral and basic media. Electrochem. commun. 7, 679–684. doi:10.1016/j.elecom.2005.04.019

Pakchin, P.S., Nakhjavani, S.A., Saber, R., Ghanbari, H., Omidi, Y., 2017. Recent advances in simultaneous electrochemical multi-analyte sensing platforms. TrAC - Trends Anal. Chem. 92, 32–41. doi:10.1016/j.trac.2017.04.010

Pal, C., Cammidge, a N., Cook, M.J., Sosa-Sanchez, J.L., Sharma, a K., Ray, a K., 2011. In situ chemichromic studies of interactions between a lutetium bis-octaalkyl-substituted phthalocyanine and selected biological cofactors. J. R. Soc. Interface 74, 2848–2850. doi:10.1098/rsif.2010.0726

Pan, L., Yu, G., Zhai, D., Lee, H.R., Zhao, W., Liu, N., Wang, H., Tee, B.C.-K., Shi, Y., Cui, Y., Bao, Z., 2012. Hierarchical nanostructured conducting polymer hydrogel with high electrochemical activity. Proc. Natl. Acad. Sci. U. S. A. 109, 9287–92. doi:10.1073/pnas.1202636109

Pandey, A., Gurbuz, Y., Ozguz, V., Niazi, J.H., Qureshi, A., 2017. Graphene-interfaced

electrical biosensor for label-free and sensitive detection of foodborne pathogenic E. coli O157:H7. Biosens. Bioelectron. 91, 225–231. doi:10.1016/j.bios.2016.12.041

Park, S., Chung, T.D., Kim, H.C., 2003. Nonenzymatic glucose detection using mesoporous platinum. Anal. Chem. 75, 3046–3049. doi:10.1021/ac0263465

Pasinszki, T., Krebsz, M., 2018. Biosensors for Non-Invasive Detection of Celiac Disease Biomarkers in Body Fluids. Biosensors 8, 55. doi:10.3390/bios8020055

Patel, S., Nanda, R., Sahoo, S., Mohapatra, E., 2016. Biosensors in Health Care: The Milestones Achieved in Their Development towards Lab-on-Chip-Analysis. Biochem. Res. Int. 2016, 3130469. doi:10.1155/2016/3130469

Pattabiraman, V.R., Bode, J.W., 2011. Rethinking amide bond synthesis. Nature 480, 471–9.

Pei, R., Cheng, Z., Wang, E., Yang, X., 2001. Amplification of antigen-antibody interactions based on biotin labeled protein-streptavidin network complex using impedance spectroscopy. Biosens. Bioelectron. 16, 355–361. doi:10.1016/S0956-5663(01)00150-6

Peng, X., Koczkur, K., Nigro, S., Chen, A., 2004. Fabrication and electrochemical properties of novel nanoporous platinum network electrodes. Chem. Commun. (Camb). 1, 2872–2873. doi:10.1039/b412677g

Pereira-Rodrigues, N., Albin, V., Koudelka-Hep, M., Auger, V., Pailleret, A., Bedioui, F., 2002. Nickel tetrasulfonated phthalocyanine based platinum microelectrode array for nitric oxide oxidation. Electrochem. commun. 4, 922–927. doi:10.1016/S1388-2481(02)00489-7

Pérez-López, B., Merkoçi, A., 2011. Nanomaterials based biosensors for food analysis applications. Trends Food Sci. Technol. 22, 625–639. doi:10.1016/j.tifs.2011.04.001

Perrin, D.D., Armarego, W.L.F., 1989. Purification of Laboratory Chemicals. Pergamon Press.

Peters, A.L., Buschur, E.O., Buse, J.B., Cohan, P., Diner, J.C., Hirsch, I.B., 2015. Euglycemic diabetic ketoacidosis: A potential complication of treatment with sodium-glucose cotransporter 2 inhibition. Diabetes Care 38, 1687–1693.

Piao, Y., Han, D.J., Azad, M.R., Park, M., Seo, T.S., 2015. Enzyme incorporated microfluidic device for in-situ glucose detection in water-in-air microdroplets. Biosens. Bioelectron. 65, 220–225.

Poitout, V., Hagman, D., Stein, R., Artner, I., Robertson, R.P., Harmon, J.S., 2006. Recent Advances in Nutritional Sciences Regulation of the Insulin Gene by Glucose and Fatty Acids 1 873–876.

PRESSEPORTAL, 2015. The world's first portable glucometer [WWW Document]. URL https://www.presseportal.de/pm/34011/3183412 (accessed 7.31.18).

Puoci, F., Curcio, M., 2013. Smart Materials for Drug Delivery. Smart Mater. Drug Deliv. Vol. 2 2, 153–179. doi:10.1039/9781849734318

Pushkarev, V.E., Tolbin, A.Y., Zhurkin, F.E., Borisova, N.E., Trashin, S.A., Tomilova, L.G., Zefirov, N.S., 2012. Sandwich double-decker lanthanide(III) "intracavity" complexes based on clamshell-type phthalocyanine ligands: Synthesis, spectral, electrochemical, and spectroelectrochemical investigations. Chem. - A Eur. J. 18, 9046–9055. doi:10.1002/chem.201200361

Qu, Z., Xu, H., Gu, H., 2015. Synthesis and biomedical applications of poly((meth)acrylic acid) brushes. ACS Appl. Mater. Interfaces 7, 14537–14551.

Quy, T., 2011. Electrochemistry of PANI/metal composites in basic solutions. UNLV Theses/Dissertations/Professional Pap.

Radhakrishnan, S., Deshpande, S.D., 2002. Conducting Polymers Functionalized with Phthalocyanine as Nitrogen Dioxide Sensors. Sensors 2, 185–194. doi:10.3390/s20500185

Ragavan, K. V., Kumar, S., Swaraj, S., Neethirajan, S., 2018. Advances in biosensors and optical assays for diagnosis and detection of malaria. Biosens. Bioelectron. 105, 188–210. doi:10.1016/j.bios.2018.01.037

Rahman, M.M., Ahammad, A.J.S., Jin, J.H., Ahn, S.J., Lee, J.J., 2010. A comprehensive review of glucose biosensors based on nanostructured metal-oxides. Sensors 10, 4855–4886. doi:10.3390/s100504855

Rahy, A., Rguig, T., Cho, S.J., Bunker, C.E., Yang, D.J., 2011. Polar solvent soluble and hydrogen absorbing polyaniline nanofibers. Synth. Met. 161, 280–284.

Ramanavičius, A., Ramanavičiene, A., Malinauskas, A., 2006. Electrochemical sensors based on conducting polymer-polypyrrole. Electrochim. Acta 51, 6025–6037. doi:10.1016/j.electacta.2005.11.052

Randles, J.E.B., 1947. KINETICS OF RAPID ELECTRODE REACTIONS 11–19.

Randviir, E.P., Banks, C.E., 2013. Electrochemical impedance spectroscopy: an overview of bioanalytical applications. Anal. Methods 5, 1098. doi:10.1039/c3ay26476a

Rao, H., Chen, M., Ge, H., Lu, Z., Liu, X., Zou, P., Wang, X., He, H., Zeng, X., Wang,

Y., 2017. A novel electrochemical sensor based on Au@PANI composites film modified glassy carbon electrode binding molecular imprinting technique for the determination of melamine. Biosens. Bioelectron. 87, 1029–1035. doi:10.1016/j.bios.2016.09.074

Raubenheimer, P., 2010. What type of diabetes does my patient have and is it relevant ? C M E 28, 1–3.

Ren, Q., Feng, L., Fan, R., Ge, X., Sun, Y., 2016. Water-dispersible triethylenetetramine-functionalized graphene: Preparation, characterization and application as an amperometric glucose sensor. Mater. Sci. Eng. C 68, 308–316. doi:10.1016/j.msec.2016.05.124

Ren, X., Chen, D., Meng, X., Tang, F., Du, A., Zhang, L., 2009. Amperometric glucose biosensor based on a gold nanorods/cellulose acetate composite film as immobilization matrix. Colloids Surfaces B Biointerfaces 72, 188–192. doi:10.1016/j.colsurfb.2009.04.003

Ribeiro, T., Baleizão, C., Farinha, J.P.S., 2014. Functional films from silica/polymer nanoparticles. Materials (Basel). 7, 3881–3900. doi:10.3390/ma7053881

Rishpon, J., Rosen-Margalit, I., Harth, R., Ozer, D., Bettelheim, A., 1991. Mediated electron transfer for the electrooxidation of glucose oxidase by manganese tetrakis (o-aminophenyl) porphyrin. J. Electroanal. Chem. Interfacial Electrochem. 307, 1991.

Roosz, N., Euvard, M., Lakard, B., Buron, C.C., Martin, N., Viau, L., 2017. Synthesis and characterization of polyaniline-silica composites: Raspberry vs core-shell structures. Where do we stand? J. Colloid Interface Sci. 502, 184–192.

Rorsman, P., Braun, M., 2013. Regulation of Insulin Secretion in Human Pancreatic

Islets. Annu. Rev. Physiol. 75, 155–179. doi:10.1146/annurev-physiol-030212-183754

Rudolph, M., Reddy, D., Feldberg, S., 1994. A simulator for cyclic voltammetric responses. Anal. Chem. 66, 589A–600A. doi:10.1021/ac00082a725

Ruiyi, L., Fangchao, C., Haiyan, Z., Xiulan, S., Zaijun, L., 2018. Electrochemical sensor for detection of cancer cell based on folic acid and octadecylamine-functionalized graphene aerogel microspheres. Biosens. Bioelectron. 119, 156–162. doi:10.1016/j.bios.2018.07.060

Ryskova, L., Buchta, V., Karaskova, M., Rakusan, J., Cerny, J., Slezak, R., 2012. In vitro antimicrobial activity of light-activated phthalocyanines. Cent. Eur. J. Biol. 8, 168–177. doi:10.2478/s11535-013-0118-0

Saeed, A.M., 2013. Temperature effect on swelling properties of commercial polyacrylic acid hydrogel beads . 1, 1614–1627.

Salahandish, R., Ghaffarinejad, A., Naghib, S.M., Majidzadeh-A, K., Zargartalebi, H., Sanati-Nezhad, A., 2018. Nano-biosensor for highly sensitive detection of HER2 positive breast cancer. Biosens. Bioelectron. 117, 104–111. doi:10.1016/j.bios.2018.05.043

Salek-Maghsoudi, A., Vakhshiteh, F., Torabi, R., Hassani, S., Ganjali, M.R., Norouzi, P., Hosseini, M., Abdollahi, M., 2018. Recent advances in biosensor technology in assessment of early diabetes biomarkers. Biosens. Bioelectron. 99, 122–135. doi:10.1016/j.bios.2017.07.047

Salimi, A., Compton, R.G., Hallaj, R., 2004. Glucose biosensor prepared by glucose oxidase encapsulated sol-gel and carbon-nanotube-modified basal plane pyrolytic graphite electrode. Anal. Biochem. 333, 49–56.

Sanger, K., 2017. Design and Development of Electrochemical Polymer-Based Lab-on-a-Disc Devices for Biological Applications.

Santonico, M., Pennazza, G., D.asimakopoulos, A., Fabbro, D. Del, Miano, R., Capuano, R., Finazzi-Agrò, E., D'Amico, A., 2014. Chemical sensors for prostate cancer detection oriented to non-invasive approach. Procedia Eng. 87, 320–323. doi:10.1016/j.proeng.2014.11.672

Saravanan, S., Anantharaman, M.R., Venkatachalam, S., 2006. Structural and electrical studies on tetrameric cobalt phthalocyanine and polyaniline composites. Mater. Sci. Eng. B Solid-State Mater. Adv. Technol. 135, 113–119. doi:10.1016/j.mseb.2006.08.048

Sardar, M., Roy, I., Gupta, M.N., 2000. Simultaneous purification and immobilization of Aspergillus niger xylanase on the reversibly soluble polymer Eudragit(TM) L-100. Enzyme Microb. Technol. 27, 672–679. doi:10.1016/S0141-0229(00)00257-X

Saydan, N., Durmuş, M., Dizge, M.G., Yaman, H., Gürek, A.G., Antunes, E., Nyokong, T., Ahsen, V., 2009. Water-soluble phthalocyanines mediated photodynamic effect on mesothelioma cells. J. Porphyr. Phthalocyanines 13, 681–690. doi:10.1142/S1088424609000863

Schuit, F., Huypens, P., Heimberg, H., Pipeleers, D., 2001. Glucose Sensing in Pancreatic β-Cells. Diabetes 50, 1–11.

Scott, K., 2016. Microbial Electrochemical and Fuel Cells, Microbial Electrochemical and Fuel Cells. Elsevier. doi:10.1016/B978-1-78242-375-1.00005-8

Şenel, M., 2011. Construction of reagentless glucose biosensor based on ferrocene conjugated polypyrrole. Synth. Met. 161, 1861–1868.

Setford, S.J., Newman, J.D., 2005. Enzyme Biosensors, in: Microbial Enzymes and Biotransformations. pp. 29–60. doi:10.1385/1-59259-846-3:029

Sezgin, N., Balkaya, N., 2015. Adsorption of heavy metals from industrial wastewater by using polyacrylic acid hydrogel. Desalin. Water Treat. 3994, 1–15. doi:10.1080/19443994.2015.1030453

Shafiee, G., Mohajeri-Tehrani, M., Pajouhi, M., Larijani, B., 2012. The importance of hypoglycemia in diabetic patients. J. Diabetes Metab. Disord. 11, 17.

Shamsipur, M., Karimi, Z., Amouzadeh Tabrizi, M., Rostamnia, S., 2017. Highly sensitive non-enzymatic electrochemical glucose sensor by Nafion/SBA-15-Cu (II) modified glassy carbon electrode. J. Electroanal. Chem. 799, 406–412. doi:10.1016/j.jelechem.2017.06.029

Shan, C., Yang, H., Han, D., Zhang, Q., Ivaska, A., Niu, L., 2010. Graphene/AuNPs/chitosan nanocomposites film for glucose biosensing. Biosens. Bioelectron. 25, 1070–1074. doi:10.1016/j.bios.2009.09.024

Sharma, R.K., Gulati, S., 2012. Manganese phthalocyanine immobilized on silica gel: Efficient and recyclable catalyst for single-step oxidative esterification of aldehydes with alcohols. J. Mol. Catal. A Chem. 363–364, 291–303.

Shenoy, V., 2013. CMOS Analog correlator based glucose sensor readout circuit. The university of Texas at Arlington.

Shinohara, Hisanori, Ashutosh, 2015. Graphene: An Introduction to the Fundamentals and Industrial Applications, John Wiley & Sons.

Shirakawa, H., Louis, E.J., MacDiarmid, A.G., Chiang, C., Heeger, A.J., 1977. Synthesis of electrically conducting organic polymers: halogen derivates of

polyacetylene. J. Chem. Soc. Chem. Commun. 578–580. doi:10.1039/c39770000578

Shui, B., Tao, D., Florea, A., Cheng, J., Zhao, Q., Gu, Y., Li, W., Jaffrezic-Renault, N., Mei, Y., Guo, Z., 2018. Biosensors for Alzheimer's disease biomarker detection: A review. Biochimie 147, 13–24. doi:10.1016/j.biochi.2017.12.015

Simic-Glavaski, B., 1989. Phthalocyanines in molecular electronic devices. IEEE Eng. Med. Biol. 11th Annu. Int. Conf. 1325–1326.

Singh, M., Kathuroju, P.K., Jampana, N., 2009. Polypyrrole based amperometric glucose biosensors. Sensors Actuators, B Chem. 143, 430–443.

Siswana, M.P., Ozoemena, K.I., Nyokong, T., 2006. Electrocatalysis of asulam on cobalt phthalocyanine modified multi-walled carbon nanotubes immobilized on a basal plane pyrolytic graphite electrode. Electrochim. Acta 52, 114–122.

Skoog, D.A., West, D.M., Holler, F.J., 1988. Foundamentals of Analytical Chemistry.

Smith, J.L., 2013. The Pursuit of Noninvasive Glucose : "Hunting the Deceitful Turkey," 3rd ed.

Sode, K., Loew, N., Ohnishi, Y., Tsuruta, H., Mori, K., Kojima, K., Tsugawa, W., LaBelle, J.T., Klonoff, D.C., 2017. Novel fungal FAD glucose dehydrogenase derived from Aspergillus niger for glucose enzyme sensor strips. Biosens. Bioelectron. 87, 305–311. doi:10.1016/j.bios.2016.08.053

Song, J., Wang, X., Chang, C.-T., 2014. Preparation and characterization of graphene oxide. J. Nanomater. 2014. doi:10.1155/2014/276143

Soomro, R.A., Ibupoto, Z.H., Sirajuddin, Abro, M.I., Willander, M., 2015. Electrochemical sensing of glucose based on novel hedgehog-like NiO

nanostructures. Sensors Actuators, B Chem. 209, 966–974. doi:10.1016/j.snb.2014.12.050

Sorokin, A.B., Buisson, P., Pierre, A.C., 2001. Encapsulation of iron phthalocyanine in sol-gel materials. Microporous Mesoporous Mater. 46, 87–98.

Spahn, C., Minteer, S., 2008. Enzyme Immobilization in Biotechnology. Recent Patents Eng. 2, 195–200. doi:10.2174/187221208786306333

Sreenivasa, B., Kumar, G. V., Sreenivasa, B., 2015. Comparative study of blood glucose levels in neonates using glucometer and laboratory glucose oxidase method. Curr. Pediatr. Res. 19, 29–32.

Stejskal, J., Gilbert, R.G., 2006. Polyaniline preparation of a conducting ploymer (IUPAC Technical Report). Pure Appl. Chem. doi:10.1351/pac200274050857

Stoller, M.D., Park, S., Yanwu, Z., An, J., Ruoff, R.S., 2008. Graphene-Based ultracapacitors. Nano Lett. 8, 3498–3502. doi:10.1021/nl802558y

Sun, C., Chen, L., Xu, F., Zhu, P., Luan, J., Mao, C., Shen, J., 2013. Hemocompatible and antibiofouling PU-F127 nanospheres platform for application to glucose detection in whole blood. J. Mater. Chem. B 1, 801–809. doi:10.1039/c2tb00396a

Sun, D.W., 2009. Infrared spectroscopy for food quality analysis and control. Academic Press.

Sun, T., Qing, G., Su, B., Jiang, L., 2011. Functional biointerface materials inspired from nature. Chem. Soc. Rev. 40, 2909. doi:10.1039/c0cs00124d

Sun, X.F., Jing, Z., Wang, G., 2013. Preparation and swelling behaviors of porous hemicellulose-g-polyacrylamide hydrogels. J. Appl. Polym. Sci. 128, 1861–1870. doi:10.1002/app.38240

Sun, Z., Cui, G., Li, H., Liu, Y., Tian, Y., Yan, S., 2016. Multifunctional optical sensing probes based on organic–inorganic hybrid composites. J. Mater. Chem. B 4, 5194–5216. doi:10.1039/C6TB01468B

Swoboda, B.E.P., Massey, V., 1965. Purification and Properties of the Glucose Oxidase from Aspergillus niger. J. Biol. Chem. 240, 2209–2215.

Tabish, S.A., 2007. Is Diabetes Becoming the Biggest Epidemic of the Twenty-first Century? Int. J. Health Sci. (Qassim). 1, V–VIII.

Tang, C.K., Vaze, A., Rusling, J.F., 2012. Fabrication of immunosensor microwell arrays from gold compact discs for detection of cancer biomarker proteins. Lab Chip 12, 281–286. doi:10.1039/C1LC20833K

Tang, L., Cheng, J., 2013. Nonporous silica nanoparticles for nanomedicine application. Nano Today 8, 290–312. doi:10.1016/j.nantod.2013.04.007

Tang, Q., Wu, J., Li, Y., Lin, J., Tang, Z., Huang, M., 2011. Facile secondary-template synthesis of polyaniline microtube array for enhancing glucose biosensitivity. J. Mater. Chem. 21, 12927. doi:10.1039/c1jm12037a

Taşdelen, B., 2017. Conducting hydrogels based on semi-interpenetrating networks of polyaniline in poly(acrylamide-co-itaconic acid) matrix: synthesis and characterization. Polym. Adv. Technol. doi:10.1002/pat.4073

Teo, R.D., Termini, J., Gray, H.B., 2016. Lanthanides: Applications in Cancer Diagnosis and Therapy. J. Med. Chem. acs.jmedchem.5b01975. doi:10.1021/acs.jmedchem.5b01975

Thirumalraj, B., Palanisamy, S., Chen, S.-M., Yang, C.-Y., Periakaruppan, P., Lou, B.-S., 2015. Direct electrochemistry of glucose oxidase and sensing of glucose at a

glassy carbon electrode modified with a reduced graphene oxide/fullerene-C60 composite. RSC Adv. 5, 77651–77657. doi:10.1039/C5RA12018G

Tian, K., Prestgard, M., Tiwari, A., 2014. A review of recent advances in nonenzymatic glucose sensors. Mater. Sci. Eng. C 41, 100–118. doi:10.1016/j.msec.2014.04.013

Tirimacco, R., Tideman, P.A., Dunbar, J., Simpson, P.A., Philpot, B., Laatikainen, T., Janus, E., 2010. Should capillary blood glucose measurements be used in population surveys? Int. J. Diabetes Mellit. 2, 24–27.

Tiwari, A., Patra, H.K., Turner, A.P., 2015. Advanced bioelectronics materials. John Wiley Sons 373.

Tobias, C.W., Eisenberg, M., Wilke, C.R., 1952. Diffusion and convection in electrodialysis - A theoretical review. J. Electrochem. Soc. 99, 359–365. doi:10.1149/1.2779636

Toghill, K.E., Compton, R.G., 2010. Electrochemical non-enzymatic glucose sensors: A perspective and an evaluation. Int. J. Electrochem. Sci. 5, 1246–1301.

Tonyushkina, K., Nichols, J.H., 2009. Glucose meters: A review of technical challenges to obtaining accurate results. J. Diabetes Sci. Technol. 3, 971–980. doi:10.1177/193229680900300446

Transparency Market Research, 2018. Glucose Biosensors Market - Global Industry Analysis, Size, Share, Growth, Trends, and Forecast 2016 - 2024 [WWW Document]. URL https://www.transparencymarketresearch.com/glucose-biosensors-market.html (accessed 7.29.18).

Trzebinski, J., 2011. NOVEL APPROACHES TO ENGINEER GLUCOSE BIOSENSORS. Brunel University.

Turner, A.P.F., 2013. Biosensors: sense and sensibility. Chem. Soc. Rev. 42, 3184. doi:10.1039/c3cs35528d

ul Hasan, K., Asif, M.H., Hassan, M.U., Sandberg, M.O., Nur, O., Willander, M., Fagerholm, S., Strålfors, P., 2015. A Miniature Graphene-based Biosensor for Intracellular Glucose Measurements. Electrochim. Acta 174, 574–580. doi:10.1016/j.electacta.2015.06.035

Ulijn, R. V., Bibi, N., Jayawarna, V., Thornton, P.D., Todd, S.J., Mart, R.J., Smith, A.M., Gough, J.E., 2007. Bioresponsive hydrogels. Mater. Today 10, 40–48. doi:10.1016/S1369-7021(07)70049-4

Ullah, S., Hamade, F., Bubniene, U., Engblom, J., Ramanavicius, A., Ramanaviciene, A., Ruzgas, T., 2018. In-vitro model for assessing glucose diffusion through skin. Biosens. Bioelectron. 110, 175–179. doi:10.1016/j.bios.2018.03.039

University of Delaware, 2018. Micromertics ASAP 2020 [WWW Document]. URL https://sites.udel.edu/amcl/micromertics-asap-2020/ (accessed 7.2.18).

Unnikrishnan, B., Palanisamy, S., Chen, S.M., 2013. A simple electrochemical approach to fabricate a glucose biosensor based on graphene-glucose oxidase biocomposite. Biosens. Bioelectron. 39, 70–75. doi:10.1016/j.bios.2012.06.045

Vanýsek, P., 1994. Introduction to electrochemical impedance 1–76.

Volpati, D., Alessio, P., Zanfolim, A.A., Storti, F.C., Job, A.E., Ferreira, M., Riul, A., Oliveira, O.N., Constantino, C.J.L., 2008. Exploiting distinct molecular architectures of ultrathin films made with iron phthalocyanine for sensing. J. Phys. Chem. B 112, 15275–15282. doi:10.1021/jp804159h

WADA, 2016. WADA President Blog: Expanding Funding for Clean Sport [WWW

Document]. The World Anti-Doping Agency. URL https://www.wada-ama.org/en/media/news/2016-05/wada-president-blog-expanding-funding-for-clean-sport (accessed 7.17.18).

Wang, A.J., Li, Y.F., Li, Z.H., Feng, J.J., Sun, Y.L., Chen, J.R., 2012. Amperometric glucose sensor based on enhanced catalytic reduction of oxygen using glucose oxidase adsorbed onto core-shell Fe3O4@silica@Au magnetic nanoparticles. Mater. Sci. Eng. C 32, 1640–1647. doi:10.1016/j.msec.2012.04.055

Wang, B., Li, B., Deng, Q., Dong, S., 1998. Amperometric glucose biosensor based on sol-gel organic-inorganic hybrid material. Anal. Chem. 70, 3170–3174.

Wang, F., Han, L., Zhang, Z., Fang, X., Shi, J., Ma, W., 2012. Surfactant-free ionic liquid-based nanofluids with remarkable thermal conductivity enhancement at very low loading of graphene. Nanoscale Res. Lett. 7, 1–7. doi:10.1186/1556-276X-7-314

Wang, H.-C., Lee, A.-R., 2015. Recent developments in blood glucose sensors. J. Food Drug Anal. 23, 191–200. doi:10.1016/j.jfda.2014.12.001

Wang, H., Bu, Y., Dai, W., Li, K., Wang, H., Zuo, X., 2015. Well-dispersed cobalt phthalocyanine nanorods on graphene for the electrochemical detection of hydrogen peroxide and glucose sensing. Sensors Actuators, B Chem. 216, 298–306.

Wang, H.B., Zhang, Y.H., Yang, H.L., Ma, Z.Y., Zhang, F.W., Sun, J., Ma, J.T., 2013. Palladium immobilized in the nanocages of SBA-16: An efficient and recyclable catalyst for Suzuki coupling reaction. Microporous Mesoporous Mater. 168, 65–72. doi:10.1016/j.micromeso.2012.09.025

Wang, J., 2008. Electrochemical glucose biosensors. Chem. Rev. 108, 814–825.

doi:10.1016/B978-012373738-0.50005-2

Wang, J., 2006. Electrochemical biosensors: Towards point-of-care cancer diagnostics. Biosens. Bioelectron. 21, 1887–1892. doi:10.1016/j.bios.2005.10.027

Wang, J., 2001. Glucose biosensors: 40 Years of advances and challenges. Electroanalysis 13, 983–988. doi:10.1002/1521-4109(200108)13:12<983::AID-ELAN983>3.0.CO;2-#

Wang, J., Thomas, D.F., Chen, A., 2008. Nonenzymatic electrochemical glucose sensor based on nanoporous PtPb networks. Anal. Chem. 80, 997–1004. doi:10.1021/ac701790z

Wang, K., Xu, J.J., Chen, H.Y., 2005. A novel glucose biosensor based on the nanoscaled cobalt phthalocyanine-glucose oxidase biocomposite. Biosens. Bioelectron. 20, 1388–1396. doi:10.1016/j.bios.2004.06.006

Wang, K., Zhang, X., Li, C., Zhang, H., Sun, X., Xu, N., Ma, Y., 2014. Flexible solid-state supercapacitors based on a conducting polymer hydrogel with enhanced electrochemical performance. J. Mater. Chem. A 2, 19726–19732. doi:10.1039/c4ta04924a

Wang, Y., Liu, L., Li, M., Xu, S., Gao, F., 2011. Multifunctional carbon nanotubes for direct electrochemistry of glucose oxidase and glucose bioassay. Biosens. Bioelectron. 30, 107–111. doi:10.1016/j.bios.2011.08.038

Wang, Y., Zheng, H., Jia, L., Li, H., Li, T., Chen, K., Gu, Y., 2014. Optimizing the Polymerization Conditions of Soluble Polyaniline Doped with Itaconic Acid. J. Macromol. Sci. Part A 51, 577–581.

Wang, Y., Zheng, H., Jia, L., Li, H., Li, T., Chen, K., Gu, Y., 2014. Optimizing the

Polymerization Conditions of Soluble Polyaniline Doped with Itaconic Acid. J. Macromol. Sci. Part A 51, 577–581.

Wang, Z., Liu, S., Wu, P., Cai, C., 2009. Detection of glucose based on direct electron transfer reaction of glucose oxidase immobilized on highly ordered polyaniline nanotubes. Anal. Chem. 81, 1638–1645. doi:10.1021/ac802421h

Webb, P. a, 2003. Introduction to Chemical Adsorption Analytical Techniques and their Applications to Catalysis. MIC Tech. Publ. 13, 1–4.

Wei, H., Gu, H., Guo, J., Wei, S., Liu, J., Guo, Z., 2013a. Silica doped nanopolyaniline with endured electrochemical energy storage and the magnetic field effects. J. Phys. Chem. C 117, 13000–13010. doi:10.1021/jp403656q

Wei, H., Gu, H., Guo, J., Wei, S., Liu, J., Guo, Z., 2013b. Silica Doped Nano-polyaniline with Endured Electrochemical Energy Storage and the Magnetic Field Effects. Phys. Chem. 13000–13010. doi:10.1021/jp403656q

Welsh, M., Nielsen, D. a, MacKrell, a J., Steiner, D.F., 1985. Control of insulin gene expression in pancreatic beta-cells and in an insulin-producing cell line, RIN-5F cells. II. Regulation of insulin mRNA stability. J. Biol. Chem. 260, 13590–4.

Wild, S., Roglic, G., Green, A., Sicree, R., King, H., 2004. Global Prevalence of Diabetes: Estimates for the year 2000 and projections for 2030. Diabetes Care 27, 1047–1053. doi:ISBN 92 4 159493 4

Williams, D.B., Carter, C.B., 2009. Transmission Electron Microscopy, Microsc Microanal. doi:10.1007/978-3-319-26651-0

Wilson, J.S., 2005. Sensor Technology Handbook. Elsevier.

Wilson, R., Turner, A.P.F., 1992. Glucose oxidase: an ideal enzyme. Biosens.

Bioelectron. 7, 165–185. doi:10.1016/0956-5663(92)87013-F

Wöhrle, D., Eskes, M., Shigehara, K., Yamada, A., 1993. Wöhrle 1993.pdf. Synthesis (Stuttg). 2, 194–196.

Worsley, M.A., Kucheyev, S.O., Mason, H.E., Merrill, M.D., Mayer, B.P., Lewicki, J., Valdez, C. a., Suss, M.E., Stadermann, M., Pauzauskie, P.J., Satcher, J.H., Biener, J., Baumann, T.F., 2012. Mechanically robust 3D graphene macroassembly with high surface area. Chem. Commun. 48, 8428–8430. doi:10.1039/c2cc33979j

Wu, B.Y., Hou, S.H., Yin, F., Li, J., Zhao, Z.X., Huang, J.D., Chen, Q., 2007. Amperometric glucose biosensor based on layer-by-layer assembly of multilayer films composed of chitosan, gold nanoparticles and glucose oxidase modified Pt electrode. Biosens. Bioelectron. 22, 838–844. doi:10.1016/j.bios.2006.03.009

Wu, C., Sun, H., Li, Y., Liu, X., Du, X., Wang, X., Xu, P., 2015. Biosensor based on glucose oxidase-nanoporous gold co-catalysis for glucose detection. Biosens. Bioelectron. 66, 350–355. doi:10.1016/j.bios.2014.11.037

Xia, L., Wei, Z., Wan, M., 2010. Conducting polymer nanostructures and their application in biosensors. J. Colloid Interface Sci. 341, 1–11. doi:10.1016/j.jcis.2009.09.029

Xiao, K., Liu, J., Chen, H., Zhang, S., Kong, J., 2017. A label-free and high-efficient GO-based aptasensor for cancer cells based on cyclic enzymatic signal amplification. Biosens. Bioelectron. 91, 76–81. doi:10.1016/j.bios.2016.11.057

Xie, J., Wang, S., Aryasomayajula, L., Varadan, V.K., 2007. Platinum decorated carbon nanotubes for highly sensitive amperometric glucose sensing. Nanotechnology 18. doi:10.1088/0957-4484/18/6/065503

Yang, W., Zhang, C.G., Qu, H.Y., Yang, H.H., Xu, J.G., 2004. Novel fluorescent silica nanoparticle probe for ultrasensitive immunoassays. Anal. Chim. Acta 503, 163–169. doi:10.1016/j.aca.2003.10.045

Ye, J.S., Wen, Y., De Zhang, W., Cui, H.F., Xu, G.Q., Sheu, F.S., 2005. Electrochemical biosensing platforms using phthalocyanine-functionalized carbon nanotube electrode. Electroanalysis 17, 89–96. doi:10.1002/elan.200403124

Yin, Y., Dang, Q., Liu, C., Yan, J., Cha, D., Yu, Z., Cao, Y., Wang, Y., Fan, B., 2017. Itaconic acid grafted carboxymethyl chitosan and its nanoparticles: Preparation, characterization and evaluation. Int. J. Biol. Macromol. 102, 10–18.

Yoo, E.-H., Lee, S.-Y., 2010. Glucose Biosensors: An Overview of Use in Clinical Practice. Sensors 10, 4558–4576. doi:10.3390/s100504558

Yu, C., Zhu, Z., Wang, L., Wang, Q., Bao, N., Gu, H., 2014. A new disposable electrode for electrochemical study of leukemia K562 cells and anticancer drug sensitivity test. Biosens. Bioelectron. 53, 142–147. doi:10.1016/j.bios.2013.09.044

Yu, E.H., Cheng, S., Logan, B.E., Scott, K., 2009. Electrochemical reduction of oxygen with iron phthalocyanine in neutral media. J. Appl. Electrochem. 39, 705–711. doi:10.1007/s10800-008-9712-2

Yu, J., Tu, J., Zhao, F., Zeng, B., 2010. Direct electrochemistry and biocatalysis of glucose oxidase immobilized on magnetic mesoporous carbon. J. Solid State Electrochem. 14, 1595–1600.

Yu, J.S., Liao, H.X., Gerdon, A.E., Huffman, B., Scearce, R.M., McAdams, M., Alam, S.M., Popernack, P.M., Sullivan, N.J., Wright, D., Cliffel, D.E., Nabel, G.J., Haynes, B.F., 2006. Detection of Ebola virus envelope using monoclonal and polyclonal antibodies in ELISA, surface plasmon resonance and a quartz crystal

microbalance immunosensor. J. Virol. Methods 137, 219–228. doi:10.1016/j.jviromet.2006.06.014

Yuan, J., Wang, K., Xia, X., 2005. Highly ordered platinum-nanotubule arrays for amperometric glucose sensing. Adv. Funct. Mater. 15, 803–809. doi:10.1002/adfm.200400321

Yue, R., Lu, Q., Zhou, Y., 2011. A novel nitrite biosensor based on single-layer graphene nanoplatelet-protein composite film. Biosens. Bioelectron. 26, 4436–4441. doi:10.1016/j.bios.2011.04.059

Zagal, J., Bindra, P., Yeager, E., 1980. A mechanistic study of O2 reduction on water soluble phthalocyanines adsorbed on graphite electrodes. J. Electrochem. Soc. 127, 1506–1517.

Zagal, J.H., 1992. Metallophthalocyanines Reactions As Catalysts in Electrochemical. Coord. Chem. Rev. 119, 89–136. doi:10.1016/0010-8545(92)80031-L

Zebda, A., Gondran, C., Le Goff, A., Holzinger, M., Cinquin, P., Cosnier, S., 2011. Mediatorless high-power glucose biofuel cells based on compressed carbon nanotube-enzyme electrodes. Nat. Commun. 2, 370.

Zeghioud, H., Lamouri, S., Safidine, Z., Belbachir, M., 2015. Chemical synthesis and characterization of highly soluble conducting polyaniline in mixtures of common solvents. J. Serb. Chem. Soc 8033513, 917–931.

Zhai, D., Liu, B., Shi, Y., Pan, L., Wang, Y., Li, W., Zhang, R., Yu, G., 2013. Highly sensitive glucose sensor based on pt nanoparticle/polyaniline hydrogel heterostructures. ACS Nano 7, 3540–3546. doi:10.1021/nn400482d

Zhang, L., Zhou, C., Luo, J., Long, Y., Wang, C., Yu, T., 2015. A polyaniline

microtube platform for direct electron transfer of glucose oxidase and biosensing. J. Mater. Chem. B Mater. Biol. Med. 3, 1116–1124. doi:10.1039/C4TB01604A

Zhang, M., Liao, C., Mak, C.H., You, P., Mak, C.L., Yan, F., 2015. Highly sensitive glucose sensors based on enzyme-modified whole-graphene solution-gated transistors. Sci. Rep. 5, 1–7. doi:10.1038/srep08311

Zhang, Y., Liu, X., Li, L., Guo, Z., Xue, Z., Lu, X., 2016. An electrochemical paracetamol sensor based on layer-by-layer covalent attachment of MWCNTs and a G4.0 PAMAM modified GCE. Anal. Methods 8, 2218–2225. doi:10.1039/c5ay03241e

Zhang, Y.Q., Fan, Y.J., Cheng, L., Fan, L.L., Wang, Z.Y., Zhong, J.P., Wu, L.N., Shen, X.C., Shi, Z.J., 2013. A novel glucose biosensor based on the immobilization of glucose oxidase on layer-by-layer assembly film of copper phthalocyanine functionalized graphene. Electrochim. Acta 104, 178–184.

Zhao, B., Yin, J.J., Bilski, P.J., Chignell, C.F., Roberts, J.E., He, Y.Y., 2009. Enhanced photodynamic efficacy towards melanoma cells by encapsulation of Pc4 in silica nanoparticles. Toxicol. Appl. Pharmacol. 241, 163–172.

Zhao, J., Wei, L., Peng, C., Su, Y., Yang, Z., Zhang, L., Wei, H., Zhang, Y., 2013. A non-enzymatic glucose sensor based on the composite of cubic Cu nanoparticles and arc-synthesized multi-walled carbon nanotubes. Biosens. Bioelectron. 47, 86–91. doi:10.1016/j.bios.2013.02.032

Zhao, Y., Liu, B., Pan, L., Yu, G., 2013. 3D nanostructured conductive polymer hydrogels for high-performance electrochemical devices. Energy Environ. Sci. 6, 2856. doi:10.1039/c3ee40997j

Zhao, Y., Trewyn, B.G., Slowing, I.I., Lin, V.S., 2009. Mesoporous Silica Nanoparticle-

based Double Drug Delivery System for Glucose Responsive Controlled Release of Insulin and Cyclic AMP. Synthesis (Stuttg). 1–9.

Zheng, H., Xue, H., Zhang, Y., Shen, Z., 2002. A glucose biosensor based on microporous polyacrylonitrile synthesized by single rare-earth catalyst. Biosens. Bioelectron. 17, 541–545.

Zheng, W., Wang, B.-B., Lai, J.-C., Wan, C.-Z., Lu, X.-R., Li, C.-H., You, X.-Z., 2015. Electrochromic properties of novel octa-pinene substituted double-decker Ln(III) (Ln = Eu, Er, Lu) phthalocyanines with distinctive near-IR absorption. J. Mater. Chem. C 3, 3072–3080. doi:10.1039/C5TC00020C

Zhong, J.P., Fan, Y.J., Wang, H., Wang, R.X., Fan, L.L., Shen, X.C., Shi, Z.J., 2013. Copper phthalocyanine functionalization of graphene nanosheets as support for platinum nanoparticles and their enhanced performance toward methanol oxidation. J. Power Sources 242, 208–215. doi:10.1016/j.jpowsour.2013.05.085

Zhou, M., Shang, L., Li, B., Huang, L., Dong, S., 2008. Highly ordered mesoporous carbons as electrode material for the construction of electrochemical dehydrogenase- and oxidase-based biosensors. Biosens. Bioelectron. 24, 442–447. doi:10.1016/j.bios.2008.04.025

Zhu, C., Yang, G., Li, H., Du, D., Lin, Y., 2015. Electrochemical sensors and biosensors based on nanomaterials and nanostructures. Anal. Chem. 87, 230–249. doi:10.1021/ac5039863

Zhu, C., Yang, G., Li, H., Du, D., Lin, Y., 2014. Electrochemical Sensors and Biosensors Based on Nanomaterials and Nanostructures. Am. Chem. Soc. 1, 230–249.

Zhu, H., Srivastava, R., Brown, Q., McShane, M.J., 2005. Combined physical and

chemical immobilization of glucose oxidase in alginate microspheres improves stability of encapsulation and activity. Bioconjug. Chem. 16, 1451–1458. doi:10.1021/bc050171z

Zhu, Z., Garcia-Gancedo, L., Flewitt, A.J., Xie, H., Moussy, F., Milne, W.I., 2012. A critical review of glucose biosensors based on carbon nanomaterials: carbon nanotubes and graphene. Sensors (Basel). 12, 5996–6022. doi:10.3390/s120505996

Zhuang, Q.F., Wang, J.E., Zhu, Z.J., Li, F., Wang, Z.X., 2011. Preparation of tetraamino-phthalocyanine-zinc-loaded silica nanoparticles and study of their cytotoxicity. Fenxi Huaxue/ Chinese J. Anal. Chem. 39, 1567–1571.

Zou, H., Wu, S., Shen, J., 2008a. Polymer / Silica Nanocomposites : Preparation , Characterization , Properties , and 3893–3957. doi:10.1063/1.1760212

Zou, H., Wu, S., Shen, J., 2008b. Polymer / Silica Nanocomposites : Preparation , Polymer / Silica Nanocomposites : Preparation , Characterization , Properties , and. Chem. Rev. 108, 3893–3957. doi:10.1021/cr068035q

Zugle, R., Nyokong, T., 2012. Physico-chemical properties of lutetium phthalocyanine complexes in solution and in solid polystyrene polymer fibers and their application in photoconversion of 4-nitrophenol. J. Mol. Catal. A Chem. 358, 49–57. doi:10.1016/j.molcata.2012.02.010